



National Library
of Canada

Canadian Theses Service

Ottawa, Canada
K1A 0N4

Bibliothèque nationale
du Canada

Service des thèses canadiennes

NOTICE

The quality of this microform is heavily dependent upon the quality of the original thesis submitted for microfilming. Every effort has been made to ensure the highest quality of reproduction possible.

If pages are missing, contact the university which granted the degree.

Some pages may have indistinct print especially if the original pages were typed with a poor typewriter ribbon or if the university sent us an inferior photocopy.

Reproduction in full or in part of this microform is governed by the Canadian Copyright Act, R.S.C. 1970, c. C-30, and subsequent amendments.

AVIS

La qualité de cette microforme dépend grandement de la qualité de la thèse soumise au microfilmage. Nous avons tout fait pour assurer une qualité supérieure de reproduction.

S'il manque des pages, veuillez communiquer avec l'université qui a conféré le grade.

La qualité d'impression de certaines pages peut laisser à désirer, surtout si les pages originales ont été dactylographiées à l'aide d'un ruban usé ou si l'université nous a fait parvenir une photocopie de qualité inférieure.

La reproduction, même partielle, de cette microforme est soumise à la Loi canadienne sur le droit d'auteur, SRC 1970, c. C-30, et ses amendements subséquents.

UNIVERSITY OF ALBERTA

**STRENGTH AND STABILITY OF REINFORCED CONCRETE
PLATES UNDER COMBINED INPLANE AND LATERAL LOADS**

BY

MASHHOUR G. GHONEIM

A THESIS

SUBMITTED TO THE FACULTY OF GRADUATE STUDIES AND RESEARCH
IN PARTIAL FULFILLMENT OF THE REQUIREMENTS FOR THE DEGREE
OF

DOCTOR OF PHILOSOPHY

IN STRUCTURAL ENGINEERING

DEPARTMENT OF CIVIL ENGINEERING

EDMONTON, ALBERTA

SPRING 1992



National Library
of Canada

Bibliothèque nationale
du Canada

Canadian Theses Service Service des thèses canadiennes

Ottawa, Canada
K1A 0N4

The author has granted an irrevocable non-exclusive licence allowing the National Library of Canada to reproduce, loan, distribute or sell copies of his/her thesis by any means and in any form or format, making this thesis available to interested persons.

The author retains ownership of the copyright in his/her thesis. Neither the thesis nor substantial extracts from it may be printed or otherwise reproduced without his/her permission.

L'auteur a accordé une licence irrévocable et non exclusive permettant à la Bibliothèque nationale du Canada de reproduire, prêter, distribuer ou vendre des copies de sa thèse de quelque manière et sous quelque forme que ce soit pour mettre des exemplaires de cette thèse à la disposition des personnes intéressées.

L'auteur conserve la propriété du droit d'auteur qui protège sa thèse. Ni la thèse ni des extraits substantiels de celle-ci ne doivent être imprimés ou autrement reproduits sans son autorisation.

ISBN 0-315-73097-8

Canada

UNIVERSITY OF ALBERTA

RELEASE FORM

NAME OF AUTHOR: MASHHOUR G. GHONEIM

TITLE OF THESIS: STRENGTH AND STABILITY OF REINFORCED
CONCRETE PLATES UNDER COMBINED INPLANE
AND LATERAL LOADS

DEGREE: DOCTOR OF PHILOSOPHY

YEAR THIS DEGREE GRANTED: SPRING 1992

Permission is hereby granted to THE UNIVERSITY OF ALBERTA LIBRARY to reproduce single copies of this thesis and to lend or sell such copies for private, scholarly or scientific research purposes only.

The author reserves other publication rights, and neither the thesis nor extensive extracts from it may be printed or otherwise reproduced without the author's written permission.

(signed) Mashhour Ghoneim

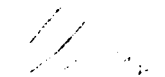
PERMANENT ADDRESS

23 Ahmed Elshattory Street
Dokki, Giza
Egypt


Date: Feb 28, 1992

THE UNIVERSITY OF ALBERTA
FACULTY OF GRADUATE STUDIES AND RESEARCH

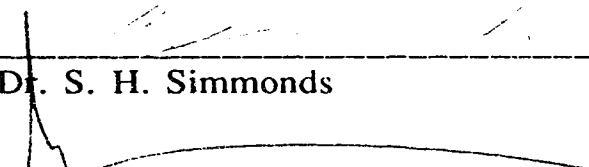
The undersigned certify that they have read, and recommended to the Faculty of Graduate Studies and Research for acceptance, a thesis entitled STRENGTH AND STABILITY OF REINFORCED CONCRETE PLATES UNDER COMBINED INPLANE AND LATERAL LOADS submitted by MASHHOUR G. GHONEIM in partial fulfillment of the requirements for the degree of DOCTOR OF PHILOSOPHY in Civil Engineering.



Dr. J. G. MacGregor, Supervisor




Dr. S. H. Simmonds




Dr. A. E. Elwi



Dr. Z. Eisenstein



Dr. A. Lipsett



Dr. A. Ghali, External Examiner

Date: Feb 5. 1992

To the memory of my parents

Abstract

Reinforced concrete plates supported on four edges and subjected to combined inplane compressive and lateral loads are encountered in many structural applications. The failure loads of these plates may be reached either by material failure due to the limited deformability of concrete in compression or by stability failure.

The experimental phase of this investigation involved testing of 19 specimens under well defined boundary conditions. The parameters included the loading type, plate slenderness, aspect ratio, inplane load level, reinforcement ratios in the orthogonal directions, and loading sequence.

A simple analytical model is developed to predict the ultimate strength of such plates. The interaction of the inplane loads and the geometrical nonlinearities is incorporated into the differential equation of equilibrium. To take into account the nonlinear material response the theory of elasticity, based on secant rigidities obtained from analytically derived moment-curvature relations, is used.

Theoretical predictions of the response of the specimens are also obtained from nonlinear finite element analyses using the bicubic three dimensional degenerated plate-shell element available in the NISA code. Geometrical nonlinearity is allowed using Updated Lagrangian formulation and material nonlinearity is allowed using an incremental hypoelastic plane stress model for concrete. The finite element investigation highlighted the sensitivity of the predicted

load-deflection response and ultimate strength of plates subjected to combined loads to the assumptions which influence the load carried by concrete in tension.

ACKNOWLEDGEMENTS

The author wishes to express his sincere gratitude and indebtedness to his research supervisor, Professor James G. MacGregor for his consistent guidance, interest, and encouragement throughout the course of this study. Professor MacGregor's valuable comments and suggestions during the research program and his efforts in reviewing the manuscript are greatly appreciated.

The assistance of L. Burden and R. Helfrich of the I. F. Morrison Structural Laboratory, University of Alberta, in conducting the experimental program is gratefully acknowledged.

Financial support for this study was provided by the Natural Science and Engineering Research Council of Canada through Operating Grant A1673.

The author deeply appreciates the support and patience of his wife throughout the course of this study.

Table of Contents

Chapter	Page
1. Introduction	1
1.1 Background	1
1.2 Review of Previous Work.....	3
1.3 Objectives	7
1.4 Scope	8
1.5 Organization of the Thesis	8
2. Experimental Program	13
2.1 Introduction	13
2.2 Test Specimens	13
2.3 Fabrication of Specimens	15
2.4 Material Properties	16
2.4.1 Reinforcing Steel	16
2.4.2 Concrete	17
2.5 Test Set-Up	18
2.5.1 Supporting Frame.....	19
2.5.2 Lateral Loading System	20
2.5.3 Inplane Loading System.....	20
2.6 Instrumentation	22
2.6.1 Steel Strains.....	23
2.6.2 Average Curvatures	23
2.6.3 Displacement Measurements	24
2.7 Test Procedure	25
3. Test Results	55

3.1	Introduction	55
3.2	Ultimate Loads	55
3.3	Crack Patterns and Modes of Failure	56
3.3.1	Specimens Tested under Lateral Loads Only	56
3.3.2	Specimens Tested under Uniaxial Inplane and Lateral Loads	58
3.3.3	Specimens Tested under Biaxial Inplane and Lateral Loads	62
3.4	Load-Deflection Characteristics	62
3.4.1	Out-of-plane Deflections	62
3.4.2	Inplane Deflections	66
3.4.3	Edge Rotations	67
3.5	Deflected Shapes	67
3.6	Measured Steel Strains and Average Curvatures	68
4.	Evaluation of Test Results	92
4.1	Introduction	92
4.2	Effect of Load Type and Plate Slenderness	92
4.2.1	Load-Deflection Response and Ultimate Strength	93
4.2.2	Failure Modes	97
4.2.2.1	Specimens Tested under Lateral Loads Only	97
4.2.2.2	Specimens Tested under Combined Inplane and Lateral Loads	99
4.3	Effect of Inplane Load Level	100
4.4	Effect of the Reinforcement Ratios in the Orthogonal Directions	102
4.5	Effect of Aspect Ratio	103
4.6	Effect of Loading Sequence	104

5.	Analytical Model	122
5.1	Introduction	122
5.2	Load-Moment-Curvature Relationship	123
5.3	Tension Stiffening Effect and Moment-Curvature Relations	124
5.4	Load-Moment-Curvature Relationship for the Present Study	127
5.4.1	Basic Assumptions	127
5.4.2	Material Constitutive Laws	129
5.4.2.1	Concrete in Compression	129
5.4.2.2	Concrete in Tension	131
5.4.2.3	Reinforcing Steel	133
5.4.3	Numerical Procedure	133
5.5	Analytical Model for Plates Subjected to Combined Inplane and Lateral Loads	135
5.5.1	General Background	135
5.5.2	Formulation	138
5.6	Comparison of Analytical Predictions with Test Results	143
6.	Finite Element Analysis	154
6.1	Introduction	154
6.2	Description of NISA	154
6.3	Material Models for Concrete and Reinforcing Steel ...	156
6.4	Modelling of the Test Specimens with NISA	160
6.5	Analysis of Plates under Combined Loads	161
6.5.1	Effect of Tension Stiffening	162
6.5.2	Effect of the Compressive Strength of Concrete	165

6.5.3	Predicted Behaviour of Selected Specimens	166
6.6	Analysis of Plates under Lateral Loads Only	168
7.	Summary, Conclusions, and Recommendations	189
7.1	Summary	189
7.2	Conclusions	190
7.3	Recommendations for Future Work	193
References	195
Appendix A	Ancillary Tests Results	203
Appendix B	Calculation of Shrinkage Induced Stresses	210
Appendix C	Experimental Lateral Load versus Center Deflection Curves	214

List of Tables

Table	Page
2.1 Side Dimensions and Average Measured Thickness of Specimens	28
2.2 Area of Reinforcement in X- and Y-Directions	29
2.3 Average Locations of Top and Bottom Reinforcement from Compressive Face	30
2.4 Concrete Properties	31
3.1 Maximum Loads and Corresponding Out-of-Plane Center Deflections	73
4.1 Test Results and Predicted Yield-Line Capacities for Specimens Tested under Lateral Loads Only	107
4.2 Levels of Applied Inplane Loads	108
5.1 Tensile Stresses Due to Shrinkage and Effective Modulus of Rupture	145
5.2 Maximum Lateral Loads: Test versus Analytical Predictions	146
6.1 Concrete Properties and Effective Reinforcement Ratios Used in the Analyses of Specimens under Combined Loads	171
6.2 Comparison of the Finite Element Predictions to the Test Results for Specimens under Combined Loads	172
6.3 Concrete Properties and Effective Reinforcement Ratios Used in the Analyses of Specimens under Lateral Loads Only	173
6.4 Comparison of the Finite Element Predictions to the Test Results for Specimens under Lateral Loads Only	174
A.1 Ancillary Tests Results for Series A	205
A.2 Ancillary Tests Results for Series B	206
A.3 Ancillary Tests Results for Series C	207

A.4	Ancillary Tests Results for Series D	209
B.1	Calculation of Shrinkage Strains	212
B.2	Parameters Used to Calculate the Tensile Stresses Due to Shrinkage	213

List of Figures

Figure	Page
1.1 The Hull of a Typical Concrete Floating Structure	1 1
1.2 Loads Acting on the Bottom Plate of a Hull	1 2
2.1 General Reinforcing Layout for a Typical Plate Section	3 2
2.2 Reinforcement Cage for a Specimen Ready for Casting	3 3
2.3 Stress-Strain Curve for Reinforcing Steel	3 4
2.4 Schematic Plan of the Test Frame	3 5
2.5 Section A-A Through the Test Frame	3 6
2.6 Loading Frame and Test Set-Up	3 7
2.7 Schematic of the Rocker-Roller Assembly	3 8
2.8 Locations of the Lateral Load and Support Points for Series A	3 9
2.9 Locations of the Lateral Load and Support Points for Series B	4 0
2.10 Locations of the Lateral Load and Support Points for the Square Specimens	4 1
2.11 Schematic of a Corner Support Frame	4 2
2.12 Knife Edge Assembly	4 3
2.13 Arrangement of the Inplane Loading Plates for Specimens Loaded along the Short Sides	4 4
2.14 Arrangement of the Inplane Loading Plates for Specimen B4	4 5
2.15 Arrangement of the Inplane Loading Plates for the Biaxially Loaded Square Specimens	4 6
2.16 Typical Strain Gauge Layout for Series A	4 7
2.17 Typical Strain Gauge Layout for Series B	4 8

2.18	Typical Strain Gauge Layout for Series C.....	49
2.19	Typical Strain Gauge Layout for Series D	50
2.20	Curvature Meter.....	51
2.21	The Edge Rotation Measuring Device.....	51
2.22	Locations of the Displacement Measurements for Series A	52
2.23	Locations of the Displacement Measurements for Series B	53
2.24	Locations of the Displacement Measurements for Square Specimens	54
3.1	Tension Face of Specimen B1 after Failure	75
3.2	Compression Face of Specimen B1 after Failure	75
3.3	Tension Face of Specimen A2 after Failure	76
3.4	Compression Face of Specimen A2 after Failure	76
3.5	Tension Face of Specimen B4 after Failure	77
3.6	Compression Face of Specimen B4 after Failure	77
3.7	Tension Face of Specimen C3 after Failure	78
3.8	Compression Face of Specimen C3 after Failure.....	78
3.9	Tension Face of Specimen C6 after Failure	79
3.10	Compression Face of Specimen C6 after Failure.....	79
3.11	Lateral Load versus Out-of-Plane Center Deflection for Specimen C1	80
3.12	Lateral Load versus Out-of-Plane Center Deflection for Specimen A4.....	80
3.13	Lateral Load versus Out-of-Plane Center Deflection for Specimen C2	81
3.14	Lateral Load versus Out-of-Plane Center Deflection for Specimen D2	81
3.15	Lateral Load versus Out-of-Plane Center Deflection for Specimen C8	82

3.16	Lateral Load versus Inplane Deflection in the X-Direction for Specimen C1	82
3.17	Lateral Load versus Inplane Deflection in the X-Direction for Specimen A4.....	83
3.18	Lateral Load versus Inplane Deflection in the Y-Direction for Specimen A4.....	83
3.19	Lateral Load versus Inplane Deflection in the X-Direction for Specimen C2	84
3.20	Lateral Load versus Inplane Deflection in the Y-Direction for Specimen C2	84
3.21	Lateral Load versus Edge Rotation about the Edge Parallel to the X-Direction for Specimen A4	85
3.22	Lateral Load versus Edge Rotation about the Edge Parallel to the Y-Direction for Specimen A4	85
3.23	Lateral Load versus Edge Rotation about the Edge Parallel to the X-Direction for Specimen C2.....	86
3.24	Lateral Load versus Edge Rotation about the Edge Parallel to the Y-Direction for Specimen C2.....	86
3.25	Out-of-Plane Deflection Profiles in the X-Direction for Specimen A4	87
3.26	Out-of-Plane Deflection Profiles in the Y-Direction for Specimen A4	87
3.27	Out-of-Plane Deflection Profiles in the X-Direction for Specimen C2	88
3.28	Out-of-Plane Deflection Profiles in the Y-Direction for Specimen C2	88
3.29	Steel Strains along the Bottom Transverse Bar at the Center of Specimen A4	89
3.30	Steel Strains at the Center of Specimen A4 in Bottom Bars Running in the Direction of the Inplane Load	89
3.31	Steel Strains along the Bottom Transverse Bar at the Center of Specimen C2	90

3.32	Steel Strains at the Center of Specimen C2 in Bottom Bars Running in the Direction of the Inplane Load	90
3.33	Lateral Load versus Transverse Steel Strains at the Center of Specimen C2	91
4.1	Effect of Loading Type for Slender Square Plates	109
4.2	Effect of Loading Type for Rectangular Plates, $a/b=2.17$	110
4.3	Effect of Loading Type for Stocky Square Plates	111
4.4	Lateral Load versus Transverse Bottom Steel Strains for Specimens D1 and D2	112
4.5	Interaction Curve for a Section of Unit Width of Specimen C2 in the Direction of the Inplane Load	113
4.6	Interaction Curve for a Section of Unit Width of Specimen C4 in the Direction of the Inplane Load	113
4.7	Effect of Inplane Load Level for Rectangular Plates, $a/b=1.5$	114
4.8	Effect of Inplane Load Level for Slender Square Plates	115
4.9	Effect of the Reinforcement Ratios in the Two Directions for Square Plates	116
4.10	Effect of the Reinforcement Ratios in the Two Directions for Rectangular Plates, $a/b=2.17$	117
4.11	Effect of Aspect Ratio	118
4.12	Loading Sequences	119
4.13	Effect of Loading Sequence for Slender Square Plates, Specimens C2, C3, and C8	120
4.14	Effect of Loading Sequence for Slender Square Plates, Specimens C2 and C9	121
5.1	Uniaxial Stress-Strain Curve for Concrete in Compression	147
5.2	Adopted Tension Stiffening Curve	147

5.3	Derivation of the Load-Moment-Curvature Relationship	148
5.4	Effect of Axial Load Level on the Moment-Curvature Relationship	149
5.5	Effect of Tension Stiffening on the Moment-Curvature Relationship	149
5.6	Plate Dimensions, Coordinate Axes and Loading	150
5.7	Lateral Load-Deflection Curves for Specimen C2 : Test versus Model.....	151
5.8	Lateral Load-Deflection Curves for Specimen C4 : Test versus Model.....	151
5.9	Lateral Load-Deflection Curves for Specimen C6 : Test versus Model.....	152
5.10	Lateral Load-Deflection Curves for Specimen C7 : Test versus Model.....	152
5.11	Lateral Load-Deflection Curves for Specimen B3 : Test versus Model.....	153
5.12	Lateral Load-Deflection Curves for Specimen A4 : Test versus Model.....	153
6.1	The 3D Degenerated Plate-Shell Element	175
6.2	Failure Envelope.....	176
6.3	Stress-Equivalent Uniaxial Strain Curve for Concrete in Compression.....	176
6.4	Tension Softening Curve for Plain Concrete.....	177
6.5	Tension Stiffening Curve for Reinforced Concrete.....	177
6.6	Modelling of Specimens of Series A	178
6.7	Modelling of Specimens of Series B.....	179
6.8	Modelling of the Square Specimens	180
6.9	Modified Stress-Strain Diagram for Reinforcing Steel to Account for Tension Stiffening	181
6.10	Specimen C5- Effect of Tension Stiffening.....	181

6.11	Specimen C5- Effect of the Tensile Strength of Concrete . . .	182
6.12	Specimen C5- Comparison Between Tension Stiffening Models	182
6.13	Specimen B2- Effect of the Compressive Strength of Concrete	183
6.14	Specimen C6- Effect of the Compressive Strength of Concrete	183
6.15	Experimental and Analytical Lateral Load versus Central Deflection Curves for Specimen A2	184
6.16	Experimental and Analytical Lateral Load versus Central Deflection Curves for Specimen A3	184
6.17	Experimental and Analytical Lateral Load versus Central Deflection Curves for Specimen B3	185
6.18	Experimental and Analytical Lateral Load versus Central Deflection Curves for Specimen C2	185
6.19	Experimental and Analytical Lateral Load versus Central Deflection Curves for Specimen C4	186
6.20	Experimental and Analytical Lateral Load versus Central Deflection Curves for Specimen D2	186
6.21	Predicted and Measured Strains in Bottom Reinforcement for Specimen A2	187
6.22	Predicted and Measured Strains in Bottom Reinforcement for Specimen B2	187
6.23	Experimental and Analytical Lateral Load versus Central Deflection Curves for Specimen B1	188
6.24	Experimental and Analytical Lateral Load versus Central Deflection Curves for Specimen C1	188
C.1	Lateral Load versus Center Deflection Curve for Specimen A1	215
C.2	Lateral Load versus Center Deflection Curve for Specimen A2	215
C.3	Lateral Load versus Center Deflection Curve	

	for Specimen A3	216
C.4	Lateral Load versus Center Deflection Curve for Specimen A4	216
C.5	Lateral Load versus Center Deflection Curve for Specimen B1	217
C.6	Lateral Load versus Center Deflection Curve for Specimen B2	217
C.7	Lateral Load versus Center Deflection Curve for Specimen B3	218
C.8	Lateral Load versus Center Deflection Curve for Specimen B4	218
C.9	Lateral Load versus Center Deflection Curve for Specimen C1	219
C.10	Lateral Load versus Center Deflection Curve for Specimen C2	219
C.11	Lateral Load versus Center Deflection Curve for Specimen C3	220
C.12	Lateral Load versus Center Deflection Curve for Specimen C4	220
C.13	Lateral Load versus Center Deflection Curve for Specimen C5	221
C.14	Lateral Load versus Center Deflection Curve for Specimen C6	221
C.15	Lateral Load versus Center Deflection Curve for Specimen C7	222
C.16	Lateral Load versus Center Deflection Curve for Specimen C8	222
C.17	Lateral Load versus Center Deflection Curve for Specimen C9	223
C.18	Lateral Load versus Center Deflection Curve for Specimen D1	223
C.19	Lateral Load versus Center Deflection Curve for Specimen D2	224

List of Symbols

a	Length of plate in y-direction
A_c	Area of concrete section
A'_c	Area of the age-adjusted transformed section
A_s	Total area of steel in the section
A_{sx}	Tension reinforcement area in the x-direction
A_{sy}	Tension reinforcement area in the y-direction
b	Length of plate in x-direction
B	Effective torsional rigidity
D_x	Bending rigidity per unit width in x-direction
D_y	Bending rigidity per unit width in y-direction
$2D_t$	Torsional rigidity per unit width
E_s	Modulus of elasticity of reinforcement
E_c	Modulus of elasticity of concrete at the age of testing
E'_c	Age-adjusted elasticity modulus of concrete
f_c	Compressive stress in concrete
f'_c	Compressive strength of concrete at the age of testing
f''_c	Compressive strength of concrete in flexure
f'_t	Direct tensile strength of concrete
f_{sp}	Splitting strength of concrete
f_r	Modulus of rupture
f_{re}	Effective modulus of rupture
F_{CC}	Compression force carried by concrete
F_{CT}	Tension force carried by concrete
F_{SC}	Compression force carried by steel
F_{ST}	Tension force carried by steel

M_x	Bending moment per unit width in x-direction
M_y	Bending moment per unit width in y-direction
M_{xy}	Twisting moment per unit width
N	Resultant axial compression force
N_x	Inplane load per unit length in x-direction
N_y	Inplane load per unit length in y-direction
N_u	Ultimate axial compression force
q	Lateral uniform load per unit area of the plate
q_u	Maximum Lateral uniform load per unit area of the plate
R	Curvature ratio at the center of the plate
$r-s-t$	Plate-Shell element coordinate axes
h	Thickness of plate
w	Lateral deflection at point (x,y)
w_o	Lateral deflection at the center of the plate
w_{ou}	Lateral deflection at the center of the plate at the maximum lateral load
α	Principal stress ratio
α_{ss}	Factor to account for the size effect on shrinkage
α_{RH}	Factor to account for the relative humidity
α_{sL}	Factor to account for the slump and cement content
β_s	Factor to account for the rate at which shrinkage develops
χ	Aging coefficient of concrete
ϵ	Strain in concrete
ϵ_o	Concrete strain at maximum compressive stress
ϵ_{cu}	Ultimate concrete compressive strain
ϵ_s	Steel strain
ϵ_{sh}	Shrinkage strain occurring at time t = age of the specimen at

testing

ϵ_{shu}	Basic shrinkage strain at time = ∞ for a member with an effective thickness of 152 mm.
ϵ_t	Tensile strain in concrete
ϵ_y	Yield strain
ϕ	Creep coefficient of concrete
κ_x	Curvature in x-direction
κ_y	Curvature in y-direction
κ_{xy}	Twist of the midplane of the plate with respect to x- and y-axes
κ_{xo}	Curvature in x-direction at the center of the plate
κ_{yo}	Curvature in y-direction at the center of the plate
ν_x	Poisson's ratio in x-direction
ν_y	Poisson's ratio in y-direction
ρ_x	Tension reinforcement ratio in x-direction
ρ_y	Tension reinforcement ratio in y-direction
ρ_{effx}	Effective reinforcement ratio in x-direction
ρ_{effy}	Effective reinforcement ratio in y-direction
σ_A, σ_B	Principal stresses
σ_{cu}	Ultimate concrete compressive strength in biaxial state of stresses

1. Introduction

1.1 Background

Reinforced concrete plates supported along all edges and subjected to combined inplane compressive and lateral (out-of-plane) loads are commonly used as structural elements. These plates resist loads in two-way action and develop biaxial curvatures.

Barge-like concrete structures, such as floating barges, bridge pier caissons, docks, bridges and breakwaters often consist of a network of slender internal stiffening walls supporting the exterior sidewalls and bottom. A schematic diagram of the hull of a typical floating concrete structure is shown in Fig. 1.1. As shown in Fig. 1.2, the loads acting on these plate elements include hydrostatic water pressures on the surface of the plate as well as compressive inplane loads due to longitudinal hull bending and transverse forces in the plane of the hull bottom arising directly from water pressure on the hull sides, (ACI Committee 357, 1988). There may also be edge moments which are not shown in the figure. Precast exterior wall panels used in high-rise buildings and bridge decks are other applications of such plates.

The sequence of application of combined inplane and lateral loads varies. Generally, any load application sequence can be imagined. Two loading sequences, however, are more common; the inplane load may be applied to its full value and held constant while

the lateral load is applied from zero to failure or both inplane and lateral loading may be applied simultaneously while maintaining a constant ratio between them. Although this investigation is primarily concerned with these two loading sequences, the effect of different loading sequences was included as a parameter in the experimental program.

Most of the research carried out on plates under combined loads have been conducted on steel or aluminium alloy plates. The results of these investigations, however, can not be extended directly to reinforced concrete plates due to the unique characteristics of the axial load-moment interaction curve of a reinforced concrete section.

The effects of moderate values of inplane compressive forces on the behaviour of reinforced concrete plates may be interpreted as being made up of two compensating effects. The inplane load causes an increase in the flexural rigidity and the moment capacity of the member in the direction of its application. This is offset partially or completely by the geometrical nonlinearity which magnifies the load effects. The failure loads of these plates may be reached either by material failure or by stability failure. Material failure is associated with crushing of concrete when the strength of the cross section is reached before or after excessive yielding of the tensile reinforcement. In some cases, however, the geometrical nonlinearity of the plate increases the external moments more rapidly than the internal resisting moments and this leads to stability failure before the critical cross sections are loaded to the limits of their strengths.

The modelling of concrete properties plays an important role when analyzing the behaviour of reinforced concrete plates under combined loads. The presence of compressive inplane loads demands an accurate representation of the characteristics of concrete in compression. On the other hand, the possibility of stability failure of such slender members makes a realistic representation of the stiffness of the section including the tension stiffening of concrete a necessity.

There are insufficient experimental and theoretical studies which address the problem of the strength and stability of reinforced concrete plates under combined loads. More tests are required to develop a better understanding of the parameters that affect the behaviour of these structural components and to establish a satisfactory level of confidence in the available numerical techniques. Also, a simple analytical model is highly desirable for use in design.

1.2 Review of Previous Work

In this section mention will be made of the experimental work available for reinforced concrete plates. Developments in other areas of particular relevance to the work presented herein, such as existing analyses of reinforced concrete plates under combined loads and moment-curvature relationships for reinforced concrete beams and slabs will be dealt with in the particular chapter in which these topics are discussed.

An extensive review of the available experimental investigations of reinforced concrete plates under lateral loads only is given by Park and Gamble (1980).

Most of the experimental investigations of reinforced concrete plates under combined inplane load and bending moments have been on panels in one-way action (i.e., simply supported only along the two loaded edges). The investigations of Oberlander and Everard (1977) and Saheb and Desayi (1989) have led to certain recommendations in the different codes of practice.

Studies on the strength and behaviour of reinforced concrete plates supported on all edges and subjected to inplane loads or combined inplane loads and bending moments, however, have been scarce.

Ernst (1952) tested ten reinforced concrete plates simply supported on all four edges under eccentric uniaxial compressive inplane loads. Five of the panels were square while the others were rectangular with an aspect ratio of 2. All the panels were centrally reinforced with welded wire fabric mesh. Width-to-thickness ratios varied from 27 to 80. Ultimate axial loads were achieved due to either crushing of concrete or instability of the panels.

Girolami et al. (1970) tested six reinforced concrete panels under combined biaxial compressive inplane and lateral loads. Each panel was 1830 mm square and 44 mm thick and was cast monolithically with 152 mm deep by 76 mm wide spandrel beams.

Three of the test specimens were supported only at the intersections of the spandrel beams, while three were supported at several points along the spandrel beams. The main purpose of these tests was to investigate the strength of panels subjected to controlled reactive inplane forces at the edges. In all cases, yield-line patterns similar to those developed under lateral loads only were observed at the ultimate lateral loads and the measured lateral load capacities were higher than the loads calculated by Johansen's yield-line theory applied without considering the enhanced moment capacity at the yield-lines due to inplane loads or the second order effect of the inplane loads.

Swartz et al. (1974) carried out tests on twenty-four plates with an aspect ratio of 2.0, simply supported along the boundaries and subjected to an inplane concentric compressive load applied along the short side. The ultimate loads were 1 to 24 percent higher than the buckling loads. It was also observed that the panels generally failed in a collapse mechanism approaching that for simply supported plates subjected to uniform lateral loads. Based on these tests, they presented a method for evaluating the carrying capacity of slender plates under concentric inplane load without any lateral loads using the isotropic tangent modulus approach.

Kordina et al. (1973, 1979, 1982) tested sixteen square reinforced concrete plates under uniaxially eccentrically applied inplane loads. The plates were simply supported along the four edges without inplane restraints and were tested in a vertical position. They also tested plates supported only along the loaded edges to

determine experimentally the influence of the horizontal or transverse bending on the inplane load capacity of a plate. In all cases, failure occurred suddenly along a failure line similar to that of a simply supported plate under lateral loads. Failure loads of plates supported along the four edges were approximately twice the wide column capacity expressed in terms of the uniaxial load bearing capacity of the plain cross-section.

Aghayere and MacGregor (1988) tested nine slender reinforced concrete plates, simply supported on all four edges, under combined inplane and lateral loads. These tests provided a first insight into the behaviour of such structural elements. The experimental program consisted of tests of nine specimens. Seven of them had an aspect ratio of 1.0, while two had an aspect ratio of 1.5. Width-to-thickness ratios varied from 27.3 to 33.0. Eight plates were tested under combined loads and one square plate was tested under transverse load alone to give an indication of the reduction in transverse load capacity for the other plates in the same series. The applied inplane loads ranged from 24 to 45 percent of the uniaxial inplane load capacity of the plate cross sections. In all the specimens, the presence of an axial inplane load led to a reduction of the transverse load capacity of the plates.

Saheb and Desayi (1990) tested twenty-four reinforced concrete plates simply supported on all the four edges and subjected to uniaxial inplane load. The inplane loads were applied at an eccentricity to represent possible accidental eccentricity that occurs in practice due to constructional imperfections. The influences of

aspect ratio, slenderness ratio and reinforcement ratios in the orthogonal directions on the ultimate inplane load were studied. An empirical and a semi-empirical equation were developed to predict the ultimate capacity of eccentrically loaded reinforced concrete plates supported along the four edges.

1.3 Objectives

This study is a continuation of an investigation of the behaviour of reinforced concrete plates under combined inplane compressive and lateral loads that has been underway at the University of Alberta since 1986. Preliminary tests were performed by Aghayere and MacGregor (1988), and a numerical investigation was carried out by Massicotte et al. (1988).

The present research has the following objectives:

1. To carry out an extensive experimental program that would lead to a better understanding of the behaviour of reinforced concrete plates under combined loads.
2. To develop a simple method for predicting the capacity of simply supported plates under combined loads which allows for geometric and material nonlinear effects in a sufficiently accurate manner.
3. To establish a satisfactory level of confidence in the results obtained from the finite element analysis of such highly nonlinear members and to highlight the factors that affect their modelling.

1.4 Scope

The experimental phase of the investigation involved the testing of 19 specimens under well defined boundary conditions. The parameters included the loading type, panel slenderness, aspect ratio (length/width), inplane load level, reinforcement ratios in the orthogonal directions, and loading sequence.

A simple analytical model was developed that predicts the strength of such plates. The scope of this model is limited to the cases in which the inplane load is applied first to its full value or both the inplane and lateral loads are applied simultaneously.

Theoretical predictions of the response of the specimens were also obtained from nonlinear finite element analyses. The analysis program NISA was used, where material nonlinearity was represented using an incremental hypoelastic material model for concrete and geometrical nonlinearity was allowed using the Updated Lagrangian formulation. The effect of varying the material parameters on such predictions were examined.

1.5 Organization of the Thesis

In addition to this chapter, six more chapters and three appendices form this thesis.

The experimental phase of the present study is described in Chapter 2. Details of the test set-up, the geometry of the specimens, material properties, instrumentation and test procedure are given.

In Chapter 3, the test results are presented including the failure loads for all the specimens, quantitative information about the load-deflection behaviour and qualitative behavioural observations regarding the strain distributions.

Chapter 4 consists of an evaluation of the parameters included in the experimental program.

In Chapter 5, the development of a simple analytical model for the prediction of the lateral load capacity of panels under combined loads is presented and its limits of application are examined. Material nonlinearities are included in the formulation using analytically derived load-moment-curvature relationships and geometrical nonlinearities are included in the governing equilibrium equations. The model is also calibrated against the test data.

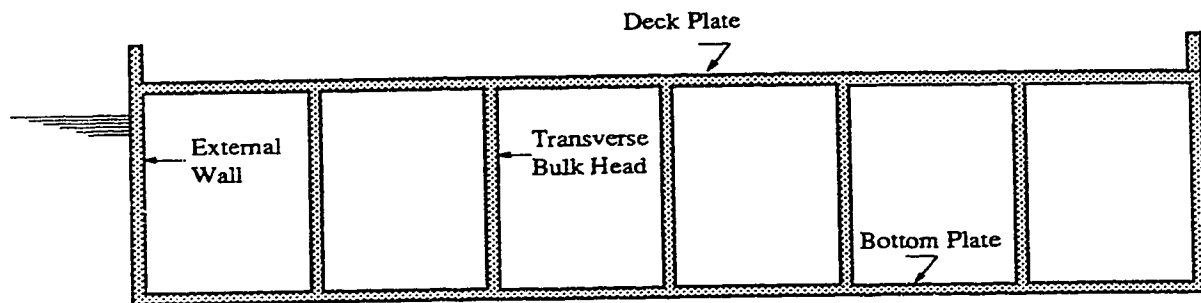
In Chapter 6, the application of nonlinear finite element analysis to this type of problems is discussed. A suitable program, NISA, having adequate sophistication for this type of analysis is used.

A summary of the significant experimental observations and the conclusions that can be drawn from the numerical analyses are presented in Chapter 7, together with recommendations for future work.

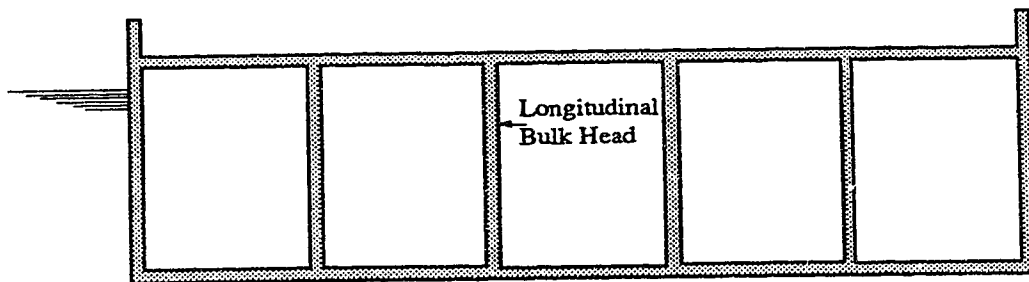
In Appendix A, the results of the ancillary tests conducted to determine the concrete properties are presented.

Appendix B contains the calculation of the shrinkage induced tensile stresses for all the specimens.

Appendix C contains the lateral load versus center deflection curves for all the specimens.



Longitudinal Section of the Hull of a Floating Plant



Cross-Section of the Hull of a Floating Plant

Figure 1.1 The Hull of a Typical Concrete Floating Structure

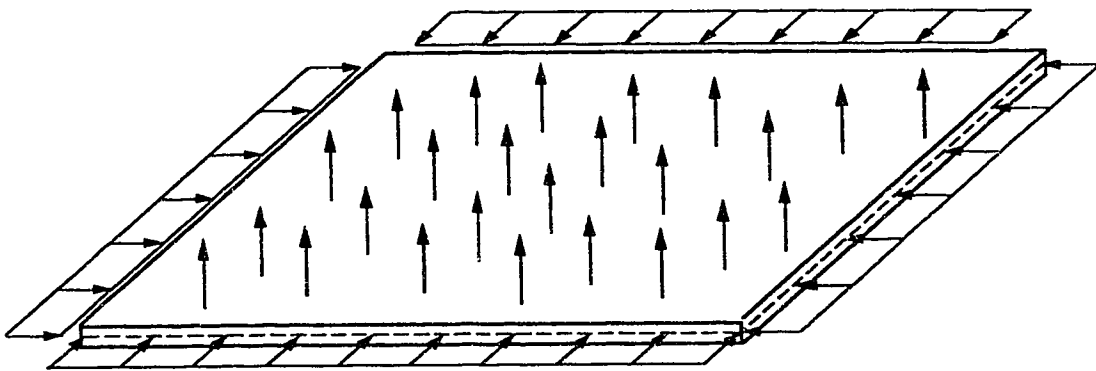


Figure 1.2 Loads Acting on the Bottom Plate of the Hull

2. Experimental Program

2.1 Introduction

This chapter presents a detailed description of the test specimens, the experimental set-up, and the test procedure. The experimental program consisted of tests of 19 reinforced concrete plates simply supported on four edges. The overall objective of this program was to develop a more complete understanding of the behaviour of reinforced concrete plates under combined inplane compressive and lateral loads. The specimens were heavily instrumented to obtain as much information as possible about their behaviour at each stage of loading.

2.2 Test Specimens

The test specimens were divided into four series: series A consisted of four rectangular specimens with side dimensions of 1829 mm by 4267 mm center-to-center of supports. Three of these specimens were tested under combined inplane and lateral loads with the inplane loads applied along the shorter edge and one was tested under lateral load only. Series B consisted of four rectangular specimens of side dimensions of 1829 mm by 2745 mm center-to-center of supports. Two of these specimens were tested under combined loads with the inplane loads applied along the shorter edge, one was tested under combined loads with the inplane load

applied along the longer edge, and one was tested under lateral load only. Series C consisted of nine square specimens of side dimensions of 1829 mm center-to-center of supports. Six of these specimens were tested under combined uniaxial compression and lateral loads, two were tested under combined biaxial compression and lateral loads, and one was tested under lateral load only. Series D consisted of two square specimens having the same side dimensions as series C but with smaller width-to-thickness ratio. One of these specimens was tested under combined inplane uniaxial compression and lateral loads while the other was tested under lateral load only. The specimen tested under lateral load only in each series was for comparison with those tested under combined loads.

The plates also had overhangs of 152 mm all round. These overhangs were required to accommodate the support assemblies and to achieve near uniform compressive inplane load starting at the support line. Plate thicknesses were measured at several points all over the plate before as well as after the completion of the test. Table 2.1 lists the side dimensions and the average measured thicknesses of all the specimens.

Plate reinforcement for all specimens consisted of top and bottom equally reinforced layers. Each layer comprised of steel running in both orthogonal directions. The top and bottom steel cages were secured in their positions using aluminium spacers. The areas of reinforcement for the specimens in both orthogonal directions are given in Table 2.2. Fig. 2.1 shows reinforcement arrangement in a typical plate section. The reinforcement positions at the top and

bottom of the specimens were measured after the test by chipping out concrete at several locations on the plate. The average locations of the top and bottom steel in both orthogonal directions measured from the compressive face of the plate are shown in Table 2.3. Fig. 2.2 shows a reinforcement cage for a specimen ready for casting.

2.3 Fabrication of Specimens

All specimens were cast flat on stiff wooden forms. The formwork consisted of two 16 mm thick plywood sheets, covered with form release oil, supported on 50 mm by 200 mm joists spaced at 300 mm. The joists were tied at the ends using 50 mm by 200 mm beams. The sides of the forms were 16 mm wood cut to the required thickness of the specimen. To accommodate the steel tie rods used for the application of lateral loads, holes 44.5 mm in diameter were formed by installing thin-walled steel conduits in the formwork. Steel washers-screws assemblies were used to cover the conduits during the casting of concrete. The distance between consecutive hole positions was 610 mm which was chosen to line up with the hole positions on the laboratory strong floor.

Each orthogonal layer of reinforcement was assembled into a mat with the aid of jigs before placement in the forms. About three-fourths of the bar intersections were tied. The strain gauge lead wires for gauges on the reinforcement were allowed to exit the specimen through drilled holes in the bottom of the form, thereby kept out of the way during casting. To achieve proper consolidation,

the concrete was vibrated with an electric vibrator. At the end of the casting operation, the top of the specimen was screeded using a long aluminium channel section. After casting, the specimens were left for about three hours to allow for partial set. Then, the top surface was finished with a steel trowel following which a curing compound (Rescoat 3001) was spread over the surface to control shrinkage cracks. After about seven hours, the specimens were covered with polythene and allowed to cure for about 7 days. At the end of this period, the specimens were air cured until they were tested. Standard cylinders and modulus of rupture beams were cured in the same manner as the specimens.

Lift hooks were provided at four points on the surface of the square specimens, six points on the surface of the rectangular specimens of series B, and eight points on the surface of the rectangular specimens of series A. The locations of these points were chosen to prevent cracking due to lifting of the specimens from the forms, where they were stored, into the test frame. The top surface during casting was the top of the specimen during testing.

2.4 Material Properties

2.4.1 Reinforcing Steel

All specimens were reinforced with 6.35 mm diameter deformed bars with a nominal area of 31.6 mm^2 . This steel was obtained from the Portland Cement Association. Tension tests were

performed on sample coupons in the MTS 1000 kN universal testing machine. A typical stress-strain plot from a coupon test is given in Fig. 2.3. The reinforcement had an ultimate strength of 620 MPa with no defined yield point. The 0.2 percent offset yield was 450 MPa.

2.4.2 Concrete

Normal weight concrete for all specimens except two was batched by a local concrete supplier and delivered by ready-mix trucks. Concrete placing was done in four phases and the same concrete mix was ordered for each. Each plate series was cast in one phase. The mix had 7 mm aggregate size and a specified 28 day compressive strength of 25 MPa. The concrete used for casting specimens C5 and C9 was produced in the laboratory.

Concrete test cylinders and modulus of rupture beams were cast at the same time as the specimens. Cylinders were nominally 150 mm in diameter and 300 mm long. Beams were 152x152x914 mm. Five concrete cylinders and two beams were tested the same day as each plate test. Of the five cylinders, three were tested in compression to determine the compressive strength and the static modulus of elasticity of concrete in compression. The remaining two cylinders were used for a split cylinder tensile test. These tests were conducted in accordance with CSA A23.2-3C (CSA, 1990). The results of the ancillary tests are given in detail in Appendix A.

The data from the control tests for each of the main four castings were fitted with regression lines of the form $f'_c(t) = a + bt$ by

the method of least squares, where t is the age of the concrete. Table 2.4 gives the age at which the specimen was tested together with the concrete properties determined for each specimen from the regression equations. As mentioned earlier, specimens C5 and C9 were cast at different times using concrete produced in the laboratory and hence their concrete properties did not follow the regression equations. Their strengths were taken from the tests made at the time these specimens were tested.

2.5 Test Set-Up

A test apparatus was especially constructed for this study. It is similar to the set-up used by Aghayere and MacGregor (1988), with some new features added to minimize uncertainties in the boundary conditions and in the method of inplane load application. The frame was designed to accommodate tests of square as well as rectangular specimens of different aspect ratios. The inplane load could be applied either uniaxially or biaxially. The test set-up consisted of the supporting frame for the plates, lateral loading system, and independent loading units for applying the inplane load. The different parts of the apparatus are described in the following sections. A schematic plan and a section through the testing frame are shown in Figs. 2.4 and 2.5. An overview of the test frame is shown in Fig. 2.6.

2.5.1 Supporting Frame

The specimens were tested in a horizontal position supported above the laboratory strong floor on two W200x71 (8W48) beams spanning between built-up beams 460 mm deep. These in turn were supported by steel columns.

Simple support conditions without inplane restraint were achieved by using a series of rocker-roller units onto which the plates were bedded by a thin layer of plaster. Each support point consisted of a 125 mm diameter half round, a 51 mm high strength plate, and 72 ball bearings used as rollers as shown in Fig. 2.7. The balls had a diameter of 12.5 mm and were guided by 125 mm by 125 mm by 8 mm thick plastic template that had a mesh of 72 subsquares. The distances between the support points were chosen to simulate as close as possible the continuous support conditions assumed in the analysis. 28 support points were used for the rectangular plates of series A, 22 support points were used for the rectangular specimens of series B, and 16 support points were used for the square plates as shown in Figs. 2.8 to 2.10.

No supports were provided under the plates at the corners since the plate corners tend to lift up from the supports once the lateral loads were applied. Each corner was held down by a frame consisting of a rocker-roller assembly as shown in Fig. 2.11. The adequacy of the corner lifting supports was checked by monitoring the deflection of the plate with respect to the reaction frame by means of dial gauges placed near the respective corner.

2.5.2 Lateral Loading System

The uniformly distributed lateral load was simulated by the application of eighteen concentrated loads to the rectangular specimens of series A, twelve concentrated loads to the rectangular specimens of series B, and nine concentrated loads to the square specimens at the locations shown in Figs. 2.8 to 2.10. The concentrated loads were applied by means of 120 kN capacity hydraulic jacks underneath the laboratory strong floor, pulling on 19 mm diameter threaded mild steel rods which passed through 38.1 mm diameter holes through the specimen. The load in the rods was transmitted by spherical nuts fitting into spherical depressions in 125 mm by 125 mm by 12.7 mm thick steel plates resting on the specimen. A thin plaster layer was provided between the plate and the specimen.

A manifold system was used to apply equal oil pressure to all the loading jacks plus an additional jack that reacted against a 120 kN load cell in a closed frame. The jack loads were measured in this way and checked by oil pressure measurements.

2.5.3 Inplane Loading System

The inplane loads were applied by independent loading units located 444 mm center to center. These are shown in Figs. 2.4 and 2.5. The loading units were supported by the test specimen as shown in Fig. 2.5 so that vertical deflection of the plate would not develop a vertical reaction in the horizontal loading system. As the edge of the

plate deflected up or down, the inplane loading frame also moved up or down.

Each loading unit consisted of 500 kN capacity hydraulic jack at one end of the specimen, reacting against a closed frame used to transfer the load to the opposite end of the specimen. The closed frame consisted of two vertical steel members at each end which were held in position by a steel beam passing on top of the specimen and 25.4 mm diameter high strength rod passing underneath the specimen. The inplane load was applied to the specimen by attaching the cylinders of the hydraulic jacks to high strength steel knife edges along one edge of the specimen as shown in Fig. 2.12. At the opposite edge of the specimen, another high strength knife edge was bolted to the vertical steel member of the closed frame to provide the reaction for the applied inplane load. At each loaded edge of the plate, the knife edges, 125 mm long, reacted against 380 mm long plates that had grooves to accommodate the knife edges and ensure concentric application of the inplane load as the edges of the specimens rotate due to the application of the lateral load. The 380 mm long plates were clamped to the edges of the specimen using top and bottom 190 mm long steel plates of 8 mm thickness as shown in Figs. 2.13 to 2.15. Discrete clamps spaced along the loaded edges were used instead of one clamp along the entire edge to allow the edge of the specimen to twist and accommodate the slab deflections. A detail of the knife edge assembly is shown in Fig. 2.12.

Four loading units were used to simulate uniform uniaxial inplane load for the square specimens and the rectangular specimens

loaded along the short sides. In specimen B4, loaded along the long sides, six loading units were used. For specimens C6 and C7, with biaxial inplane load, four loading units were used in each direction. The different arrangements of the inplane loading plates are shown in Figs. 2.13 through 2.15.

A manifold system was used which supplied equal oil pressure to all the jacks used to apply the inplane load and to an extra one of the same capacity that reacted against a 500 kN capacity load cell in a closed frame. The jack loads were measured in this way and checked by oil pressure measurements.

The average weights of the inplane loading units per meter of the loaded edge were 2.5 kN/m for rectangular specimens of series A, 1.6 kN/m for rectangular specimens of series B, and 1.5 kN/m for square specimens. These acted as downward line loads along the loaded edges.

2.6 Instrumentation

Instrumentation was arranged to provide information on both global and local responses of the test specimens. All instrumented readings were monitored and recorded using the FLUKE data acquisition system through which the signals were conditioned, converted from analog to digital form and stored on a disk.

2.6.1 Steel Strains

The strains in the reinforcing steel were measured using electrical resistance strain gauges. Forty-four electrical resistance Showa foil strain gauges, type N11-FA-5-120-11, with nominal resistance of 120 ohms and a gauge length of 5 mm, were placed on the top and bottom mats of each specimen. The gauges were then sealed from the wet concrete by means of an epoxy coating. All strain gauges were zeroed shortly before testing, hence strains due to shrinkage and those due to the self weight of the specimen were not recorded. Typical steel strain gauge layouts for specimens of series A, B, C, and D are shown in Figs. 2.16 through 2.19.

2.6.2 Average Curvatures

In series B, C, and D average curvatures were measured in the two orthogonal directions at the center of the plate. The basic tool for measuring the average curvature angle was an adaptation of the rotation meter used by Breen (1964) and others. The meter, shown in Fig. 2.20, consisted of two threaded steel rods, each attached to the plate by 12.5 mm coupling cast with the plate. Lock nuts were used for attachment, so that the exact location of contact could be controlled. LVDTs were mounted on the ends of the extending steel rods in order to measure the change in the horizontal distance between them. Average curvatures were calculated by summing the changes in the LVDTs readings on the two sides and dividing by the lateral distance between the LVDTs. On the assumption that a linear

strain distribution applies, the values can be further interpreted to give average strains for the inner and outer fibers of the cross section. The gauge length between rods was 180 mm.

2.6.3 Displacement Measurements

The following displacements were recorded during the course of a typical test:

- Out-of-plane surface deflections of the plate.
- Inplane deflections of one edge of the plate relative to the other in the x- and y-directions.
- Rotations of the plate edges along the center lines in the x- and y-directions.

The out-of-plane displacements were recorded electronically using linear variable displacement transducers (LVDTs) supported on a reference frame above the specimen. The inplane deflections in each direction were measured using LVDTs mounted directly on the specimen. The edge rotations were measured by LVDTs mounted to reference frames above the specimen as shown in Fig. 2.21.

The detailed locations of the out-of-plane deflection measurement stations, inplane deflections, and edge rotations for rectangular specimens of series A and series B and for the square specimens are shown in Figs. 2.22, 2.23, and 2.24, respectively.

2.7 Test Procedure

At the beginning of each plate test series, the test frame was first adjusted to accommodate the new plate dimensions. Prior to testing, each specimen was checked for alignment within the testing apparatus which allowed for minor adjustments. Inplane and transverse loading plates were then plastered in their positions to provide a complete contact with the specimen. All the instruments were positioned, and hooked up to the data acquisition system. The electrical instrumentation readings were initialized to zero using the testing software of the FLUKE system.

Specimens A1, B1, C1, and D1 were tested under lateral loads only. Load increments of 0.5 kN per jack were used until inelastic behaviour became noticeable, then smaller load increments or displacement increments were used depending on the behaviour of the specimen on that stage. As load was applied, loads, steel strains and the center deflection were monitored continuously on the data acquisition screen. When the required load or deflection was reached at any test increment, the hydraulic system was closed to maintain the load (as closely as relaxation would allow) while a set of readings were taken.

The loading process for other specimens was complicated by the fact that two different loadings had to be applied to the test specimens.

For specimens in which the inplane load was applied first, the inplane load was applied in regular increments up to a predetermined value and maintained constant as the lateral load was applied monotonically and incrementally from zero to a maximum value and then allowed to drop off steadily beyond the maximum value. At the completion of each lateral load increment, the inplane load was re-checked and adjusted if necessary. Usually, lateral load increments of about 0.5 kN per jack were used until noticeable inelastic behaviour was observed. Smaller load increments were then applied. Depending on the behaviour of the specimen, the loading rate was adjusted beyond the peak to avoid, as possible, sudden failure.

Specimen C3 was tested with the inplane and lateral loads applied simultaneously from zero until peak loads were reached. Thereafter, the lateral load was allowed to drop off while keeping the inplane load constant until failure.

In specimen C8, the lateral load was first applied incrementally while monitoring the steel strains on the FLUKE system. When the steel strain at the center of the plate reached about 0.0019, the valve supplying oil to the hydraulic jacks, used to apply the lateral loads, was closed eliminating any movement of the ram and leaving any previously applied lateral load subject to the behaviour of the specimen. The inplane load was then incrementally applied to a predetermined value. This loading path was chosen to represent the case in which a service lateral load acted prior to the application of

the inplane load. During the application of the inplane load, it was noticed that the specimen started to deflect upwards, rather than continuing to deflect downwards, and hence pressed against the lateral load jacks causing the lateral load to increase. No attempt was made to adjust the lateral load during the application of the inplane load. The inplane load was then held constant and the lateral load was increased until reaching its maximum value. Finally, the lateral load was allowed to drop while keeping the inplane load constant until failure.

In specimen C9, the lateral load was applied incrementally up to a predetermined value and maintained at constant value after which the inplane load was applied from zero until failure. Due to the large deflection the plate experienced before applying the inplane load, the lateral load had to be adjusted frequently to its predetermined value during the application of the inplane load.

The overall behaviour of each specimen was also monitored during the course of each test by plotting the lateral load versus central deflection. In all tests, the loading system was initially controlled by load increments but near the maximum load, the further loading was controlled by imposing deflection increments. Most of the tests took approximately about three hours to complete.

Table 2.1 Side Dimensions and Average Measured Thickness of Specimens

Specimen Designation	a (mm)	b (mm)	h (mm)
A1	4267	1829	67.3
A2	4267	1829	64.7
A3	4267	1829	65.3
A4	4267	1829	65.3
B1	2745	1829	68.2
B2	2745	1829	66.8
B3	2745	1829	66.7
B4	2745	1829	65.3
C1	1829	1829	67.8
C2	1829	1829	67.6
C3	1829	1829	68.5
C4	1829	1829	70.0
C5	1829	1829	70.1
C6	1829	1829	67.4
C7	1829	1829	66.5
C8	1829	1829	67.8
C9	1829	1829	66.9
D1	1829	1829	92.8
D2	1829	1829	92.7

Table 2.2 Area of Reinforcement in X- and Y-Directions

Specimen Designation	X- Direction*		Y- Direction*	
	Area of Top Rebar mm ² /m	Area of Bottom Rebar mm ² /m	Area of Top Rebar mm ² /m	Area of Bottom Rebar mm ² /m
A1	260.0	260.0	260.0	260.0
A2	260.0	260.0	260.0	260.0
A3	260.0	260.0	520.0	520.0
A4	520.0	520.0	260.0	260.0
B1	260.0	260.0	260.0	260.0
B2	260.0	260.0	260.0	260.0
B3	260.0	260.0	260.0	260.0
B4	260.0	260.0	260.0	260.0
C1	260.0	260.0	260.0	260.0
C2	260.0	260.0	260.0	260.0
C3	260.0	260.0	260.0	260.0
C4	260.0	260.0	520.0	520.0
C5	520.0	520.0	260.0	260.0
C6	260.0	260.0	260.0	260.0
C7	260.0	260.0	260.0	260.0
C8	260.0	260.0	260.0	260.0
C9	260.0	260.0	260.0	260.0
D1	364.0	364.0	364.0	364.0
D2	364.0	364.0	364.0	364.0

* X- and Y-directions are consistent with those in Figures 2.8 through 2.10.

Table 2.3 Average Locations of Top and Bottom Reinforcement from Compressive Face

Specimen Designation	X- Direction*		Y- Direction*	
	d_x mm	d'_x mm	d_y mm	d'_y mm
A1	54.5	22.2	48.2	15.9
A2	52.6	20.2	46.3	14.2
A3	52.7	20.6	46.4	14.3
A4	52.5	20.4	46.2	14.5
B1	55.0	22.3	48.7	16.0
B2	53.5	20.5	47.2	14.2
B3	53.3	20.2	47.0	13.9
B4	50.3	19.70	44.0	13.4
C1	56.8	21.9	50.5	15.6
C2	57.6	19.7	51.3	13.4
C3	57.6	19.9	51.3	13.6
C4	58.5	20.9	52.2	14.6
C5	52.5	14.4	58.8	20.7
C6	56.1	18.1	49.8	11.8
C7	55.3	17.9	49.0	11.6
C8	56.6	19.1	50.3	12.8
C9	56.3	17.8	50.0	11.5
D1	82.7	20.4	76.4	14.1
D2	82.6	18.9	76.3	12.6

* X- and Y-directions are consistent with those in Figures 2.8 through 2.10.

Table 2.4 Concrete Properties

Specimen Designation	Age (Days)	f'_c (MPa)	E_c (MPa)	f_{sp} (MPa)	f_r (MPa)
A1	52	22.26	21085	1.95	3.62
A2	70	22.66	21215	2.18	3.74
A3	80	22.87	21285	2.31	3.81
A4	86	23.00	21330	2.39	3.85
B1	32	18.70	20590	1.78	2.68
B2	65	19.27	20805	1.84	2.87
B3	80	19.53	20900	1.86	2.96
B4	154	20.82	21385	1.98	3.41
C1	29	25.21	21300	2.31	3.46
C2	34	25.27	21400	2.32	3.52
C3	37	25.30	21460	2.33	3.55
C4	42	25.35	21560	2.34	3.61
C5*	24	25.81	21800	2.55	2.96
C6	50	25.44	21720	2.35	3.71
C7	61	25.56	21940	2.36	3.85
C8	83	25.80	22380	2.40	4.11
C9*	39	24.94	19200	2.70	2.85
D1	32	26.12	20800	2.65	3.26
D2	36	26.12	20800	2.65	3.26

* Concrete for these two specimens was produced in the Laboratory.

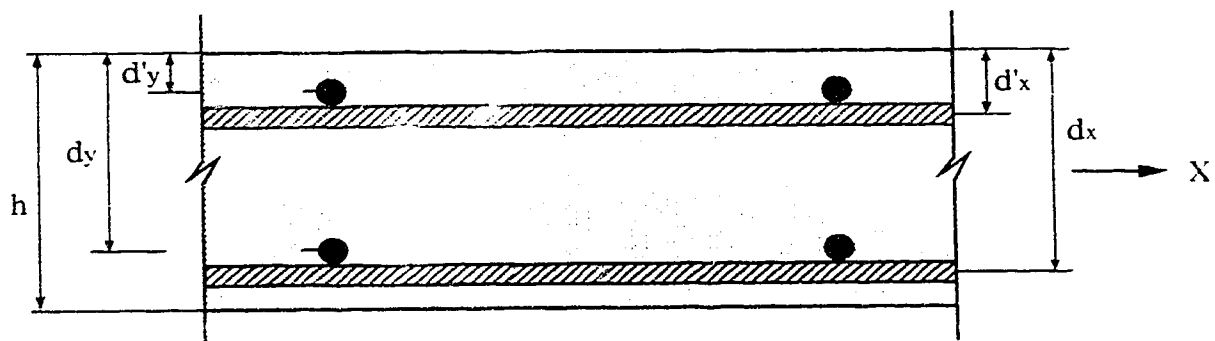


Figure 2.1 General Reinforcing Layout for a Typical Plate Section

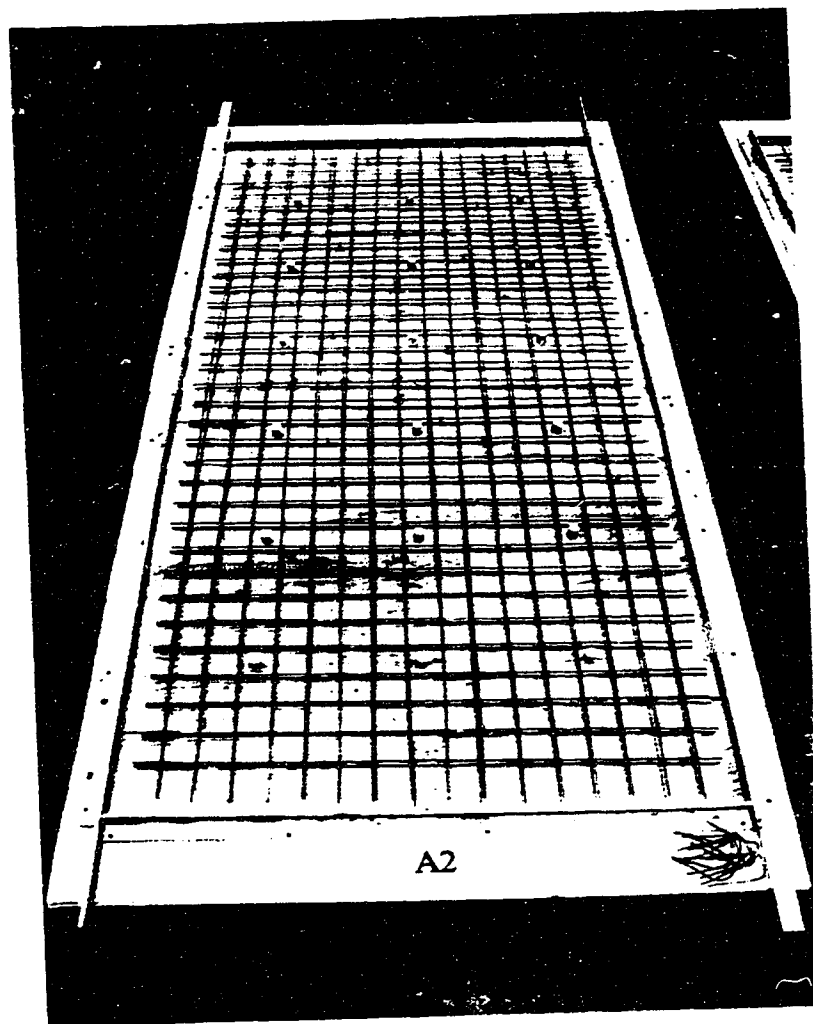


Figure 2.2 Reinforcement Cage for a Specimen Ready for Casting

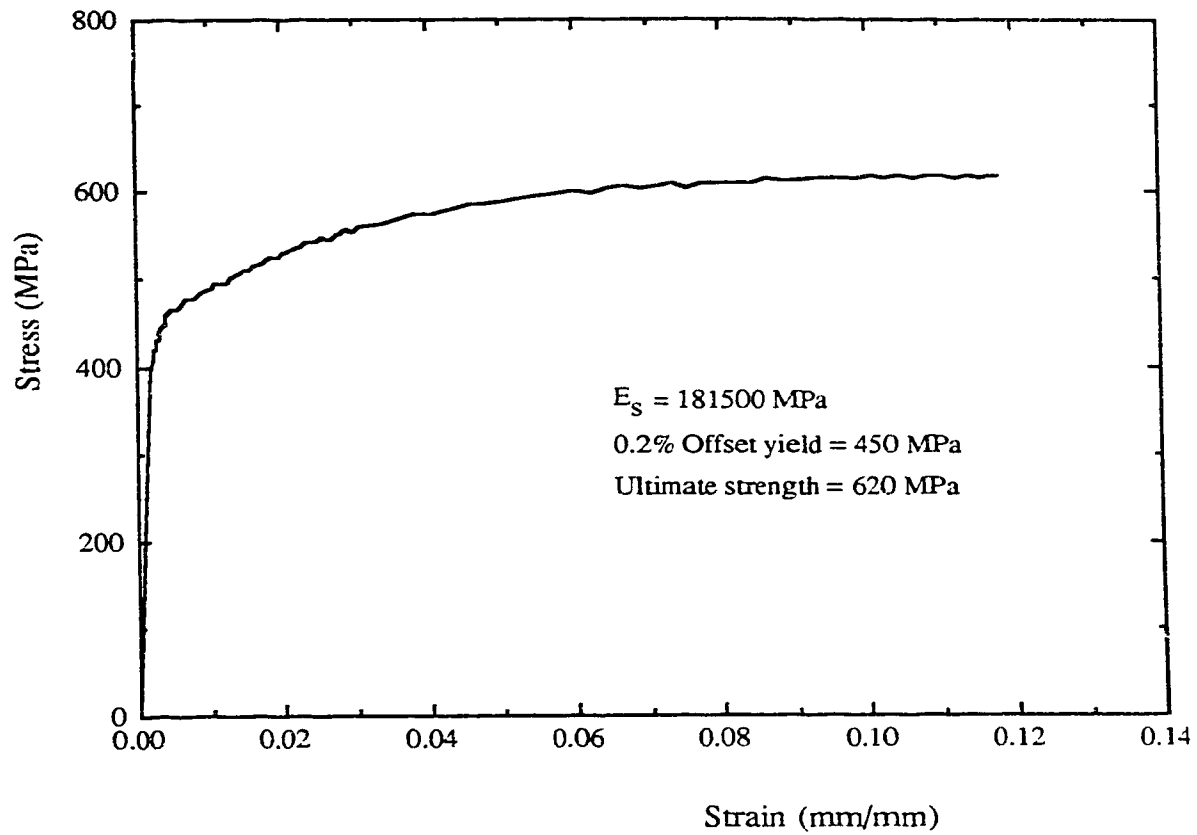


Figure 2.3 Typical Stress-Strain Curve for Reinforcing Steel

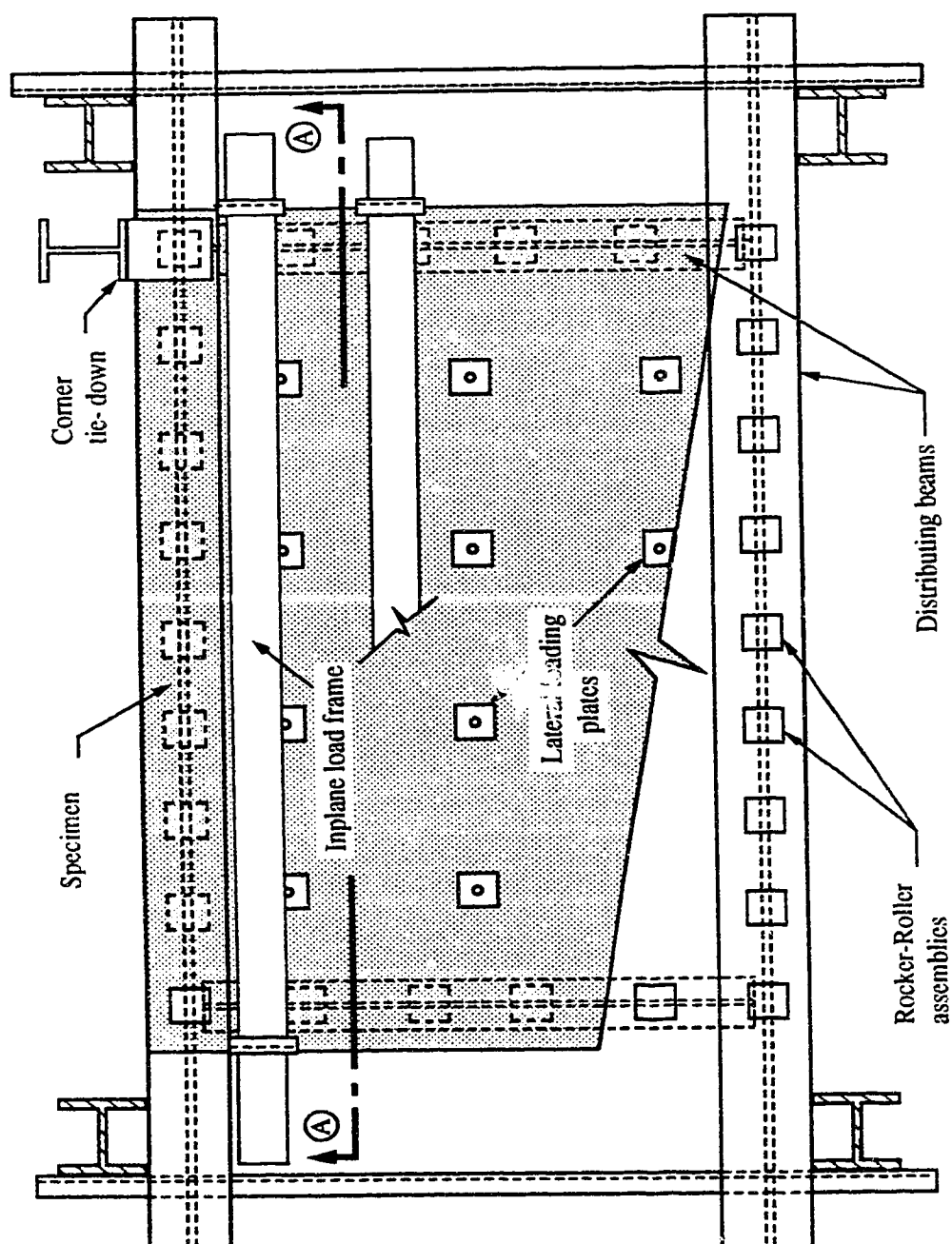


Figure 2.4 Schematic Plan of the Test Frame

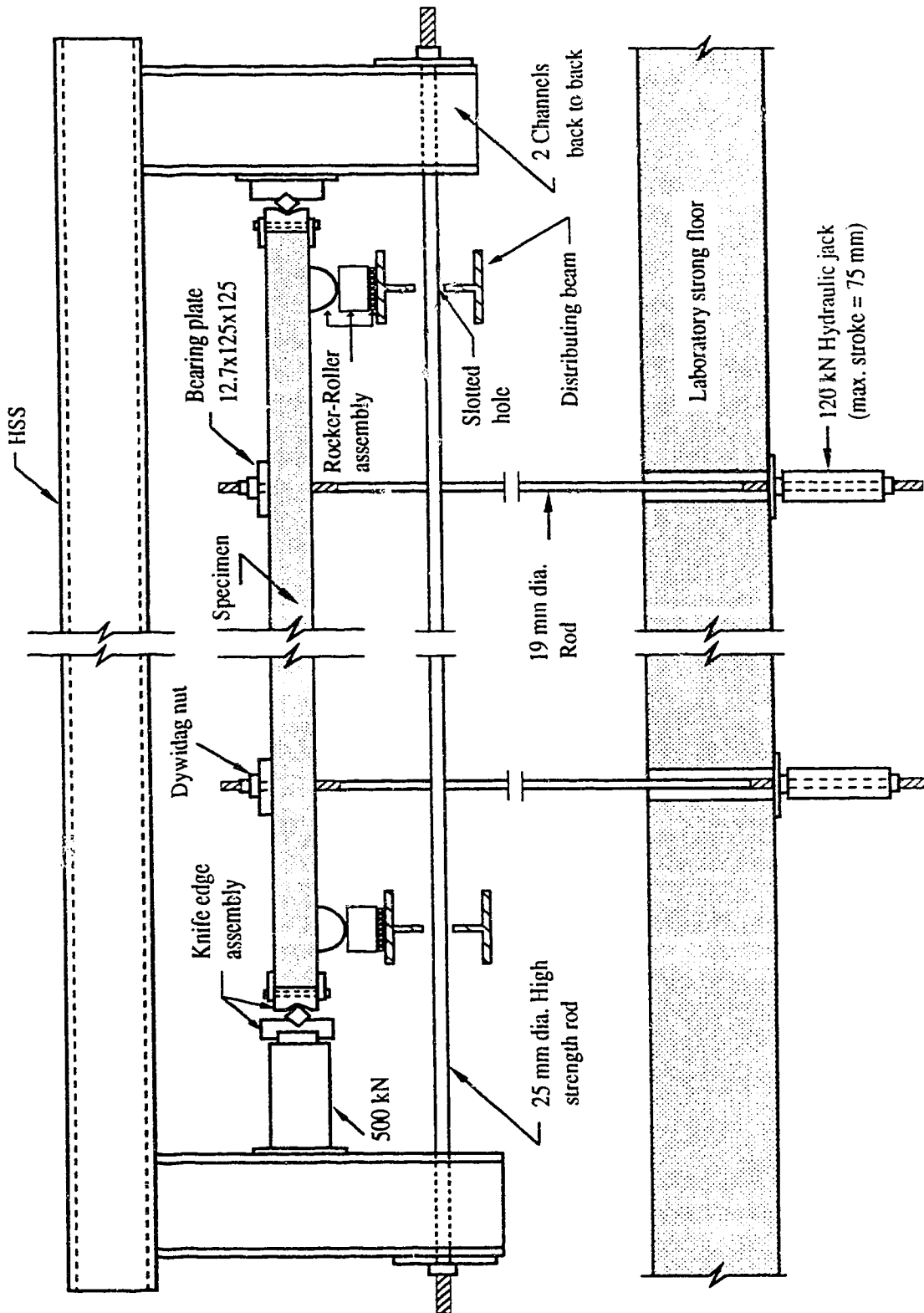
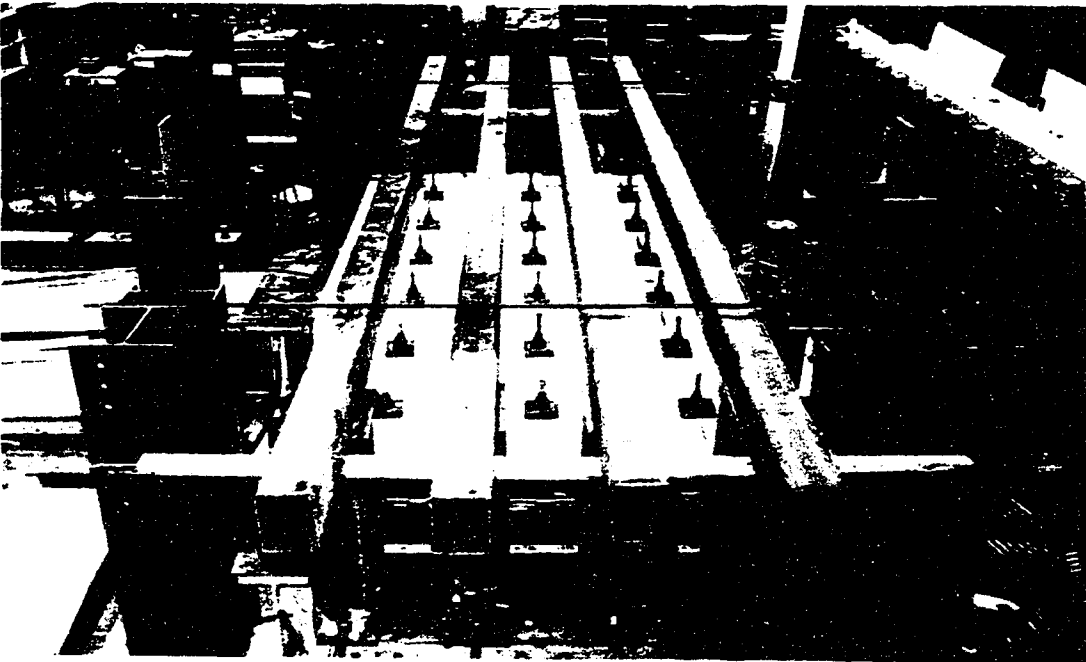


Figure 2.5 Section A-A Through the Test Frame (See Figure 2.4)



a- Typical Test Set-Up for Specimens Tested under Lateral Loads Only



b- Typical Test Set-Up for Specimens Tested under Combined Uniaxial Inplane and Lateral Loads

Figure 2.6 Loading Frame and Test Set-Up

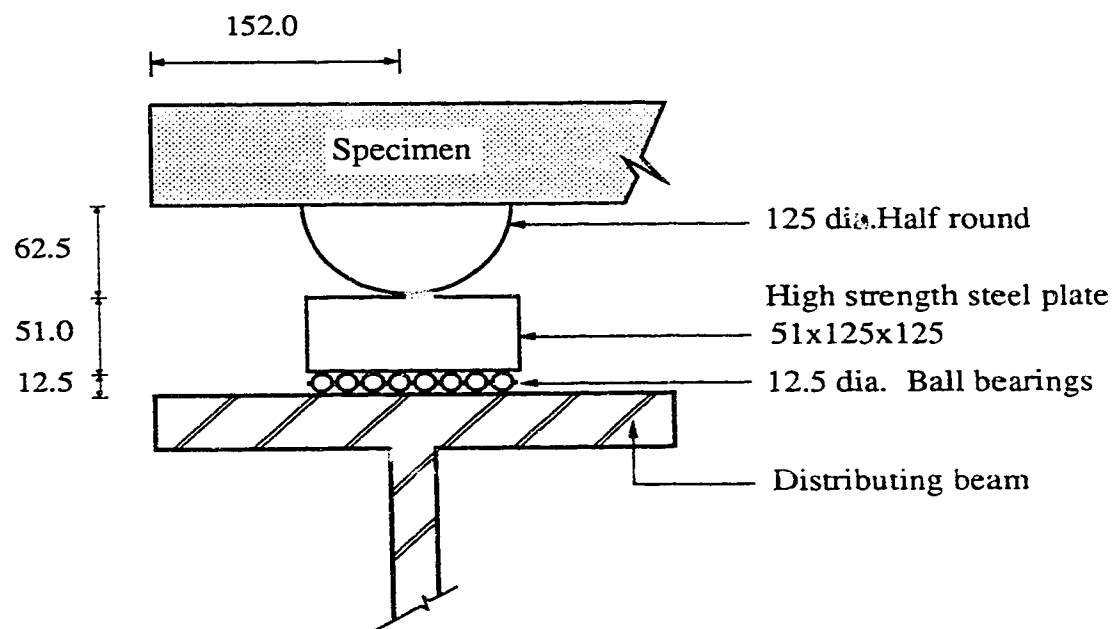


Figure 2.7 Schematic of the Rocker-Roller Assembly

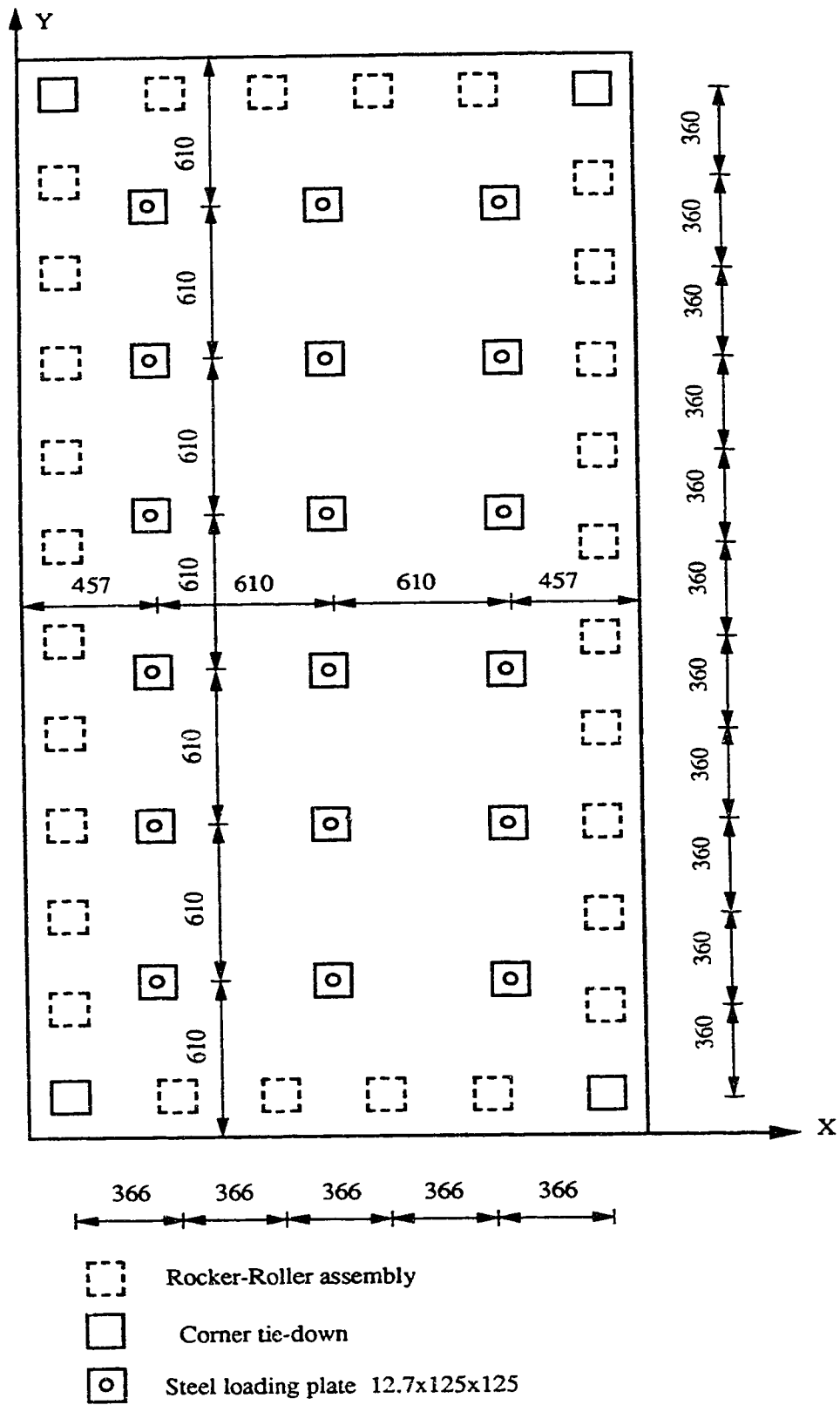


Figure 2.8 Locations of the Lateral Load and Support Points for Series A

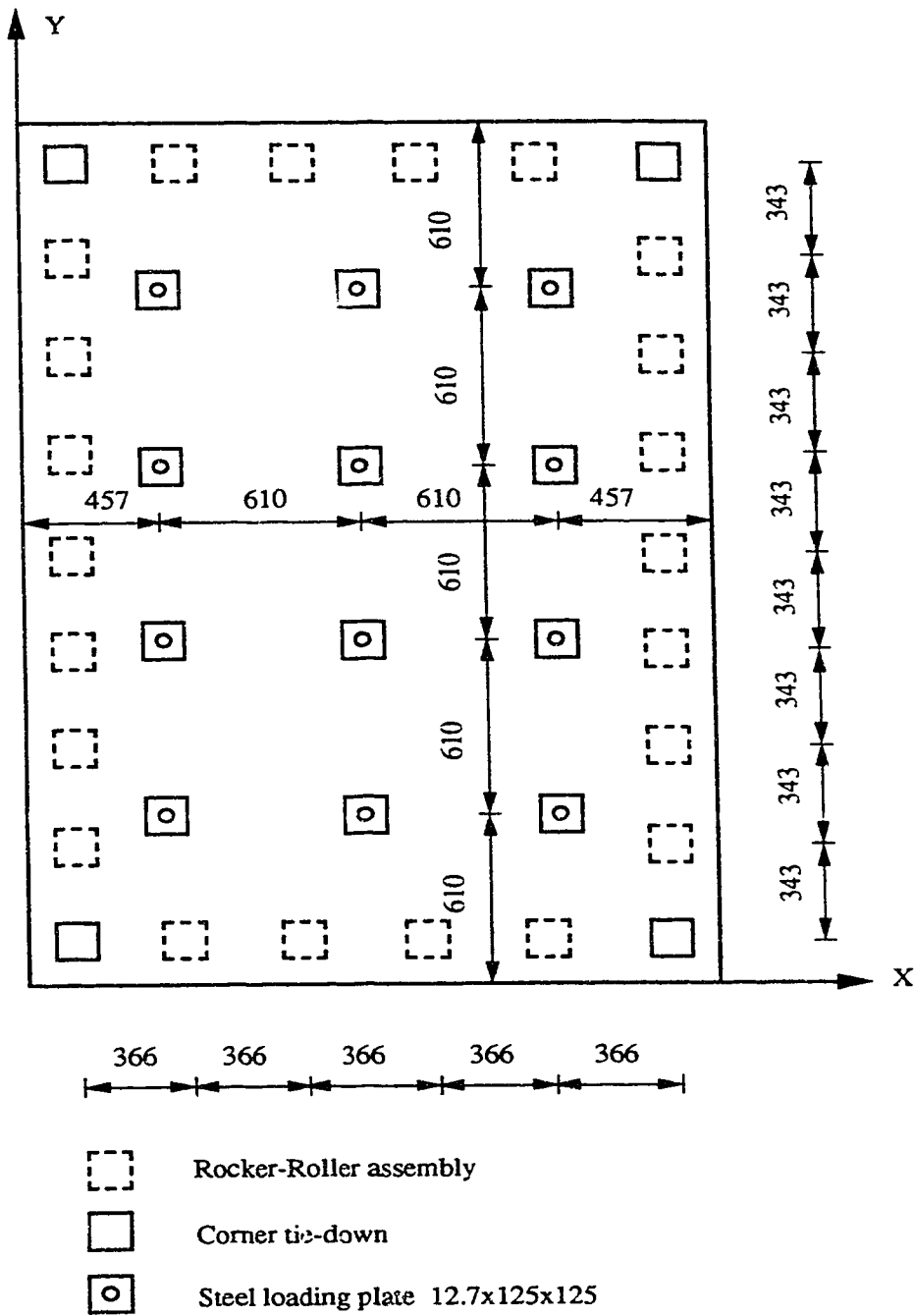


Figure 2.9 Locations of the Lateral Load and Support Points for Series B

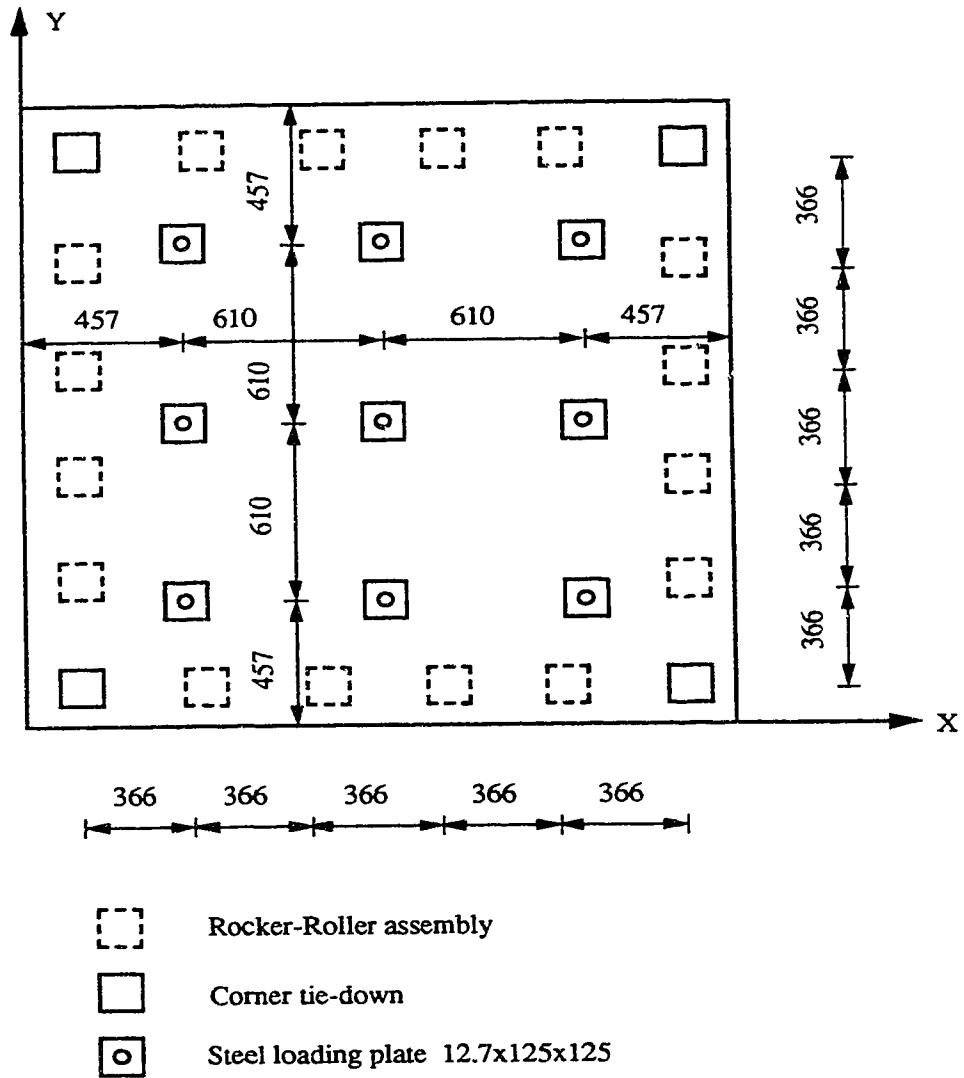


Figure 2.10 Locations of the Lateral Load and Support Points for the Square Specimens

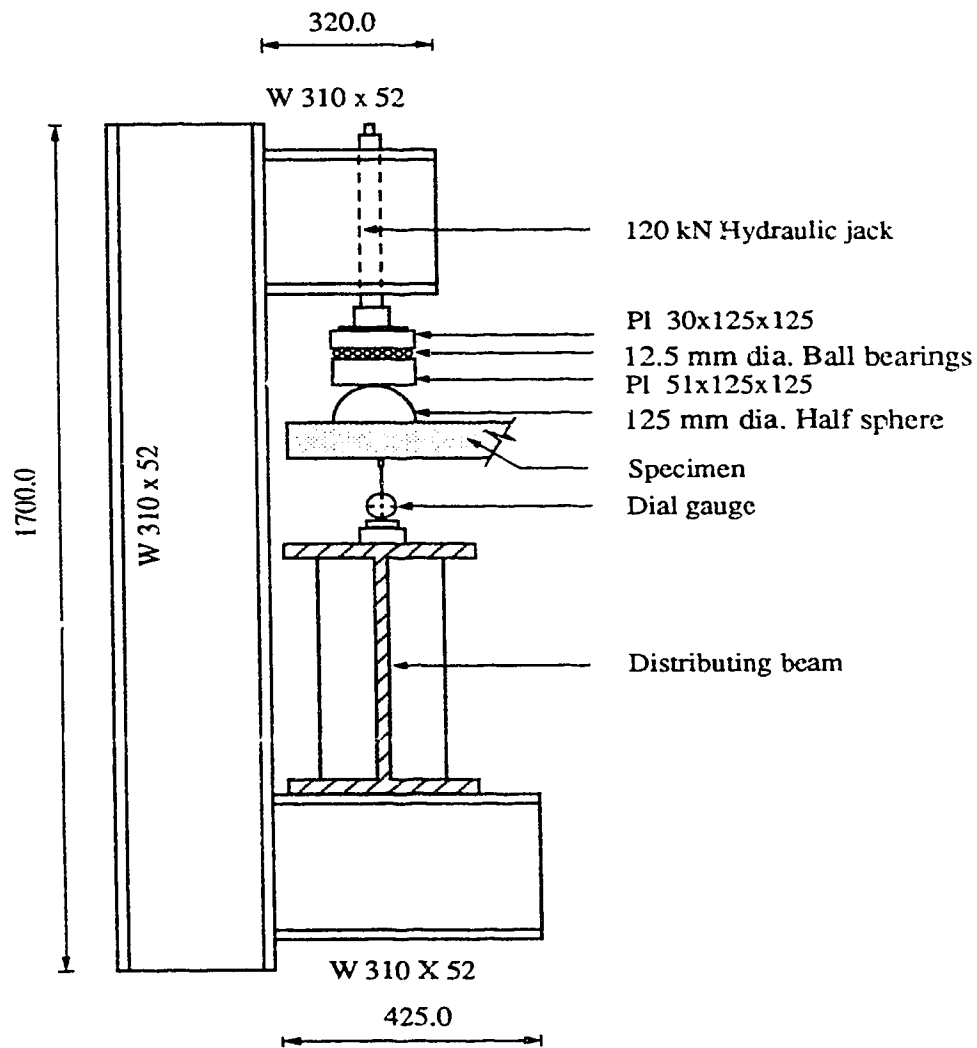


Figure 2.11 Schematic of a Corner Support Frame

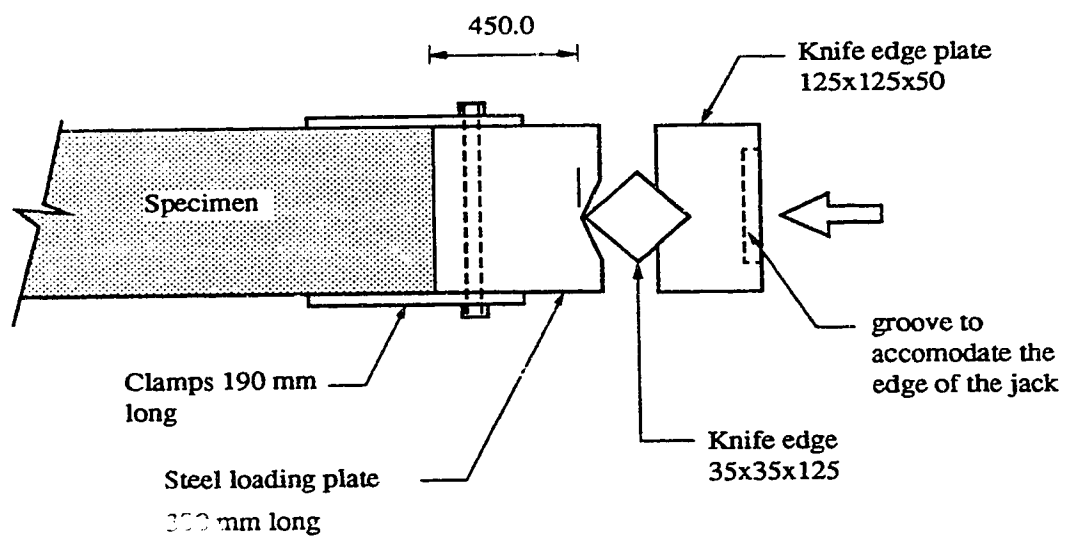


Figure 2.12 Knife Edge Assembly

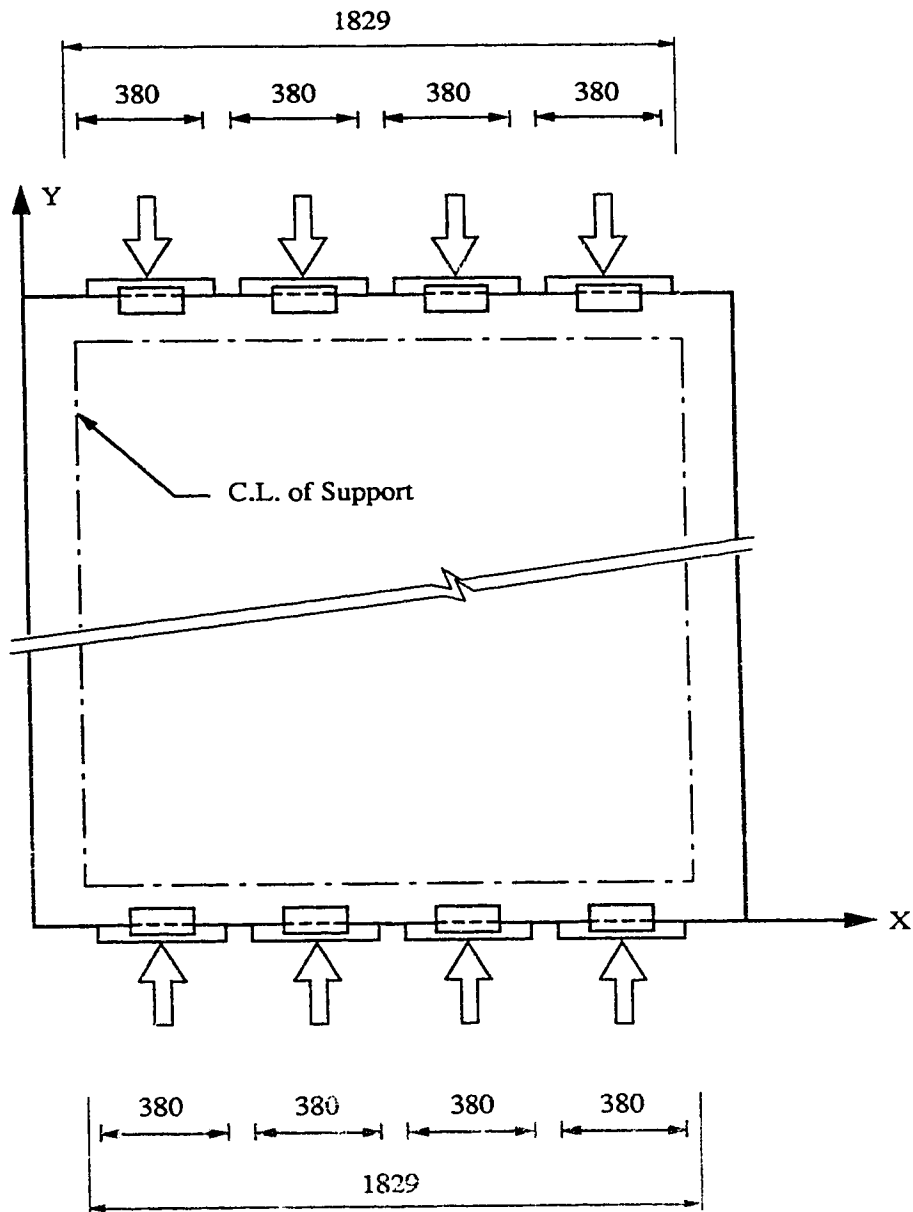


Figure 2.13 Arrangement of the Inplane Loading Plates for Specimens Loaded along the Short Sides

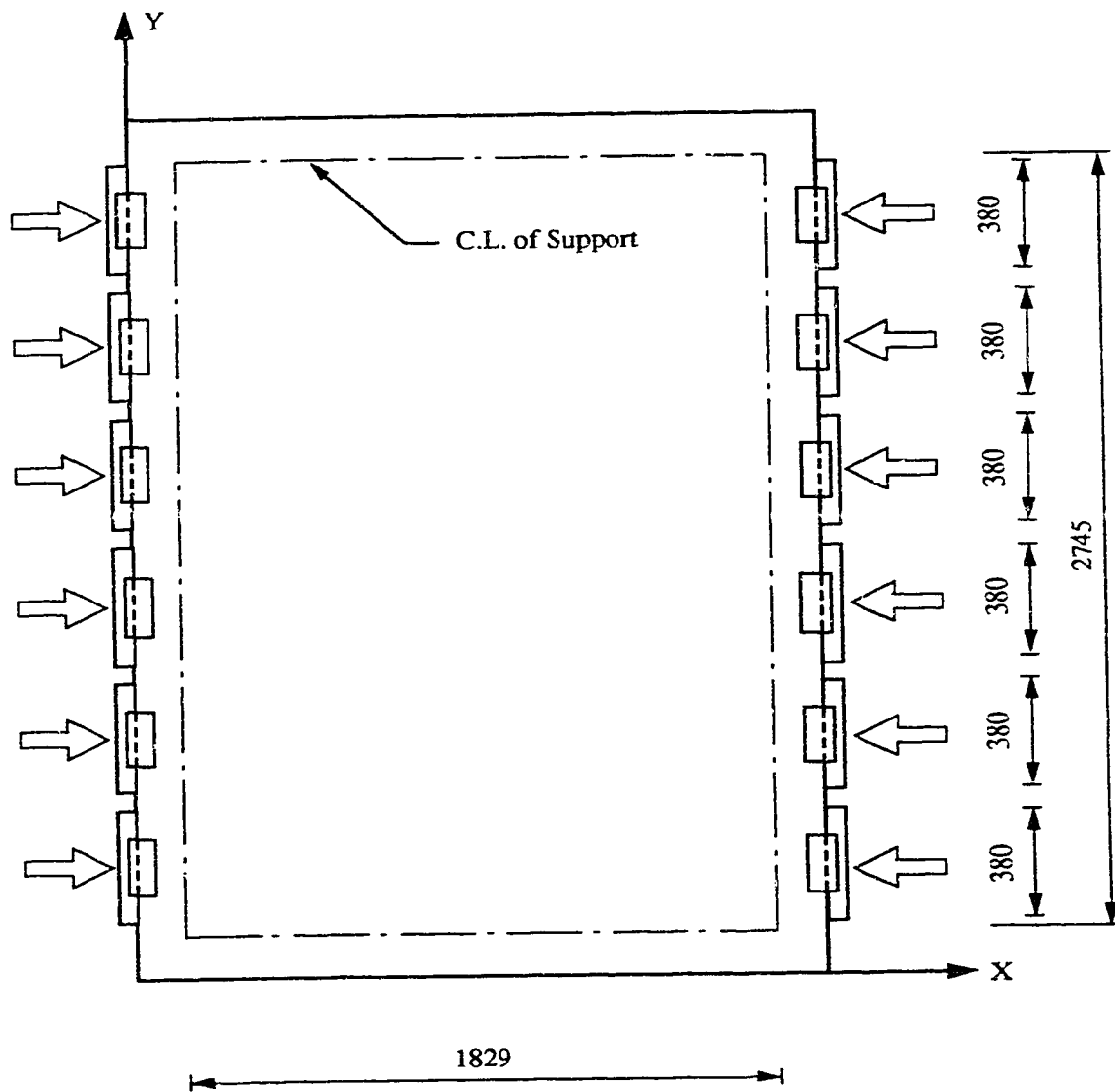


Figure 2.14 Arrangement of the Inplane Loading Plates for Specimen B4

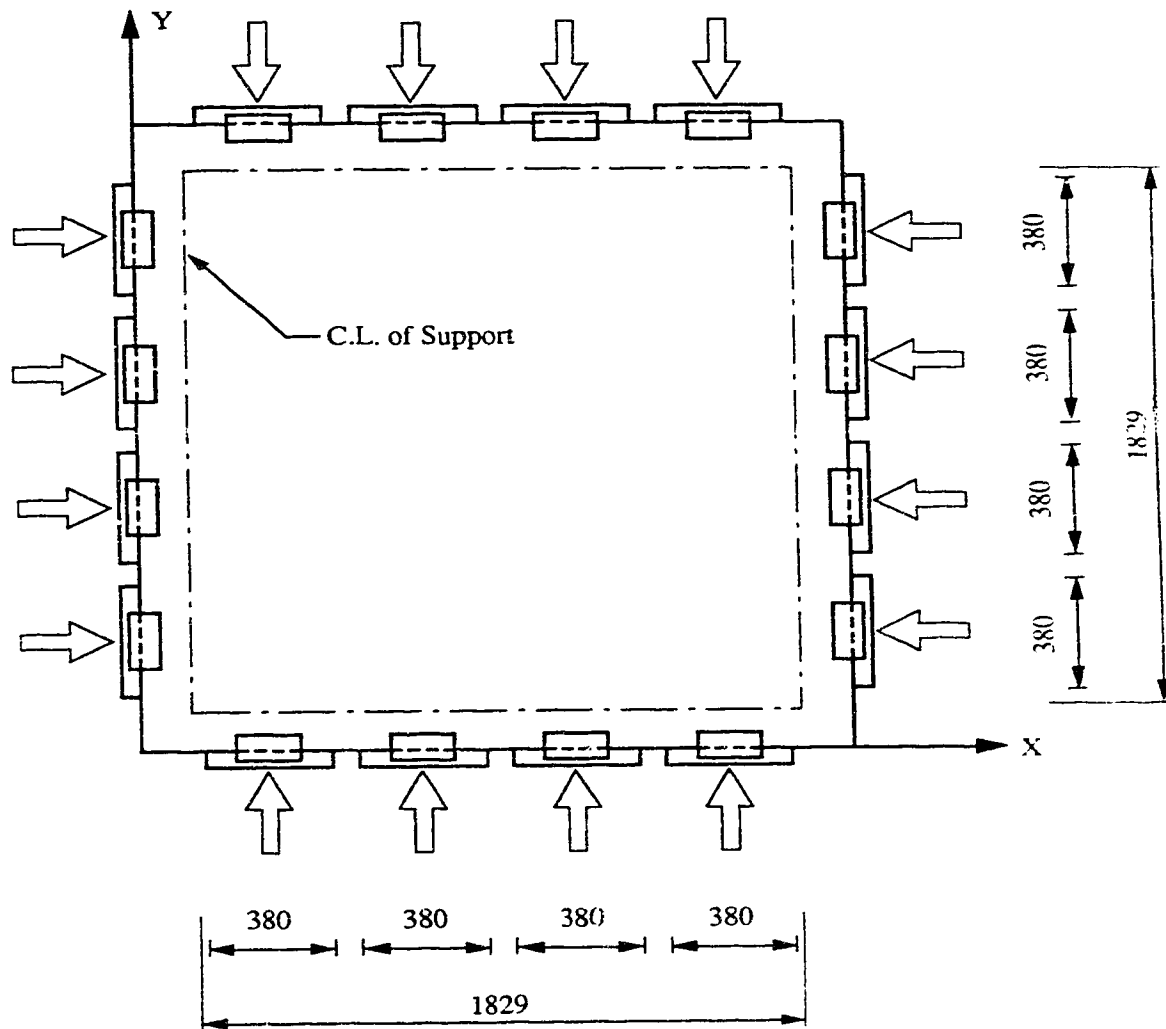


Figure 2.15 Arrangement of the Inplane Loading Plates for the Biaxially Loaded Square Specimens

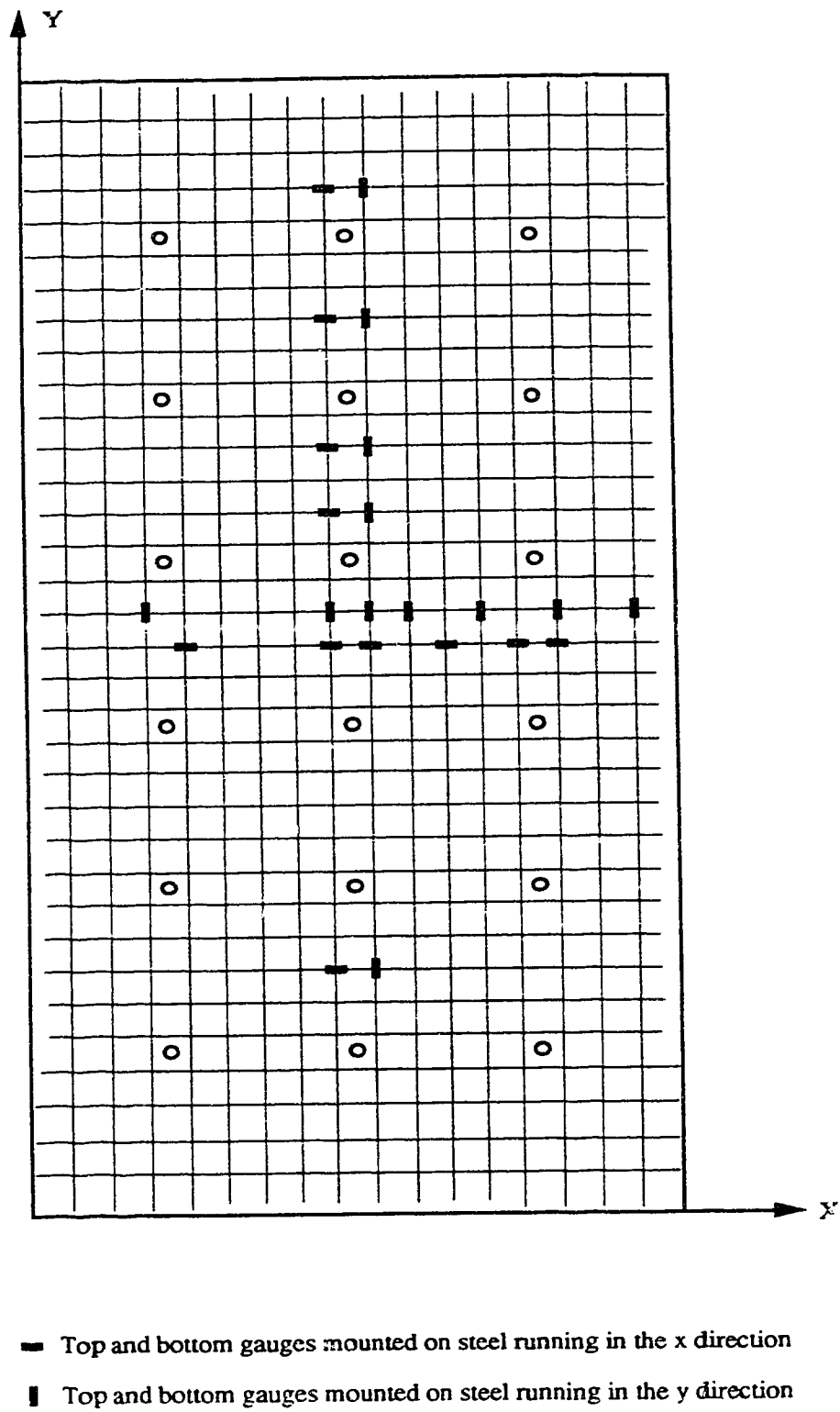


Figure 2.16 Typical Strain Gauge Layout for series A

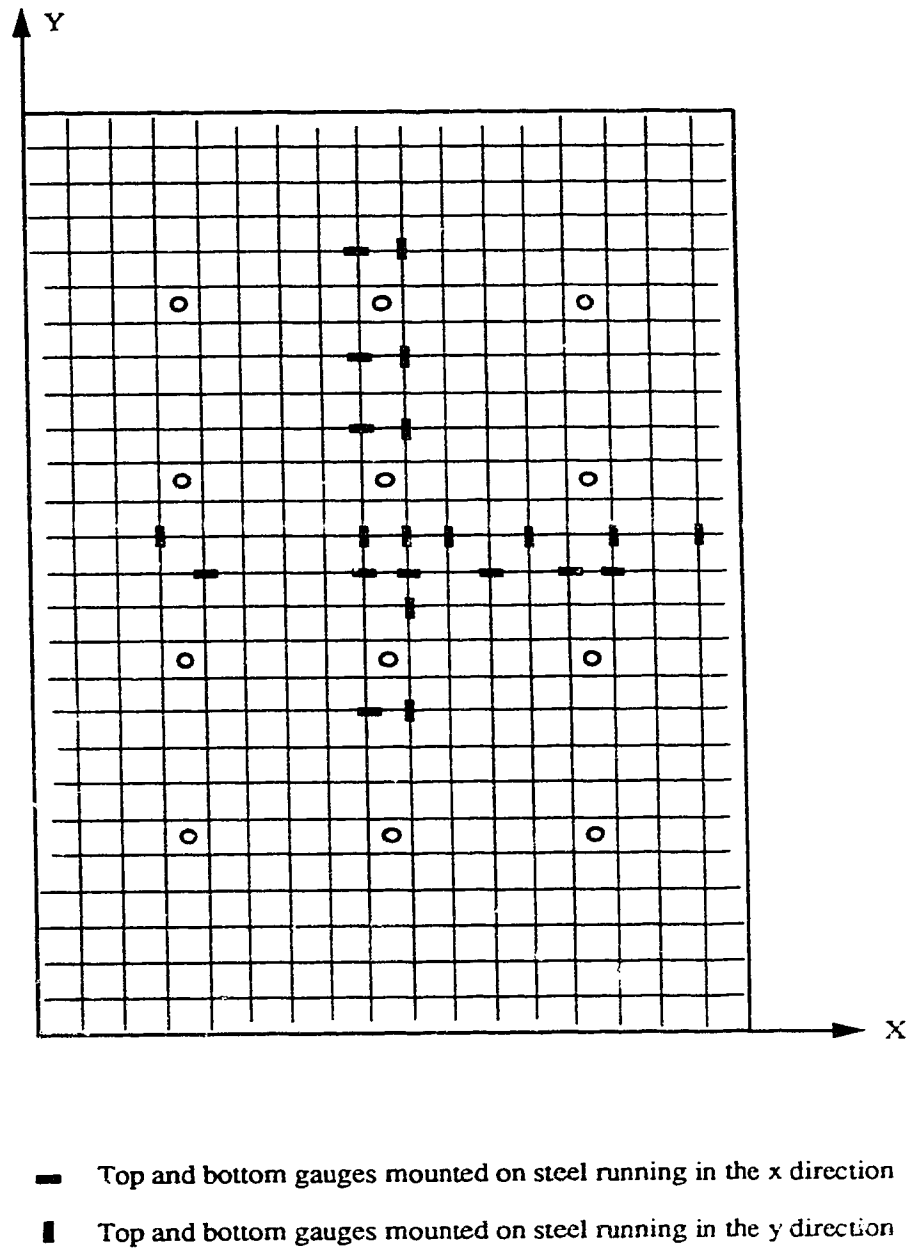


Figure 2.17 Typical Strain Gauge Layout for Series B

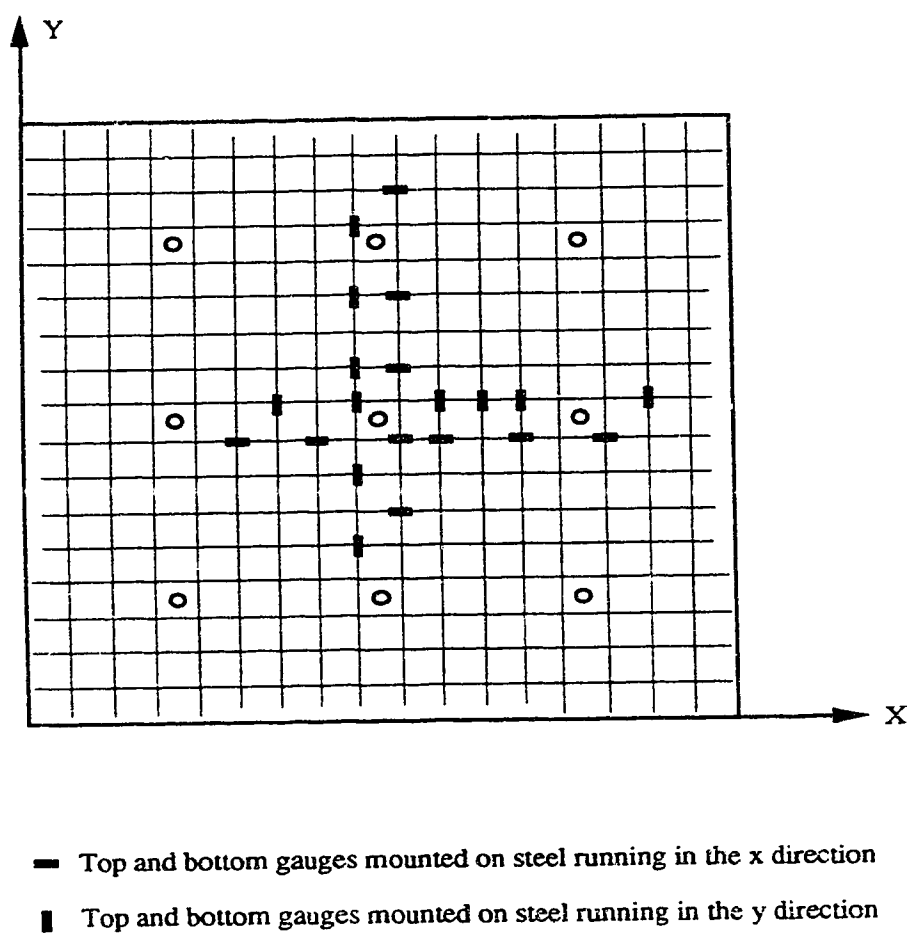


Figure 2.18 Typical Strain Gauge Layout for Series C

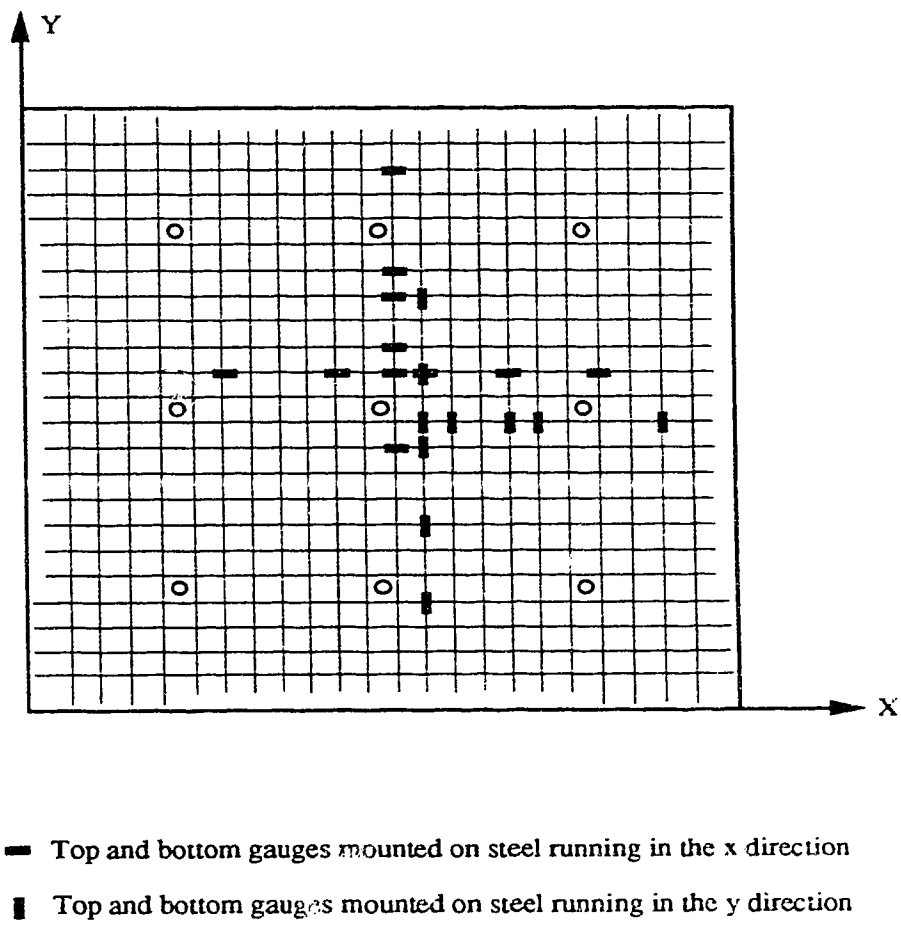


Figure 2.19 Typical Strain Gauge Layout for Series D

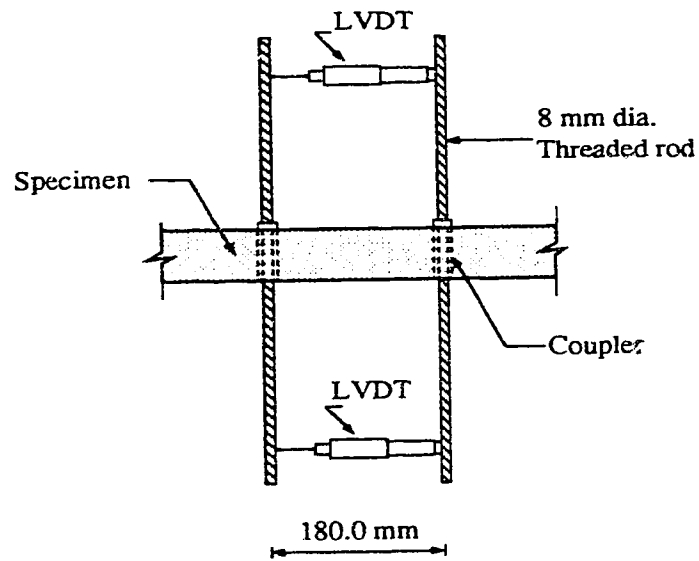


Figure 2.20 Curvature Meter

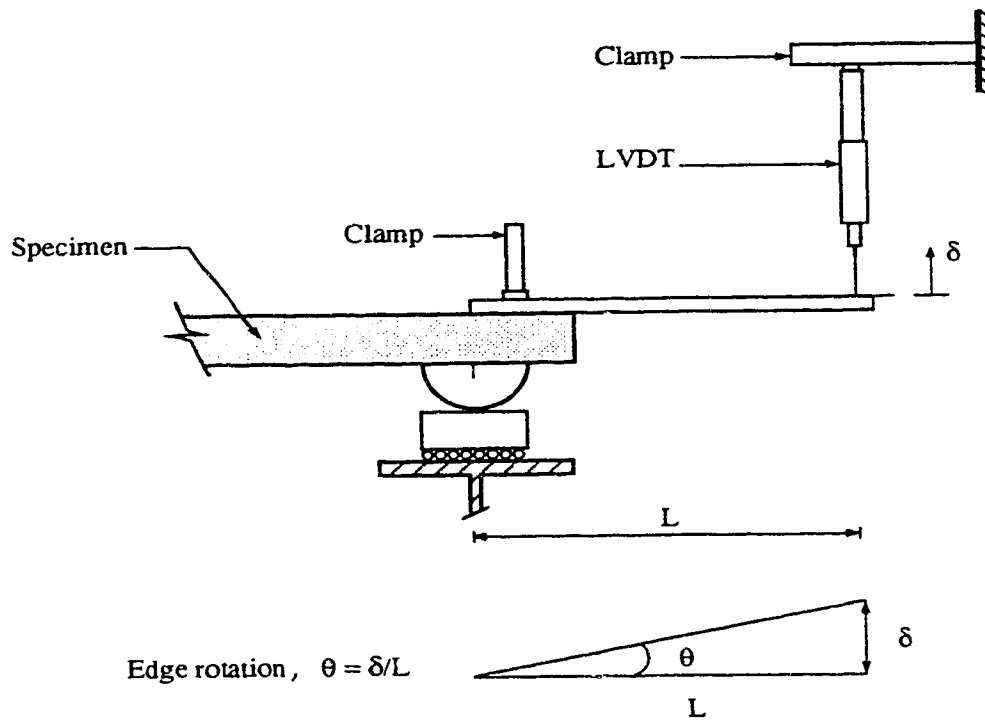


Figure 2.21 The Edge Rotation Measuring Device

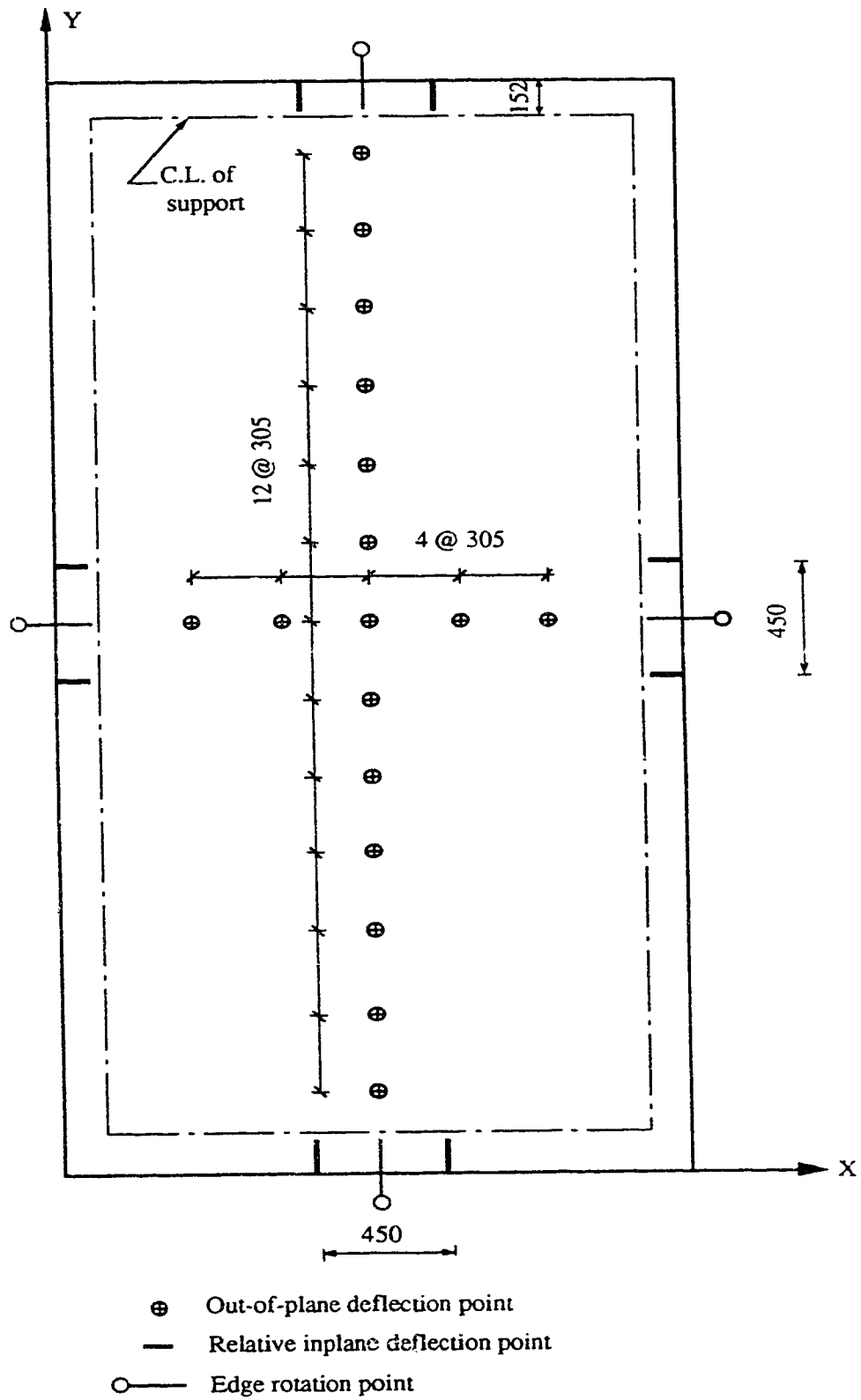


Figure 2.22 Locations of the Displacement Measurements for Series A

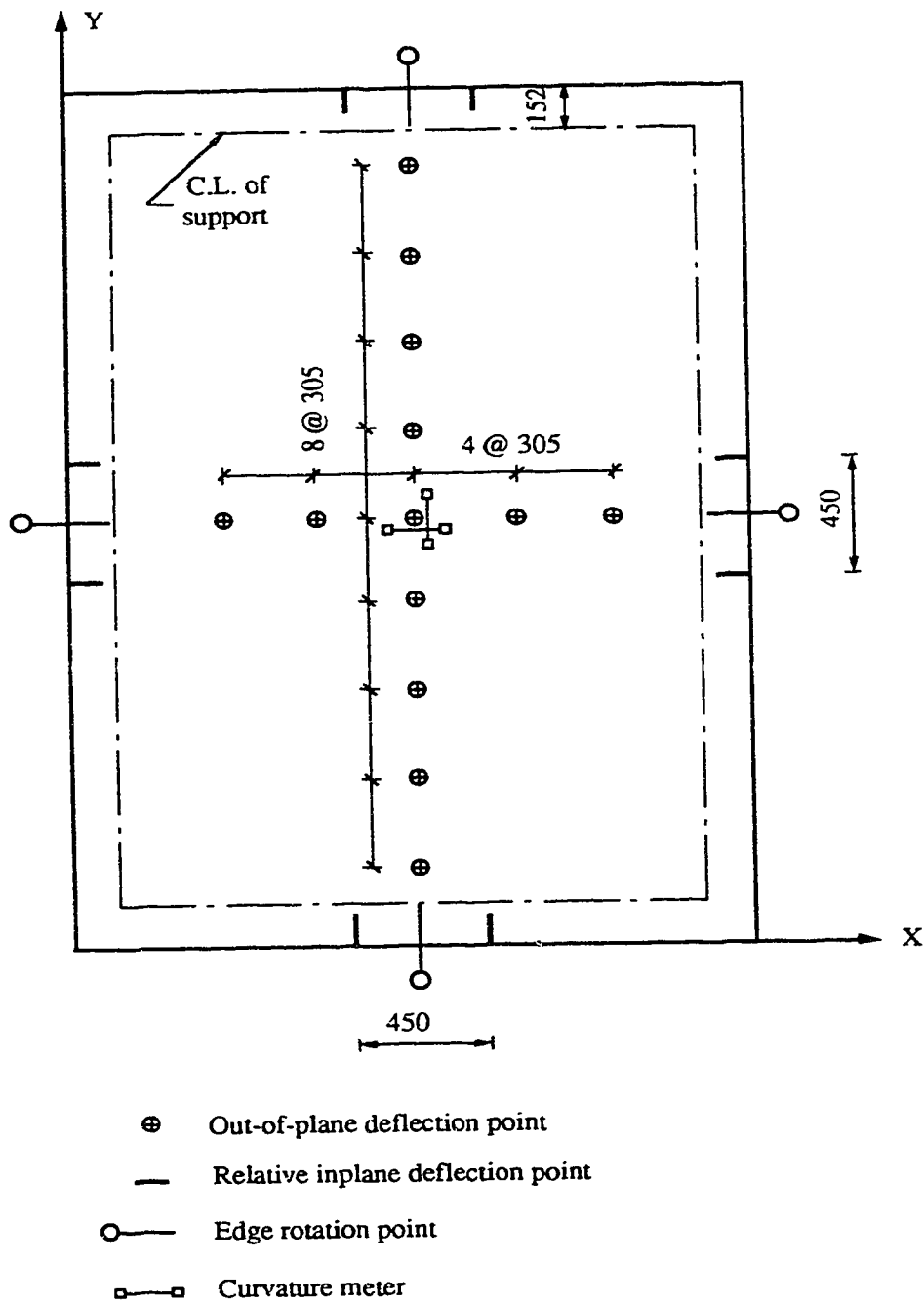


Figure 2.23 Locations of the Displacement Measurements and Curvature Meters for Series B

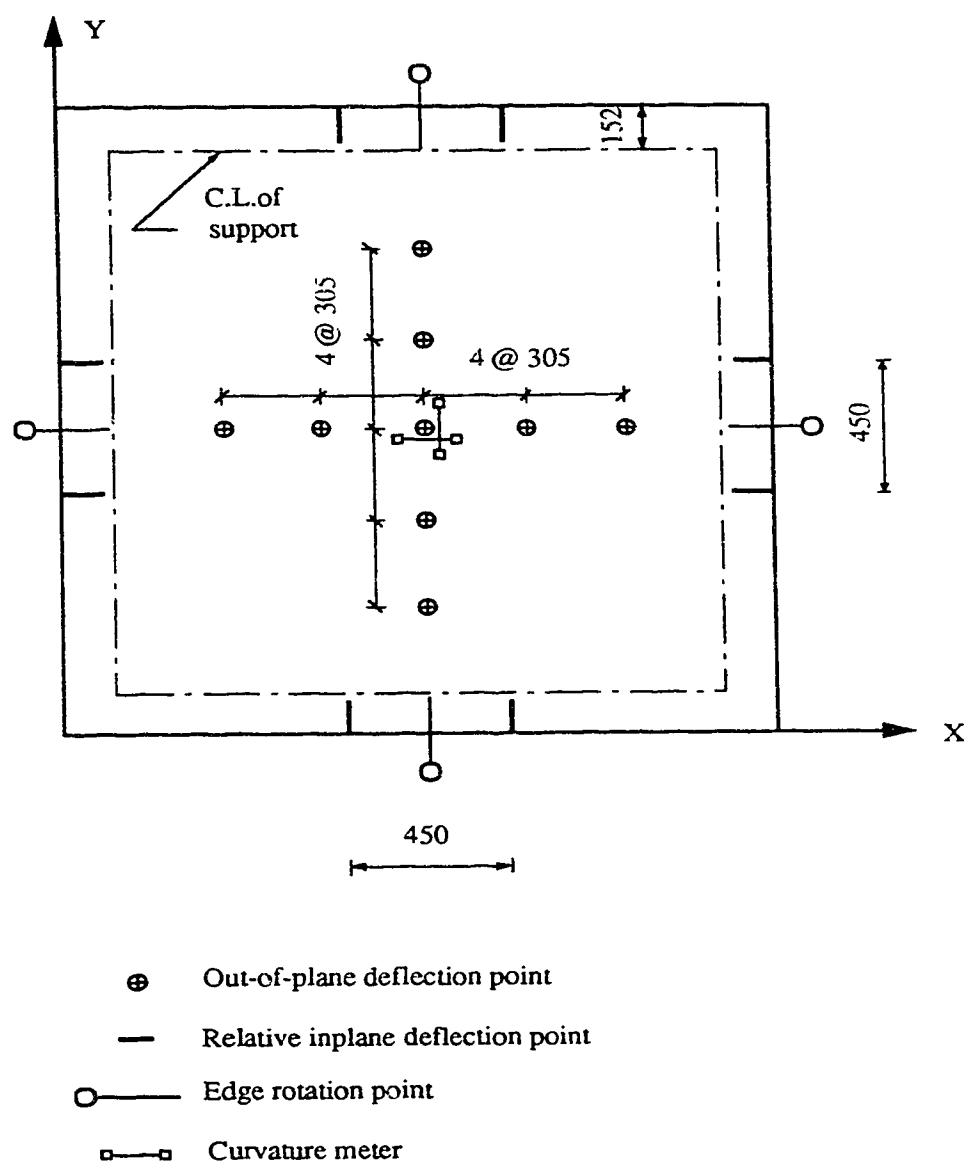


Figure 2.24 Locations of the Displacement Measurements and Curvature Meters for Square Specimens

3. Test Results

3.1 Introduction

This chapter presents the test results and the observed behaviour for all of the specimens. The test conditions included different aspect ratios, presence or absence of inplane compressive forces which were to be applied uniaxially or biaxially, different reinforcement ratios in the orthogonal directions, and different loading sequences. Topics to be covered in this chapter include ultimate loads, crack patterns and apparent failure modes, load-deflection characteristics, deflected shapes, and the distribution of steel strains and the average curvature. Evaluation of test results and observed behaviour is presented in Chapter 4.

3.2 Ultimate Loads

The measured ultimate loads at failure (peak values) and the corresponding deflections at the center of the plate are given in Table 3.1. The lateral load is given as pressure in kPa computed as the sum of the jack loads divided by the area of the plate within the center-lines of the supports. The inplane load is given as a line load in kN/m computed as the sum of the horizontal jack loads divided by the plate width along which the inplane load was applied, i.e. the plate width between support lines. Specimens A1, B1, C1, and D1 were tested under lateral load only.

3.3 Crack Patterns and Modes of Failure

Specimens of series B developed minor shrinkage cracking over partial widths of the underside as well as on the top surface of the plate prior to testing. These cracks did not have a preferred direction and were visible to the naked eye. In all other specimens, the first cracks to be observed were associated with flexural stresses. The cracking patterns developed in specimens of series A, which had an aspect ratio of 2.17, indicated that the plate strips in the middle region were essentially behaving in a one-way manner. The other specimens developed crack patterns which reflected the reinforcing pattern and indicated two-way action. At the ultimate loads, the crack patterns for plates tested under combined loads approached that of a similar plate under lateral loads only. The final failure of most of the specimens tested under combined loads was violent and abrupt.

3.3.1 Specimens Tested under Lateral Loads Only

In specimen A1, cracks were first observed in the long direction at a lateral load of 5.2 kPa, with each crack following the path of a reinforcing bar. Cracks were first observed in specimen B1 at a load of 1.65 kPa. This relatively small value is attributed to the low tensile strength of concrete of series B (see Table 2.4) and to the tensile stresses that were developed before testing due to restrained shrinkage. In specimens C1 and D1, orthogonal patterns of cracks,

coinciding with the reinforcement layout, were first noticed on the tension face at lateral loads of 9.1 kPa and 26.4 kPa, respectively.

In all the above specimens, as loads increased, cracks developed into yield-line hinge fields or bands of cracking extending towards each of the corners. In addition, cracks developed perpendicular to the diagonals on the top surface of the corners of the plate. These cracks resulted from the holding down of the plate corners permitting the development of anticlastic corner surfaces. The twisting moments near the corners caused torsional cracks on the edges of the plate near the corners. At Johansen's predicted yield-line loads, all plates had clear signs of fully developed yield patterns, but in no case was there any sign of imminent collapse. Indeed all plates continued to take further increments of load. The effect of the additional load was to increase the width of existing cracks rather than to cause the formation of new cracks.

When the central deflections exceeded approximately 1.2 times the thickness of the plate, the tensile cracking at the central region extended to the top surface of the plate and crushing of concrete started along the top diagonals. Although the stiffness of the plates became very low, there was often no fall-off in load carrying capacity and tests were sometimes terminated because of the excessive deflections at the center and the rotation of the supports. The tension and compression faces of specimen B1 are shown in Figs. 3.1 and 3.2.

3.3.2 Specimens Tested under Uniaxial Inplane and Lateral Loads

In specimen A2, cracks were first observed at the bottom face in the direction of the inplane load at a lateral load of 5.6 kPa. As the lateral load increased, the crack pattern approached that of specimen A1. Final failure of the specimen was explosive and occurred when a failure mechanism was formed in one half of the plate. Concrete crushing lines were observed at the top of the specimen and the compression reinforcement in the direction of the inplane load buckled. The tension and compression faces of this plate are shown in Figs. 3.3 and 3.4.

Hairline cracks were observed on the bottom face of specimen A3 in the long direction at the full application of the inplane load and before any lateral load was applied. In specimen A4, cracks were first noticed on the tension face in the long direction at a lateral load of 5.8 kPa. Final failures of these two specimens were explosive and similar to that of specimen A2.

In specimens B2 and B3, shrinkage cracks did not propagate further during the application of the inplane load. However, flexural cracks, in the direction of the inplane load, appeared on the bottom middle region at early stages of the lateral load application. With further loading, cracking similar to that observed in specimen B1 occurred on the tension face of the plate. Although final failure of specimen B2 was explosive, that of specimen B3 was more gradual. In both cases failure mechanisms were formed in one half of the

plate accompanied by crushing of concrete on the top face and buckling of the compression reinforcement in the crushed areas.

For specimen B4, the inplane load was applied parallel to the short edges. Distinct flexural cracks appeared on the bottom middle region in the direction of the inplane load (the short direction) at a lateral load of 7.20 kPa. As lateral loading continued, new cracks developed and extended towards the corners but remained very narrow. The specimen showed very gradual unloading. Final failure occurred near the end of the unloading stage with the failure mechanism formed in one half of the plate. Concrete crushing lines were observed at the top face of the specimen and buckling of the compression reinforcement in the direction of the inplane load occurred. The tension and compression faces of this specimen are shown in Figs. 3.5 and 3.6.

During loading of specimen C2, flexural cracks were first observed at the center of the bottom face in the direction of the inplane load at a lateral load of 20.8 kPa. As the lateral load increased thereafter, the crack pattern approached that of specimen C1 which was tested under lateral load only. At the maximum lateral load, most of the cracks in the direction of the inplane load did not open sufficiently to be diagnosed as yield lines. Final failure was explosive and occurred when a failure mechanism was formed in one half of the plate. Crushing of concrete in the top surface and buckling of the compression reinforcement in the direction of the inplane load occurred near the end of the unloading stage.

The inplane and lateral loads were applied simultaneously in the test of specimen C3. The inplane load was applied in steps of 18.5 kN/m and the lateral load in steps of 1.25 kPa up to the peak loads. Beyond the peak loads, the lateral load was allowed to drop off as the deflection increased, while keeping the inplane load constant at the peak value. Cracks were first observed in the direction of the inplane load on the tension face at inplane and lateral loads of 225.0 kN/m and 17.8 kPa, respectively. The tension and compression faces of specimen C3 are shown in Figs. 3.7 and 3.8.

In specimens C4 and C5, cracks were first noticed in the direction of the inplane load on the tension face at lateral loads of 23.7 kPa and 24.1 kPa, respectively and the failure modes were similar to specimen C2.

In specimen C8, lateral load was first applied in increments of about 1.5 kPa. Cracks were first observed at the bottom face at a lateral load of 9.0 kPa. The valve supplying oil to the hydraulic jacks applying the lateral load was closed at a lateral load of 25.4 kPa. This value was corresponding to a maximum steel strain of about 0.0019, less than yield, and a central deflection of 10.0 mm. The inplane load was then applied monotonically in small increments until reaching a full value of 655.0 kN/m. Previously opened flexural cracks normal to the inplane load direction closed due to the application of the axial compression. Hence, the inplane load initially had the effect of straightening the plate. This upward movement of the plate, during the application of the inplane load, pressed against the jacks applying

the lateral load resulting in a slight increase in the lateral load. Finally, the inplane load was held constant and the plate was tested to failure by further increase in the lateral load. Final mode of failure was similar to that of specimen C2.

In specimen C9, the lateral load was first applied in increments of about 1.5 kPa to a level of 52.5 kPa corresponding to the lateral load capacity of specimen C2. Cracks were first noticed at the bottom face at a lateral load of 10.45 kPa. At the lateral load of 52.5 kPa, the central deflection was 41.3 mm. The lateral load was then held constant at this value while the inplane load was applied monotonically and incrementally from zero to its maximum value. The maximum steel strain prior to applying the inplane load was about 0.006. Previously opened flexural cracks in the direction of the inplane load widened quickly because of the continuous shifting in the neutral axis location due to the second order effect of the inplane load. Crushing of concrete was noted at the top surface just before failure. Failure was sudden and violent and the likely reason for it was the inability of the section to develop the compressive force required to balance the externally applied axial force.

Cracks were observed in specimen D2 in the direction of the inplane load at a lateral load of 54.2 kPa. As the lateral load increased, these cracks widened and cracks normal to the inplane load developed and both extended towards the corners. Light spalling in the concrete on the top surface preceded the maximum lateral load and the specimen showed a brittle type of failure in

which sudden extensive crushing began shortly after reaching its maximum lateral load.

3.3.3 Specimens Tested under Biaxial Inplane and Lateral Loads

Specimens C6 and C7 were subjected to combined biaxial compression and lateral loads. The progression of cracking in specimen C6 was gradual, with flexural cracks still emerging as the lateral load increased beyond 33.4 kPa. With further load, cracks extended towards the corners but remained very narrow. Final failure was explosive with concrete crushing lines on the top surface of the specimen and buckling of the compression reinforcement in the two orthogonal directions. In specimen C7, in which the inplane load was half that of C6, cracks were first observed at a lateral load of 28.7 kPa. Near the end of the test, the lateral load approached zero. The tension and compression faces of specimen C6 are shown in Figs. 3.9 and 3.10.

3.4 Load-Deflection Characteristics

3.4.1 Out-of-Plane Deflections

The reference values for the deflection measurements of the specimens were taken at the start of the loading tests, i.e. deflections due to dead load were not measured. During the application of the inplane load, very small out-of-plane deflections occurred in some of

the specimens in which the inplane loads were applied first. The maximum recorded out-of-plane deflection was less than 1 percent of the deflection at the maximum lateral load. These small values indicate that the inplane load was concentrically applied through the knife edges.

The lateral load versus out-of-plane deflection curves for all of the specimens are presented and discussed in Chapter 4. In this section, however, some of these specimens are described in some detail.

The lateral load versus out-of-plane deflection relationships of specimens tested under lateral loads only exhibited similar features. Each diagram is essentially a straight line up to the start of cracking. Beyond cracking, as the tension is lost by the concrete, a rapid change of slope in the load-deflection curve is observed. The stiffness deterioration caused by cracking occurred mainly at first cracking, and less during progressive cracking. With further load, yielding of the reinforcement started in one or more regions of high moments and spread through the plate as moments were redistributed from yielded regions to areas that were still elastic. This continued until the yield-line mechanism developed. Although the yield lines divided the plate to form a plastic mechanism, the plate continued to withstand appreciably higher loads. This was, however, accompanied with pronounced degradation of stiffness. The lateral load versus out-of-plane center deflection for specimen C1 is shown in Fig. 3.11. The drop in load at a deflection of about 70 mm occurred when the test was stopped to reset the jacks.

Fig. 3.12 shows the lateral load-deflection response of the rectangular specimen A4. This specimen had inplane load in the y-direction. The initial behaviour of the plate was linear up to a lateral load of 6.6 kPa, which is close to the value of the cracking load detected during testing. The change of slope in the load-deflection curve reflects the formation of cracks in the direction of the inplane load at the central region of the plate. The load under which first yielding of short span reinforcement was detected during testing is indicated on the load-deflection curve. As load increased, yielding of short direction reinforcement spread causing a rapid deterioration of stiffness. It can be observed that the specimen failed almost immediately after reaching the peak lateral load. This abrupt collapse is attributed to the development of an unstable panel mechanism.

The lateral load-deflection characteristics of specimens C1, C4, and C5 displayed similar features. Fig. 3.13 shows the lateral load versus out-of-plane center deflection curve of specimen C2. Examination of this curve reveals that the load-deflection relationship deviates from a linear function at about 25.0 kPa. The loads under which first cracking, in the direction of the inplane load, and yielding of tension reinforcement normal to the direction of the inplane load were detected during testing are indicated on the load-deflection curve. It can be observed that the load-deflection curve was insensitive to the initiation of flexural cracks in the direction of the inplane load. Signs of first flexural cracks were camouflaged because of the combination of two effects: the redundancy of the

plate and the delay of cracking normal to the inplane load direction since the presence of the inplane compressive load increased the cracking moment in its direction. However, the plate softened appreciably as a result of yielding of the reinforcement normal to the inplane load. In fact, initiation of yielding in that reinforcement may be termed the beginning of the failure process in slender square plates. At the ultimate load, the interaction between the axial force and the lateral deflection of the plate began to affect the behaviour. Any attempt to maintain the lateral load increased plate deflection significantly. Since the static moments can not exceed the cross sectional capacity, unloading of the lateral loads started and continued with increasing deflection until the moments about an axis normal to the inplane load direction reached their peak values. This was accompanied by decisive crushing failure of concrete. It is clear that crushing of concrete was a postfailure phenomenon which occurred after the plate achieved an unstable condition.

The lateral load versus out-of-plane center deflection curve of specimen D2 is shown in Fig. 3.14. This square specimen had a width-to-depth ratio of 19.7 and was tested under combined uniaxial and lateral loads. It can be seen that the specimen exhibited essentially linear load-deflection response well beyond the load at which flexural cracks were first observed during the test. The load corresponding to yielding of reinforcement normal to the inplane load direction, as indicated by the strain gauges is shown on the curve. As can be seen, the overall stiffness of the plate was strongly affected by first yielding of that reinforcement. With the continuance

of loading, crushing of concrete on the top surface was noticed just before reaching the ultimate load. The load-deflection curve showed a brittle type of failure in which the specimen was unable to sustain any further loading after reaching the maximum load.

Fig. 3.15 shows the lateral load versus out-of-plane center deflection curve for specimen C8. This specimen was loaded first with lateral loads then with inplane loads followed by more lateral loads. During the application of the inplane load, the flexural cracks normal to its direction closed. Subsequently, the effective area of the uncracked section was increased and concrete resumed its role in resisting compressive stresses. As can be seen in Fig. 3.15, this led to a substantial increase in the overall stiffness of the specimen. As the lateral load increased again, cracks in the direction of the inplane load widened quickly and those normal to it reopened leading to a gradual deterioration of stiffness. No crushing of concrete was observed at the maximum lateral load and it was possible to extend the test well into post-peak stage.

3.4.2 Inplane Deflections

The lateral load versus the relative inplane deflection of the plate ends in the x-direction for the square specimen C1 and in the x- and y-directions for the square specimen C2 and the rectangular specimen A4 are shown in Figs. 3.16 through 3.20. The readings are the average of two gauges measured 225 mm on either side of the plate center-lines. A positive deflection corresponds to a shortening

of the plate. In specimen C1, tested under lateral load only, the relative end deflection accelerated after initial cracking and increased at a relatively constant rate thereafter. Specimens C2 and A4 were axially loaded in the y-direction. In Figs. 3.18 and 3.20, the horizontal offsets at zero lateral loads indicate the shortening of the plates in the direction of the inplane loads as they were applied.

3.4.3 Edge Rotations

Representative plots of the lateral load versus edge rotations about the edges parallel to the x- and y-directions along the center lines are shown in Figs. 3.21 through 3.24 for specimens under combined uniaxial compression and lateral loads.

3.5 Deflected Shapes

Out-of-plane deflections of the plate surface were measured at several points along the center-lines in the two orthogonal directions. From these, the out-of-plane deflection profiles at various load levels in both the x- and y-directions were obtained. The deflection profiles for the square specimen C2, and for the rectangular specimen A4 are shown in Figs. 3.25 through 3.28.

The deflected shapes across the square plates and in the short directions of the rectangular plates approach a half sine wave shape. The deflected shapes in the long directions of specimens of series A suggest that there may have been a region of one-way load transfer in the middle of these plates.

3.6 Measured Steel Strains and Average Curvatures

Several behavioural trends can be observed from the measured steel strains. The general shapes of the load-steel strain curves are similar to the load-deflection curves or load-curvature curves and indicate changes of stiffness accompanying cracking of concrete and yielding of reinforcement. However, since the strain measurements give indications of local deformation while deflection and curvature measurements indicate only gross deformations, it is possible to have high strains at particular locations and still have only relatively small curvatures at the same applied load level.

Due to the large deformation experienced by specimens tested under lateral loads only, some of the gauges showing the highest strains malfunctioned before the maximum load was reached. However, large reinforcement strains were measured at many strain gauge locations in those plates. The maximum recorded steel strain exceeded 0.015 in specimens A1, B1, C1, and D1, with the greatest recorded being 0.0173 in specimen A1.

Large reinforcement strains were also measured at one or more strain gauge locations in rectangular specimens under combined loads in which the inplane loads were applied along the short sides, with the plates with lower reinforcement ratios and lower levels of axial force tending to have larger strains. The maximum recorded strain was 0.0146 in strain gauges installed on bars running in the

short direction of specimen A2. In square specimens under combined uniaxial compression and lateral loads, the greatest measured steel strain at the maximum lateral load was about 0.008 in the stocky specimen D2 in gauges installed on bars running normal to the inplane load direction. In specimen B4, the maximum recorded steel strains at the maximum lateral load was 0.00076 in gauges on bars running in the long direction.

Figs. 3.29 and 3.30 contain bottom steel strain distributions measured in specimen A4 for three loading stages: (1) immediately after application of inplane load, (2) at a lateral load about 50% of the ultimate, and (3) near the ultimate lateral load. In each figure, the locations of the strain gauges are indicated. In Fig. 3.29, strain measurements on the rebar running in the short direction, normal to the inplane load direction, show extensive yielding of that steel and confirm the full development of the yield mechanism at the ultimate load. This proves that there was sufficient plasticity at the critical sections in the short direction to allow for the redistribution of bending moments with the specimen maintaining its stability during that process. As can be seen in Fig. 3.30, the application of axial compressive forces along the short sides of the specimen caused compressive strains in the reinforcement running in the longitudinal direction. Before applying the lateral load, these strains were fairly uniform across the width of the plate. Near the maximum lateral load, compressive strains at the center were overcome by moments due to the lateral load while those near the edges increased (became more compressive). This suggests that there was a significant

redistribution of the applied inplane load in this specimen near the maximum lateral load.

Figs. 3.31 and 3.32 contain bottom steel strains measured in specimen C2 for three loading stages: (1) immediately after the application of the inplane load, (2) at 50% of the ultimate lateral load, and (3) at the ultimate lateral load. Fig. 3.31 shows that the application of the lateral load caused tensile strains in the bottom gauges that overcome the previously induced compressive strains.

Lateral load-steel strain curves are given in Fig. 3.33 for top and bottom steel strain gauges at the center of specimen C2 installed on a rebar running normal to the direction of the inplane load. The offset at zero lateral load was due to Poisson's ratio. As can be seen, when the lateral load was applied at constant inplane load, the strains in the transverse top steel increased (became more tensile) rather than decreasing. Since the plate sections were lightly reinforced, the height of the compression zone was small in the direction normal to the inplane load. As the lateral load increased, the location of the neutral axis shifted towards the extreme compressive fibre and the top steel in that direction was subjected to increasing tensile stresses.

While the average measured curvatures can not be interpreted accurately in terms of moment, they do record the average concrete strains occurring at the center of the plates over a 180.0 mm gauge length. In view of the few and narrow cracks which were observed at the maximum lateral loads in specimens in which the inplane loads were applied first, reasonable estimates of the concrete

compressive strains should be expected in the direction of the inplane load application.

In specimens B2 and B3, the curvature meter readings at the maximum lateral load indicated compressive strains on the top surface in the direction of the inplane load, for the 180.0 mm gauge length, of 0.0032 and 0.0029, respectively. It should be noted, however, that the measured strains in these two specimens do not necessarily represent the maximums which occurred at the maximum lateral loads since concrete crushing, which occurred during unloading, was first observed at a distance from the curvature meter location in the longitudinal direction.

In specimen B4, the compressive strain of the top surface in the direction of the inplane load, measured on a 180.0 mm gauge length, at the maximum lateral load was 0.00282.

At the maximum lateral load, a compressive strain of 0.00273 was measured in specimen C2 in the direction of the inplane load. In specimens C4 and C5, compressive strains of 0.00292 and 0.00316 were measured at the maximum lateral loads although no visible crushing was noted.

In specimens C6 and C7, compressive strains of 0.00278 and 0.00234, respectively, were measured at the maximum lateral loads.

In specimen D2, the compressive strain in the direction of the inplane load at the maximum lateral load was 0.00498. Signs of slight surface crushing were noted at that strain level. This indicates that

the practical strength of the plate section at the center, in the direction of the inplane load, was almost fully developed at the maximum lateral load.

Table 3.1 Maximum Loads and Corresponding Out-of-Plane Center Deflections

Specimen Designation	a/b	b/h	ρ_x^*	ρ_y^*	N_x (kN/m)	N_y (kN/m)	q_{li} (kPa)	w_{ou} (mm)
A1	2.17	27.18	0.00386	0.00386	0.0	0.0	39.69	132.43
A2	2.17	28.27	0.00402	0.00402	0.0	584.5	21.96	46.14
A3	2.17	28.01	0.00398	0.00796	0.0	586.8	23.90	63.91
A4	2.17	28.01	0.00796	0.00398	0.0	587.0	33.80	55.59
B1	1.50	26.82	0.00383	0.00383	0.0	0.0	45.91	101.22
B2	1.50	27.38	0.00385	0.00385	0.0	514.0	23.27	40.09
B3	1.50	27.42	0.00390	0.00390	0.0	353.80	25.52	45.83
B4	1.50	28.01	0.00398	0.00398	516.0	0.0	19.51	25.96
C1	1.00	26.98	0.00383	0.00383	0.0	0.0	73.88	91.15
C2	1.00	27.06	0.00385	0.00385	0.0	653.9	52.59	24.02
C3	1.00	26.70	0.00380	0.00380	0.0	647.0	51.56	24.68
C4	1.00	26.13	0.00371	0.00742	0.0	656.5	59.47	25.70
C5	1.00	26.09	0.00742	0.00371	0.0	652.5	67.83	31.00

(See next page for the remaining part of the table)

Table 3.1 Maximum Loads and Corresponding Out-of-Plane Center Deflections (continued)

Specimen Designation	a/b	b/h	ρ_x^*	ρ_y^*	N_x (kN/m)	N_y (kN/m)	q_u (kPa)	w_{ou} (mm)
C6	1.00	27.14	0.00386	0.00386	657.8	657.8	69.16	17.23
C7	1.00	27.50	0.00391	0.00391	362.5	362.5	60.03	20.10
C8	1.00	26.98	0.00383	0.00383	0.0	654.6	50.88	25.73
C9	1.00	27.34	0.00389	0.00389	0.0	342.4	50.02	51.85
D1	1.00	19.71	0.00392	0.00392	0.0	0.0	109.39	101.73
D2	1.00	19.73	0.00393	0.00393	0.0	883.8	121.68	29.70

Notes:

- In all the specimens which were tested under combined loads except C3, C8, and C9 the full inplane load was applied first, before lateral loading was commenced. In C3, the inplane and lateral loads were applied proportionally. In C8, a lateral load of 24.5 kPa was applied first followed by the full inplane load then by the rest of the lateral load. In C9, the full lateral load was applied first before inplane loading was commenced.

- X- and Y-directions are consistent with those in Figures 2.8 through 2.10.

* The reinforcement ratios are based on steel in one layer.

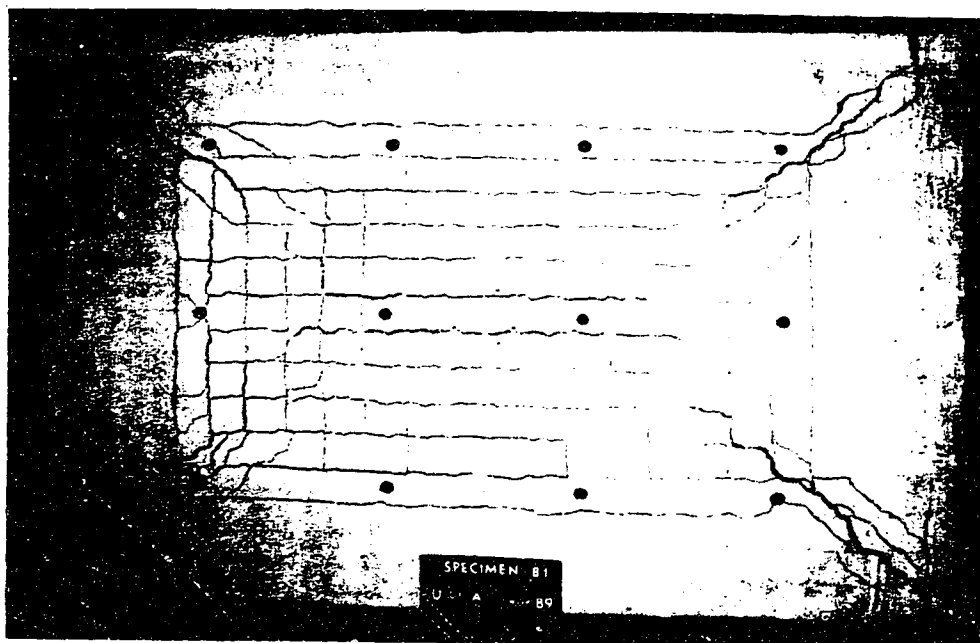


Figure 3.1 Tension Face of Specimen B1 after Failure



Figure 3.2 Compression Face of Specimen B1 after Failure

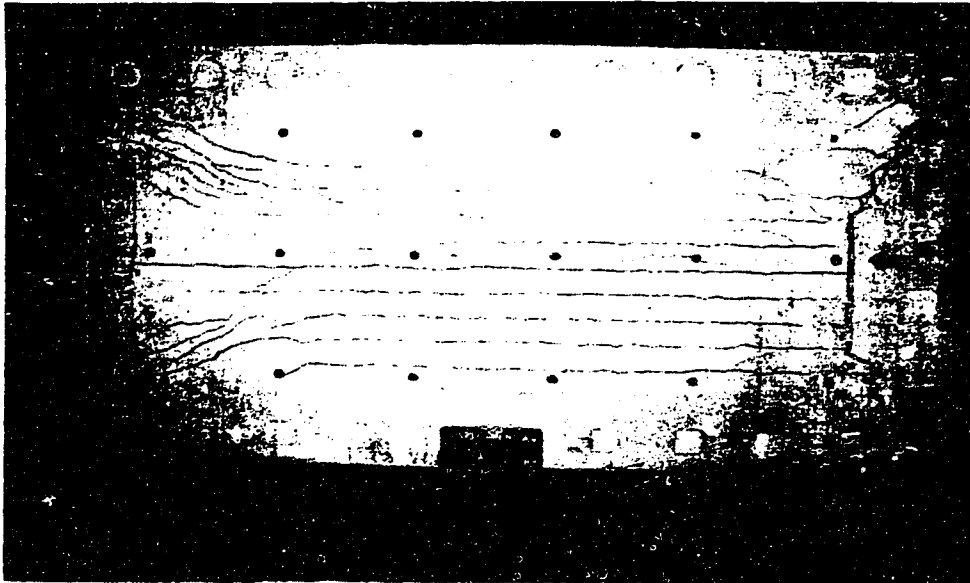


Figure 3.3 Tension Face of Specimen A2 after Failure

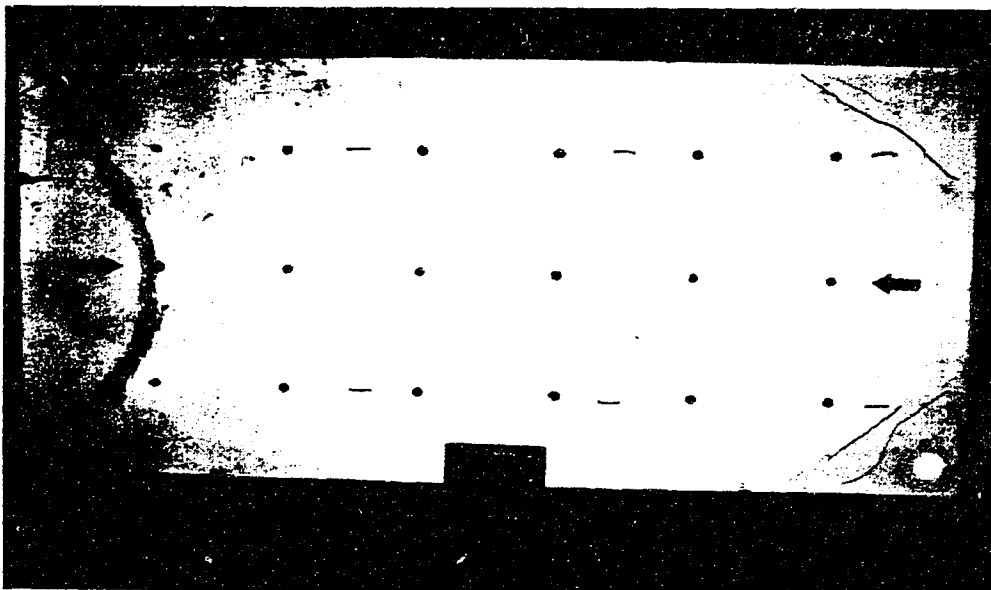


Figure 3.4 Compression Face of Specimen A2 after Failure

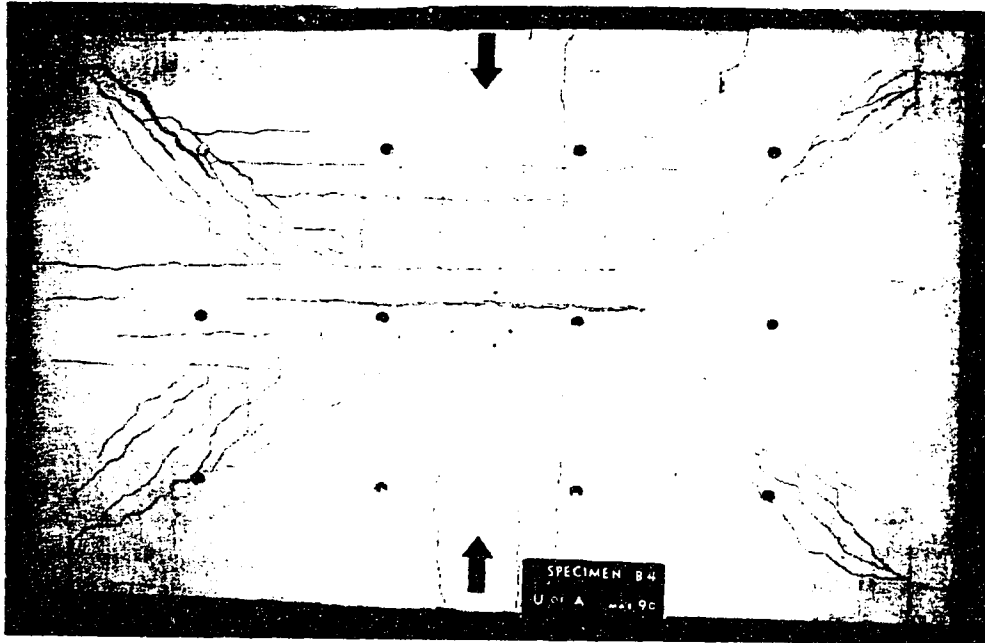


Figure 3.5 Tension Face of Specimen B4 after Failure

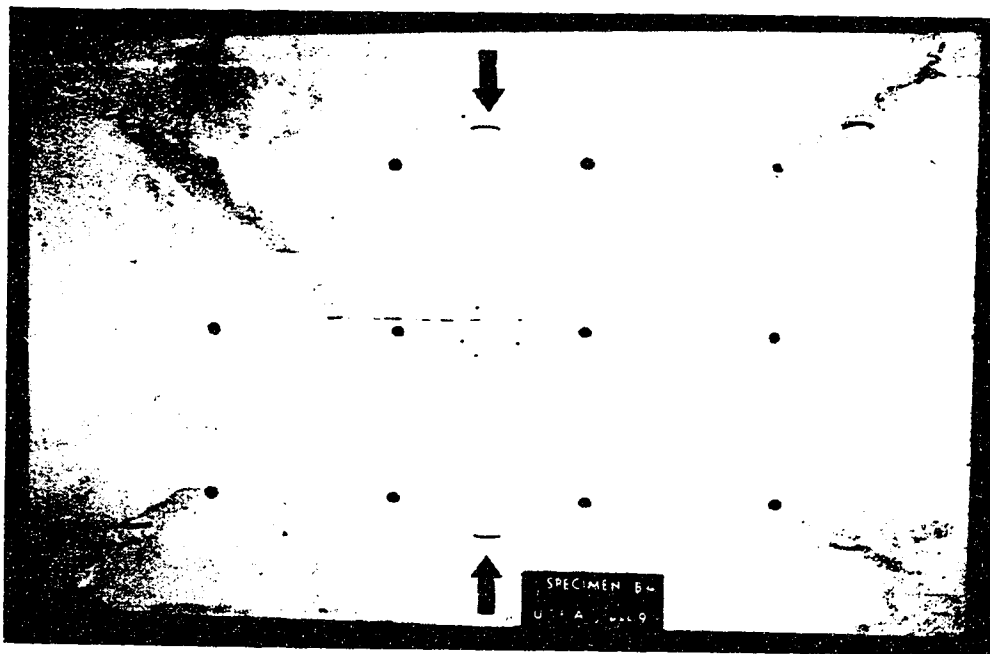


Figure 3.6 Compression Face of Specimen B4 after Failure

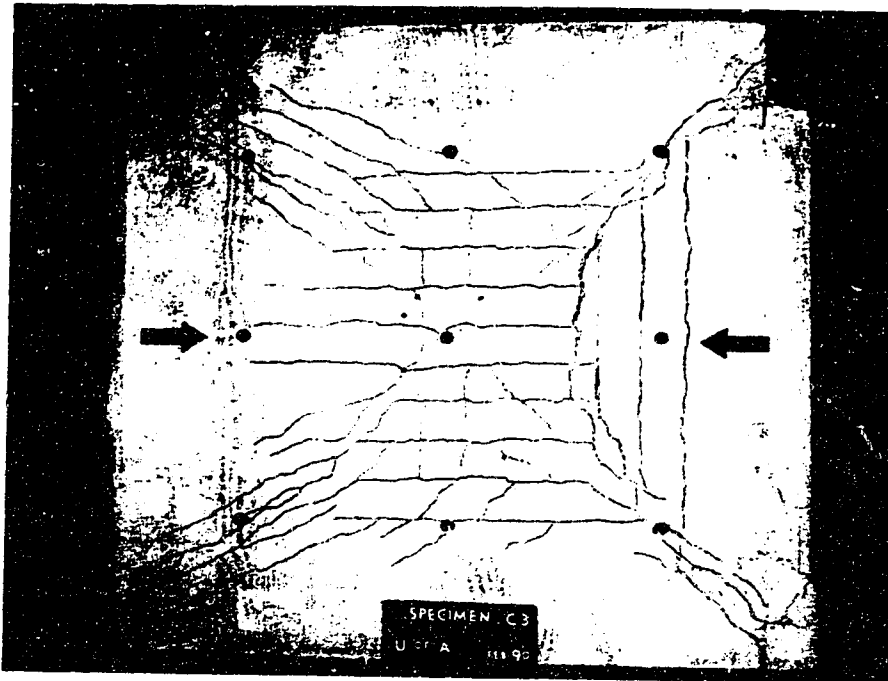


Figure 3.7 Tension Face of Specimen C3 after Failure

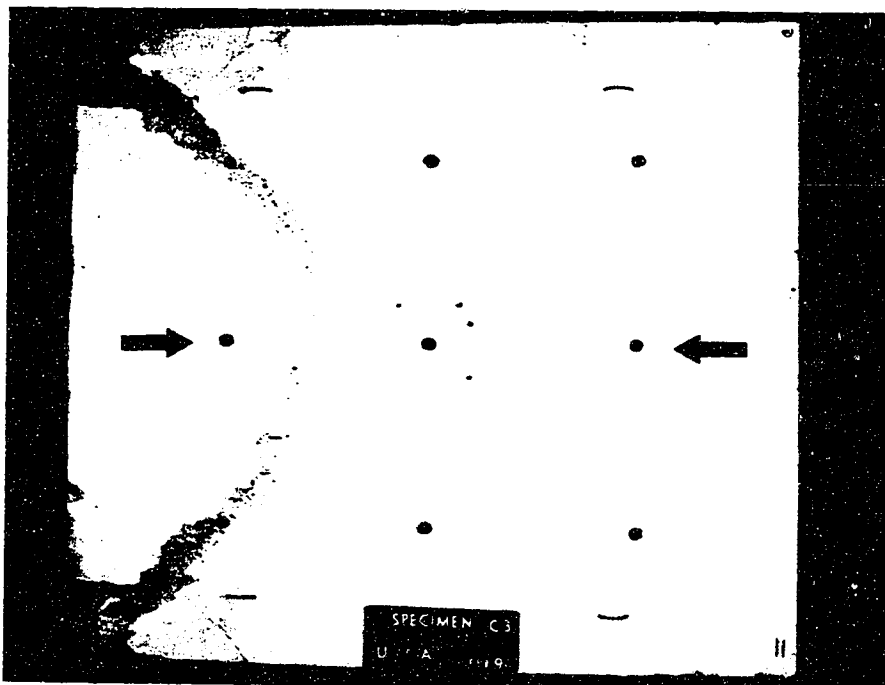


Figure 3.8 Compression Face of Specimen C3 after Failure

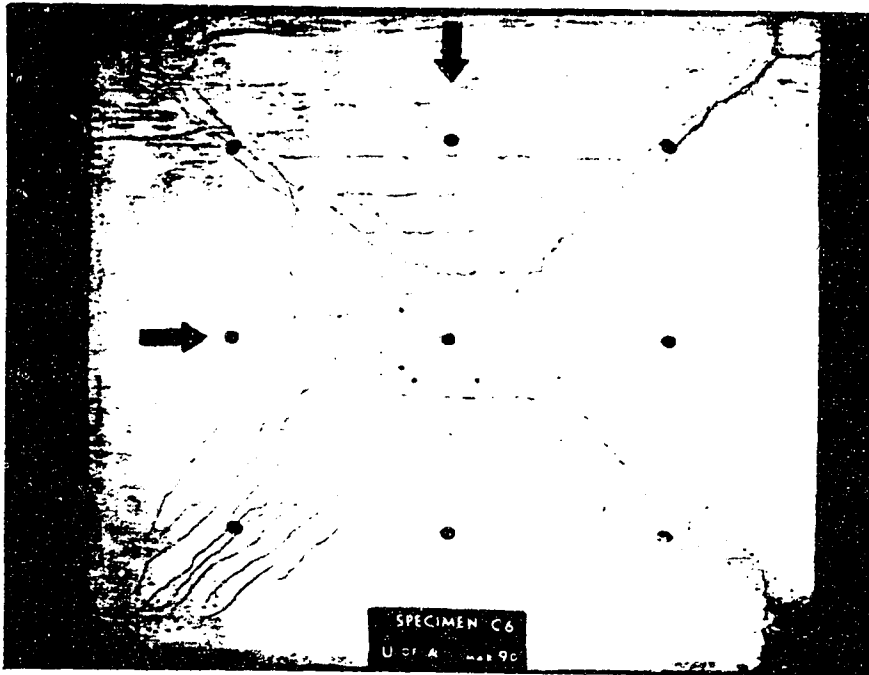


Figure 3.9 Tension Face of Specimen C6 after Failure

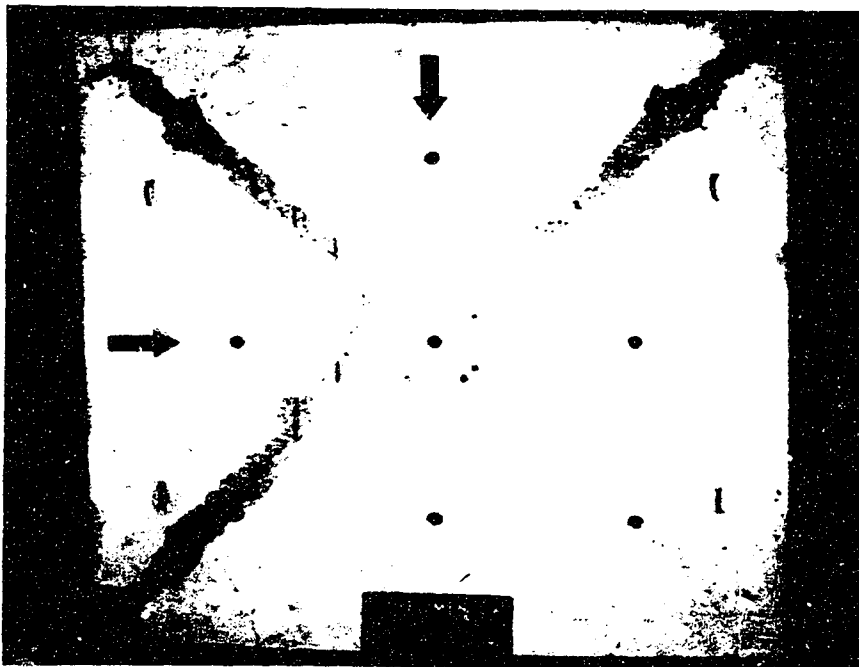


Figure 3.10 Compression Face of Specimen C6 after Failure

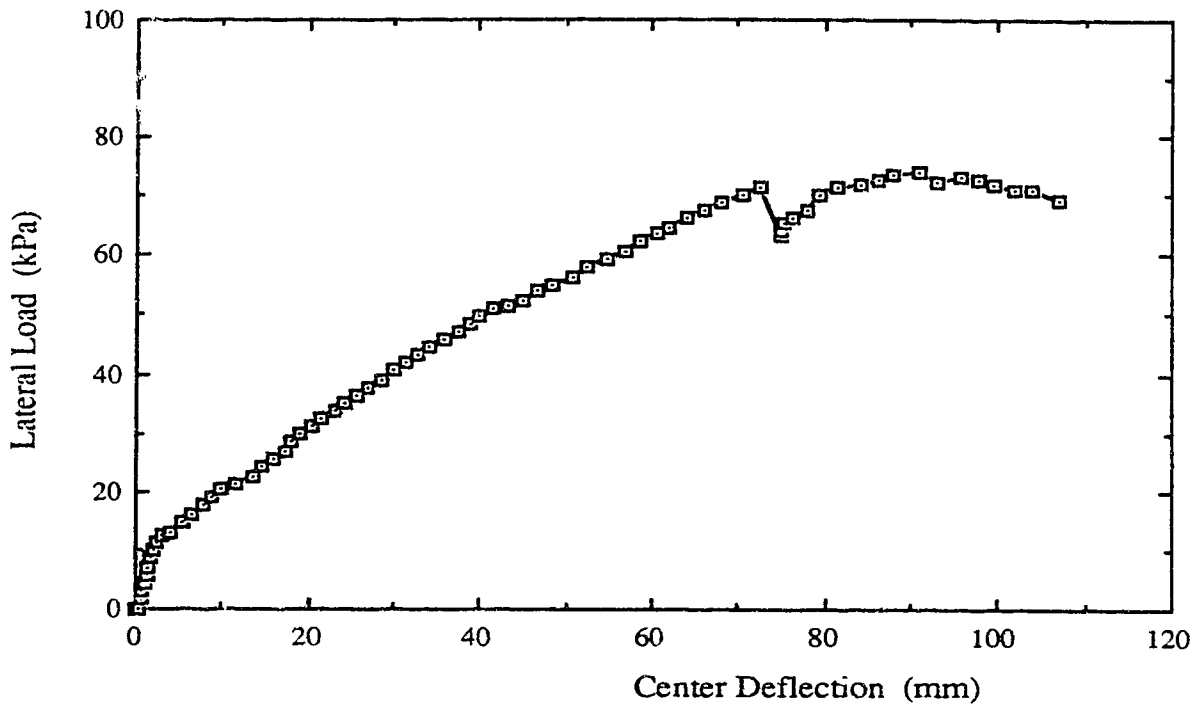


Figure 3.11 Lateral Load versus Out-of-Plane Center Deflection for Specimen C1

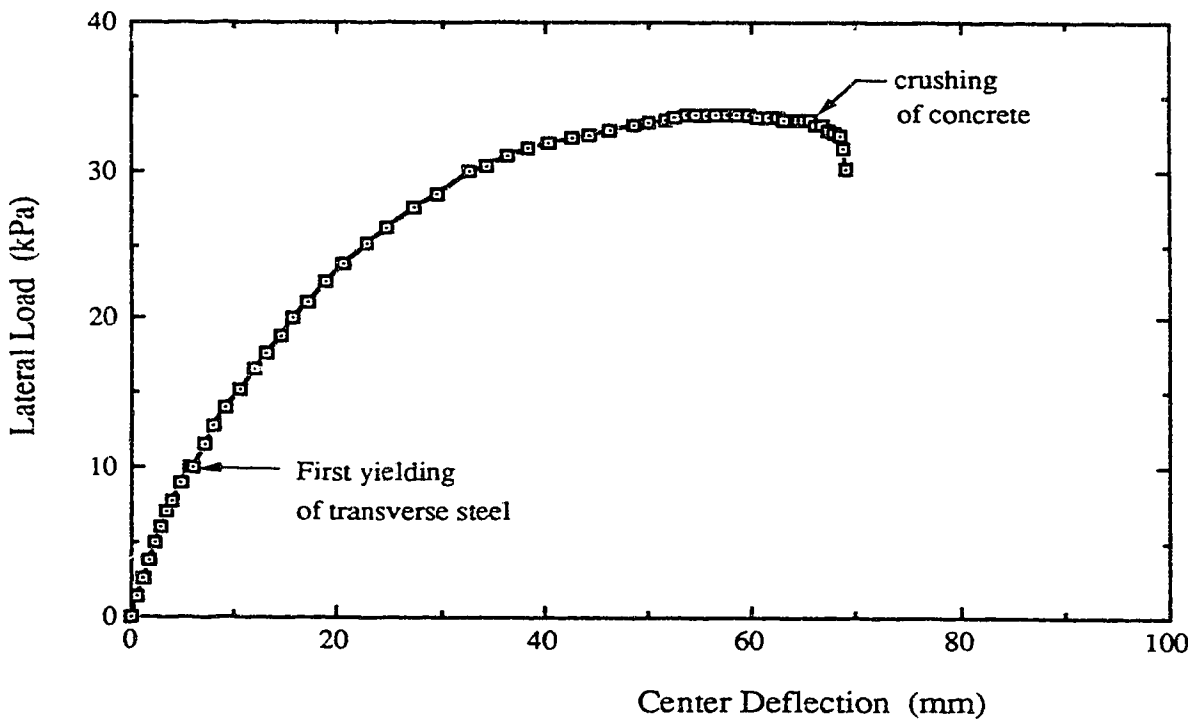


Figure 3.12 Lateral Load versus Out-of-Plane Center Deflection for Specimen A4

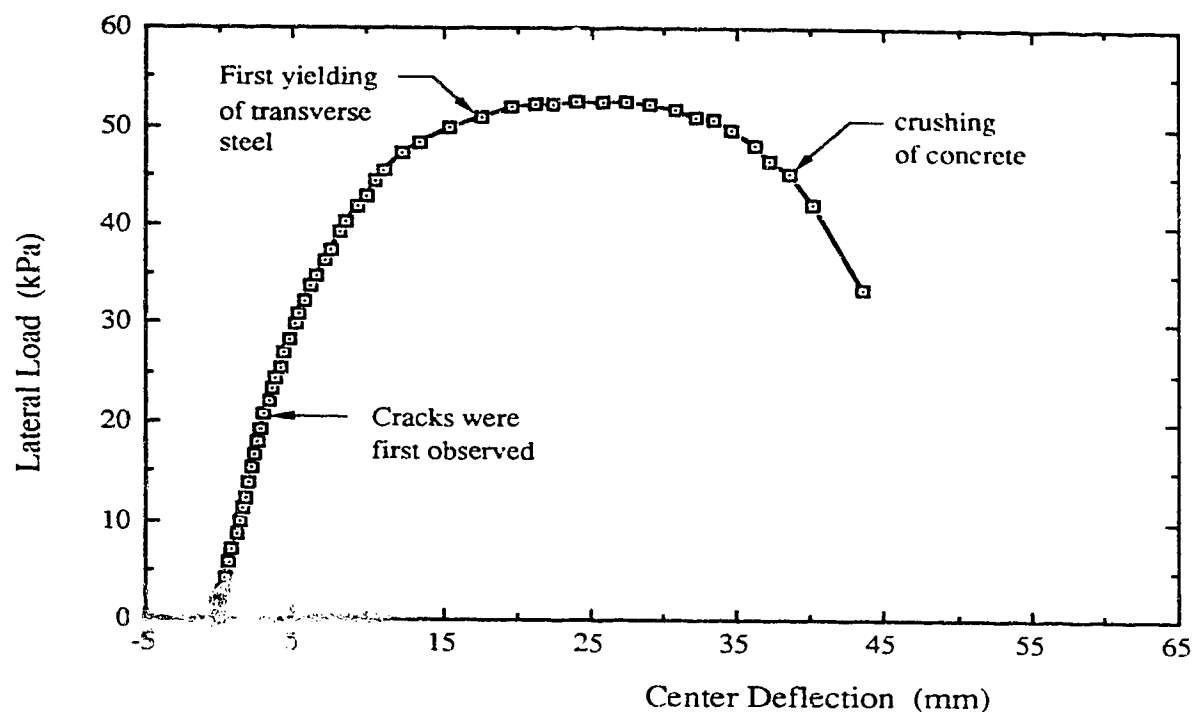


Figure 3.13 Lateral Load versus Out-of-Plane Center Deflection for Specimen C2

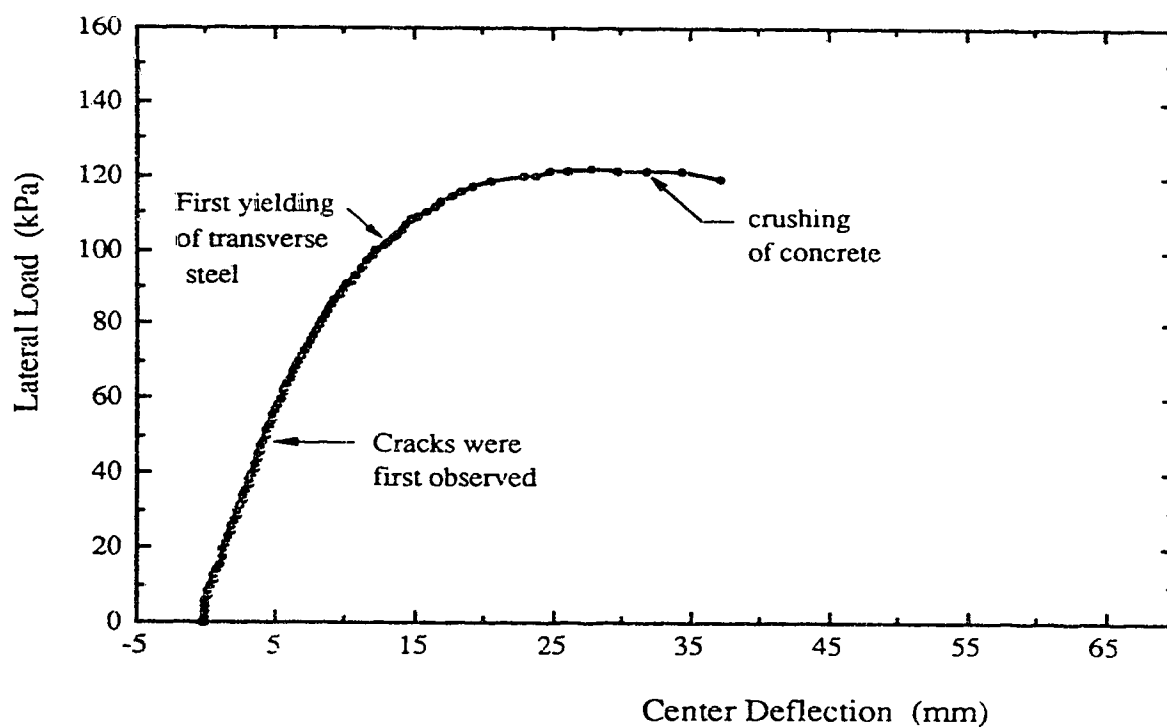


Figure 3.14 Lateral Load versus Out-of-Plane Center Deflection for Specimen D2

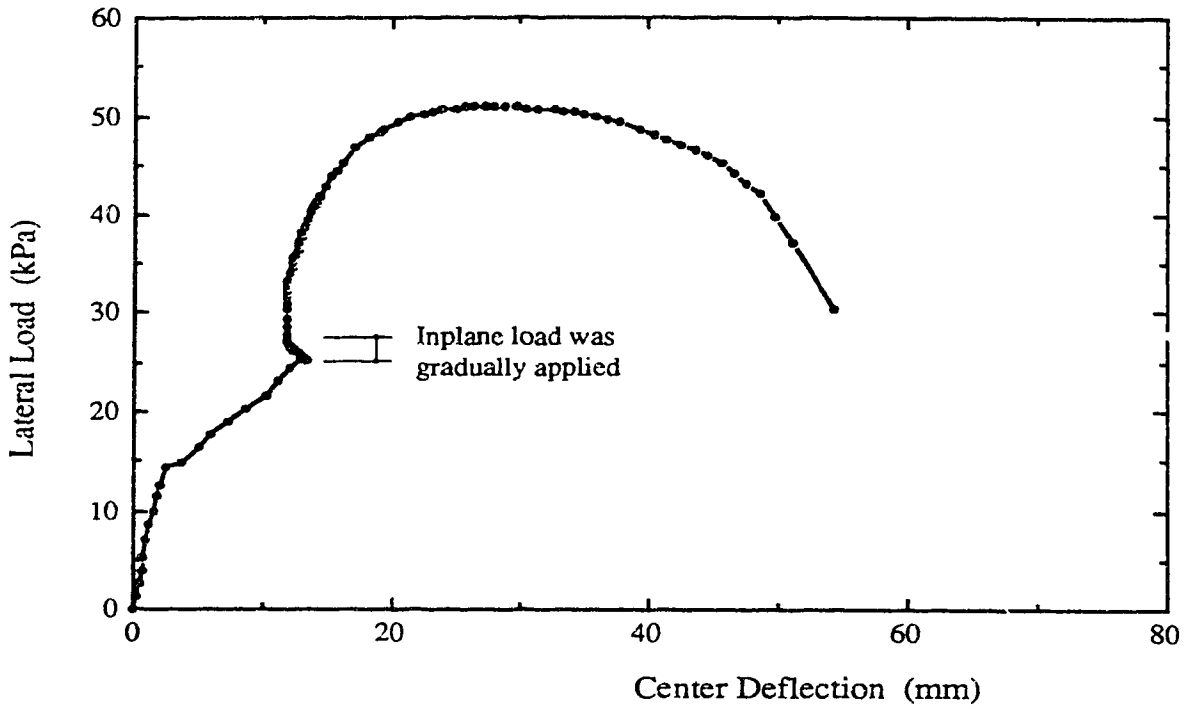


Figure 3.15 Lateral Load versus Out-of-Plane Center Deflection for Specimen C8

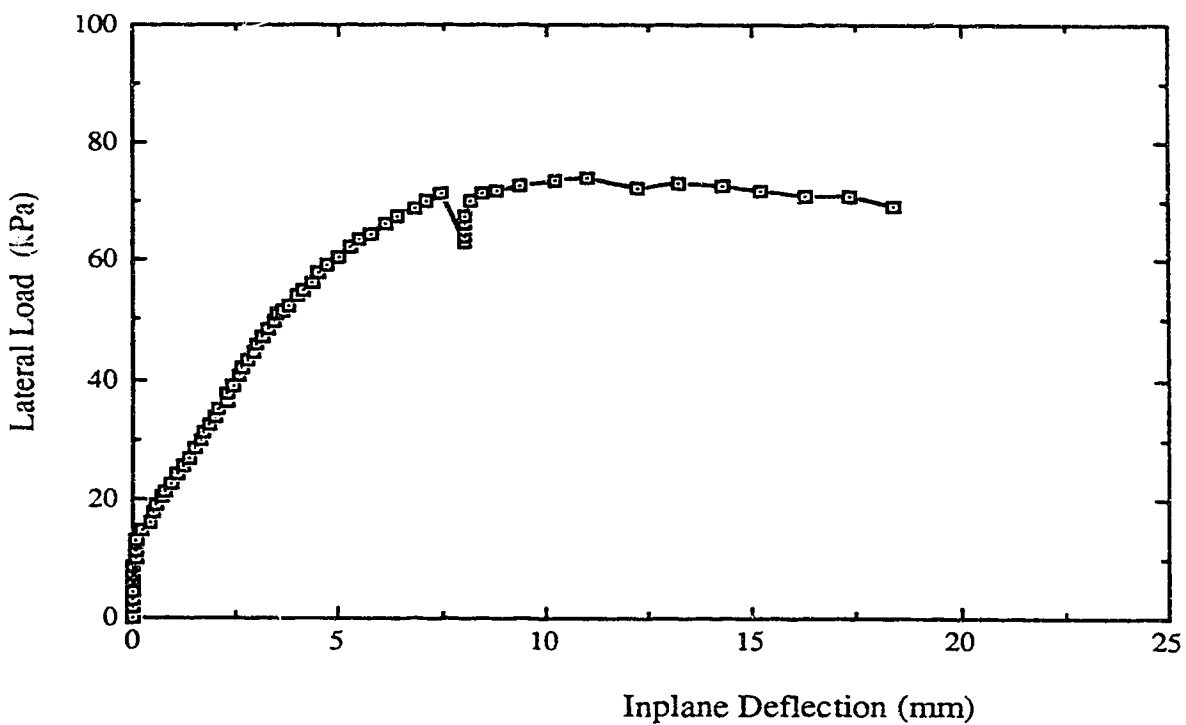


Figure 3.16 Lateral Load versus Inplane Deflection in the X-Direction for Specimen C1

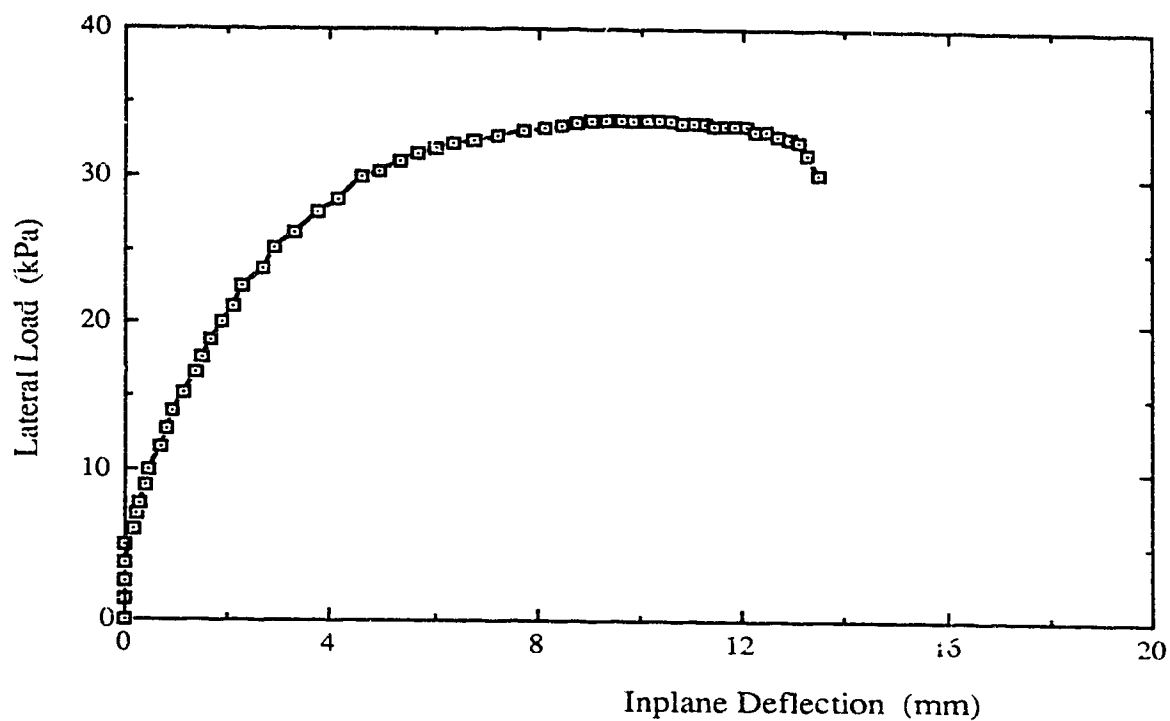


Figure 3.17 Lateral Load versus Inplane Deflection in the X-Direction for Specimen A4

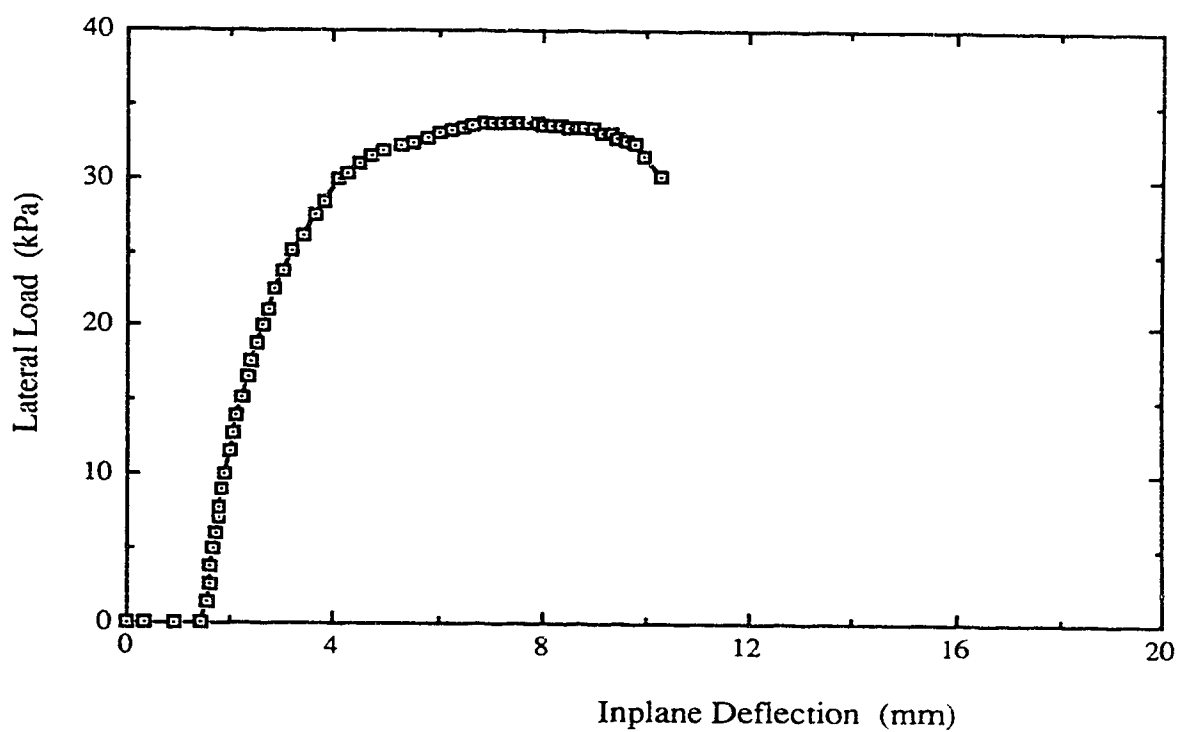


Figure 3.18 Lateral Load versus Inplane Deflection in the Y-Direction for Specimen A4

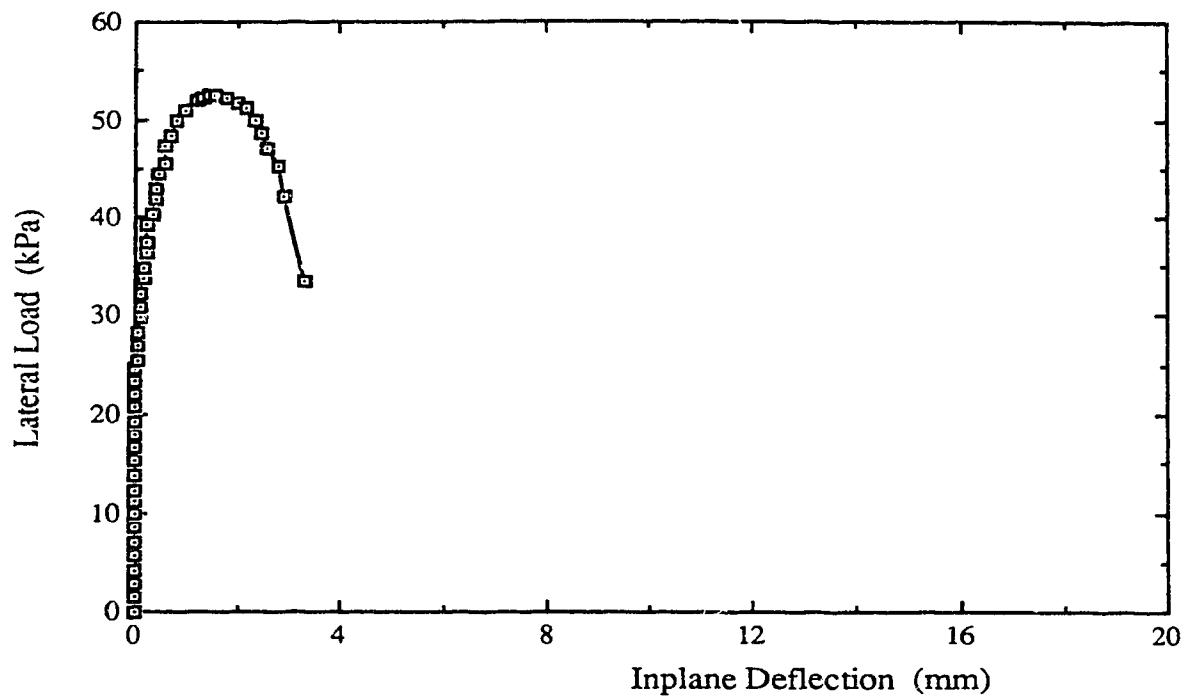


Figure 3.19 Lateral Load versus Inplane Deflection in the X-Direction
for Specimen C2

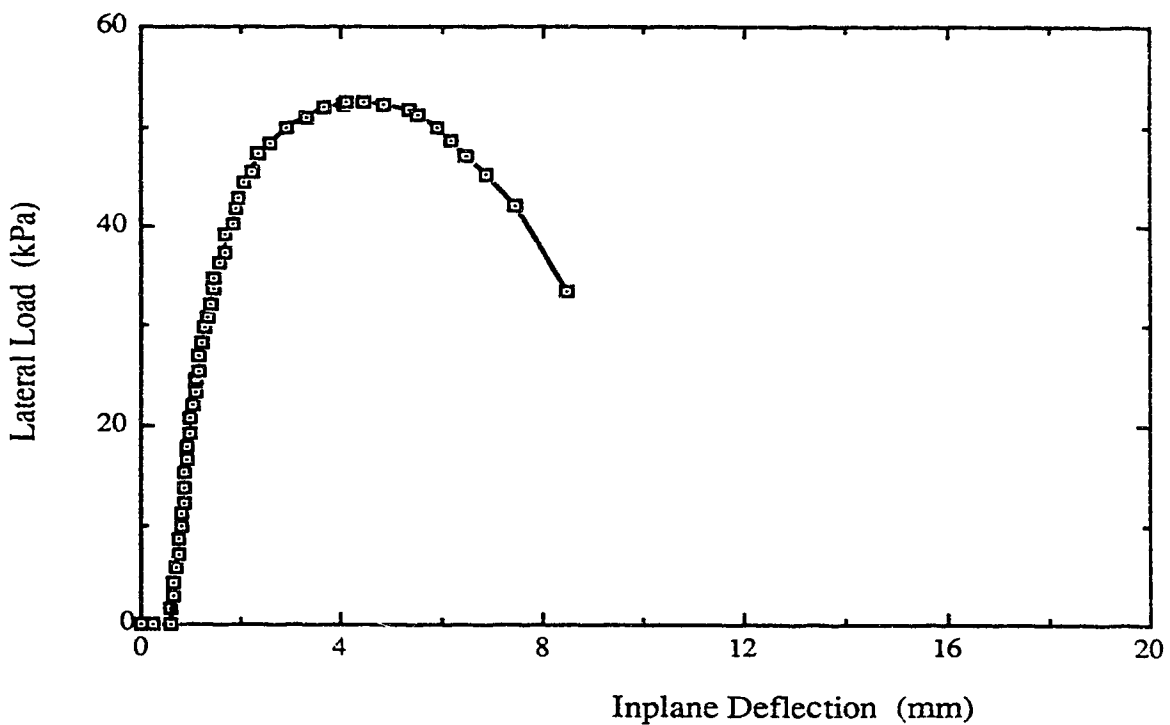


Figure 3.20 Lateral Load versus Inplane Deflection in the Y-Direction
for Specimen C2

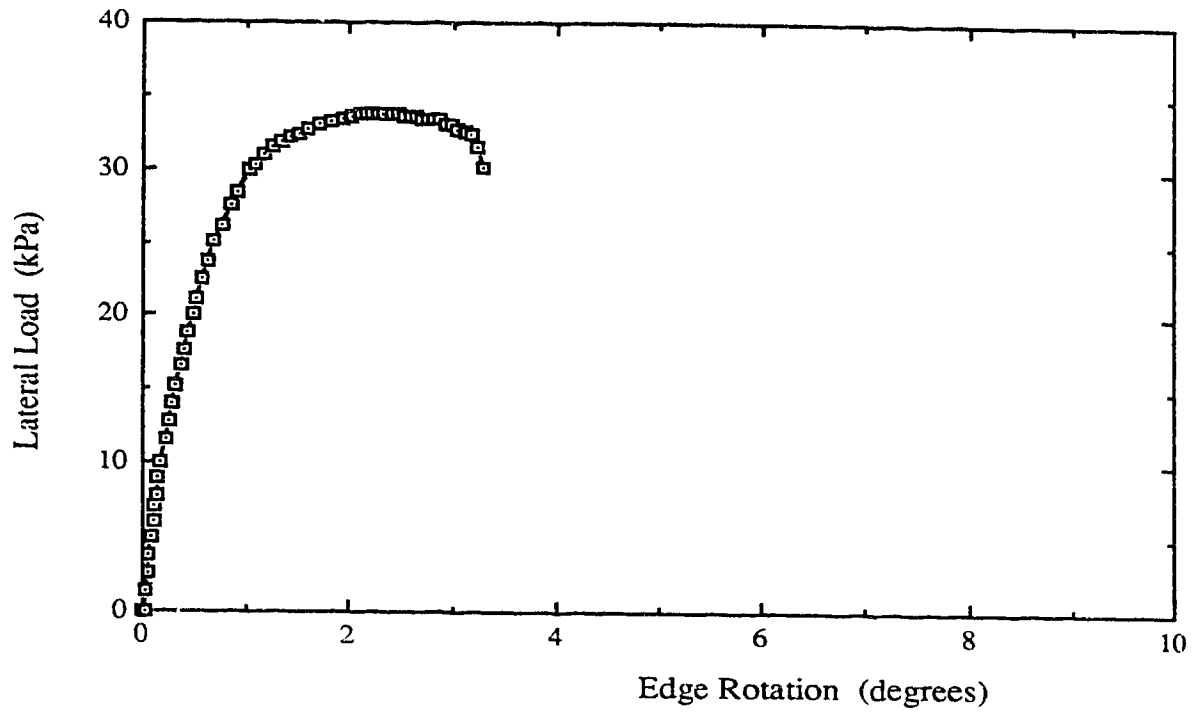


Figure 3.21 Lateral Load versus Edge Rotation about the Edge Parallel to the X-Direction for Specimen A4

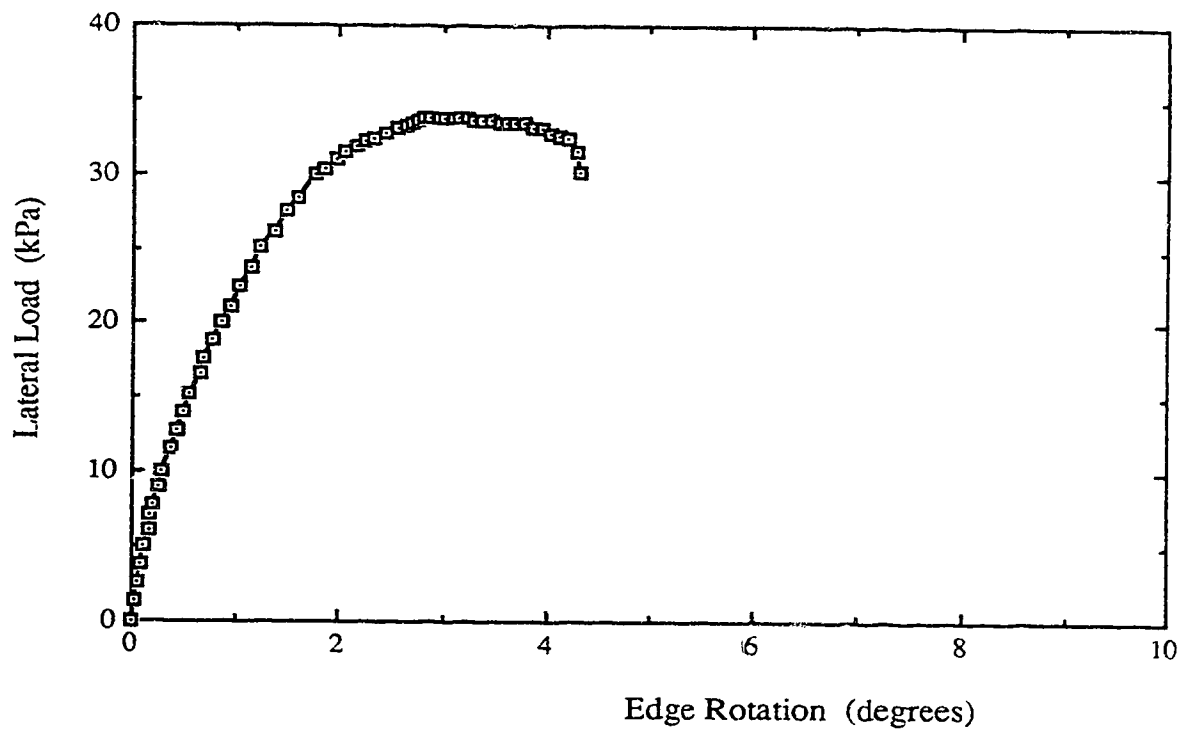


Figure 3.22 Lateral Load versus Edge Rotation about the Edge Parallel to the Y-Direction for Specimen A4

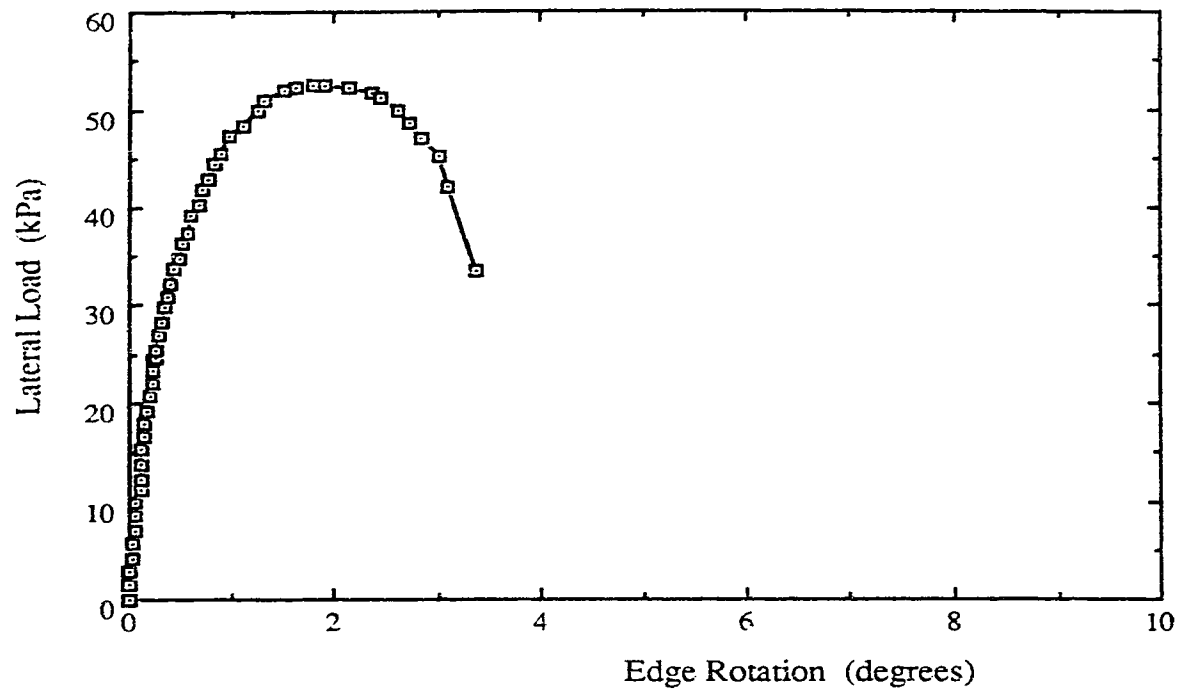


Figure 3.23 Lateral Load versus Edge Rotation about the Edge Parallel to the X-Direction for Specimen C2

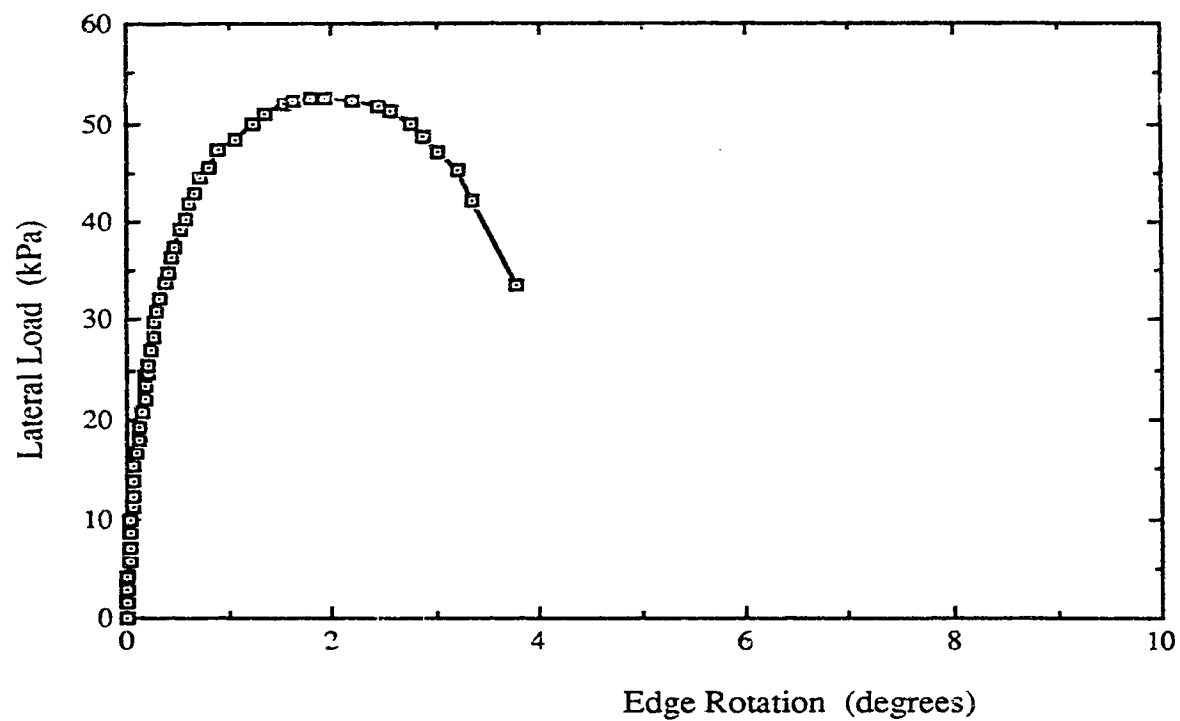


Figure 3.24 Lateral Load versus Edge Rotation about the Edge Parallel to the Y-Direction for Specimen C2

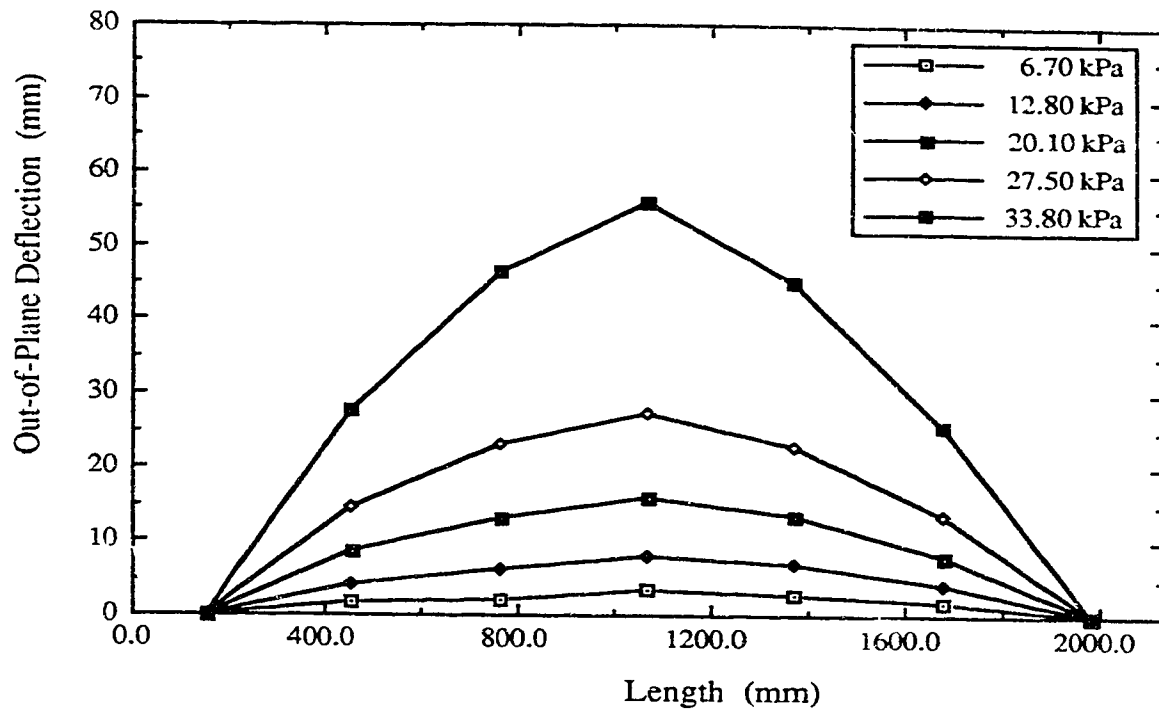


Figure 3.25 Out-of-Plane Deflection Profiles in the X-Direction for Specimen A4

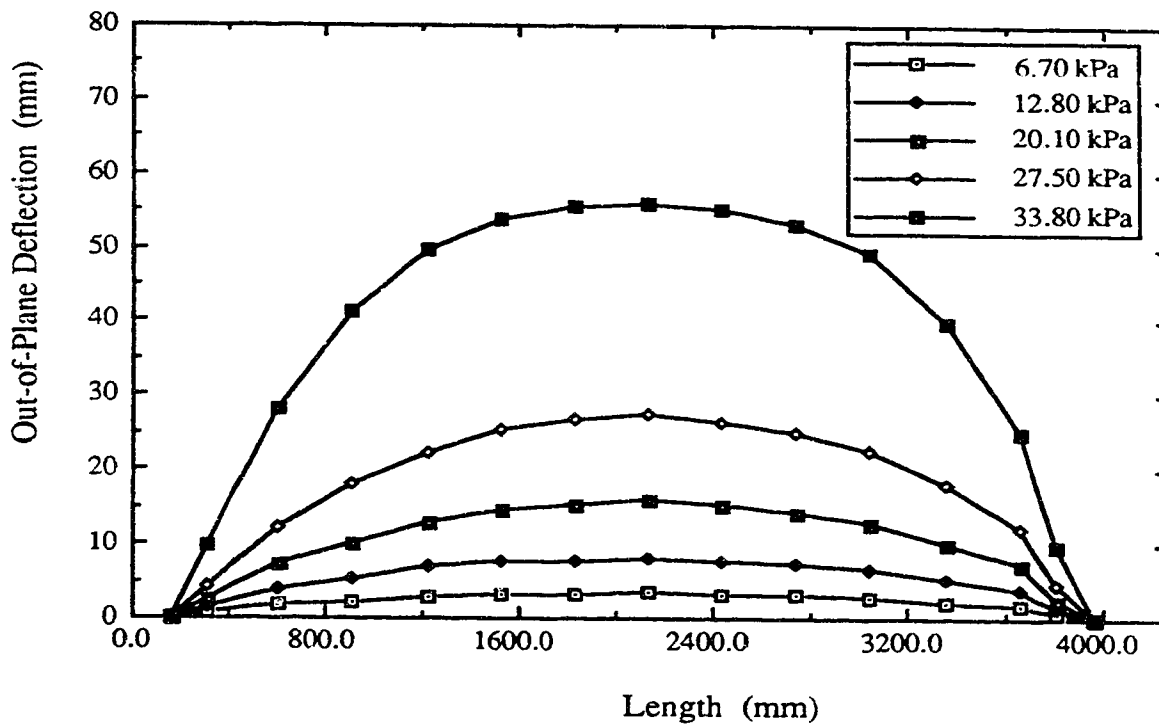


Figure 3.26 Out-of-Plane Deflection Profiles in the Y-Direction for Specimen A4

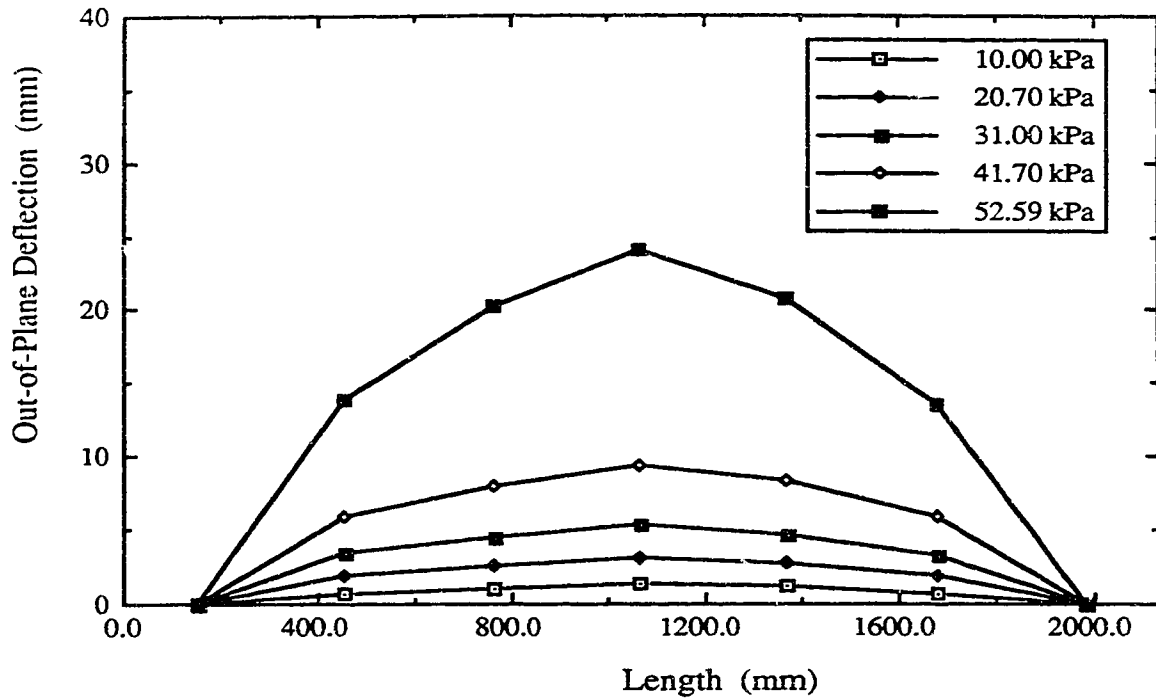


Figure 3.27 Out-of-Plane Deflection Profiles in the X-Direction for Specimen C2

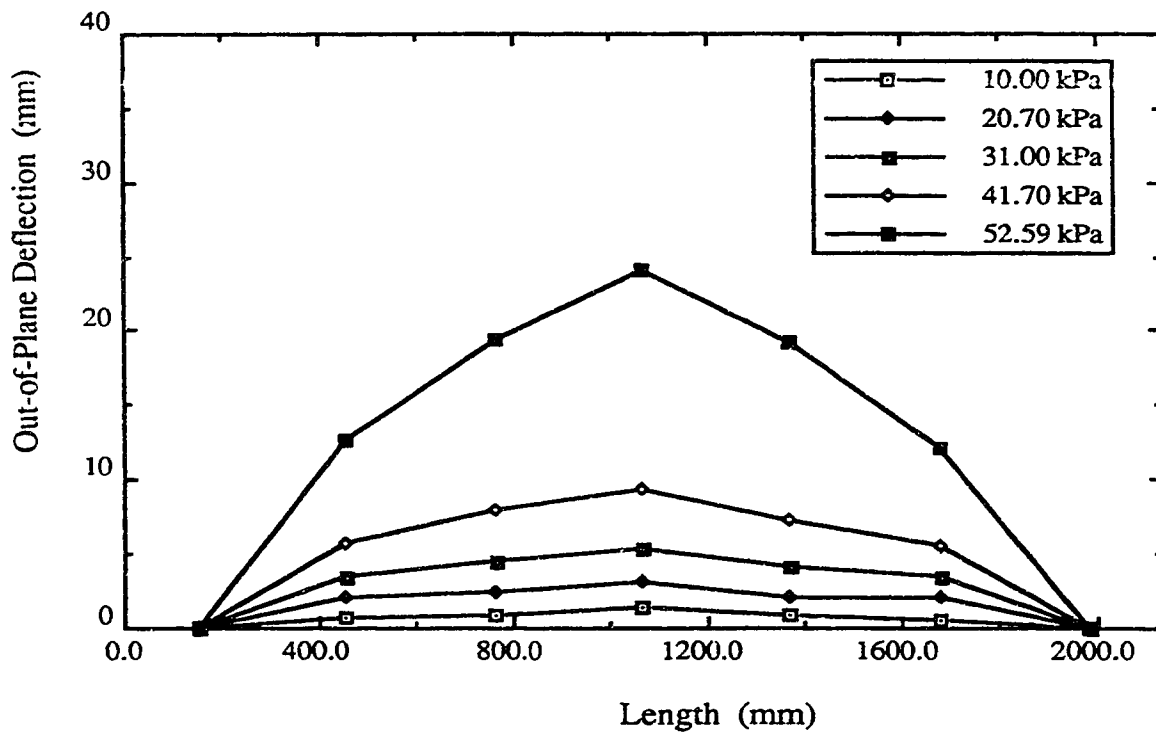


Figure 3.28 Out-of-Plane Deflection Profiles in the Y-Direction for Specimen C2

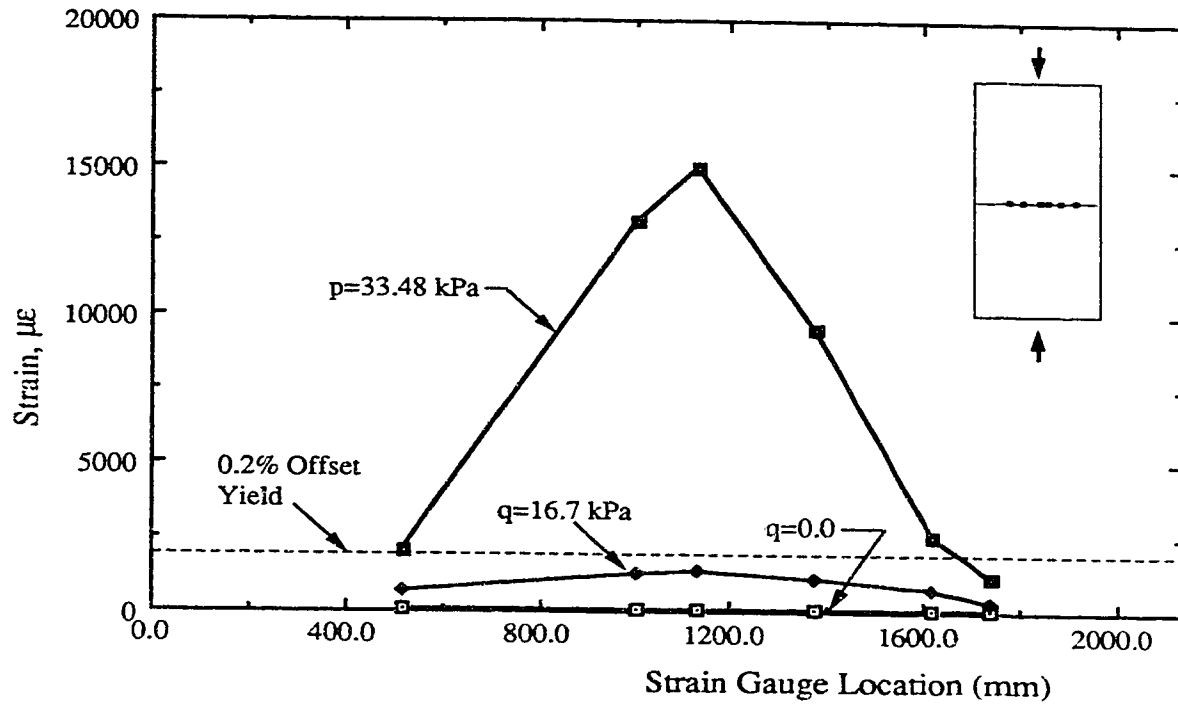


Figure 3.29 Steel Strains along the Bottom Transverse Bar at the Center of Specimen A4

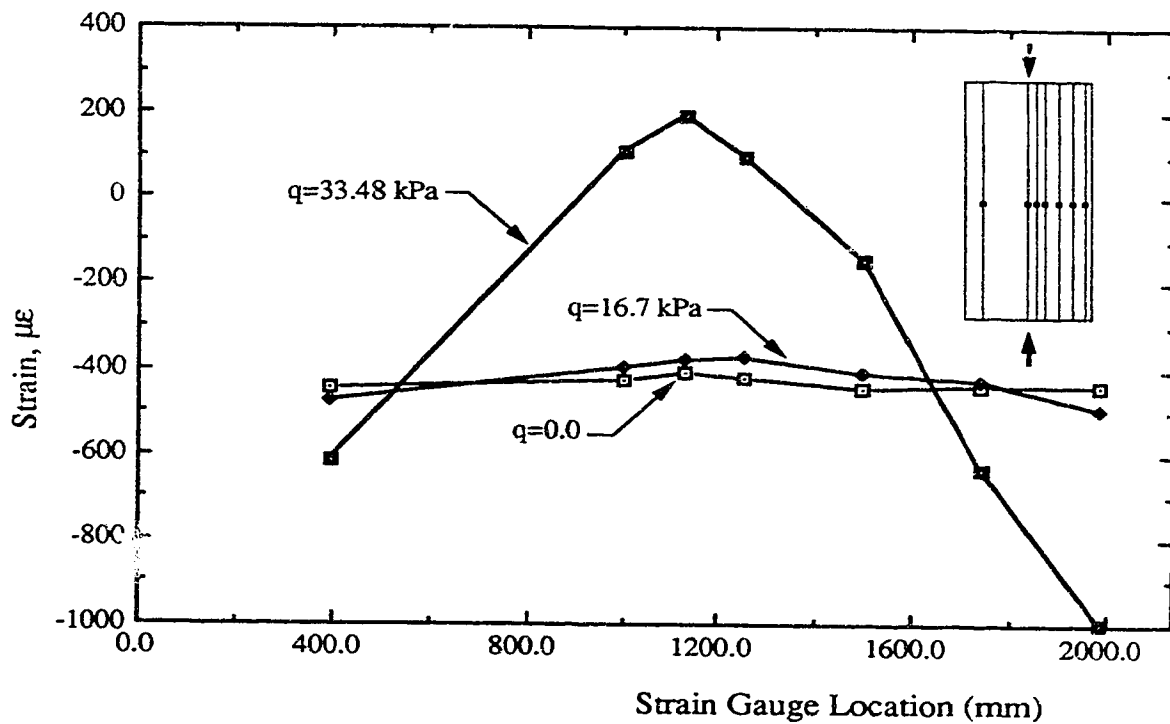


Figure 3.30 Steel Strains at the Center of Specimen A4 in Bottom Bars Running in the Direction of the Inplane Load

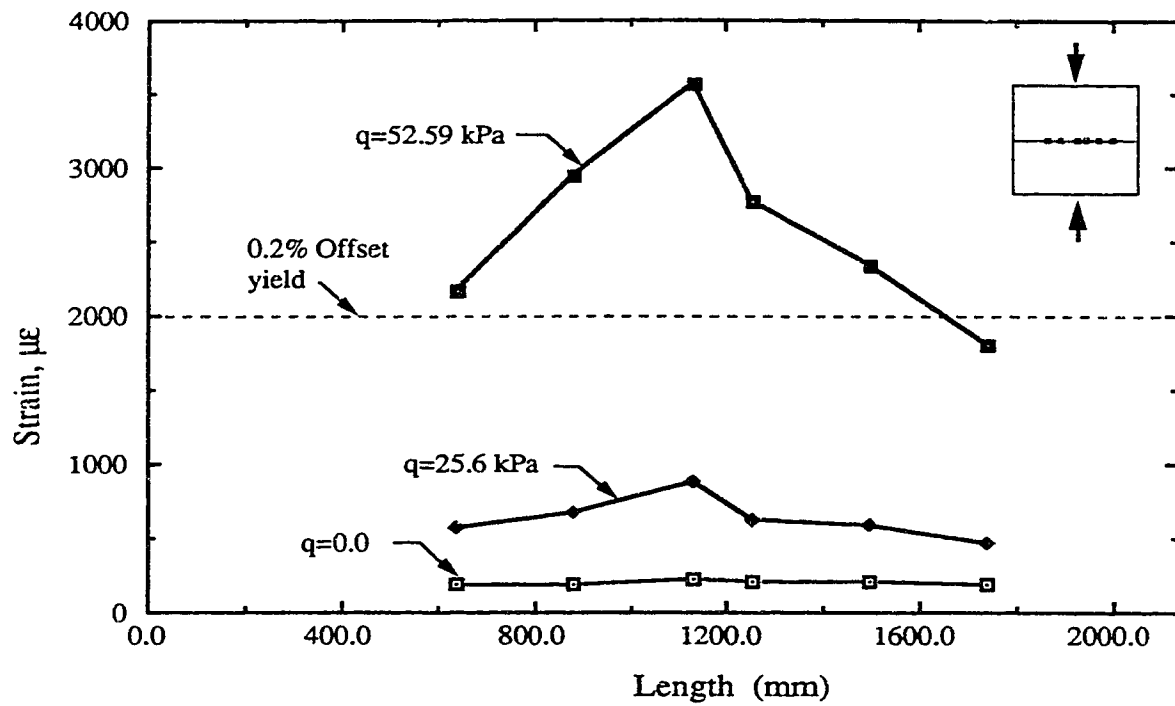


Figure 3.31 Steel Strains along the Transverse Bottom Bar at the Center of Specimen C2

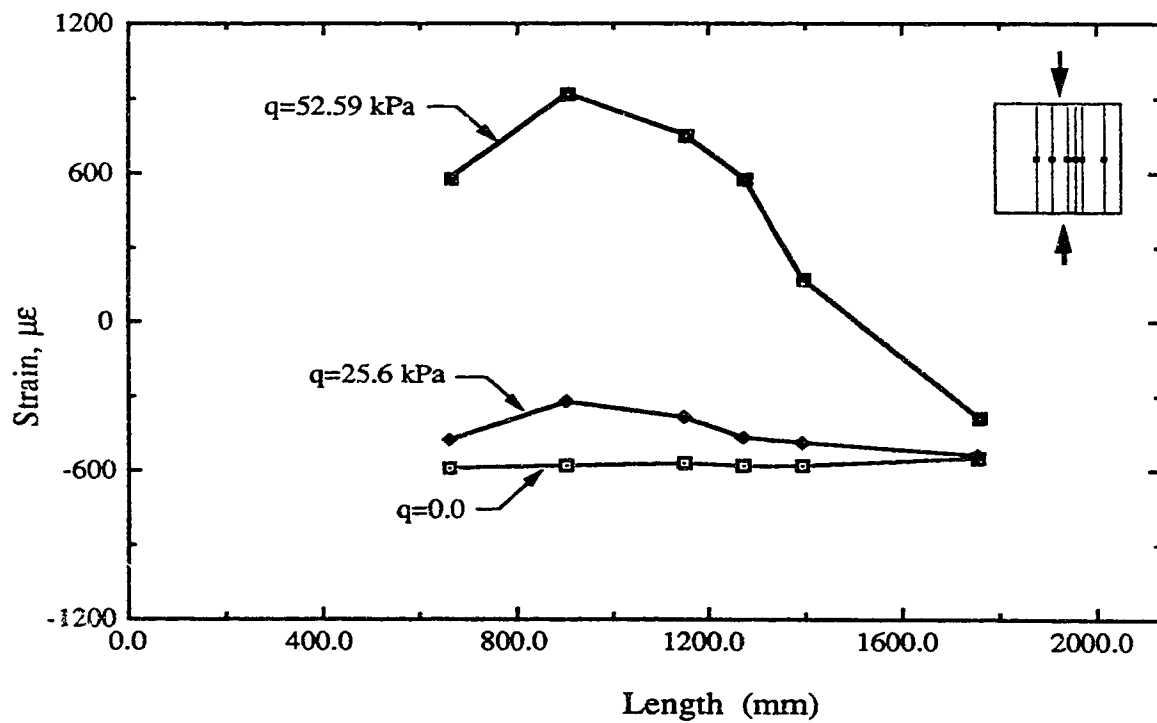


Figure 3.32 Steel Strains at the Center of Specimen C2 in Bottom Bars in the Direction of the Inplane Load

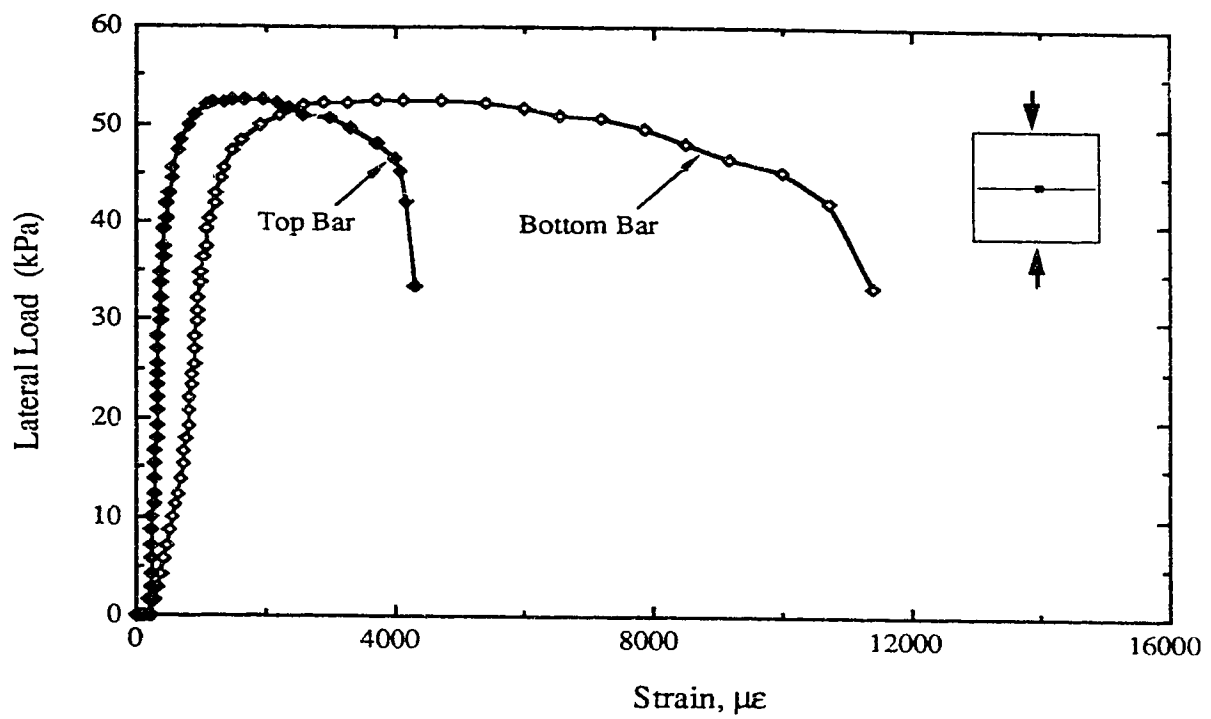


Figure 3.33 Lateral Load versus Transverse Steel Strains at the Center of Specimen C2

4. Evaluation of Test Results

4.1 Introduction

In this chapter an evaluation is made of the parameters which affect the behaviour of reinforced concrete plates which are simply supported on four edges and subjected to combined inplane compressive and lateral loads. Particular attention is paid to the effect of each parameter on the cracking behaviour, ultimate capacity, and failure mode.

For all but three of the specimens subjected to both inplane and lateral loads, the inplane load was applied first to its selected value and kept constant while the lateral load was being applied. Sections 4.2 through 4.5 deal with plates loaded in this way. The effect of the loading sequence was examined using the specimens of series C (C3, C8, and C9) tested under different loading sequences as discussed in Section 4.6.

4.2 Effect of Load Type and Plate Slenderness

Loading type and panel slenderness are two interdependent parameters that should be linked together when assessing plate behaviour. For lightly reinforced sections, the presence of a moderate value of axial force increases the cracking moment, the flexural stiffness, and the moment capacity of the cross section. On the other

hand, at the member level the effects of the inplane forces may be interpreted as being made up of two compensating effects: the flexural rigidity and the strength of the member increase in the direction of the inplane load and this translates into smaller member deflection and higher capacity. This may be offset by the interaction of the inplane load and the geometrical nonlinearity which magnifies the applied bending moments.

4.2.1 Load-Deflection Response and Ultimate Strength

Figs. 4.1, 4.2 and 4.3 illustrate the effects of load type on the response of slender square plates, slender rectangular plates, and stocky square plates.

In Fig. 4.1, the lateral load versus out-of-plane center deflection responses of slender square specimens subjected to different load combinations are presented. Specimen C1 was tested under lateral load only, specimen C2 was tested under combined uniaxial inplane and lateral loads, and specimen C6 was tested under combined biaxial inplane and lateral loads. The same level of inplane load was applied to specimens C2 and C6. It can be seen that specimen C6 had a slightly stiffer response in the precracking stage, presumably because of the increase of the initial stiffness of concrete as it was subjected to equal biaxial compressive stresses over the whole depth which delayed the formation of microcracking. Only in specimen C1 is there a perceptible change in stiffness upon first cracking. The cause of such behaviour is associated with the sudden

transfer of the force carried by concrete at the interface of the crack to the reinforcing bars. In specimens C2 and C6, no such sharp transition occurs. Instead, both specimens exhibit a slower deterioration of stiffness since the progression of cracking was much more gradual due to the presence of the inplane forces. In specimen C1, cracking occurred simultaneously in both directions, while in C2 cracking occurred first parallel to the inplane load followed some time later by cracking perpendicular to the inplane load. Relative to specimen C1, the lateral load reduction for specimen C6 was a meagre 6% while that for specimen C2 was significantly higher (29%). This indicates that for specimen C6, the geometrical nonlinearity effect was, to a great extent, counterbalanced by the increase in the section capacity of the plate in the two orthogonal directions.

The effect of the presence of inplane compressive load applied along the short sides of long rectangular plates can be presented by contrasting the behaviour of specimen A1, tested under lateral load only, and specimen A2, tested under combined inplane and lateral loads (Fig. 4.2). The lateral load capacity of specimen A2 was 55% of that of A1.

It can be observed that the lateral load carrying capacity of slender plates was reduced significantly due to the presence of the uniaxial inplane compression. The reduction is more pronounced, however, for rectangular specimens. In square plates subjected to combined uniaxial compression and lateral loads the increase of the flexural capacity of the plate in the direction of the inplane load compensated for part of the increase of the static moment due to

geometric nonlinearities. On the other hand, the flexural capacity of the short direction, which is the main contributor to the plate strength in the rectangular specimens, was not affected by the application of the inplane load along the short sides. Also, the out-of-plane deflections of rectangular plates are much larger than those of square plates and hence the interaction of the inplane load and the geometrical nonlinearity starts to play its role early in the lateral loading history.

Lateral load versus out-of-plane deflection plots of specimen D1, tested under lateral load only, and specimen D2, tested under combined uniaxial inplane and lateral loads, are given in Fig. 4.3. Both specimens had a width-to-thickness ratio of 19.7. The initial responses of the two specimens were similar. Simultaneous cracking of the two orthogonal directions in specimen D1 led to a dramatic change of slope in the load-deflection curve due to the reduction of the effective moment of inertia of the plate sections. Specimen D1, as a result of extensive yielding of the reinforcement, exhibited progressively more ductile response. Specimen D2, conversely, demonstrated a stiffer load-deflection response and a more brittle failure as a result of the presence of the inplane load. The enhanced strength of specimen D2 indicates that the secondary moments due to the inplane load consumed only a part of the increased moment capacity of the plate section in the direction of the inplane load. This behaviour is very different from that of specimens C1 and C2 in Fig. 4.1. In specimen C2, the increase in the secondary moments exceeded the increase in section capacity due to the inplane loads.

The strains developed in the bottom reinforcement at the center of specimens D1 and D2 are given in Fig. 4.4. In specimen D2, this reinforcement was normal to the inplane load direction. As the lateral load increased, cracks progressively formed at the center of specimen D1 and tensile strains developed at a considerably lower lateral load than they did in specimen D2. This is attributed to the fact that the direction of inplane load application in specimen D2 had a larger flexural rigidity as compared to the normal direction and hence attracted more lateral load.

At the ultimate load, the compressed concrete in all the specimens which were tested under combined loads was in a state of biaxial compression at the middle of the plate since the principal moments were both positive (Note that in the specimens tested under lateral loads only, the flexural cracks near the middle of the plate penetrated to the top surface of the plate). Kupfer et al. (1969), and Lui et al. (1972) have shown that under conditions of biaxial compression, the compressive strength of concrete is increased up to 25%. While that increase in the concrete strength would result in relatively small effects on the flexural behaviour of sections subjected to bending moments only, it has a significant effect on the flexural behaviour of sections subjected to combined axial forces and bending moments. For the cross sections of specimen C6, the moment-curvature diagrams indicated that an increase of concrete strength of 16%, would result in increase in the flexural strength and stiffness of about 15% at the corresponding axial load level. Also, for biaxial compression, concrete exhibits an increased initial stiffness

that may be attributed to the Poisson effect and the confining of the compression zone which increases the maximum usable strain.

4.2.2 Failure Modes

4.2.2.1 Specimens under Lateral Loads Only

Specimens tested under lateral loads only did not collapse nor did they experience an apparent overall loss in their carrying capacity even though they underwent very large deflections.

The successful redistribution of bending moments and the formation of yield-lines were to be expected in plates tested under lateral loads only since the reinforcement contents were low and hence sections were ductile. The yield-line mechanism in these plates developed early in the loading history for each plate. All that happened at the predicted yield-line capacity was that the deflections increased more rapidly, the load went on rising. Table 4.1 compares the predicted yield-line capacities, based on the 0.2% offset yield and neglecting the effect of corner levers, to the measured maximum loads for specimens tested under lateral loads only.

In this investigation, very little restraint was applied to the specimen in its plane by the reaction frame. As a result, the fact that the four plates tested under lateral loads only carried loads much higher than their theoretical collapse load determined by the yield-line theory is attributed in part to the increased flexural strength

due to the stress-strain characteristics of steel and also to the tensile membrane actions which developed at high deflections.

Because the stress-strain curve of the reinforcement used in this study did not have a yield plateau, any increase in rotation at any section met with increased resistance at all levels of loading. As a result, a stage when rotation occurred freely was never reached. A moment-curvature diagram (See Fig. 5.5 for example) would indicate an increase of about 20 percent past yielding. At large deflections the flexural cracks penetrated to the top surface in the middle third of the plate. The central region of the plates tended to move inwards but was restrained from doing so by the outer regions. The result is an outer ring of compression supporting the tensile membrane forces in the central region of the plate. This led to an increase in the carrying capacity due to the stronger combined bending and tensile membrane actions. The development of membrane forces in plates in which inplane movement of the edges can occur freely was also reported by Taylor et al. (1969).

It should be noted that although the enhancement of the strength of a plate by tensile membrane action can develop within a plate simply supported along its edges, such action occurs only at large deflections of the plates, usually after the formation of yield-lines. From observation of specimens tested under lateral loads only, it is clear that the tensile membrane action does not alter the mechanism of collapse. That is, the increasing deflections occur by rotation of the segments of the plate bounded by the yield-lines formed earlier.

4.2.2.2 Specimens under Combined Inplane and Lateral Loads

The failure of plates tested under combined loads was either caused by compressive crushing because of the limited deformability of concrete in compression or by instability of the plate because with the increase in deflection, the applied load moments and the secondary moments increased more rapidly than the internal resisting moments.

Although the modes of failure can become indistinct in some cases and it is sometimes difficult to distinguish between the two modes, the following observations can be made. The mode of failure of the rectangular specimens in which the inplane load was applied along the short sides was material failure that was associated with crushing of concrete after extensive yielding of the tension steel running in the short direction, normal to the direction of the inplane load. Large deflections, coupled with the presence of axial compression forces, resulted in large secondary moments which led to accelerated hinging at sections where yield started. Strain hardening of the steel running in the short direction, normal to the inplane load direction, contributed to a slowly increasing ultimate lateral load capacity after the formation of the collapse mechanism. Ultimately, the ductility of the load-deflection response was limited by brittle crushing of concrete. The stocky square specimen D2 failed suddenly and catastrophically shortly after reaching its maximum lateral load as the compressive strain capacity of some hinging

sections was exhausted. Concrete crushing in this specimen was accompanied by yielding of the transverse steel at the center.

Instability with partial plasticity was the cause of failure of the slender square specimens and rectangular specimen B4 in which the inplane load was applied along the long sides. Instability failures of these specimens were followed by crushing of concrete and buckling of the reinforcement in the direction of the inplane load as postfailure phenomena.

4.3 Effect of Inplane Load Level

The level of the inplane load for all specimens was moderate, in the sense that there was no possibility of collapse under the inplane load alone. Table 4.2 gives the ratio of the applied inplane load per unit width to the uniaxial strength of concrete multiplied by the panel thickness for all of the specimens. Also included in Table 4.2 are the ratios of the applied inplane load to the balanced load for each specimen. There was a difficulty in defining the balanced failure conditions in a meaningful fashion, since there was no sharp break in the steel stress-strain curve. The strengths of plate cross sections were represented by axial load-bending moment interaction curves. In constructing these diagrams, concrete in tension was neglected, the section was considered to have failed when the strain in the concrete at the extreme compression fibers reached 0.0038, the stress-strain relationship of concrete proposed by Todoshini et al. (1964), with $f_c' = 0.85 f_c'$, and the actual stress-strain relationship of

the steel were used. The load corresponding to the break point in the interaction curve was called the balanced load and used in Table 4.2. Figs. 4.5 and 4.6 show the interaction diagrams for the cross sections of specimens C2 and C4 in direction of the inplane loads.

The lateral load versus out-of-plane center deflection curves for specimens B2 and B3, tested under inplane loads of 1.09 and 0.74 times the balanced load, respectively, are shown in Fig. 4.7. At the applied inplane load levels, the moment capacity of the specimen B2 cross section is 25% higher than that of specimen B3. However, the lateral load capacity of these rectangular specimens decreased with increasing inplane load level. Due to the fact that most of the load was carried in the short direction in the rectangular plates, the beneficial effect of the inplane load on the strength of the long direction was more than offset by its second order effect.

The lateral load versus out-of-plane center deflection responses for specimens C6 and C7, tested under different levels of biaxial compression, are presented in Fig. 4.8. Although specimen C6 was subjected to inplane load of 657.8 kN/m while specimen C7 was subjected to 362.5 kN/m, the lateral load capacity of specimen C6 was about 15% higher than that of specimen C7. At the cross section level, the increase in the inplane load magnitude resulted in an increase in the moment capacity of the sections in both directions accompanied by a decrease in their curvatures at any given load. At the member level, smaller curvature translated into smaller deflection and hence smaller secondary effects while the larger moment capacity translated into larger lateral load capacity. It can

also be observed that due to the lower level of inplane load, the final failure was less sudden in specimen C7.

4.4 Effect of the Reinforcement Ratios in the Orthogonal Directions

The effects of the reinforcement ratios in the two orthogonal directions are presented in Figs. 4.9 and 4.10 for the square plates of series C and the rectangular plates of series A tested under combined uniaxial inplane and lateral loads. Specimens C2 and A2 had reinforcement contents of $260.0 \text{ mm}^2/\text{m}$ in both directions, specimens C4 and A3 had reinforcement contents of $520.0 \text{ mm}^2/\text{m}$ in the inplane load direction, and $260.0 \text{ mm}^2/\text{m}$ in the transverse direction, and specimens C5 and A4 had reinforcement contents of $260.0 \text{ mm}^2/\text{m}$ in the inplane load direction, and $520.0 \text{ mm}^2/\text{m}$ in the transverse direction.

For both the square and rectangular plates, the carrying capacity was affected more by the reinforcement transverse to the inplane load direction. This would be expected since in lightly reinforced sections under pure bending the ultimate moment capacity is affected almost linearly by the reinforcement content. On the other hand, in sections subjected to combined axial force and bending moments, the flexural strength is more affected by the level of the axial force than the reinforcement content.

The change in behaviour with the change in the reinforcement ratio was particularly noticeable for rectangular specimens. Doubling

the steel in the inplane load direction increased the lateral load capacity of the rectangular and the square specimens by 9% and 13%, respectively. On the other hand, doubling the transverse steel increased the lateral load capacity of the rectangular and square specimens by 54% and 29%, respectively. This is not surprising since in the rectangular specimens most of the applied lateral load, as well as that resulted from the second order effect, were carried to the supports by strips spanning in the short direction.

It can also be observed that plates with higher steel contents normal to the inplane load direction have a stiffer response in terms of load-deflection behaviour. This trend is primarily due to the improved moment-curvature response due to the larger amount of reinforcement.

4.5 Effect of Aspect Ratio

The aspect ratio parameter has been partially discussed in section 4.2 while comparing the behaviour of square and rectangular specimens under combined uniaxial inplane and lateral loads. In those rectangular specimens, the inplane load was applied along the short sides.

Lateral load-out-of-plane deflection characteristics for specimens B1, B2, and B4 are given in Fig. 4.11. Specimen B1 was tested under lateral load only, while specimens B2 and B4 were tested under combined uniaxial compression and lateral loads. In specimen B2 the inplane load was applied along the short sides

giving a ratio of loaded edge to unloaded edge length of 0.67 while for specimen B4 the same value of the inplane load was applied along the long sides giving a loaded to unloaded edge ratio of 1.5.

In both specimens tested under combined inplane and lateral loads, the lateral load capacity was substantially reduced compared to specimen B1. While the initial stiffness of specimen B4 was higher than that of specimen B2, there was a marked decrease in its lateral load capacity.

With the inplane load applied along the long sides, specimen B4 received less support from the short sides and its central portion became more and more like a wide beam-column. It should be noted, however, that the enhanced flexural capacity of the plate sections in the short direction, due to the presence of the inplane load, compensated for part of the reduction of the plate action and hence the effect of the aspect ratio was less than one would expect for metal plates under combined loads.

The initially stiffer response of specimen B4 is attributed to the delay of cracking of the short direction as a result of the presence of the inplane compressive load.

4.6 Effect of Loading Sequence

Four slender square specimens were subjected to different loading sequences in order to study the effect of load history on the different aspects of behaviour of plates under combined loads. In

specimen C2, the inplane load was first applied to its full value of 653.9 kN/m and then held constant while lateral load was applied giving an ultimate value of 52.59 kPa. In specimen C3, the inplane and lateral loads were applied simultaneously and proportionally based on the ultimate values of specimen C2 which had been tested earlier. This produced a failure at a lateral load of 51.56 kPa and an inplane load of 647.0 kN/m, essentially the same as specimen C2. In specimen C9, the lateral load was applied up to 52.5 kPa and kept essentially constant as explained in Section 2.7 while the inplane load was increased until failure. In this case, the inplane failure load was 342.4 kN/m which is about 52.0% its value in specimen C2. Specimen C8 was first subjected to a lateral load of 24.5 kPa which resulted in a steel strain of about 0.0019 at the center of the plate. This value of the lateral load was kept constant while the inplane was increased from zero to 654.0 kN/m, which was the same value applied to specimen C2. Finally, this value of the inplane load was maintained constant and the lateral load was increased again until failure. The maximum lateral load was 50.88 kPa. The four loading sequences are shown in Fig. 4.12.

The lateral load versus out-of-plane center deflection curves for the above four specimens are shown in Figs. 4.13 and 4.14. It can be seen that the overall behaviour as well as the ultimate strength of plates tested under combined loads are largely affected by the sequence of loading. The first two loading paths resulted in very little difference both in the ultimate strength and the stiffness of the plates. Although the behaviour of specimen C8 was softer in the

initial part due to the cracks caused by the lateral load in the absence of the inplane load, its ultimate strength was not significantly affected by the load path. The reduction in strength due to different load sequences was more pronounced in specimen C9 since the beneficial effects of the inplane load could not be utilized due to the extensive cracking and large deflections caused by the lateral load.

It seems unlikely that reinforced concrete plates would, in normal practice, be subjected to a loading of the sequence occurred in specimen C9. Primarily, however, the test was included to serve as an extreme boundary in assessing the effect of loading sequence. Hence, it would appear that for slender square plates, subjected to combined uniaxial inplane and lateral loads, the influence of load path on the maximum strength is insignificant even if the lateral load is applied first to a level that results in stresses in steel and cracks in concrete within the serviceability limit states. This conclusion can not, however, be extended directly to plates of other aspect ratios.

Table 4.1 Test Results and Predicted Yield-Line Capacities for Specimens Tested under Lateral Loads Only

Specimen	$\frac{a}{b}$	$\frac{b}{h}$	q(Test)	q(Yield-line)*	$\frac{q(\text{Test})}{q(\text{Yield-line})}$
Designation			(kPa)	(kPa)	
A1	2.17	27.18	39.69	23.62	1.68
B1	1.50	26.82	45.91	29.12	1.58
C1	1.00	26.98	73.88	42.80	1.72
D1	1.00	19.71	109.39	89.26	1.23

* Based on 0.2% offset yield and neglecting the effect of corner levers.

Table 4.2 Levels of Applied Inplane Loads

Specimen Designation	N_x	N_y	N_x	N_y
	$f'_c \cdot h$	$f'_c \cdot h$	N_x balanced	N_y balanced
A1	0.0	0.0	0.0	0.0
A2	0.0	0.399	0.0	1.063
A3	0.0	0.393	0.0	1.067
A4	0.0	0.391	0.0	1.067
B1	0.0	0.0	0.0	0.0
B2	0.0	0.399	0.0	1.094
B3	0.0	0.272	0.0	0.737
B4	0.380	0.0	1.173	0.0
C1	0.0	0.0	0.0	0.0
C2	0.0	0.383	0.0	1.089
C3*	0.0	0.373	0.0	1.106
C4	0.0	0.370	0.0	1.094
C5	0.0	0.361	0.0	1.088
C6	0.384	0.384	1.096	1.164
C7	0.214	0.214	0.604	0.647
C8*	0.0	0.374	0.0	1.138
C9*	0.0	0.206	0.0	0.590
D1	0.0	0.0	0.0	0.0
D2	0.0	0.365	0.0	1.040

* For loading sequence, refer to Figure 4.12.

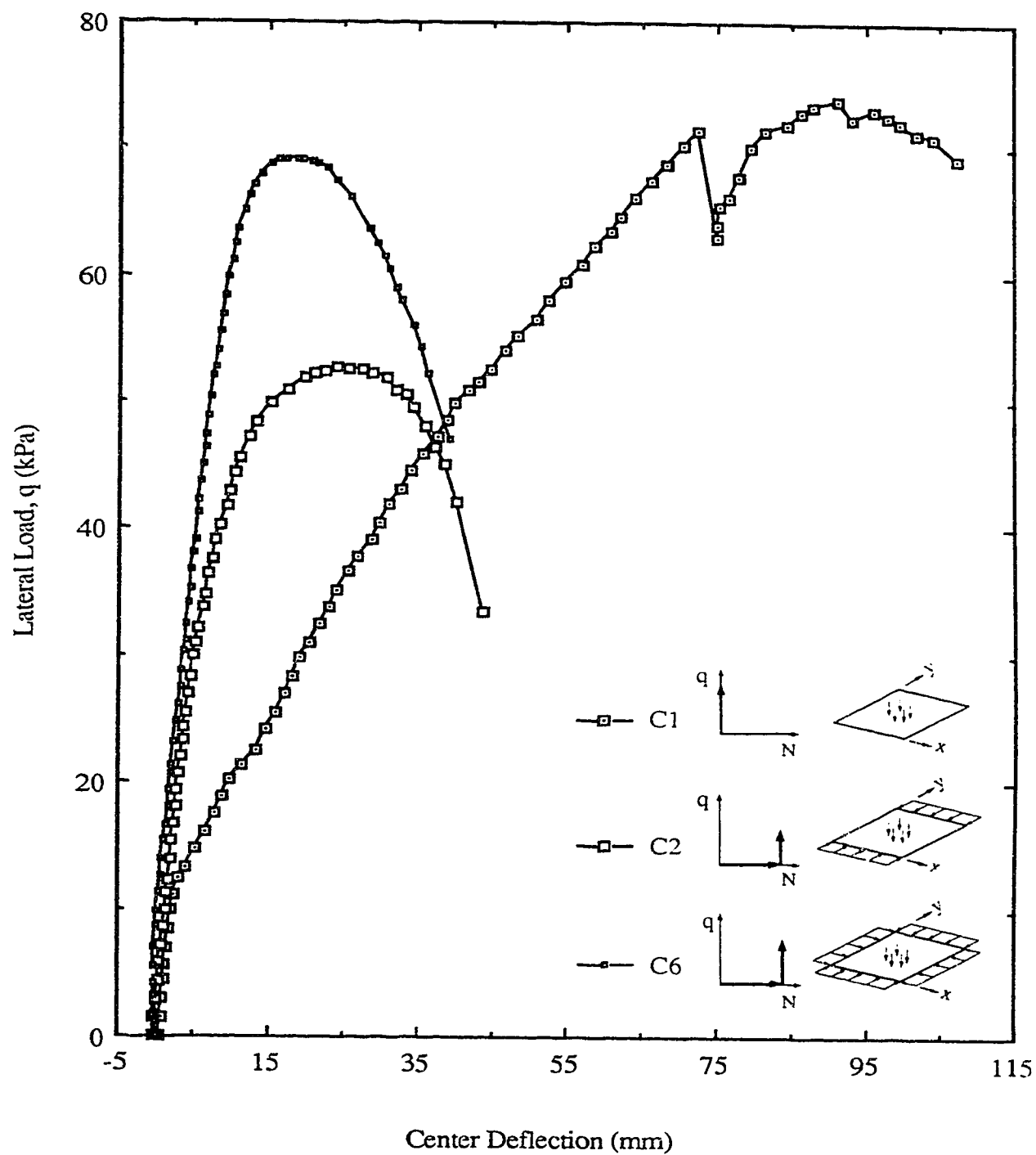


Figure 4.1 Effect of Loading Type for Slender Square Plates

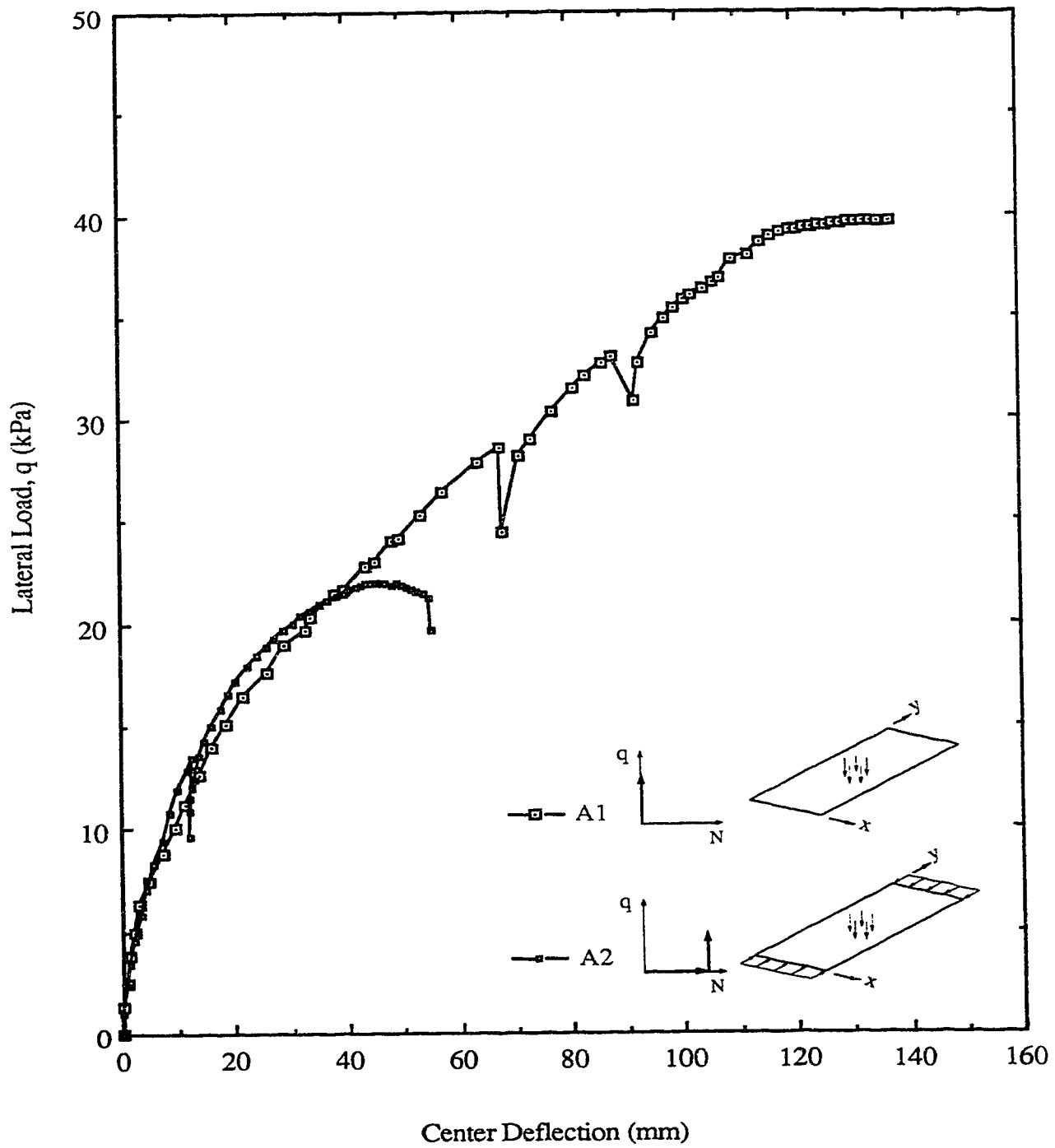


Figure 4.2 Effect of Loading Type for Rectangular Plates, $a/b = 2.17$

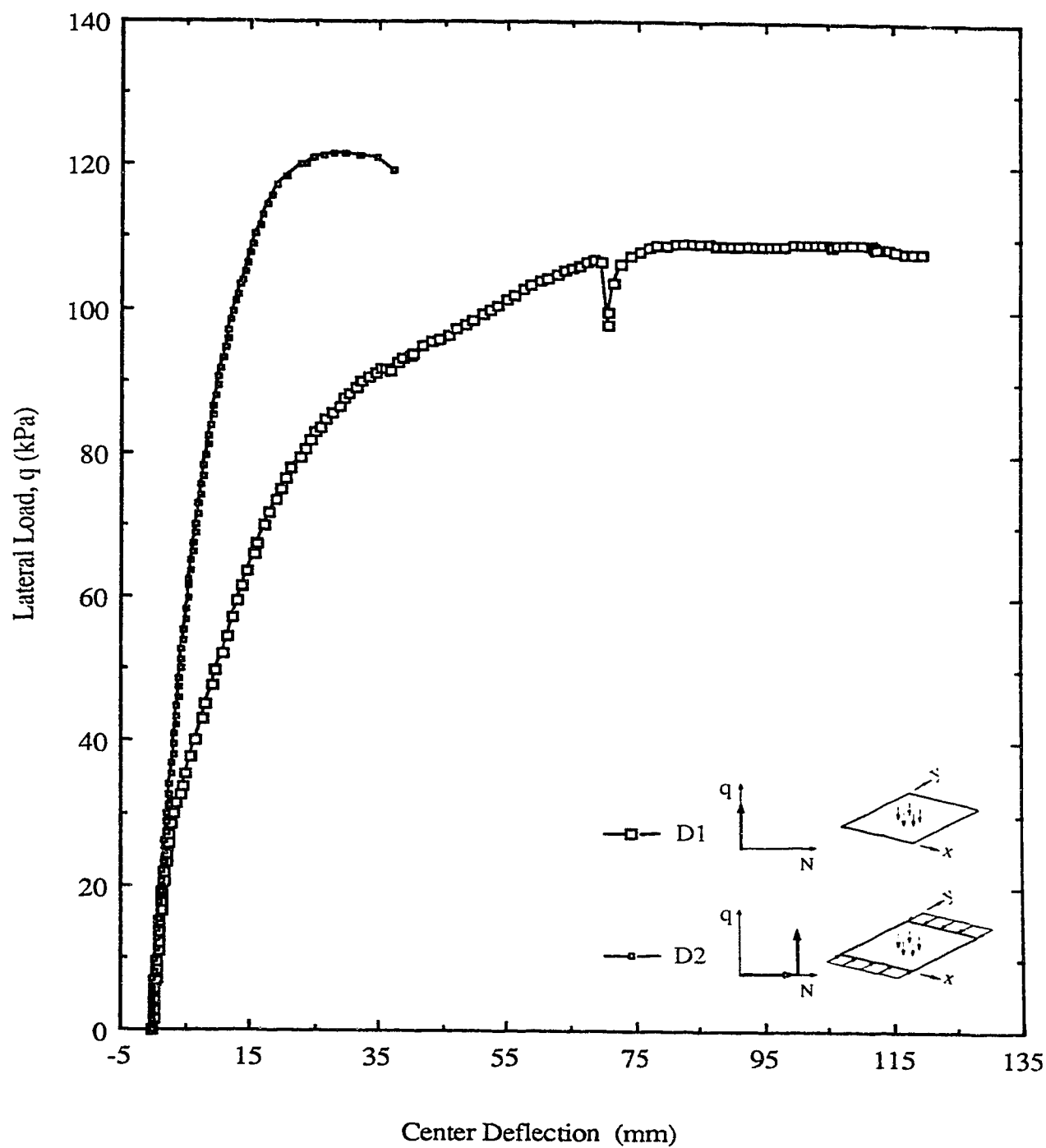


Figure 4.3 Effect of Loading Type for Stocky Square Plates

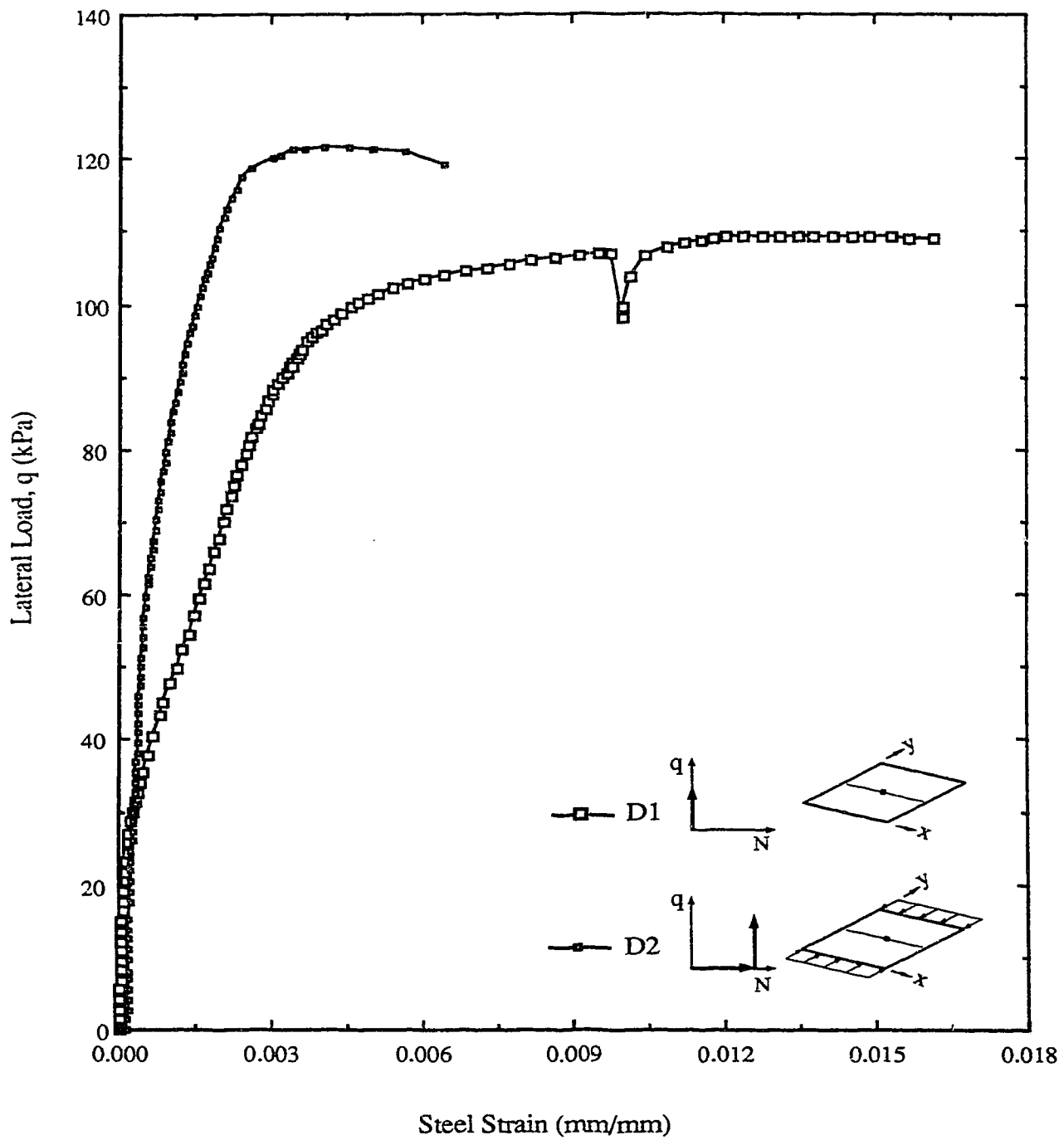


Figure 4.4 Lateral Load versus Transverse Bottom Steel Strains for Specimens D1 and D2

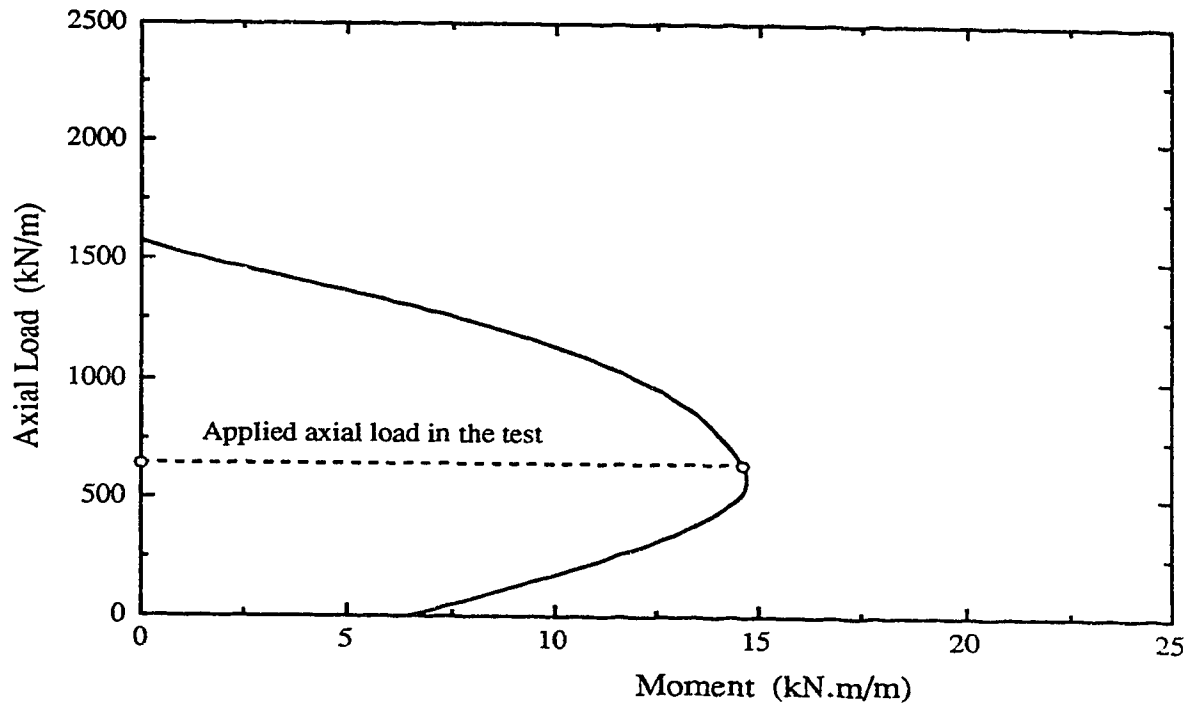


Figure 4.5 Interaction Curve for a Section of Unit Width of Specimen C2
in the Direction of the Inplane Load

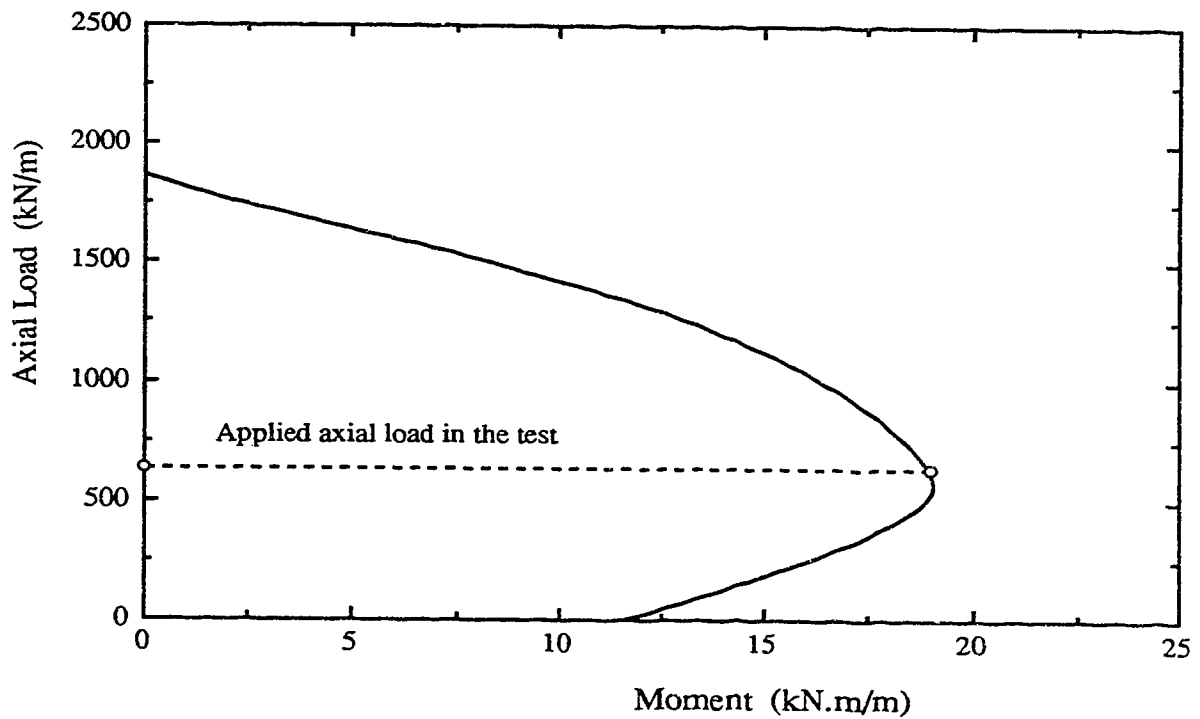


Figure 4.6 Interaction Curve for a Section of Unit Width of Specimen C4
in the Direction of the Inplane Load

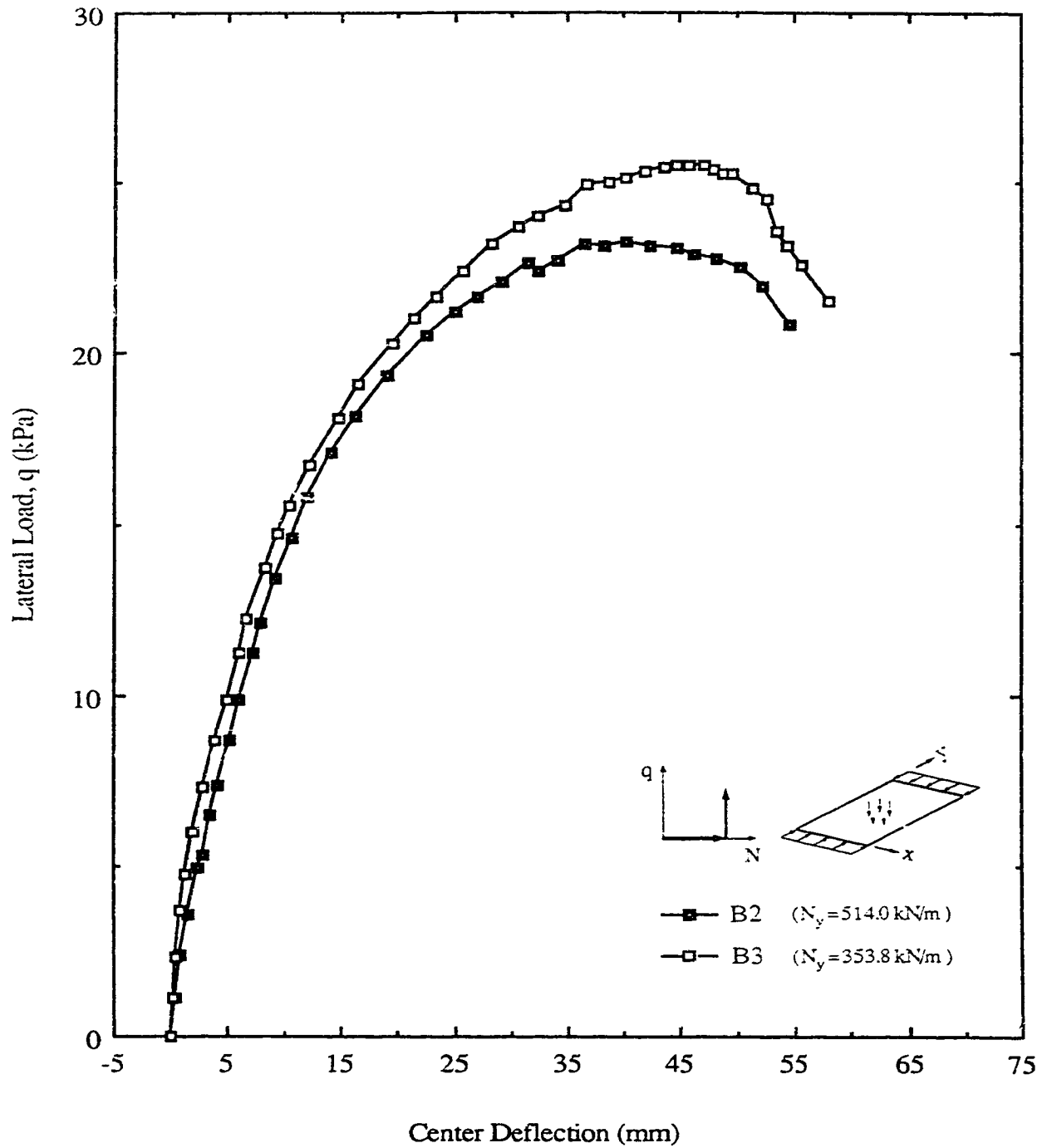


Figure 4.7 Effect of Inplane Load Level for Rectangular Plates, $a/b = 1.5$

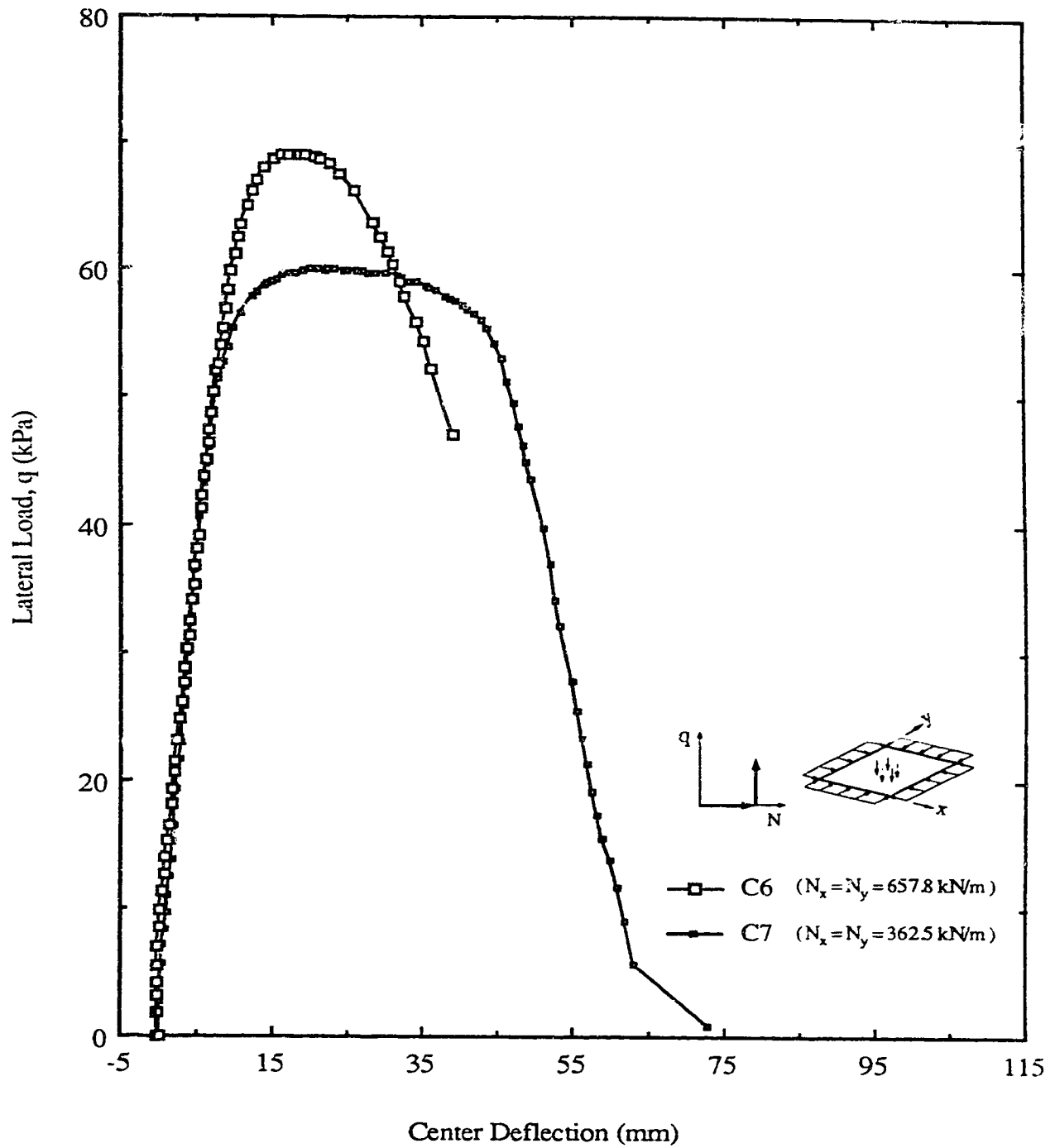


Figure 4.8 Effect of Inplane Load Level for Slender Square Plates

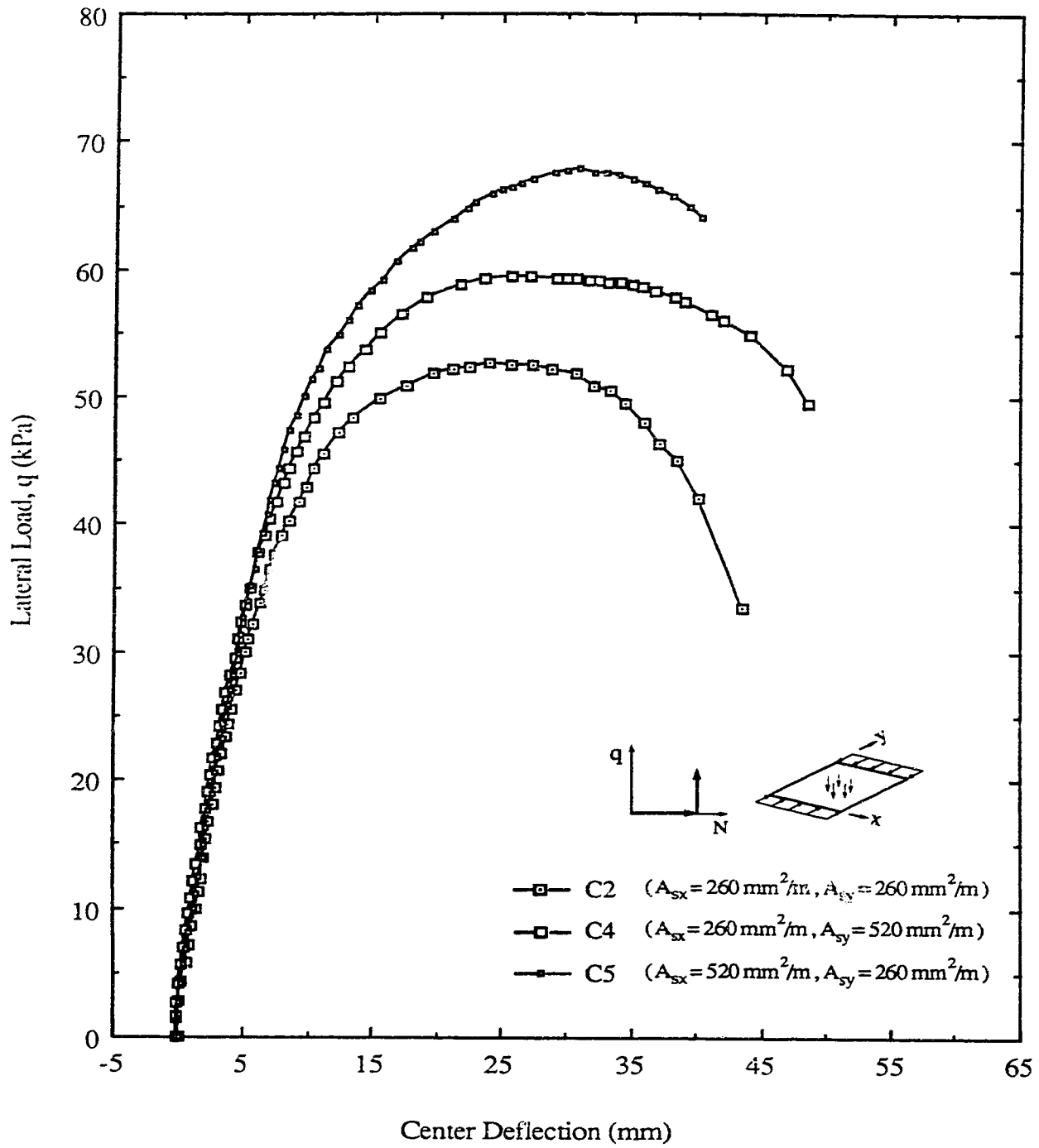


Figure 4.9 Effect of the Reinforcement Ratios in the Two Directions for Square Plates

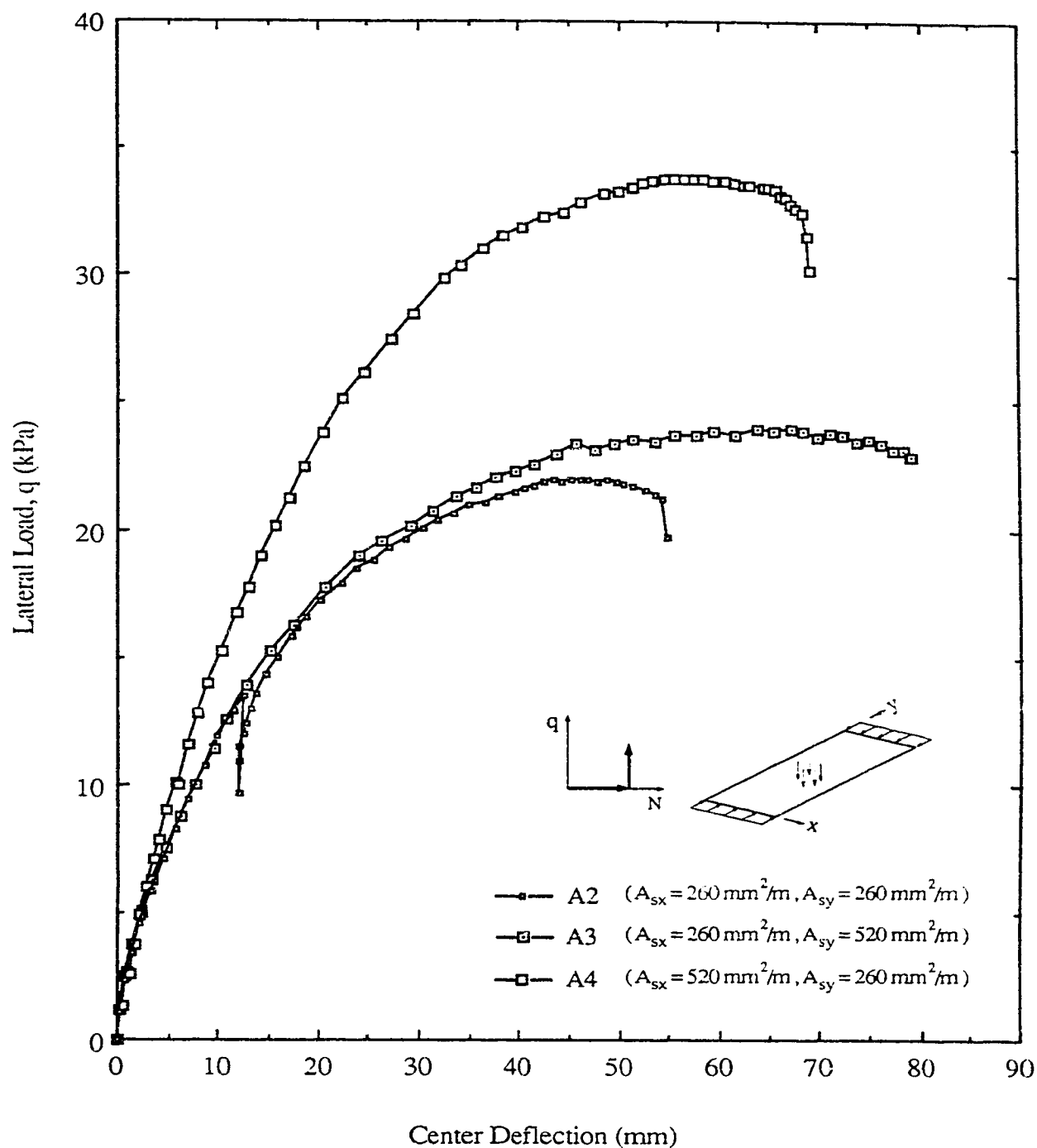


Figure 4.10 Effect of the Reinforcement Ratios in the Two Directions for Rectangular Plates, $a/b = 2.17$

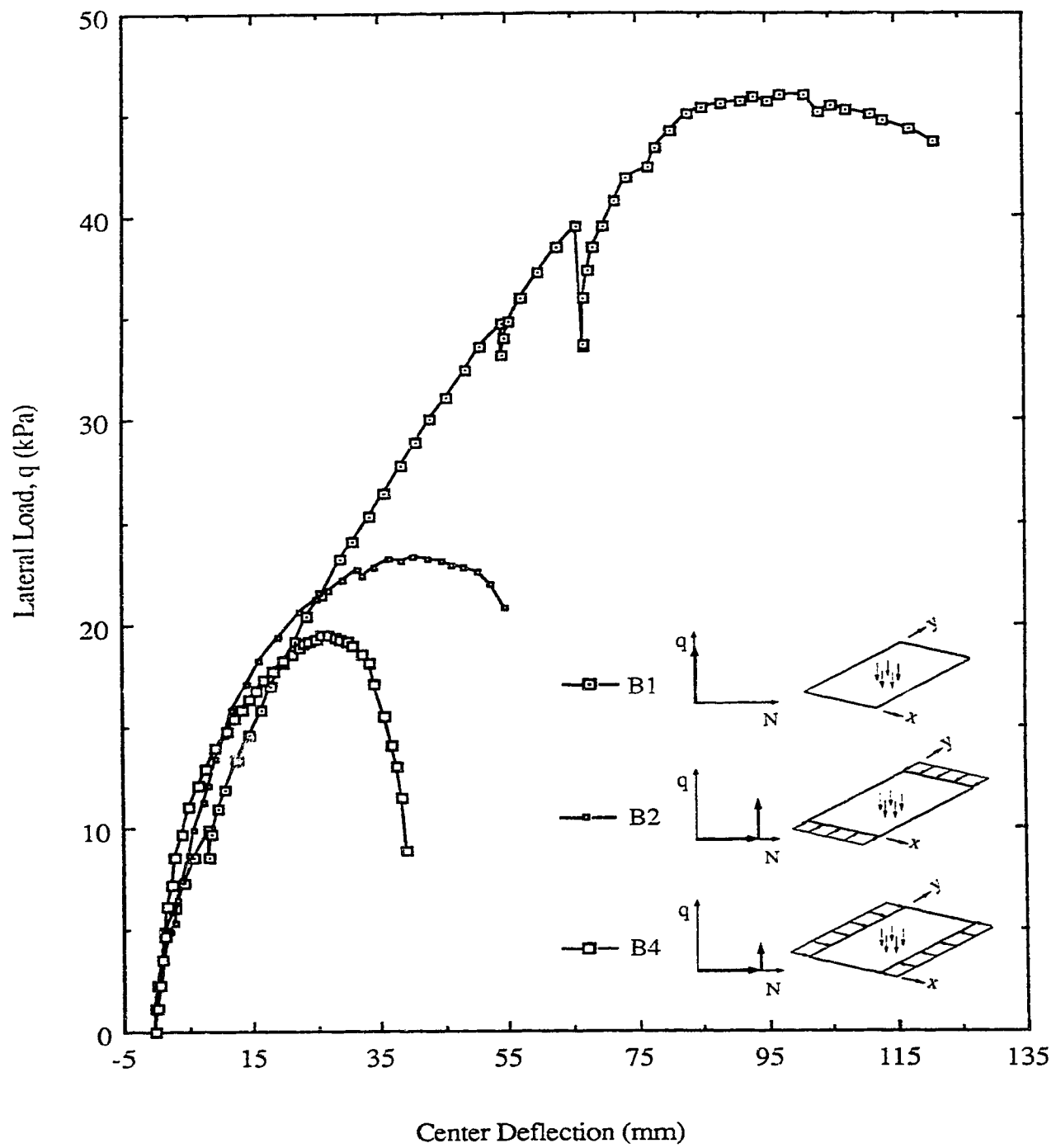
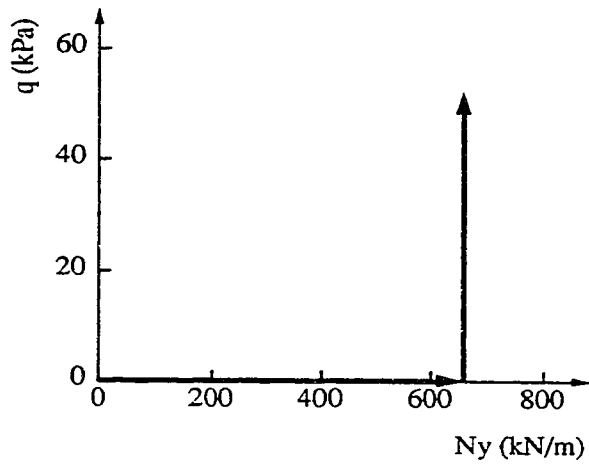
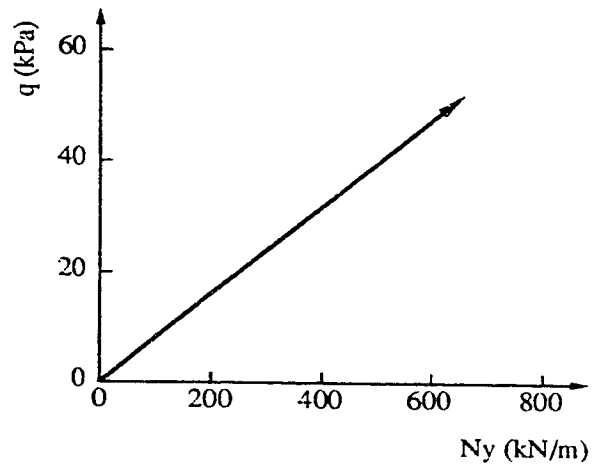


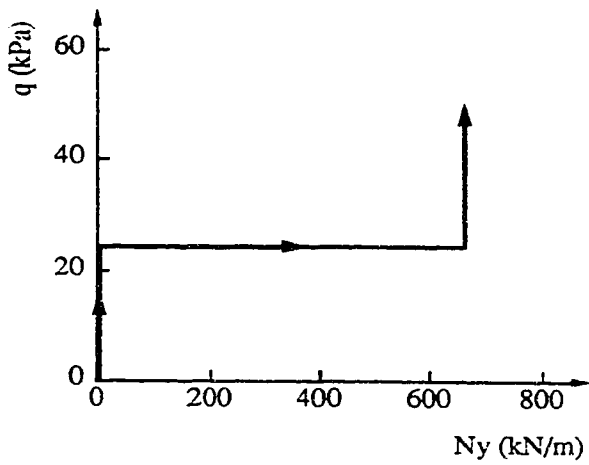
Figure 4.11 Effect of Aspect Ratio



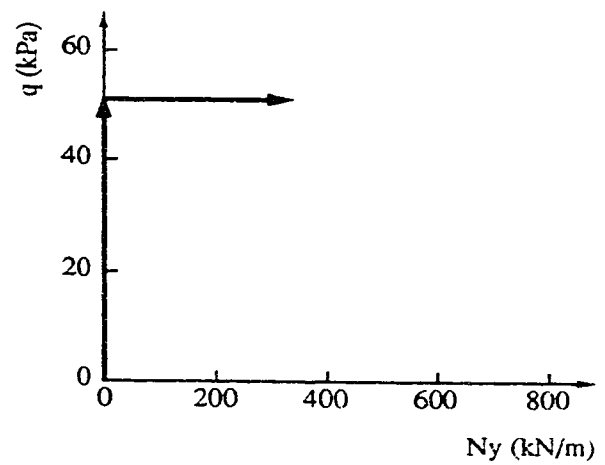
(a) Specimen C2



(b) Specimen C3



(c) Specimen C8



(d) Specimen C9

Figure 4.12 Loading Sequences

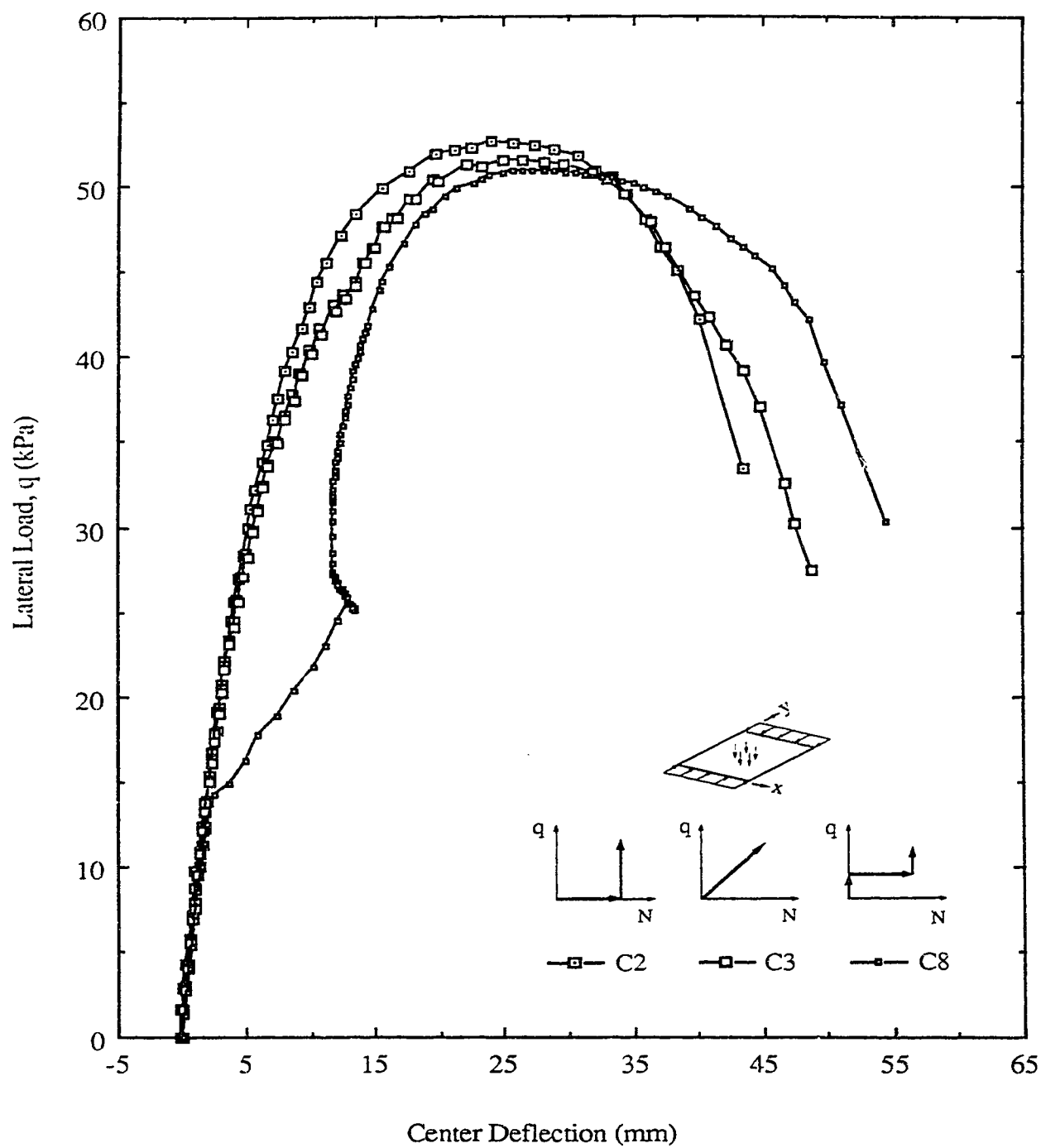


Figure 4.13 Effect of Loading Sequence for Slender Square Plates, Specimens C2, C3, and C8

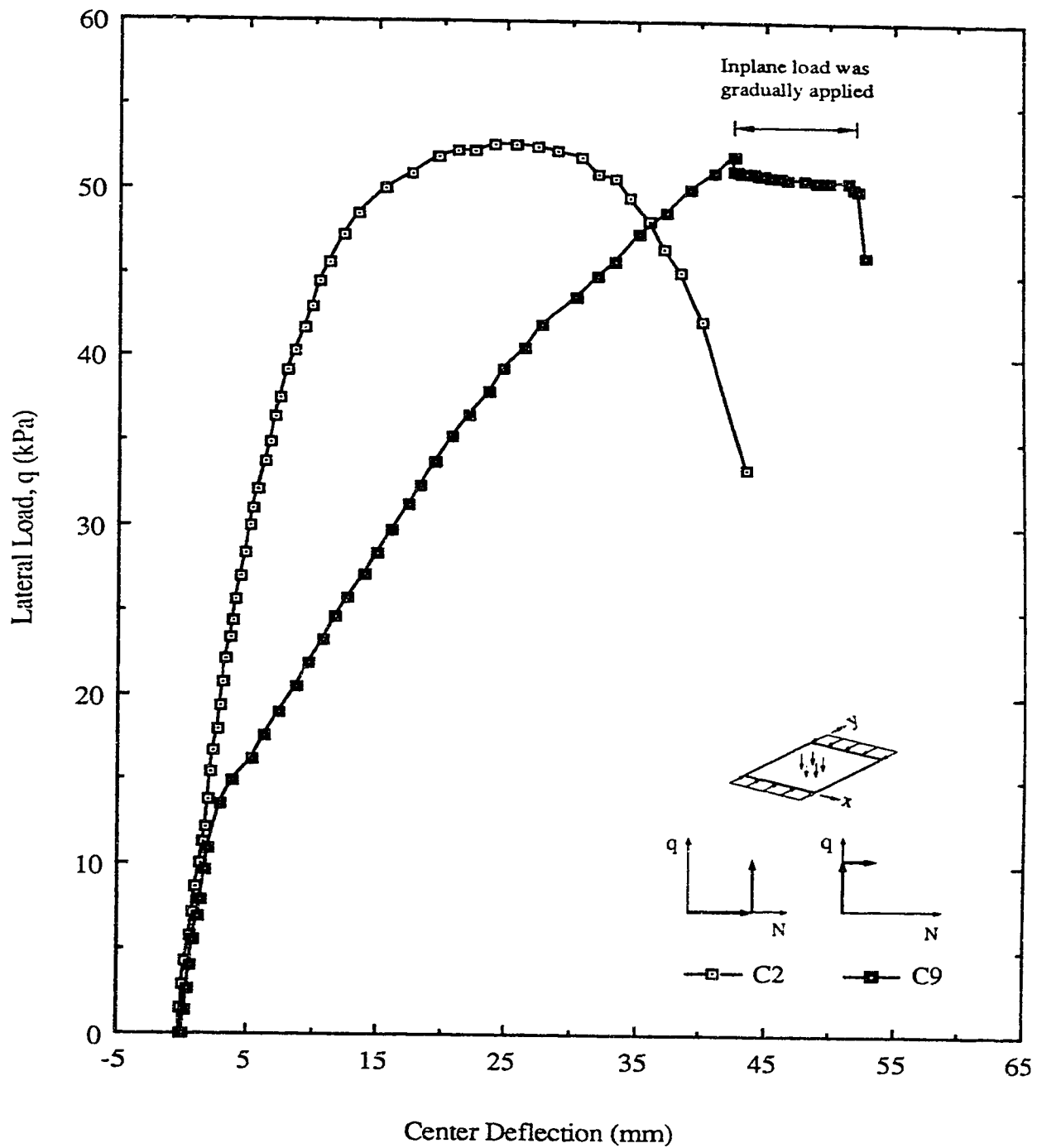


Figure 4.14 Effect of Loading Sequence for Slender Square Plates, Specimens C2 and C9

5. Analytical Model

5.1 Introduction

The prediction of the behaviour of reinforced concrete plates subjected to combined inplane and lateral loads is complicated by two types of nonlinearity. The first, geometrical nonlinearity, results from the influence of the deflections on the total moments. This effect is also often referred to as "second order effect". The second type of nonlinearity is due to the nonlinear material response of steel and concrete. The material nonlinearity results in a nonlinear moment-curvature relationship which is dependent on the reinforcement and axial load.

Several attempts have been made in the past to apply the methods of limit analysis to plates subjected to externally applied lateral loads and internally induced inplane loads (due to support conditions) Park, (1964), or externally applied inplane and lateral loads, Girolami et al. (1970). However, these methods are limited to situations where tension steel yields. This will be the case only for small inplane loads since if inplane loads are high, the tension steel will not yield at failure, and limit analysis will not be valid. To determine the ultimate lateral load using the limit analysis, the value of the central deflection at the ultimate load must be known. The determination of the deflection at the ultimate load has caused difficulty since it depends on several factors; the most acceptable

approach at present is probably to examine the range of experimentally determined values for the ratio of the deflection/span and to select a safe empirical value.

In this chapter, a simple analytical model based on Fourier series expansion of the deflection and lateral load is presented. To take into account the nonlinear material response the theory of elasticity, based on secant rigidities obtained from analytically derived moment-curvature relationships, is used to determine the behaviour of the reinforced concrete plates. The geometrical nonlinearity is incorporated in the governing differential equation.

5.2 Load-Moment-Curvature Relationship

The nonlinear behaviour of a concrete member is characterized mainly by the load-moment-curvature relationship of its cross section.

The analytical methods developed to calculate the moment-curvature relationship are based on the application of the basic principles of equilibrium of forces and strain compatibility assuming linear distribution of strain over the cross section, and using idealized but realistic stress-strain relations to represent the behaviour of the reinforcing steel and the concrete. Due to the nonlinear nature of these stress-strain relations, use of numerical procedures rather than closed form solutions has in general been adopted.

Pfrang, Siess and Sozen (1964), presented a numerical procedure to obtain the moment-curvature relationship for cross sections subjected to combined bending and axial compression. Idealized analytical expressions were used to represent the stress-strain relations for the concrete in compression and the reinforcing steel. Tension in the concrete was neglected.

An extensive analytical investigation of the moment-curvature relationships for reinforced concrete cross sections subjected to combined bending and axial compression was undertaken by Chon and Ghosh (1972). The concrete behaviour, as represented by analytical expressions for the stress-strain relationships, was assumed to be nonlinear, strain softening for the concrete in compression and elastic-brittle for concrete in tension, respectively.

The bending stiffness of unstressed or partially prestressed lightly reinforced concrete members tend to be significantly higher than those calculated based on a cracked section analysis. It is not until the tension stiffening effect of the concrete is considered that the analysis becomes realistic.

5.3 Tension Stiffening Effect and Moment-Curvature Relations

The well-established fact that concrete can display significant additional stiffness due to tension stiffening is extensively documented for prestressed and reinforced concrete. Experimental evidence from the test results of Clark and Speirs (1978) on beams

and slabs and Williams (1986) on direct tension showed that even at the strain corresponding to steel yielding, concrete exhibited 20 to 55 percent of its tensile strength.

The two primary factors that contribute to the tension stiffening phenomenon in concrete members are: (1) the effect of uncracked regions between cracked sections, and (2) the fact that concrete does not crack suddenly and completely but undergoes progressive microcracking (strain softening).

Several basically different approaches have been proposed in the literature to allow for tension stiffening effect when deriving the moment-curvature relations of reinforced concrete elements.

The European concrete committee (CEB) (1985, 1990) presented a method that accounts for the effect of tension stiffening on the curvature through an empirical interpolation between the curvatures corresponding to the uncracked and fully cracked sections. The method proved to give satisfactory results for ordinary and high strength concrete (Favre et al. 1990).

Ferry-Borges and Oliveira (1963), developed a numerical procedure for the calculation of the moment-curvature relationship for rectangular and tee-shaped beam segments subjected to combined bending and low levels of axial compression. The tensile strength of concrete was ignored, but the effect of tension stiffening was taken into account by using appropriately adjusted values for the modulus of elasticity for the tension reinforcement, thus yielding the average moment-curvature relationship for a beam segment.

An alternative to the above approaches is to simulate the effects of the tension existing between cracks, bond characteristics, and progressive cracking on the average stiffness of a concrete element by using a fictitious stress-strain relationship for concrete in tension, including a gradually descending branch representing the declining tension stiffening as cracking progresses.

Based on a fracture mechanics approach, Bazant and Oh (1984), proposed a stress-strain curve for plane concrete in tension to be used in deriving the moment-curvature relationship. Strictly, however, their curve is a representative of the strain softening defined as a fracture process zone phenomenon.

Several average "homogenized" tensile stress-strain relationships are proposed in the literature to simulate the tension stiffening effect in the context of moment-curvature analysis: Vebo and Ghali (1977), Carreira and Chu (1986), Prakhya and Morley (1990), among others. Despite the difference among the proposed diagrams, the calculated curvatures agreed well with the experimental results against which they were checked. This is because diagrams with a reasonable descending branch significantly improve the accuracy of the calculated curvatures over that of curvatures from diagrams in which concrete contribution is neglected or a complete unloading is assumed after the tensile strength is reached.

In view of the lack of information regarding the factors governing the bond characteristics, the distribution of the tensile

stress in the concrete, and the progressive development of cracks, it makes little sense to argue whether one or another approach for including the tension stiffening effect is better since only a crude approximation of the overall effects can be achieved regardless of the analytical procedure employed.

In this thesis, tension stiffening will be represented, within the context of moment-curvature relationship, by an assumed stress-strain curve for reinforced concrete in tension as discussed in Section 5.4.2.2.

5.4. Load-Moment-Curvature Relationship for the Present Study

5.4.1 Basic Assumptions

In developing the load-moment-curvature relations, a linear strain distribution is assumed over the cross section at all load levels and the strains in the steel and concrete are assumed compatible. The axial force, which is applied at the section centroid, is assumed to be applied first and held constant while the moments are monotonically increased to their failure values. Moreover, it is assumed that the moment-curvature relationship for bending about one axis is independent of moments about an orthogonal axis.

The last assumption implies that there is no interaction between the effects of the two principal moments. This is equivalent to the yield assumption applied by Johansen to rigid-perfectly-

plastic slab behaviour but in this case it is assumed to apply whether the steel has yielded or not. The effect of this assumption is to allow the slab element to be treated as a one-way slab or equivalent beam for which a simple two-dimensional moment-curvature relationship can be derived.

Although it may not be possible to include the effects of the biaxial state of stresses in the development of a "macroscopic" moment-curvature relationship, it is possible to outline the effects of such a simplification.

From the experimental investigations performed into the effects of biaxial stress states on the behaviour of concrete, it is established that the presence of biaxial compression results in increased ultimate compressive strength, increased ductility, and increased stiffness, the increases depending on the ratio of the two applied stresses. It is also proved that the opposite occurs in the case of biaxial compression and tension. The significance of these findings is that the concrete elements within the plate which are subjected to biaxial compression or biaxial tension and compression are governed by different compressive stress-strain relationships. Hence, it is obvious that in order to include the effects of the biaxial state of stresses, a "microscopic" layered technique, such as the one used in the next chapter, should be adopted.

By neglecting the effects of the biaxial state of stresses in the development of a "macroscopic" moment-curvature relationship, the model will err on the conservative side especially in the case of the

plates which are subjected to biaxial inplane and lateral loads since the confinement of potential microcracking exists all over the compression zone in both directions.

5.4.2 Material Constitutive Laws

5.4.2.1 Concrete in Compression

Under pure flexure, the strength of concrete does not have a significant influence on the flexural capacity and deformation of a section. Under combined flexure and axial compression, concrete strength plays an important role in the determination of the section capacity, particularly if the level of the axial load is significant. The ACI building code (1989) allows the use of any concrete stress-strain relationship in compression that predicts section strength in substantial agreement with the results of comprehensive tests.

The stress-strain relationship adopted for concrete in compression was proposed by Todeschini et al. (1964). For any given concrete strain ϵ , the concrete stress is given by,

$$f_c = 2 f''_c \frac{(\epsilon / \epsilon_o)}{1 + (\epsilon / \epsilon_o)^2} \quad (5.1)$$

where,

$$f''_c = \text{peak stress in flexure} = k_3 f_c$$

$$\epsilon_o = \text{concrete strain at peak stress} = 0.002$$

Tests of isolated beam-columns under moderate and large axial load levels had indicated that the parameter k_3 is less than unity. This is because the increase of the axial load level results in a less steep strain gradient and hence the beneficial effects of the strength gradient are reduced. Abbasi and Siess (1969) used the above stress-strain relationship with the parameter $k_3=0.85$ to obtain moment-curvature relationships for cross sections subjected to combined axial load and bending moments for different axial load levels. The computed moment capacity agreed very well with tests on beam-columns reinforced with high strength steel. Hence, this value is adopted in developing the moment-curvature relations in this study. Eqn. 5.1 is applicable for concrete strengths up to 45 MPa.

The value adopted for the ultimate strain of concrete in compression has a decisive influence upon the deformational characteristics of reinforced concrete sections and members, although its effect upon strength are rather insignificant. Evidence suggests two primary variables affecting the ultimate strain: the strain gradient and the degree of confinement of concrete. R  sch (1960) defined ϵ_u as the extreme compression fiber strain at which a reinforced concrete section reaches its maximum load- or moment-capacity. R  sch's definition has a mathematical significance. For a given axial load, ϵ_u corresponds to the peak of the curve relating moment and extreme compression fiber strain. This definition is very logical if it is accepted that the primary function of a member or a structure is to carry loads.

Bazant and Cedolin (1991) pointed out that the strain softening behaviour of concrete is difficult to measure in uniaxial tests since strain localization occurs right after the peak. Hence, the practice has been to assume for concrete a stress-strain diagram terminating with a sudden drop. This simplification is probably not very realistic for bending but is usually on the safe side. In this study, a limiting value of ultimate concrete compressive strain is adopted as the failure criterion. The value of 0.0038 suggested by Hognestad (1952) will be used.

5.4.2.2 Concrete in Tension

The overall tension stiffening effect is simulated using a stress-strain relationship for concrete in tension so that the strains and curvatures obtained would represent average values in the cracked zones rather than the peak values at crack locations.

The trilinear piecewise stress-strain relationship for concrete in tension suggested by Vebo and Ghali (1977) is adopted in this study. As shown in Fig. 5.2, the independent variables for this relationship are the modulus of rupture, f_r , and the modulus of elasticity of concrete in compression, E_c .

Although the modulus of rupture over-estimates the true value of the tensile strength of concrete due to the analytical procedure used, Hannant (1972) suggested that it might represent a more realistic measure of the cracking strength of concrete members

subjected to flexure. This is because the tensile strength of a concrete member is strongly influenced by the stress gradient over the cross section. Under a large stress gradient, the fibers subjected to maximum stresses are restrained by the less stressed portions of the cross sections, leading to a higher tensile strength than in the case of a small gradient.

Drying shrinkage of concrete affects the curvature in two ways. The first is direct; shrinkage produces curvature which adds or subtracts to the curvature due to loading. This effect, however, vanishes for members having equal top and bottom reinforcement as those considered herein. The second effect is indirect; shrinkage causes volumetric changes that introduce tensile stresses in concrete if restrained and therefore can lead to a significant reduction of the apparent tensile strength of concrete. In test specimens, the restraint may be caused by the embedded reinforcement. The nonlinear distribution of free shrinkage strains across the cross section may also be a contributing factor. This indirect effect of shrinkage on the curvature may be approximately accounted for by deducting the shrinkage induced tensile stresses from the measured modulus of rupture to obtain an effective modulus of rupture, f_{re} .

The shrinkage induced stresses for all the specimens were calculated using the method described by Ghali and Favre (1986). As recommended by MacGregor (1988), free shrinkage strains were computed using the CEB method (1978) but the ultimate shrinkage strains were taken from the ACI recommendations (1982). The details of the calculations are given in Appendix B. The induced

shrinkage stress and the value of the effective modulus of rupture for all the specimens are given in Table 5.1. The values of the effective modulus of rupture were used in the moment-curvature calculations.

5.4.2.3 Reinforcing Steel

The response of the reinforcing bars in tension and compression was simulated the stress-strain curve shown in Fig. 2.3 which was obtained from standard tensile tests on steel specimens.

5.4.3 Numerical procedure

For any assumed strain distribution, the resultant forces and moments can be computed as illustrated in Fig. 5.3. The moment-curvature diagram was developed by incrementing the curvature. For a particular curvature, the strain at the top of the section was altered using a trial and error procedure until the sum of the compression and tension forces in the section was essentially equal to the desired axial force. Once the forces were balanced, the moment was calculated and thus one point on the moment-curvature diagram was determined. The curvature was then incremented and the above procedure of balancing the forces and calculating the moment was repeated. This was continued until an ultimate concrete compressive strain of 0.0038 was reached.

In Fig. 5.4, the effect of axial compressive force on the moment-curvature relationship of a section is shown for

compression-to-tension steel ratio of 1.0. It is obvious from the figure that the strength of a section improves proportionally with axial compression up to a certain limit after which the effect reverses and moment capacity of the section becomes smaller under high compression than it is with low or no compression. On the other hand, the section becomes less ductile with increasing axial compression and the section ductility becomes very limited under large compressive forces. Such behaviour is well known and has been demonstrated experimentally.

Fig. 5.5 shows the tension stiffening effect on the flexural behaviour of sections subjected to pure bending and combined axial force and bending moment, respectively. In this figure, the solid curves represent the average $M-\kappa$ relationships which were obtained when including the stiffening effect of tension of concrete between the cracks and at the cracked section, by assuming a stress-strain curve for reinforced concrete in tension while the dotted curves were obtained by ignoring the tension in concrete altogether. Although the effect of tension stiffening on the strength of the section is insignificant, it is obvious that neglecting this effect significantly underestimates the stiffness of the section. The inclusion of tension stiffening is important when analyzing lightly reinforced members which are susceptible to stability failures which occur long before the sections reach their strengths.

5.5 Analytical Model for Plates Subjected to Combined Inplane and Lateral Loads

5.5.1 General Background

The analysis of plating under combined lateral and inplane loads can be dealt with at a reasonable level of accuracy using the corrected second-order small-deflection theory (Haugus, 1983). In this theory, the out-of-plane deflection of the plate due to the lateral load is included in the differential equation, thus allowing interaction with the inplane compressive forces, but no other interaction between lateral and inplane effects is considered.

Equations for orthotropic plates derived in text books on the theory of plates (Timoshenko and Woinowsky-Krieger, 1959; Szilard, 1974) are needed for use in the proposed analytical model. A typical rectangular plate as considered in the analysis is shown in Fig. 5.6. The plate is of length a , width b , and uniform thickness h . The x , y , and z axes are longitudinal, transverse and through the thickness respectively, where z is zero at mid-surface. A uniform inplane compressive force per unit length N_x is applied in the x -direction to the sides of length a , and a uniform inplane compressive force per unit length N_y is applied in the y -direction to the sides of length b . Both inplane forces are applied at mid-thickness of the plate. In addition, there is a uniform lateral pressure q at any point (x,y) , and w represents the lateral displacements from the flat surface.

Based on Kirchhoff theory, the following relationships between moments and deformations can be derived for elastic plates:

$$M_x = -D_x (w_{,xx} + \nu_y w_{,yy}) \quad (5.2)$$

$$M_y = -D_y (w_{,yy} + \nu_x w_{,xx}) \quad (5.3)$$

$$M_{xy} = 2D_t w_{,xy} \quad (5.4)$$

where,

$$2D_t = (1 - \sqrt{\nu_x \nu_y}) \sqrt{D_x D_y} \quad (5.5)$$

represents the torsional rigidity of the plate, while D_x and D_y are the bending rigidities in the x and y directions, respectively. M_x , M_y and M_{xy} are moments per unit width. The moment M_x is about the y axis, while M_y is about the x axis.

The equilibrium equation for an orthotropic plate under combined lateral load $q(x,y)$ per unit area and compressive inplane loads N_x and N_y per unit width in the x and y directions, respectively, is given as:

$$M_{x,xx} - 2 M_{xy,xy} + M_{y,yy} = -q(x,y) + N_x w_{,xx} + N_y w_{,yy} \quad (5.6)$$

The above equation is independent of material properties and hence it is valid for both elastic and plastic cases. Substituting Eqns. (5.2) through (5.5) into the equilibrium equation, the differential equation of the deflection surface of an elastic orthotropic reinforced concrete plate can be written as:

$$D_x w_{,xxxx} + 2B w_{,xxyy} + D_y w_{,yyyy} = q(x,y) - N_x w_{,xx} - N_y w_{,yy} \quad (5.7)$$

where,

$$B = \frac{1}{2} (v_y D_x - v_x D_y + 4D_t) \quad (5.8)$$

is called the "effective torsional rigidity" of the orthotropic plate.

There is experimental evidence, Clark (1972) and Lenschow and Sozen (1966), to suggest that the effective Poisson's ratio is zero on the cracked face and about 0.05 to 0.1 on the uncracked face of a slab. These figures suggest that for most practical purposes the effective Poisson's ratio can be assumed equal to zero. Hence, for a cracked plate, the following constitutive relationships can be adopted:

$$M_x = -D_x w_{,xx} \quad (5.9)$$

$$M_y = -D_y w_{,yy} \quad (5.10)$$

$$M_{xy} = 2D_t w_{,xy} \quad (5.11)$$

where now,

$$2D_t = \sqrt{D_x D_y} \quad (5.12)$$

It is debatable whether Eqn. (5.12) should be applied to a cracked reinforced concrete plate where the orthotropy is due to discontinuities (cracks) in the plate rather than to material orthotropy. Tests by Clark and White (1978) indicated that the Huber stiffness, defined by Eqn. (5.12), represents a lower bound of the

torsional stiffness after flexural cracking. This is because considerable shear may be transmitted across the crack in the forms of aggregate interlock and dowel action of the reinforcement.

Based on the above approximations, the differential equation of the problem in hand can be written as:

$$D_x w_{,xxxx} + 4D_t w_{,xxyy} + D_y w_{,yyyy} = q(x,y) - N_x w_{,xx} - N_y w_{,yy} \quad (5.13)$$

5.5.2 Formulation

The analytical approach developed herein is an extension to the "model plate" method first introduced by Aas-Jakobsen (1983). The approach is based on the following simplifications:

1. The deflected shape of the plate is assumed to be a certain function, and further, this general shape will not alter during loading but merely change its magnitude as the lateral load increases.
2. The rigidities are assumed constant over the plate. The bending rigidities, D_x and D_y , are secant rigidities determined from analytically derived moment-curvature relationships for unit widths of the plate cross sections at the center of the plate in the orthogonal directions. The torsional rigidity, $2D_t$, is obtained from Eqn. 5.12.

A plate with an assumed deflected shape and constant anisotropic properties will be referred to as the "model plate".

Assumption (1) implies that at the ultimate lateral load, the deflection of the plate is predominantly elastic. This would be the

case for square plates in which the failure is initiated due to instability. For rectangular plates in which the inplane loads were applied along the short sides, the steel in the short direction experienced significant deformation at the ultimate lateral load and hence the deflected shapes of these plates are combination of the elastic deflected shape and the failure mechanism shape. It should be borne in mind, however, that the ultimate lateral loads of these plates are not reached at a sharp peak in the load-deflection curve, and as a result the loads do not differ significantly during the spread of plasticity. Hence, it is reasonable to assume a predominant elastic deflected shape when calculating the maximum lateral load for such plates.

The assumption of using a single function to analyze member behaviour in both the elastic and plastic ranges has been employed by many investigators since it simplifies the problem drastically. This approach was used by Aghayere and MacGregor (1988) to derive a lower bound solution for reinforced concrete plates. A sinusoidal shape of the deflection curve has been also used by Toma and Chen (1983) for the analysis of tubular steel beam-columns, by Broms and Viest (1961) and recently by Bazant et al. (1991) for the analysis of reinforced concrete beam-columns. It is also the basis for the CEB model column method (1978), and is implied in the ACI's use of the magnification factor for slender columns. This is despite the fact that all the forgoing methods were applied at ultimate conditions where deflections are large.

For a plate reinforced at the corners with top and bottom steel of the same magnitude at its center, assumption (2) is consistent with the development of a lower bound estimate on the overall torsional rigidity.

The deflection surface can be expressed by a double sine series which satisfies the boundary conditions for a simply supported plate without inplane restraints:

$$w(x,y) = \sum_{m=1}^{\bar{m}} \sum_{n=1}^{\bar{n}} w_{mn} \sin \frac{m\pi x}{b} \sin \frac{n\pi y}{a} \quad (5.14)$$

The lateral load can also be expanded into a double sine series as:

$$q(x,y) = \sum_{m=1}^{\bar{m}} \sum_{n=1}^{\bar{n}} \frac{16q_0}{\pi^2 mn} \sin \frac{m\pi x}{b} \sin \frac{n\pi y}{a} \quad (5.15)$$

where m and n are positive odd integers ($m=1,3,5,\dots$ and $n=1,3,5,\dots$). Eqns. (5.14) and (5.15) are usually expressed in infinite series form. Herein, however, only a finite series in which \bar{m} and \bar{n} can be large enough to provide some acceptable convergence tolerance is considered. In this thesis six terms are used ($\bar{m} = \bar{n} = 5$).

Substituting Eqns. (5.14) and (5.15) into the governing differential Eqn. (5.13), an algebraic equation is obtained from which the unknown w_{mn} can be obtained as:

$$w_{mn} = \frac{16 q}{\pi^2 mnD \left(1 - \frac{N_x m^2 \pi^2}{b^2 D} - \frac{N_y n^2 \pi^2}{a^2 D} \right)} \quad (5.16)$$

where,

$$D = \frac{D_x m^4 \pi^4}{b^4} + \frac{D_t m^2 n^2 \pi^4}{a^2 b^2} + \frac{D_y n^4 \pi^4}{a^4} \quad (5.17)$$

The curvatures can be approximated by the second derivatives of the deflection function as:

$$\kappa_x = -w_{,xx} \quad (5.18)$$

$$\kappa_y = -w_{,yy} \quad (5.19)$$

$$\kappa_{xy} = w_{,xy} \quad (5.20)$$

Hence, the curvature in the x-direction, at the center of the plate, is related to the lateral load by the relation:

$$\kappa_{x0} = \sum_{m=1}^{\infty} \sum_{n=1}^{\infty} \frac{16qm}{b^2 D n} \frac{\sin \frac{m\pi}{2} \sin \frac{n\pi}{2}}{\lambda} \quad (5.21)$$

where κ_{x0} is the curvature at the center of the plate in the x-direction. In the above equation, λ is given by:

$$\lambda = 1 - \frac{N_x m^2 \pi^2}{b^2 D} - \frac{N_y n^2 \pi^2}{a^2 D} \quad (5.22)$$

The ratio, R , between the curvatures at the plate center in the x - and y - directions is given by:

$$R = \frac{\sum_{m=1}^{\bar{m}} \sum_{n=1}^{\bar{n}} \frac{m}{a^2 n} \frac{\sin \frac{m\pi}{2} \sin \frac{n\pi}{2}}{\lambda}}{\sum_{m=1}^{\bar{m}} \sum_{n=1}^{\bar{n}} \frac{n}{b^2 m} \frac{\sin \frac{m\pi}{2} \sin \frac{n\pi}{2}}{\lambda}} \quad (5.23)$$

Hence, the curvature at the center of the plate in the y -direction is given by:

$$\kappa_{y0} = R \kappa_{x0} \quad (5.24)$$

The method of analysis is based on an incremental procedure in which the curvature in the x -direction at the center of the plate is incremented in steps and the plate equilibrium equation is solved for the lateral load corresponding to the assumed curvatures. It should be noted that the plate rigidities obtained in step (i-1) are used in Eqn. 5.23 to obtain the relation between the curvatures in step (i).

The procedure for obtaining the total lateral load, q , for a given set of inplane loads N_x and N_y per unit width is as follows:

1. Obtain the M - N - κ relationships for a section of unit width at the center of the plate in the x and y directions for the given values of N_x and N_y as done in Section 5.4.
2. Assume a value for κ_{x0i} .

3. From Eqn. 5.24 determine $\kappa_{yoi} = R_{i-1} \kappa_{xoi}$ (for $i=1$, the rigidities used in Eqn. 5.23 are those corresponding to the uncracked section).
4. From the M-N- κ relationships derived in step (1) obtain the secant rigidities, D_{xi} and D_{yi} , corresponding to κ_{xo} and κ_{yo} , respectively, and from Eqn. 5.12 obtain the torsional rigidity, $2D_{ti}$.
5. Compute the lateral load, q_i , for a given κ_{xoi} using Eqn. 5.21.
6. Increment κ_{xo} and repeat steps (2) through (5).

This gives a plot of lateral load, q , versus the curvature at the center of the plate in the x direction κ_{xo} . The peak of this curve is taken as the lateral load capacity.

5.6 Comparison of Analytical Predictions with Test Results

The analytical model described above was used to predict the maximum lateral load the plate can carry for specimens in which the inplane loads were applied first. From observations of specimens subjected to different loading sequences, it is clear that proportional loadings or application of the inplane load prior to the lateral load leads to little difference in the load-deflection response and ultimate strength. Therefore, the method of analysis was also used to predict the maximum lateral load for specimen C3 in which the inplane and lateral loads were applied simultaneously.

Table 5.2 compares the maximum lateral loads from the proposed model with the maximum lateral loads obtained from the

tests. The average test-to-predicted ratio is 0.990 and the coefficient of variation is 6.2 percent. The calculation method is considered satisfactory in view of the nature of the problem being dealt with and the wide range of variables covered in the test program. Specimens A1, B1, C1, and D1 are omitted because they had lateral loads only. Specimens C8 and C9 had the lateral load applied first.

It should be emphasized that the main purpose of the method described above is to obtain the maximum lateral load under controlled inplane load. It is suitable for tracing the load-deflection behaviour as long as the diagram for load versus deflection is rising. The ductility and the unloading portion of the load-deflection curve, however, depend partly on the ability of the actual plate to redistribute the load and partly on how close the softening (descending) portion of the effective stress-strain relation used in the analysis models to the real behaviour of the material, (Bazant and Cedolin 1991).

Figs. 5.7 to 5.12 show comparisons between the analytical and test load-deflection curves. In the ascending branch of the load-deflection curves, the figures indicate a good agreement between test and analysis especially for square specimens. Although the model predicts the maximum lateral load capacity of the long plates, there are deviations between the test and predicted load-deflection curves for these specimens near the ultimate load. The probable reason for this deviation is the formation of bands of intense cracking near the ultimate load.

Table 5.1 Tensile Stresses Due to Shrinkage and Effective Modulus of Rupture

Specimen Designation	Uniform Tensile Stresses Due to Shrinkage (MPa)		Effective Modulus of Rupture f_{re} (MPa)	
	X-Direction	Y-Direction	X-Direction	Y-Direction
A1	0.66	0.66	2.96	2.96
A2	0.72	0.72	3.02	3.02
A3	0.74	1.30	3.07	2.51
A4	1.31	0.75	2.54	3.10
B1	0.53	0.53	2.15	2.15
B2	0.70	0.70	2.17	2.17
B3	0.73	0.73	2.23	2.23
B4	0.83	0.83	2.58	2.58
C1	0.54	0.54	2.92	2.92
C2	0.57	0.57	2.95	2.95
C3	0.56	0.56	2.99	2.99
C4	0.58	1.04	3.03	2.57
C5	0.86	0.47	2.10	2.49
C6	0.66	0.66	3.05	3.05
C7	0.69	0.69	3.16	3.16
C8	0.72	0.72	3.39	3.39
C9	0.57	0.57	2.28	2.28
D1	0.44	0.44	2.21	2.21
D2	0.44	0.44	2.21	2.21

Table 5.2 Maximum Lateral Loads: Test versus Analytical Predictions

Specimen Designation	Max. Lateral Load from Tests (kPa)	Max. Lateral Load from Analysis (kPa)	<u>Test Predicted</u>
A2	21.96	19.92	1.091
A3	23.90	21.68	1.102
A4	33.80	34.56	0.978
B2	23.27	25.20	0.923
B3	25.52	27.28	0.935
B4	19.51	21.38	0.913
C2	52.59	52.20	1.011
C3*	51.56	53.00	0.973
C4	59.47	60.48	0.983
C5	67.83	68.25	0.994
C6**	69.16	65.34	1.058
C7**	60.03	61.71	0.973
D2	121.68	130.58	0.932

Mean = 0.990

Coefficient of Variation = 6.2%

* Proportional loading

** Biaxial inplane loading

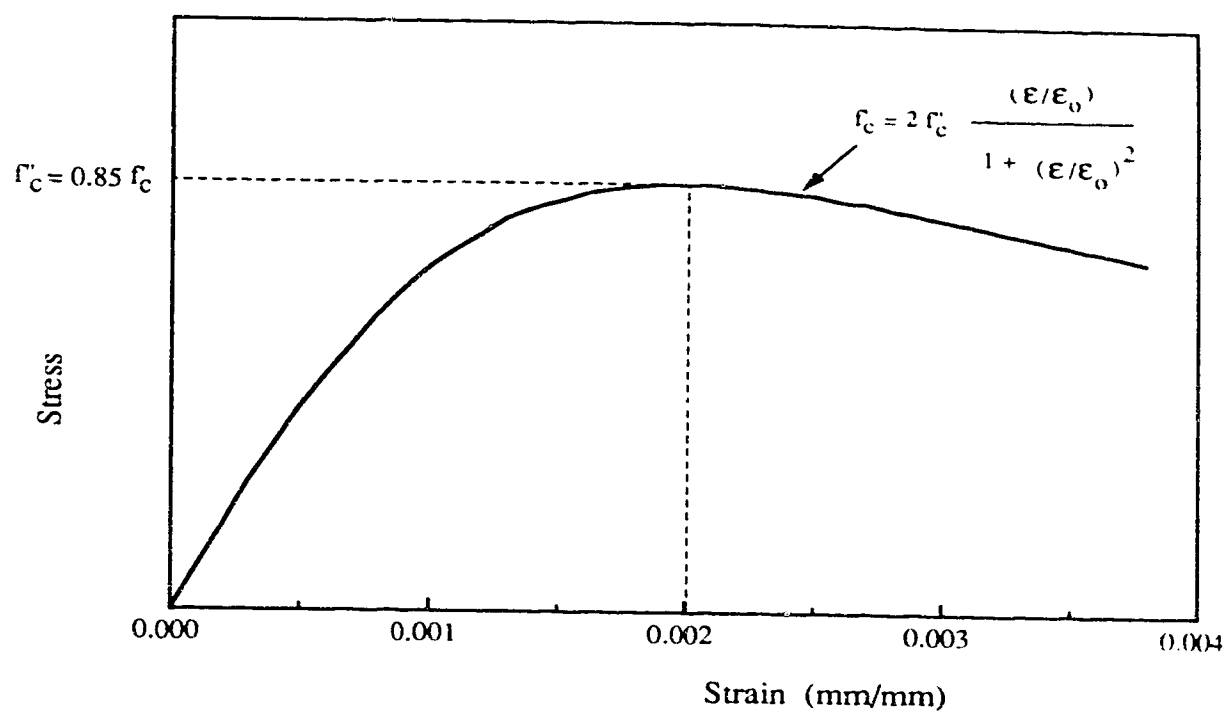


Figure 5.1 Uniaxial Stress-Strain Curve for Concrete in Compression

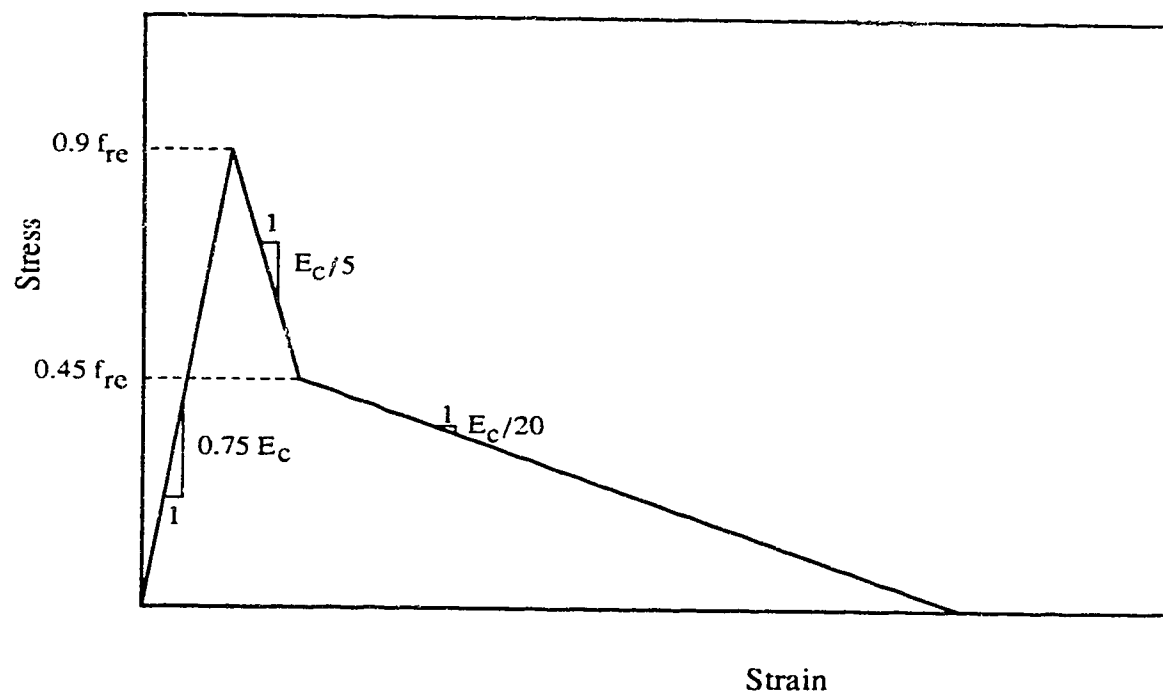


Figure 5.2 Adopted Tension Stiffening Curve

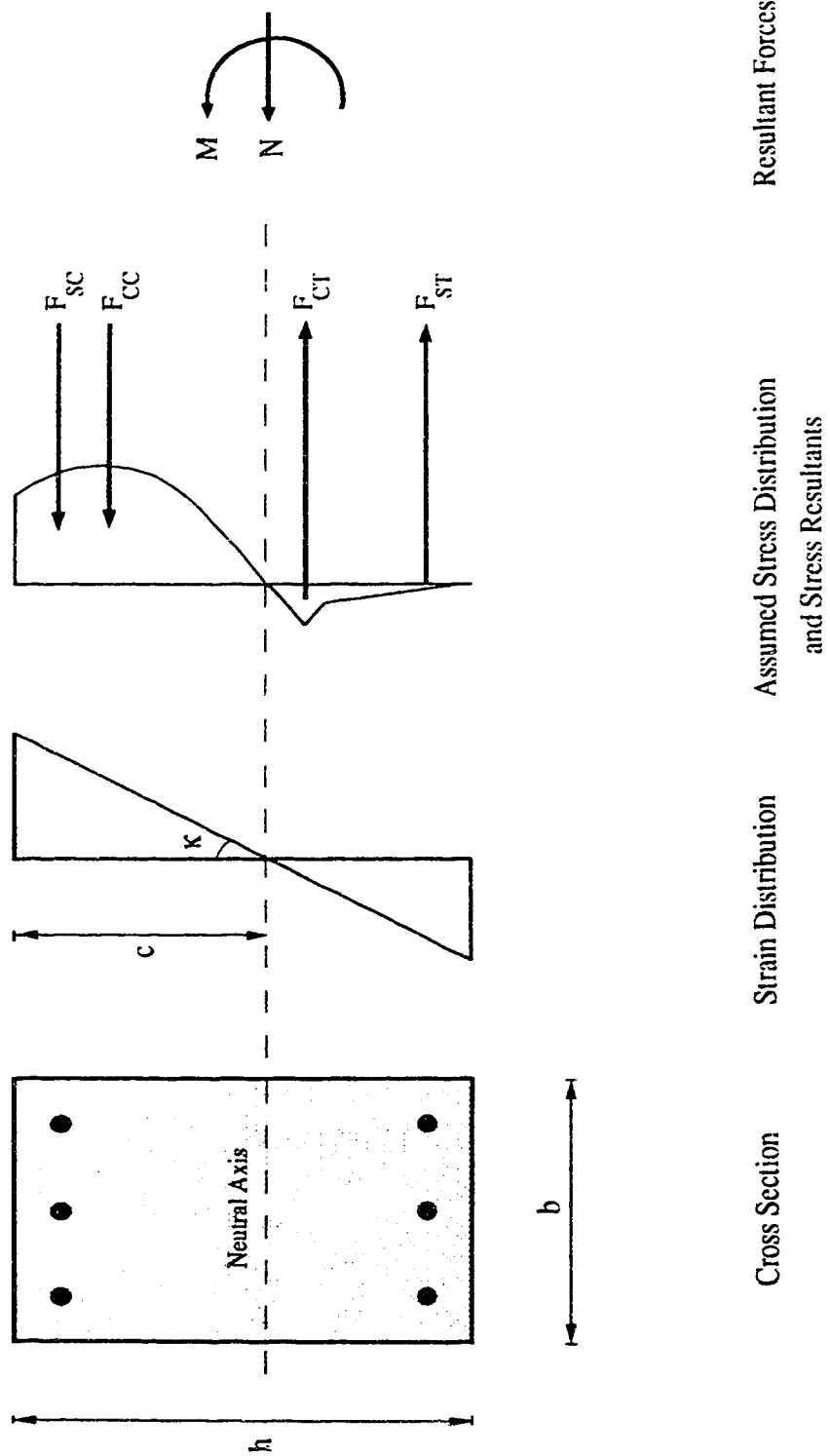


Figure 5.3 Derivation of the Load-Moment-Curvature Relationship

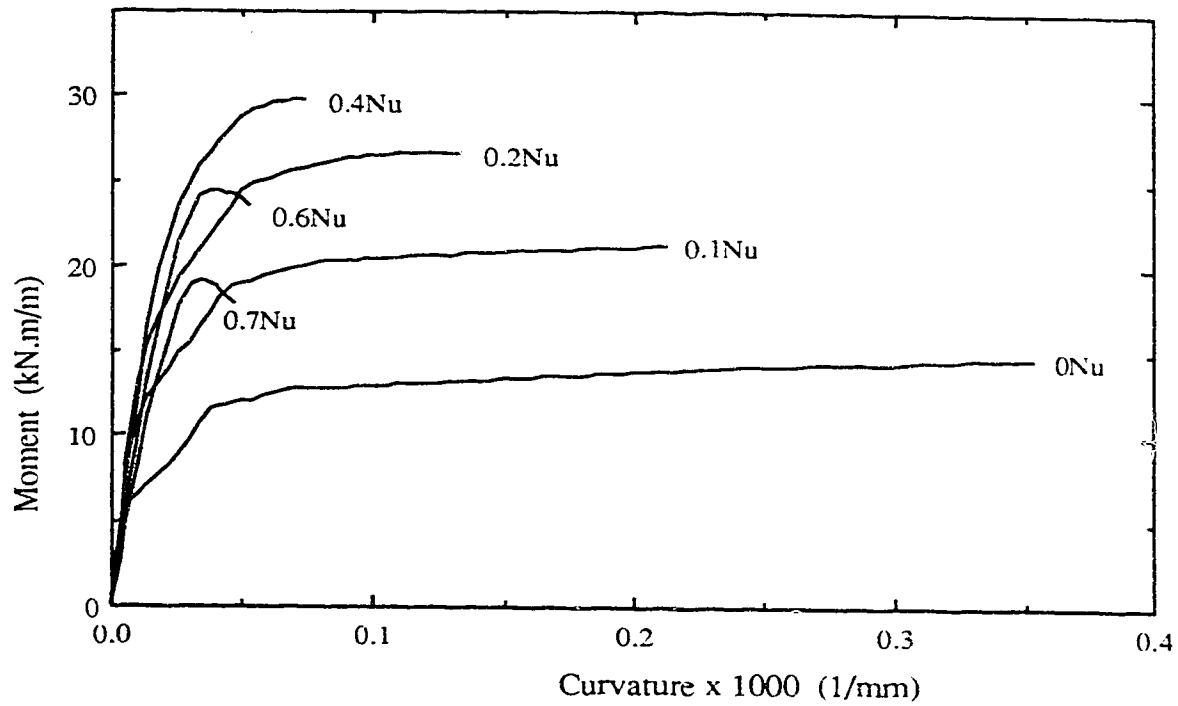


Figure 5.4 Effect of Axial Load Level on the Moment-Curvature Relationship

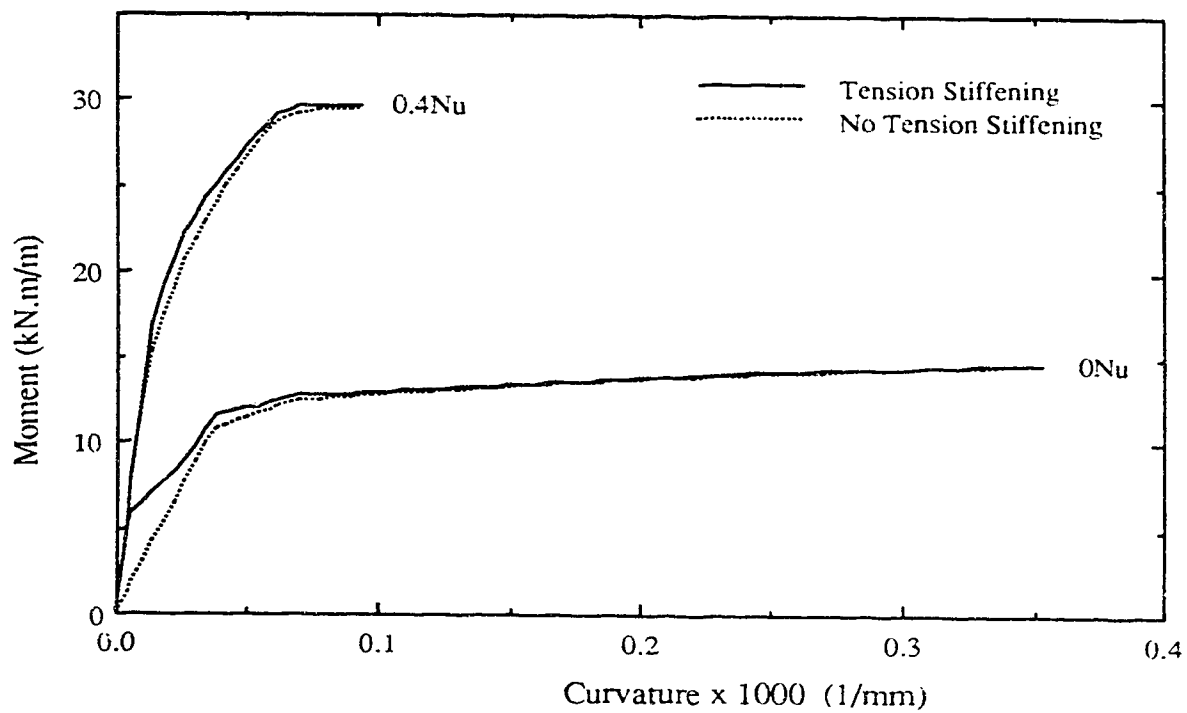


Figure 5.5 Effect of Tension Stiffening on the Moment-Curvature Relationship

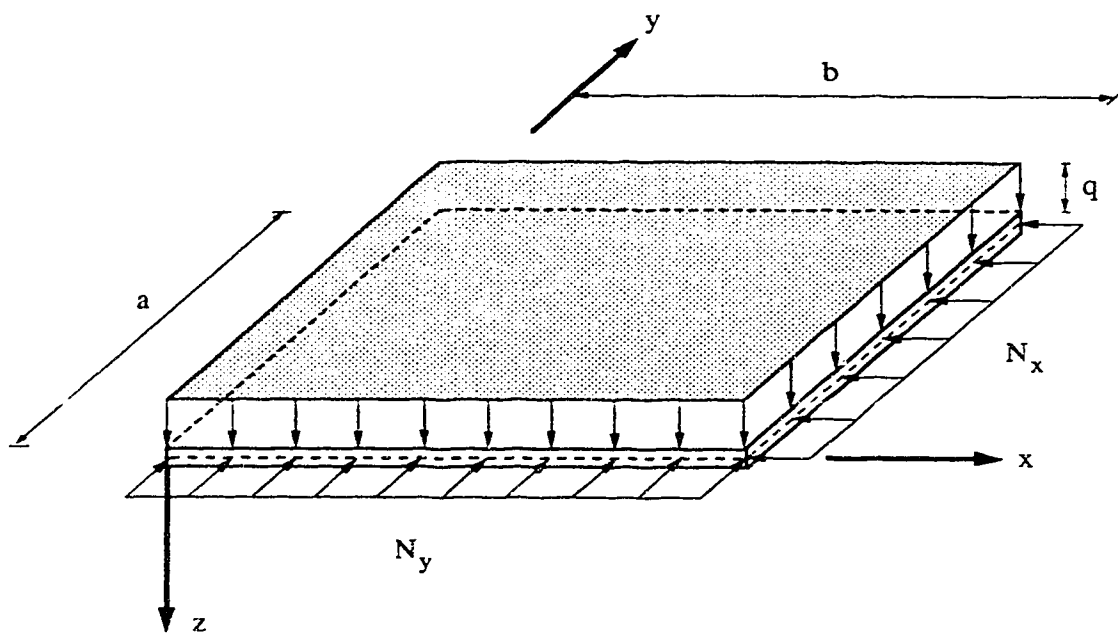


Figure 5.6 Plate Dimensions, Coordinate Axes and Loading

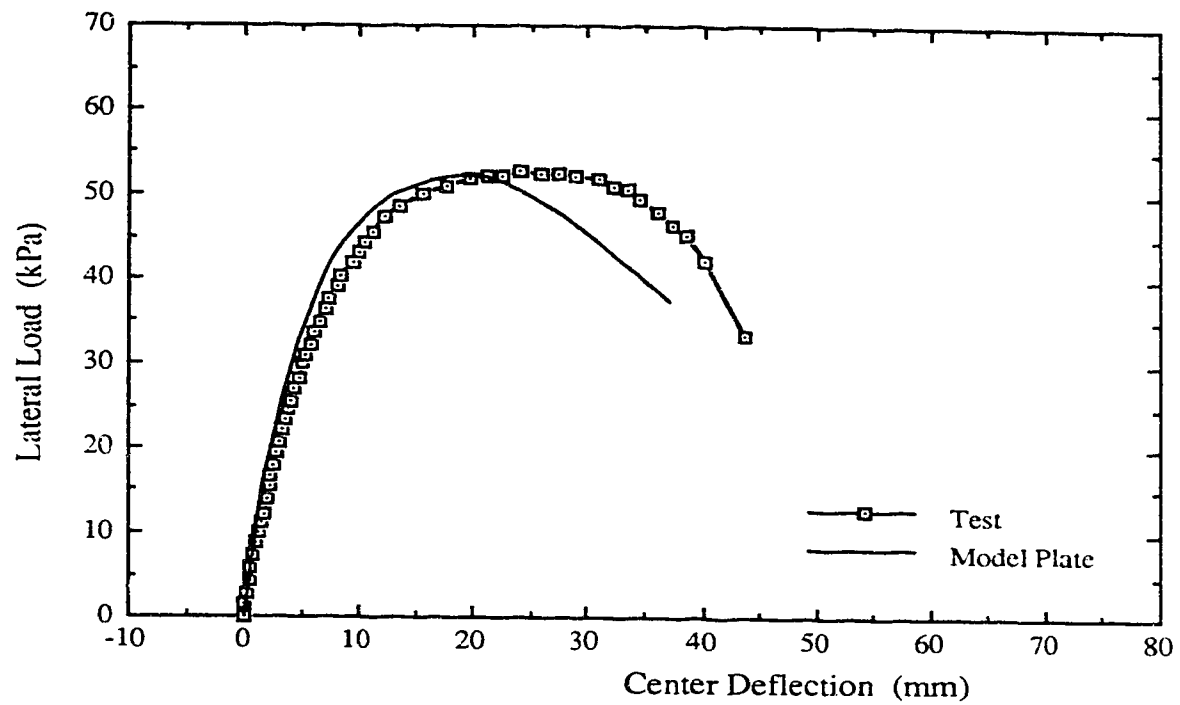


Figure 5.7 Lateral Load-Deflection Curves for Specimen C2: Test versus Model

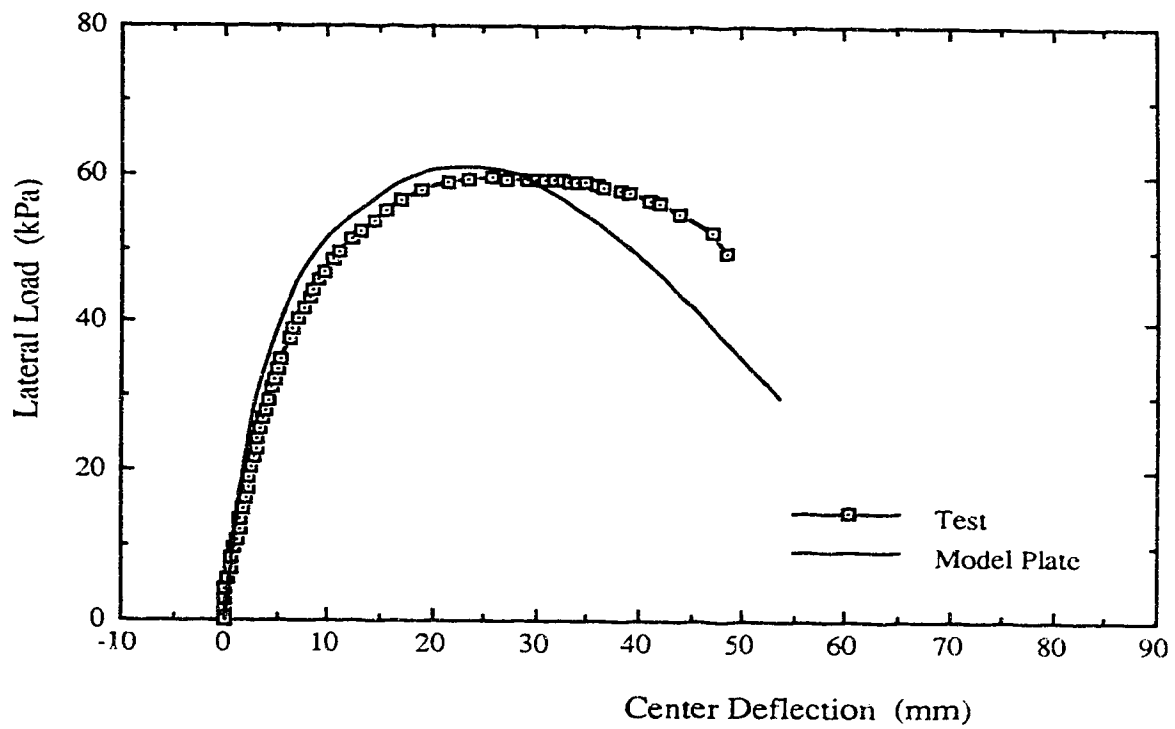


Figure 5.8 Lateral Load-Deflection Curves for Specimen C4: Test versus Model

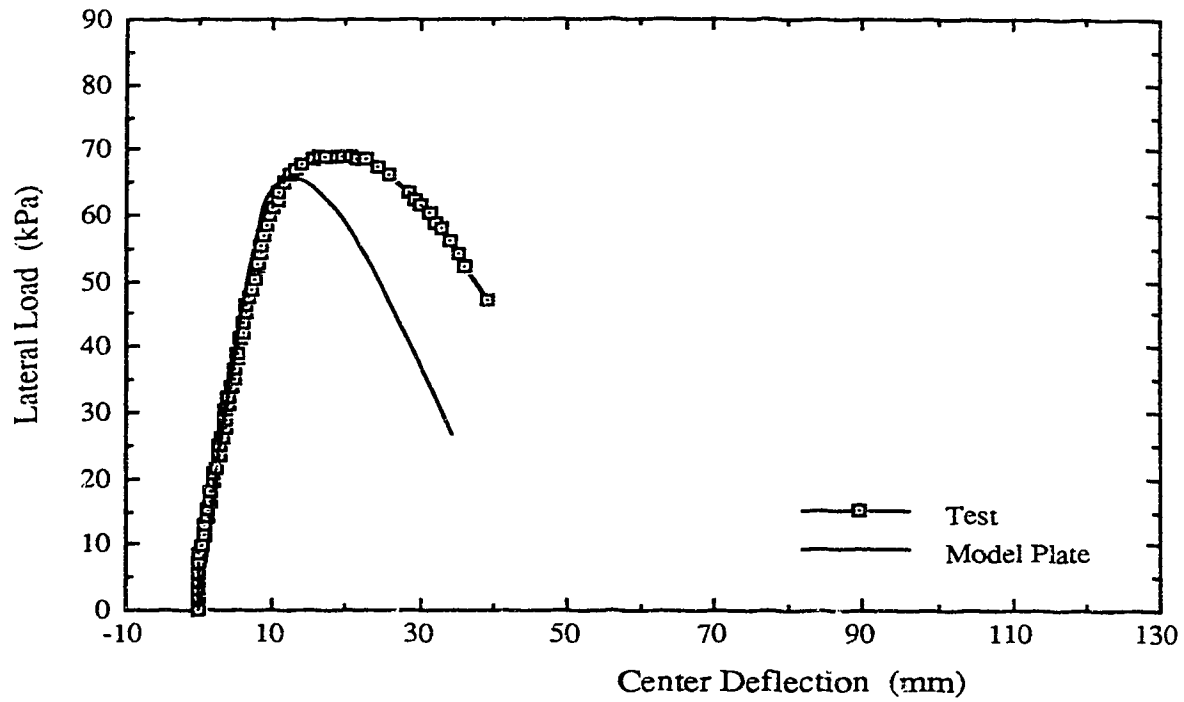


Figure 5.9 Lateral Load-Deflection Curves for Specimen C6: Test versus Model

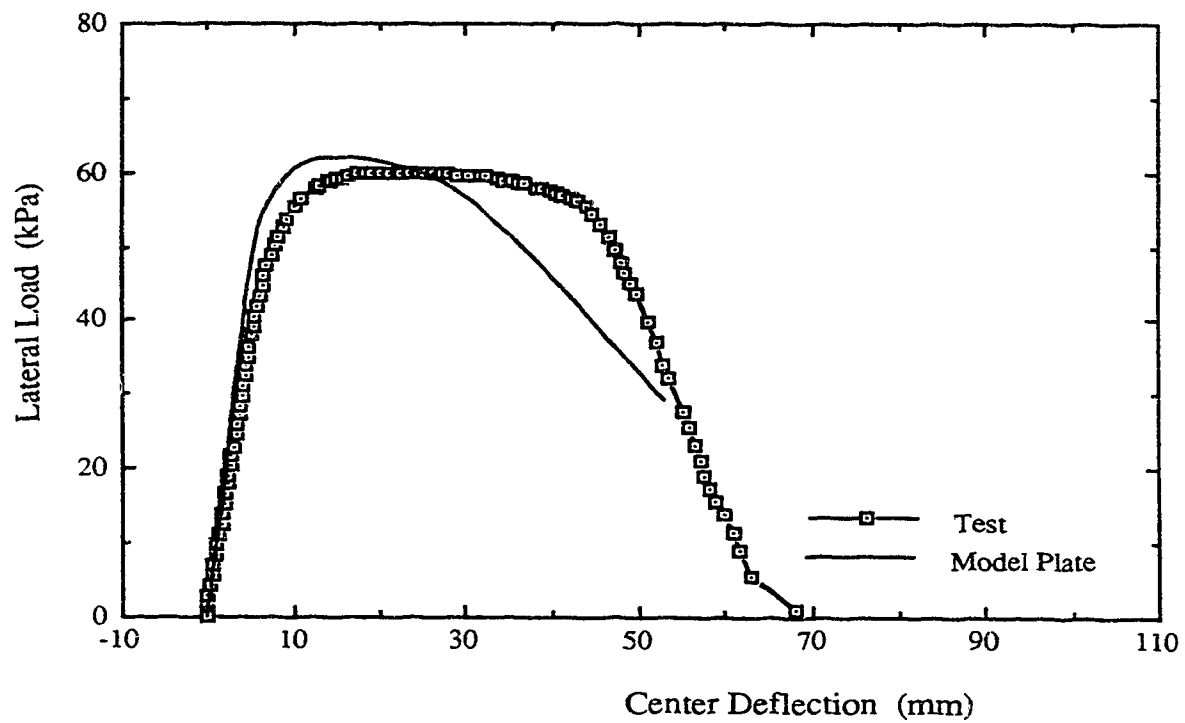


Figure 5.10 Lateral Load-Deflection Curves for Specimen C7: Test versus Model

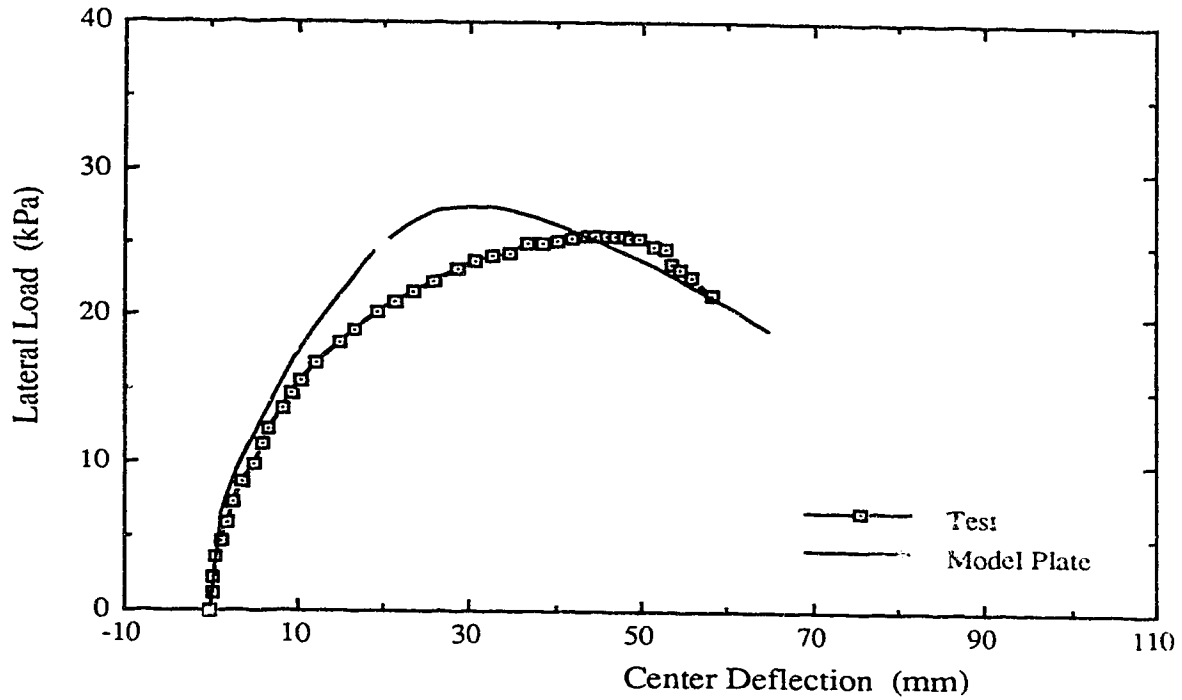


Figure 5.11 Lateral Load-Deflection Curves for Specimen B3: Test versus Model

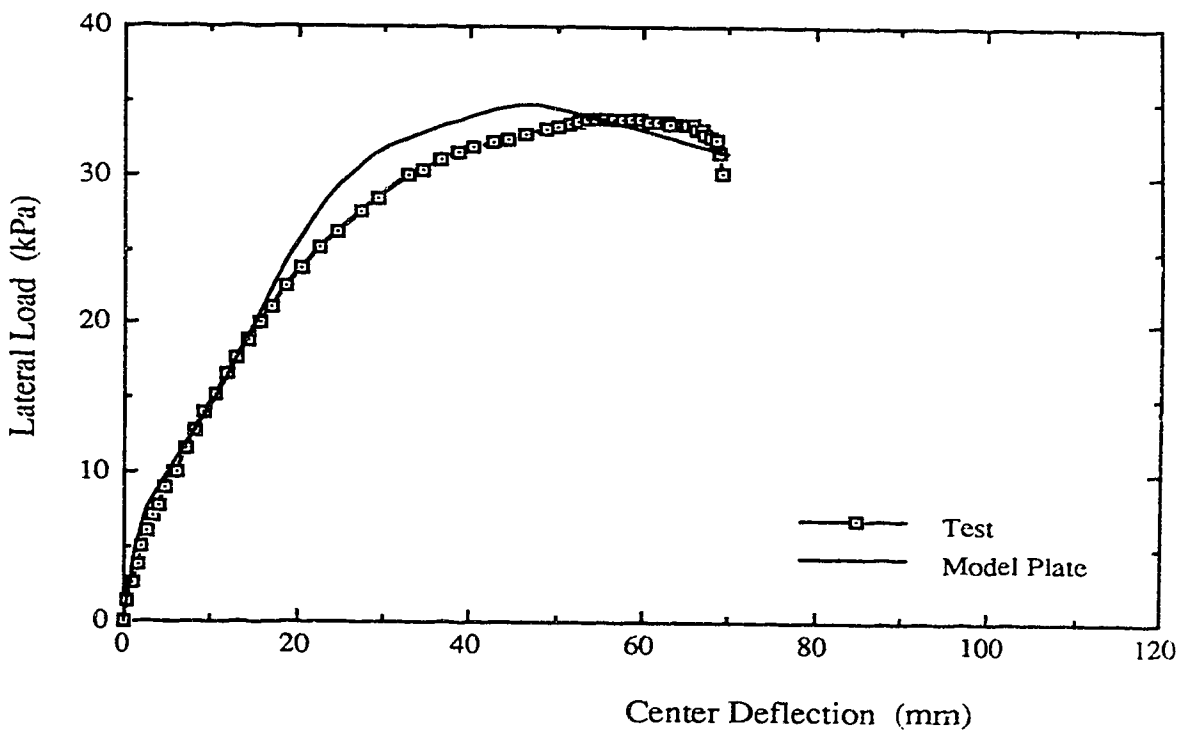


Figure 5.12 Lateral Load-Deflection Curves for Specimen A4: Test versus Model

6. Finite Element Analysis

6.1 Introduction

The objective of the finite element analysis presented in this chapter is to examine the material parameters which affect the modelling of panels subjected to combined inplane and lateral loads. The finite element predictions are also compared with the physical tests to establish a satisfactory level of confidence in the numerical modelling.

The finite element program NISA (Stegmüller et al., 1983, and Stegmüller, 1984), has been used as the numerical analysis tool for the analysis. A brief description of the program and options available are presented in the following.

6.2 Description of NISA

NISA is a nonlinear incremental finite element program for the analysis of large-displacement large-strain problems. The program was initially developed at Stuttgart University in Germany and modified later at the University of Alberta.

The type of finite element selected for the analysis reported in this study is the 16 node bicubic degenerated three-dimensional plate-shell element developed by Ramm (1976, 1977). This plate-shell element, shown in Fig. 6.1, has five degrees of freedom per

node, three displacements and two rotations. The displacement at any point through the thickness of the element is defined as a function of the midplane plane displacements and rotations. Applying the isoparametric concept, geometry and displacement fields are interpolated in the same way. The rotational degrees of freedom are independently interpolated thus shear deformations are included and continuity of displacements is ensured. The interpolation order is the same for all the three displacements and the rotational part.

A full 4x4 Gaussian integration rule over the element plane is adopted, whereas a Simpson-type integration is performed over the thickness. The strains are evaluated from the interpolation functions at each integration point at each level through the thickness and are used in the constitutive relationships to form the stiffness matrix and to evaluate the stress conditions at each level.

Geometric nonlinearities are allowed using either the Total or Updated Lagrangian formulations (Bathe, 1982). Updated Lagrangian formulation is recommended for large-displacement large-strain problems and hence it is adopted in this study.

The NISA program allows access to two main solution strategies: load control and displacement control. Load control is applied through a modified Newton-Raphson or the standard Newton-Raphson iterative strategy, while the displacement control is applied through a modified constant arc-length iterative strategy which was introduced by Ramm (1981). The latter method allows

one to trace a problem response near limit points and on unloading paths which can not be obtained with load control methods. The constant arc-length method, with an additional constant load has been used to trace the load-deflection response for specimens under combined loads. For specimens tested under lateral loads only, Newton-Raphson iteration was used to trace the load-deflection response.

6.3 Material Models for Concrete and Reinforcing Steel

There are two different approaches to treat material nonlinearity in the context of the finite element analysis of reinforced concrete plates; the modified stiffness approach and the layered element approach. In the first approach, the effect of the nonlinear behaviour is treated in a macroscopic sense by modifying the flexural rigidity of the elements, (Jofriet and McNeice, 1971 and Bell and Elms, 1971). The second approach, in which layers are used to perform an integration over the plate thickness, allows for greater flexibility and easier implementation for the complex behavioural characteristics of reinforced concrete. This advantage, however, is at the expense of the need for a considerably more complex finite element model.

In case of reinforced concrete, the plate-shell element described above is assumed to be made up of concrete. The reinforcing steel is represented by layers of uniform thickness located at a constant relative depth inside the element. Eight

different reinforcement layers can be specified each having independent but unidirectional properties. These layers can be located anywhere in the thickness of the concrete element.

The material model for concrete which is used in this application has been implemented in the plate-shell element and described in detail by Massicotte et al. (1988). Therefore, only the salient features of the model are briefly outlined herein.

It is an hypoelastic incremental model which is intended for use in a smeared cracking type of finite element analysis where cracked concrete is assumed to remain a continuum. Concrete is assumed isotropic up to either cracking or crushing.

Two cracks can form at any integration point through the plane and the element thickness. The orientation of these cracks follows different rules in each of the cracking models available in NISA, in two categories: fixed-crack models and rotating-crack models. In reinforced concrete elements which have different amounts of reinforcement in two orthogonal directions or which are subjected to different combinations of inplane and lateral loads, the internal resisting forces do not remain proportional upon cracking. For isotropically reinforced concrete elements, the proportionality of internal resisting forces is also lost if the steel in one direction yields first. Therefore in cases such as these the principal stress and strain directions do not remain fixed and the crack directions start to shift. The change in direction of the maximum stiffness was clearly observed in the tests of Vecchio and Collins (1982). The conventional

fixed-crack model can not handle this crack rotation and the superiority of the rotating crack model is quite obvious. In the rotating-crack models, cracks are assumed orthogonal and oriented in the direction of either the principal stresses or the principal strains, which give a stress-rotating-crack model and a strain-rotating-crack model, respectively. Both of these rotating crack models proved to give adequate results. The stress-rotating-crack model is adopted in this study.

The biaxial failure envelope used by Massicotte et al. (1988), shown in Fig. 6.2, is that developed by Kupfer and Gerstle (1973) with a small modification in the tension-compression zone.

The stress-strain relationship for concrete in compression in the pre-failure region is the one proposed by Saenz (1964). The biaxial failure envelope renders the limit stresses, σ_u , for each stress ratio, α . Together with the limit strain, ϵ_{cu} , taken from test results it defines the corresponding stress versus equivalent uniaxial strain curve, from which the material tangent modulus is taken. When a compression failure occurs in one direction, all concrete at this point is assumed crushed and the tangent moduli and the Poisson's ratio are set to zero in the evaluation of the stiffness matrix while the shear modulus is reduced to 0.1 of its elastic value. Strain softening in compression is allowed through the linear relationship shown in Fig. 6.3.

As shown in Fig. 6.4, the stress-strain curve for plain concrete in tension has a bilinear softening branch that was derived based on

a fracture mechanics approach. This softening behaviour is incorporated into the CEB description of the tension-stiffening phenomenon (1985) to derive a stress-strain curve for reinforced concrete in tension. Based on concrete properties in tension, given in Fig. 6.4, and the amount, spacing, and quality of reinforcement, the tension-stiffening phenomenon is represented by assuming an average stress-strain curve for reinforced concrete in tension as shown in Fig. 6.5. The coordinates of points a, b, and c as well as the equation of the nonlinear part of the stress-strain curve shown in Fig. 6.5 were derived and described in detail by Massicotte et al. (1988, 1990).

Since a strain softening branch is used to describe the stress-strain behaviour of plain concrete in tension, the tensile strength to be input is ideally obtained from direct tension tests as recommended by Massicotte et al. (1988). However, direct tension tests to obtain reliable results are difficult to perform and hence in this thesis, the direct tensile strength of concrete will be related to the splitting strength or the flexural strength.

Once cracking occurs in one direction, the elastic coefficients in the material constitutive matrix are changed as concrete becomes an orthotropic material where only the stiffening in the direction normal to the crack is set to zero, and the corresponding stress is controlled by the tension stiffening model. After cracking, the elastic shear modulus is reduced progressively as a function of the average tensile stress carried by concrete and Poisson's ratio is set to zero.

6.4 Modelling of the Test Specimens with NISA

The test specimens were modelled using the 16 node 3D degenerated plate-shell element with 5 degrees of freedom per node. Because of symmetry in both geometry and loading conditions, only one quarter of the specimen needed to be considered. The mesh layouts of the specimens of series A, B, and the square specimens are shown in Figs. 6.6, 6.7, and 6.8, respectively.

Out-of-plane displacements were restrained at nodal points corresponding to the actual positions of the rocker-roller assemblies in the specimens. At these nodal points, the rotation about an axis parallel to the edge of the panel was allowed but the rotation in the other direction was restrained to model the actual support conditions and to account for the fact that supports in the tests were 125 mm long.

A 4x4 Gaussian integration rule was used over the plane of each element, while 9-point Simpson's integration rule was used to describe the element through its thickness.

Reinforcing steel was treated as an equivalent uniaxial material layer which was smeared through the concrete (individual bars were not modelled). The response of the reinforcing steel was described using the actual stress-strain curve shown in Fig. 2.3, identical in tension and compression and four layers of smeared reinforcement were located at their actual positions. In the strips outside the

supports, only one quarter of the reinforcement existing inside the supports was considered.

Due to the difference in behaviour between specimens under combined loads and those under lateral loads only, their analyses will be discussed in separate sections.

6.5 Analysis of Plates under Combined Loads

In order to demonstrate the relative importance of the different aspects of material modelling on the prediction of the behaviour of reinforced concrete plates under combined inplane compressive and lateral loads, a number of specimens subjected to different loading conditions are analyzed in this section.

The inplane load was modelled using a uniformly distributed line load within the actual span of the plate and the lateral loading was modelled by concentrated loads located at the nodal points as close as possible to their respective positions in the specimens.

As mentioned in Chapter 2, the inplane load was applied through knife edge assemblies which allowed for the edge rotation while panels deflected and ensured a concentric application of the load. Hence, in the following analyses, the inplane loads are assumed to be applied at the middle surface of the plates with no eccentricity. Also, the inplane load is assumed to be applied to an initially perfect plate. A lateral line load was applied along the loaded edges to simulate the weight of the inplane loading frames.

6.5.1 Effect of Tension Stiffening

A parametric study consisting of four investigations has been carried out to study the effect of tension stiffening phenomenon on the behaviour of panels subjected to combined inplane and lateral loads, namely:

1. Tension stiffening was considered by assuming unloading in the concrete (Massicotte et al., 1988) and the direct tensile strength of concrete was taken equal to 0.9 times the splitting strength, as recommended by the CEB model code (1990).
2. Tension stiffening was not considered (tension cut-off) and the tensile strength of concrete was taken equal to 0.9 times the splitting strength.
3. Tension stiffening was considered by assuming unloading in the concrete (Massicotte et al., 1988) and the tensile strength of concrete was taken equal to $0.33 \sqrt{f'_c}$ as recommended by Collins and Mitchell (1987) and others.
4. Concrete was ignored after cracking and tension stiffening was modelled using an increased stiffness for the reinforcing steel. As recommended by Gilbert and Warner (1978), the stress-strain diagram of the reinforcing steel was modified as shown in Fig. 6.9 after the surrounding concrete had cracked. This approach was also used and recommended by Van Greunen (1979). The tensile strength of concrete was taken equal to 0.9 times the splitting strength.

Specimen C5 has been adopted as a reference for this investigation. All the other material properties were taken from Table 2.4 and used for the four analyses.

Fig. 6.10 shows the predicted responses for specimen C5 with tension stiffening applied by assuming a stress-strain curve for concrete in tension and with no tension stiffening (tension cut-off). The predicted ultimate loads when the tension stiffening was considered and for no tension stiffening were 65.93 kPa and 47.80 kPa, respectively, compared to an experimental ultimate load of 67.83 kPa. It can be seen that the tension cut-off analysis underestimates the actual deflection at failure and the failure load of the specimen. This was due to the fact that, for plates subjected to combined loads, reinforcing steel at least in one direction had not yielded and therefore the concrete in that direction was still capable of carrying some tension stress up to failure. Under this condition, the inclusion of the tension stiffening effect not only improves the prediction of the plate behaviour after cracking takes place, but also increases the calculated ultimate loads. It should be also noted that the tension stiffening has an indirect effect on plate behaviour because of its effect on the shear retention factor due to the assumed relation between the shear stiffness of the cracked concrete and the normal crack stress. It should also be mentioned that the solution which assumed a complete loss of the concrete tensile stress after the initiation of cracking was not as stable as the one which took account of the concrete tension stiffening stress and consequently needed more iterations and computer time to get a convergent solution.

Fig. 6.11 shows the predicted responses for specimen C5 with tension stiffening applied by assuming a stress-strain curve for concrete in tension for two different assumed values for the direct tensile strength of concrete. The predicted failure load was 65.93 kPa for an assumed tensile strength of 2.30 MPa ($0.9 f_{sp}$) and 64.10 kPa for a tensile strength of 1.68 MPa ($0.33 \sqrt{f'_c}$) compared to the measured failure load of 67.83 kPa.

Fig. 6.12 shows the predicted response for specimen C5 with tension stiffening stress applied on concrete or on steel. It can be seen that good agreement is obtained by applying the tension stiffening stress to the concrete. On the other hand, the solution calculated by using the alternative approach which applies the tension stiffening stress to the steel did not agree with test results at all. One reason for this discrepancy is that under this procedure the tension stiffening stress is always oriented in the directions parallel to steel which ignores the fact that the tension stiffening stress should also rotate with the crack. In addition, the added tension stiffening stress decreases so fast that during the final loading stage there is no tensile stress to be lumped at the steel level. Consequently no tension stiffening effect exists at all.

The results of the above study indicate that the predicted post cracking behaviour of specimen C5 depends on those assumptions which influence the load carried by the concrete in tension. The sensitivity of these results to the analytical description of tension stiffening contradicts the normally held opinion that tension

stiffening can change the shape of the load-deflection curve but not its limiting or ultimate load. The present observations are however dependent on the loading conditions.

6.5.2 Effect of the Compressive Strength of Concrete

Massicotte et al. (1988) suggested the use of a reduced concrete compressive strength equal to 90% of f'_c to reflect the actual structural compressive strength compared to the compressive strength measured in cylinder test where some confinement may exist (Kotsovos, 1983). The value of $0.9 f'_c$ was chosen based on judgement since no extensive study was available on the ratio of the compressive strength measured with different techniques.

Figs. 6.13 and 6.14 illustrate the comparisons between the experimental and the computed responses for specimens B2 and C6 using f'_c and $0.9 f'_c$ as compressive strength of concrete. Specimen B2 had an aspect ratio of 1.5 and was tested under combined uniaxial inplane and lateral loads, while specimen C6 was square and was tested under combined biaxial inplane and lateral loads.

Using a cylinder strength of concrete of $0.9 f'_c$, the predicted failure loads of specimens B2 and C6 are about 0.95 and 0.91 of the test values, respectively. On the other hand, the use of the actual cylinder strengths which were obtained directly from the tests for specimens B2 and C6 resulted in predicted ultimate loads of 0.993 and 0.989 of the test values, respectively. As can be seen, the presence of inplane compressive loads places a heavy demand on the

compressive strength of concrete, especially in the case of specimen C6 where the inplane load was applied biaxially.

6.5.3 Predicted Behaviour of Selected Specimens

The material model described by Massicotte et al. (1988) was used to predict the behaviour of selected specimens under combined inplane and lateral loads. Massicotte et al. (1988) recommended the use of concrete tensile strength equal to $0.33 \sqrt{f'_c}$ and a compressive strength of concrete equal to 90% the cylinder strength. However, the use of a tensile strength equal to $0.9 f_{sp}$, as recommended by the CEB model code (1990), and a compressive strength equal to the cylinder strength were found to be a better choice in most cases and hence they are used in the following numerical study.

In addition to the above three specimens, the responses of six specimens under different combinations of inplane and lateral loads were investigated. In all these specimens, the inplane loads were applied first and held constant while the lateral load was monotonically applied until failure.

Table 6.1 summaries the material properties and the effective steel ratios, required for the tension stiffening model, for the specimens included in the analysis. Also included in the table are the properties of the three specimens used in the studies reported in previous sections, namely specimens C5, C6, and B2.

The measured and computed peak loads and the associated deflections at the center of the selected specimens are compared in Table 6.2. Comparisons of the experimental lateral load-out-of-plane deflection responses and the numerical ones are shown in Figs. 6.15 to 6.20. In general the numerically predicted ultimate loads and the failure modes are in good agreement with the experimental data. However, the predicted load-deflection responses in all cases, especially in the rectangular plates, are too stiff compared to the experimental ones. This could be attributed, in part, to the use of an initial modulus of elasticity of concrete in tension equal to that obtained from the compression tests of the cylinders.

The predicted distributions of strains in the bottom short element at the middle of specimens A2 and B2 are shown in Figs. 6.21 and 6.22 at selected lateral load levels. Also shown on the same figures are the measured values at the corresponding lateral load levels. The measured and predicted distributions are seen to differ significantly, although they generally have the same trend. This is to be expected to a certain degree since steel strains were measured at the locations of the cross wires which were crack locations and hence they represent the maximum values rather than the average ones. In the actual situation, a crack represents a strain discontinuity which can not be modelled correctly using the smeared cracking models. In the model used, a cracked integration point does not relieve the rest of the material in the element, but it has the effect of increasing the strains at the other integration points. This deficiency, however, does not make the model unusable, but it does

clearly point out that it should be only used to predict the global behaviour since its nature restricted its ability of reproducing localized behaviours.

6.6 Analysis of Plates Under Lateral Loads Only

To evaluate the ability of the material model in modelling the flexural behaviour of plates subjected to lateral load only, the rectangular specimen B1 and the square specimen C1 were analyzed. Table 6.3 contains the material properties and the effective steel ratios, used in the tension stiffening model, for these two specimens. As mentioned earlier, Newton-Raphson iteration was used to trace the load-deflection response for these two specimens. Upon initiation of cracking, the loading level is increased by steps of 0.5% to 5% of the ultimate load.

The measured and computed ultimate loads for specimens B1 and C1 and the associated deflections at the center are compared in Table 6.4. The predicted load-center deflection curves are compared with the test results in Figs. 6.23 and 6.24.

As previously mentioned, specimens tested under lateral loads only carried loads much higher than those predicted by the yield-line analysis and the tension steel in the orthogonal directions experienced extensive yielding. Owing to the upper bound limit set in Fig. 6.5, the tension stiffening stress in concrete is automatically reduced to zero after steel yields. Therefore, the predicted ultimate load is not affected by the manner of handling the tension stiffening.

However, the predicted response is stiffer than that obtained from the tests. This is related directly to the tension stiffening model.

One inadequacy of the tension stiffening model used stems from the fact that the degree of tension stiffening in any tensile region depends not only on the concrete properties, but also on the proximity of the tensile steel. Hence, the simple addition of one unloading curve for all concrete layers, whatever their location with respect to the tension steel, does not ensure satisfactory results in all cases. Concrete layers away from the reinforcement are not greatly influenced by the stiff reinforcing layer and hence their post-cracking behaviour should be controlled by the concrete strain softening characteristics independent of the bond effects. In other words, the shape of the unloading curve should be adjusted to reflect the position of each layer relative to the reinforcement.

The assumption of using the same stress-strain curve for all concrete layers had a profound effect on the predicted load-deflection response of specimens tested under lateral loads only since the depths of the tension zones in those specimens were much higher than those in specimens tested under combined loads, under the same lateral load level and hence there was more contribution from concrete layers located far from the reinforcement.

The results of the analyses carried out in this chapter indicate that the tension stiffening effect dominates the behaviour of thin under-reinforced concrete plates. For plates tested under combined loads, the assumptions which influence the load carried by concrete

in tension affect not only the load-deflection response but also the predicted strength.

Table 6.1 Concrete Properties and Effective Reinforcement Ratios Used in the Analyses of Specimens under Combined Loads

Specimen Designation	f'_c (MPa)	E_c (MPa)	f_t^* (MPa)	ρ_{effx} (%)	ρ_{effy} (%)
A2	22.66	21215	2.01	1.03	1.03
A3	22.87	21285	2.08	1.00	1.59
B2	19.27	20805	1.65	1.00	1.00
B3	19.53	20900	1.67	1.00	1.00
C2	25.27	21400	2.10	0.99	0.99
C4	25.35	21560	2.10	0.96	1.48
C5	25.81	21800	2.30	1.48	0.95
C6	25.44	21720	2.11	0.99	0.99
D2	26.12	20800	2.39	0.078	0.078

* Direct Tensile Strength of Concrete = 0.9 x Splitting Strength.

Table 6.2 Comparison of the Finite Element Predictions to the Test Results for Specimens under Combined Loads

Specimen Designation	Test		F.E. Model		Test Predicted	
	q_u (kPa)	w_{ou} (mm)	q_u (kPa)	w_{ou} (mm)	q_u	w_{ou}
A2	21.96	46.16	24.01	37.13	0.915	1.243
A3	23.90	67.19	25.11	37.50	0.954	1.792
B2	23.27	40.09	23.11	26.40	1.007	1.519
B3	25.52	45.83	24.34	28.60	1.048	1.602
C2	52.59	24.02	52.62	16.14	0.999	1.488
C4	59.47	25.70	58.30	18.56	1.020	1.385
C5	67.83	31.00	65.93	20.10	1.029	1.542
C6	69.16	18.78	66.92	16.44	1.033	1.143
D2	121.68	29.70	127.52	14.46	0.954	2.050

Mean = 0.995 1.529

Coefficient of Variation = 4.5% 17.9%

Table 6.3 Concrete Properties and Effective Reinforcement Ratios Used in the Analyses of Specimens under Lateral Loads Only

Specimen Designation	f'_c (MPa)	E_c (MPa)	f'_t * (MPa)	ρ_{effx} (%)	ρ_{effy} (%)
B1	18.70	20590	1.60	0.98	0.98
C1	25.21	21300	2.08	0.99	0.99

* Direct Tensile Strength of Concrete = 0.9 x Splitting Strength.

Table 6.4 Comparison of the Finite Element Predictions to the Test Results for Specimens under Lateral Loads Only

Specimen Designation	Test		F.E.Model		Test Predicted	
	q_u (kPa)	w_{ou} (mm)	q_u (kPa)	w_{ou} (mm)	q_u	w_{ou}
B1	45.91	101.22	42.10	105.10	1.09	0.963
C1	73.88	91.15	72.10	132.16	1.025	0.690

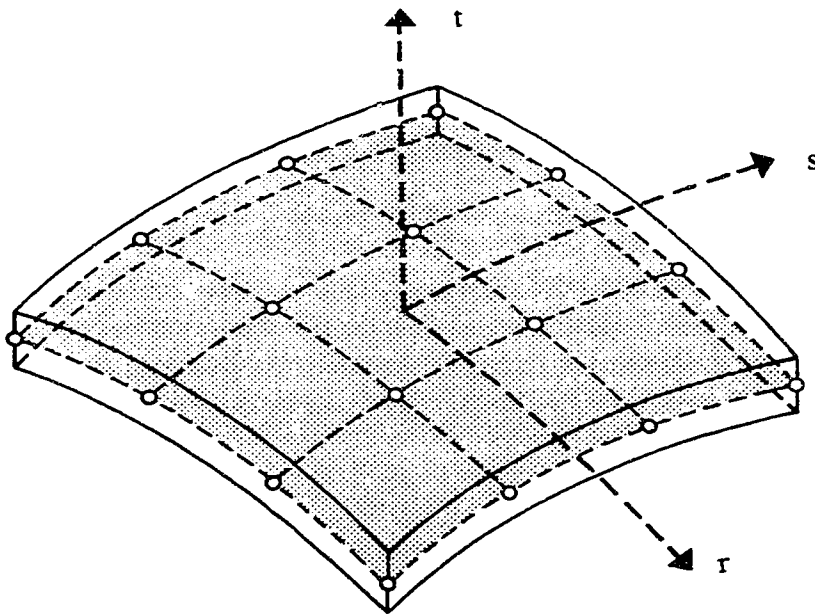


Figure 6.1 The 3D Degenerated Plate-Shell Element

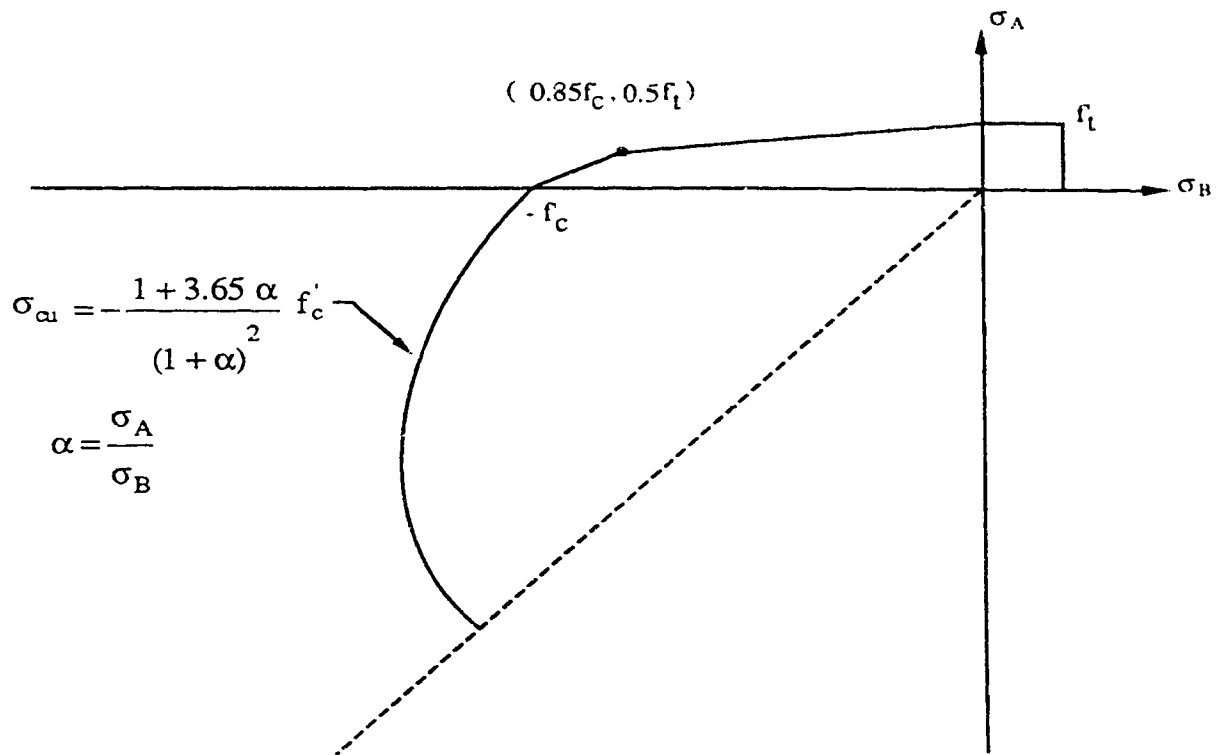


Figure 6.2 Failure Envelope

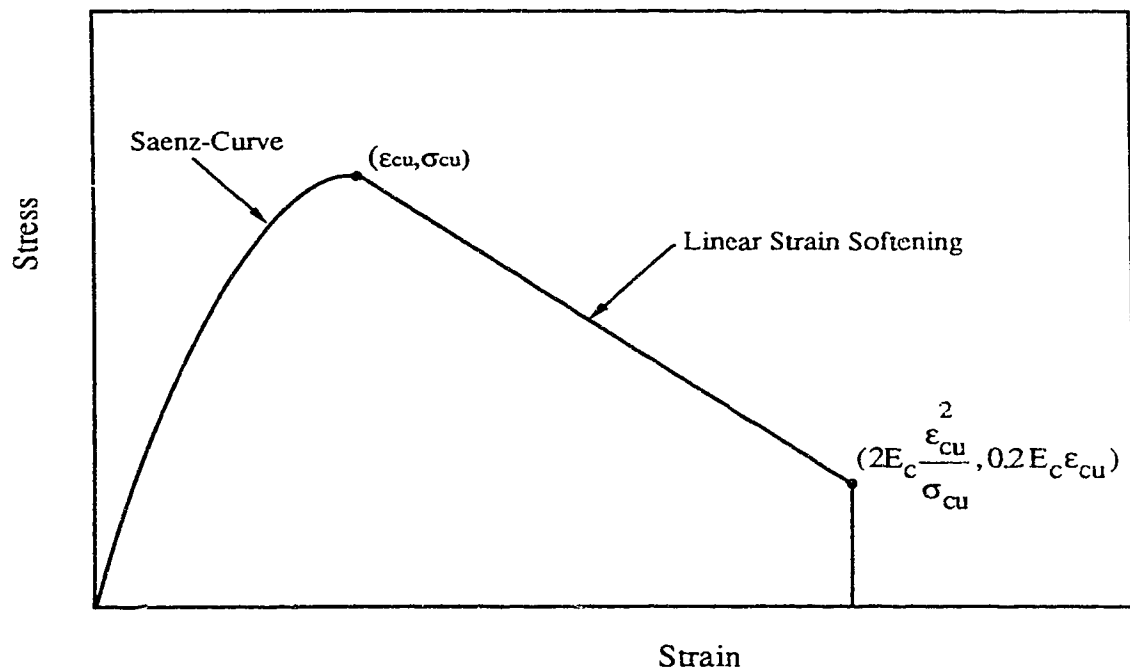


Figure 6.3 Stress-Equivalent Uniaxial Strain Curve for Concrete in Compression

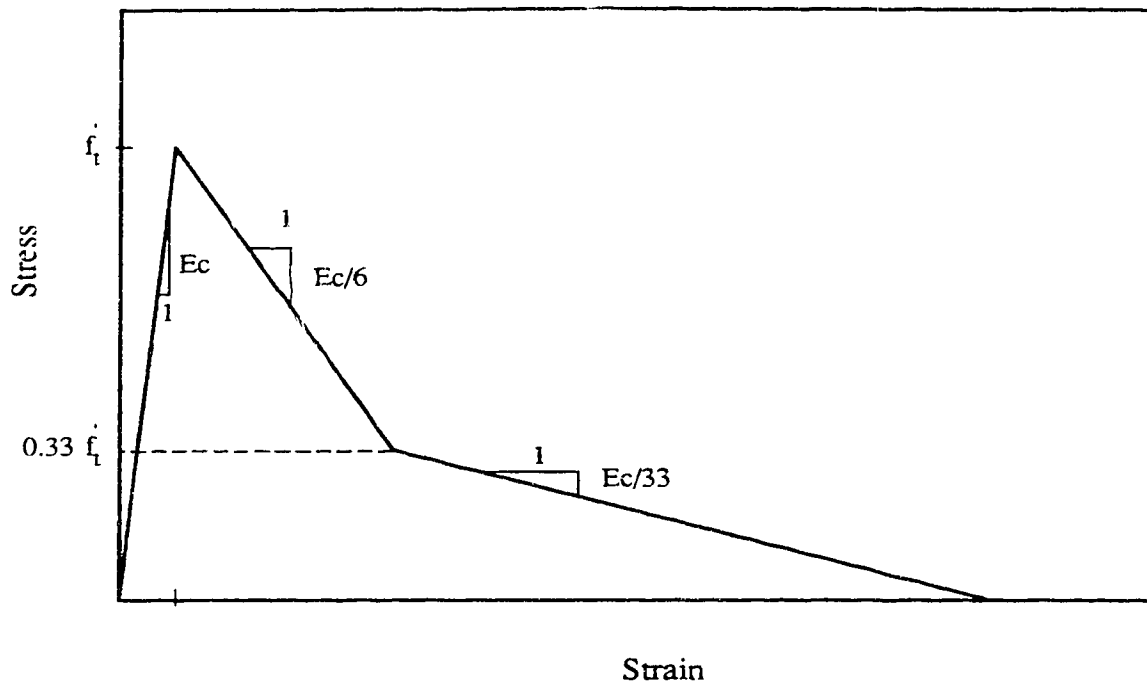


Figure 6.4 Tension Softening Curve for Plain Concrete

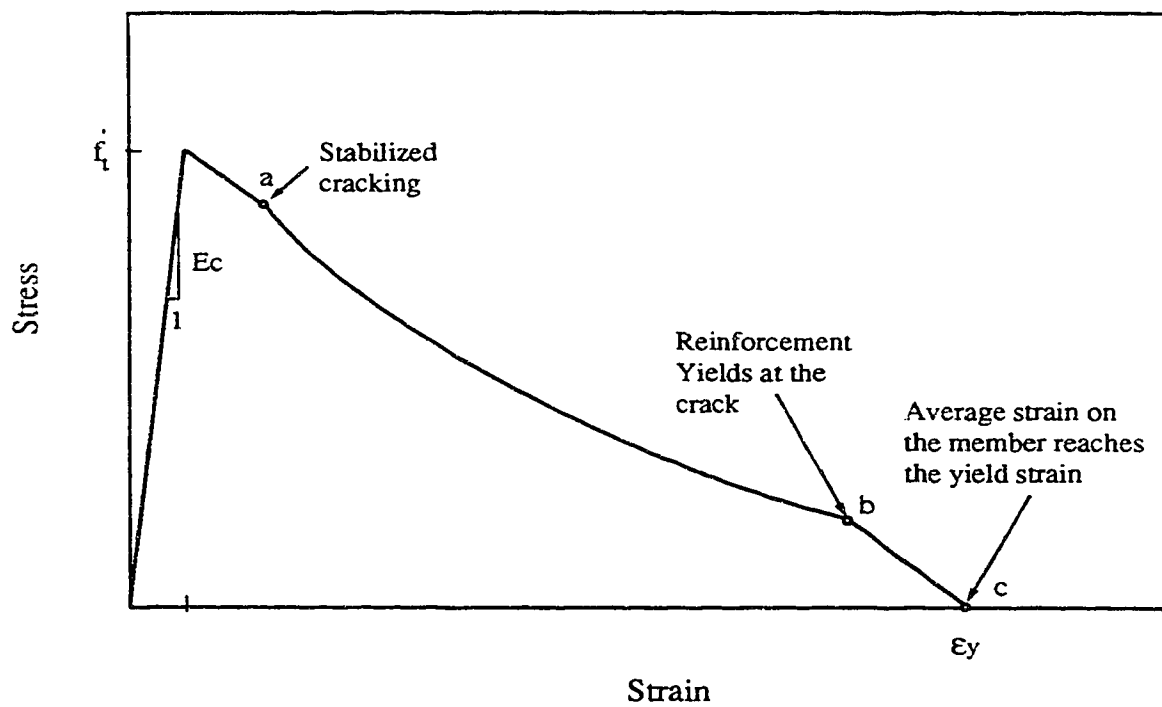
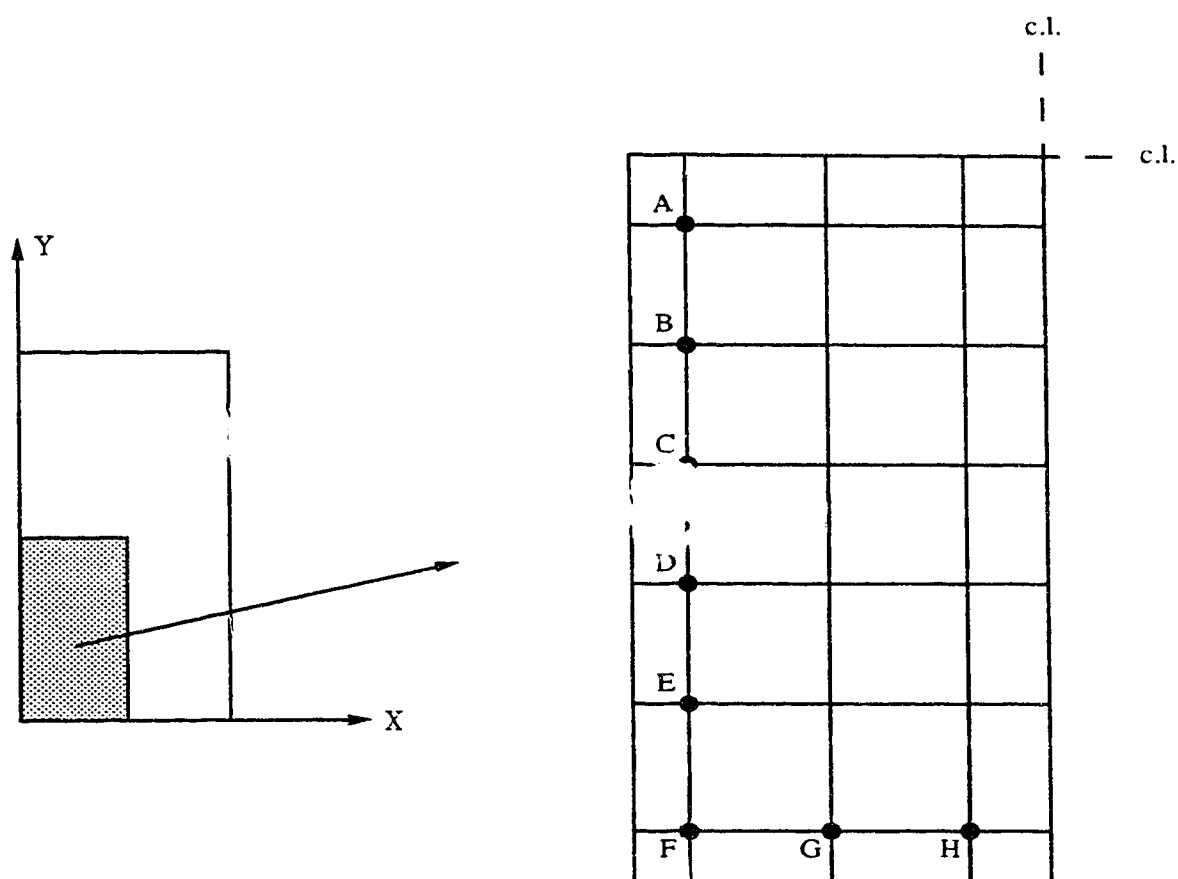


Figure 6.5 Tension Stiffening Curve for Reinforced Concrete



For Support Points A, B, C, D, and E,

$$w = 0.0, \theta_x = 0.0$$

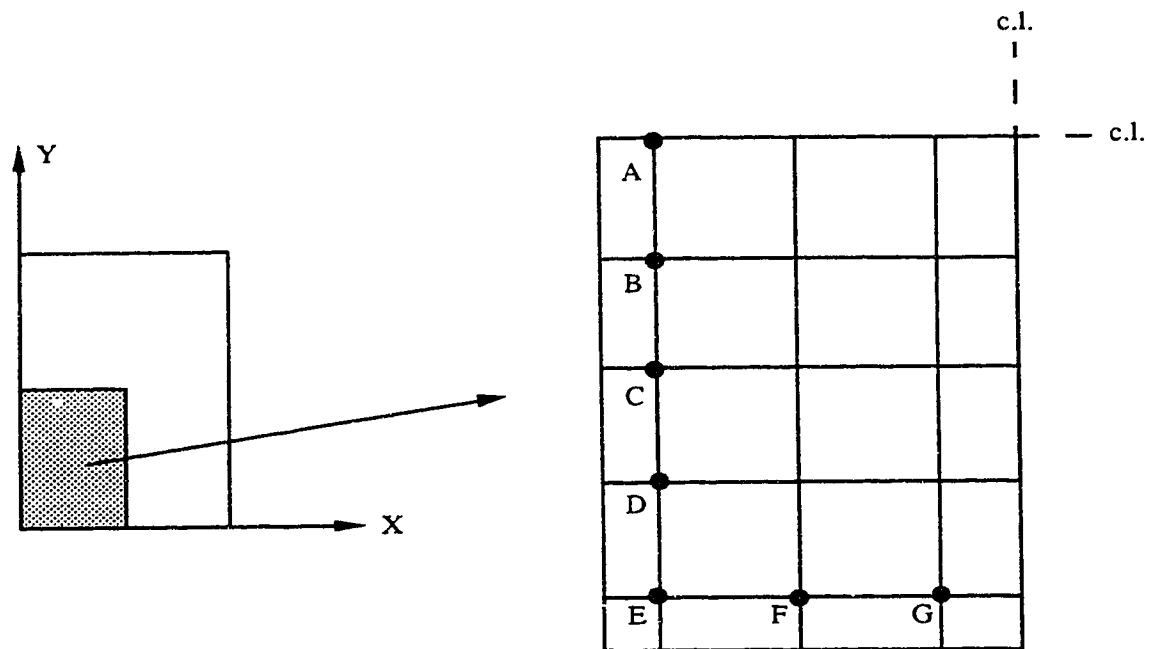
For Support Point F,

$$w = 0.0, \theta_x = \theta_y$$

For Support Points G, and H,

$$w = 0.0, \theta_y = 0.0$$

Figure 6.6 Modelling of Specimens of Series A



For Support Points A, B, C, and D,

$$w = 0.0, \theta_x = 0.0$$

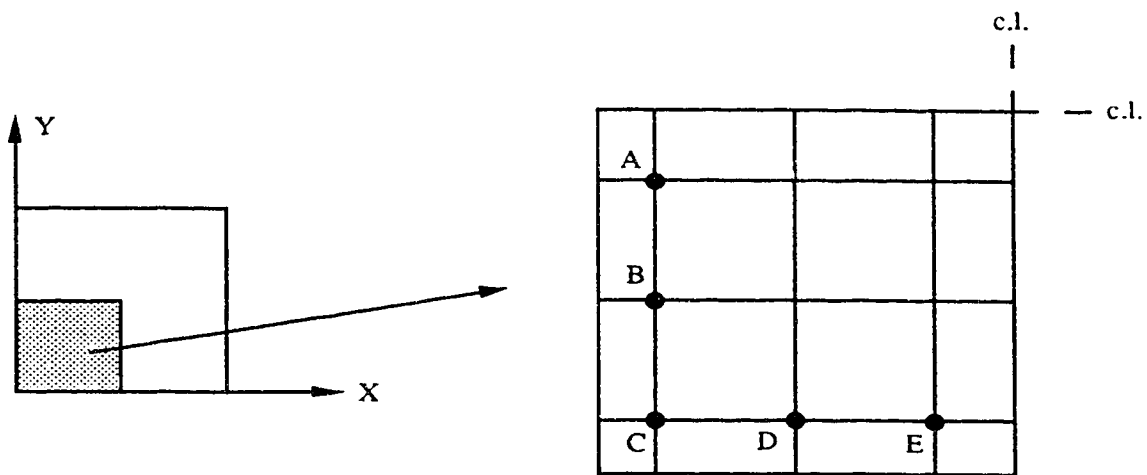
For Support Point E,

$$w = 0.0, \theta_x = \theta_y$$

For Support Points F, and G,

$$w = 0.0, \theta_y = 0.0$$

Figure 6.7 Modelling of Specimens of Series B



For Support Points A, and B,

$$w = 0.0, \theta_x = 0.0$$

For Support Point C,

$$w = 0.0, \theta_x = \theta_y$$

For Support Points D, and E,

$$w = 0.0, \theta_y = 0.0$$

Figure 6.8 Modelling of the Square Specimens

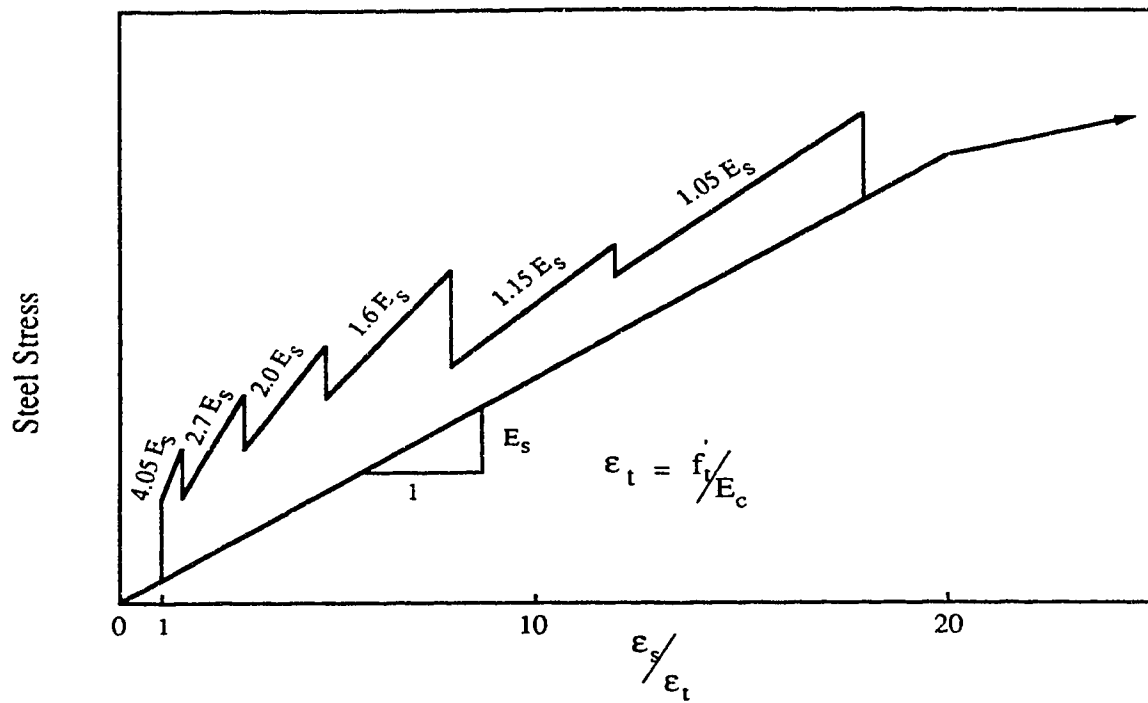


Figure 6.9 Modified Stress-Strain Diagram for Reinforcing Steel to Account for Tension Stiffening

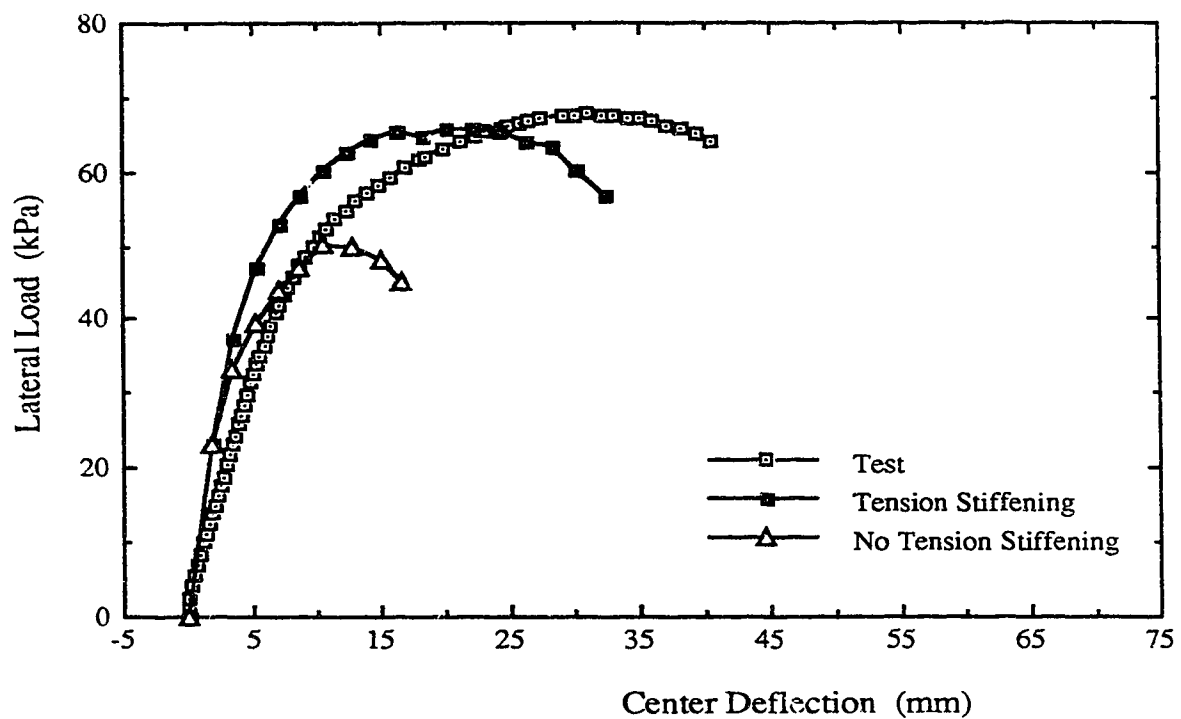


Figure 6.10 Specimen C5 - Effect of Tension Stiffening

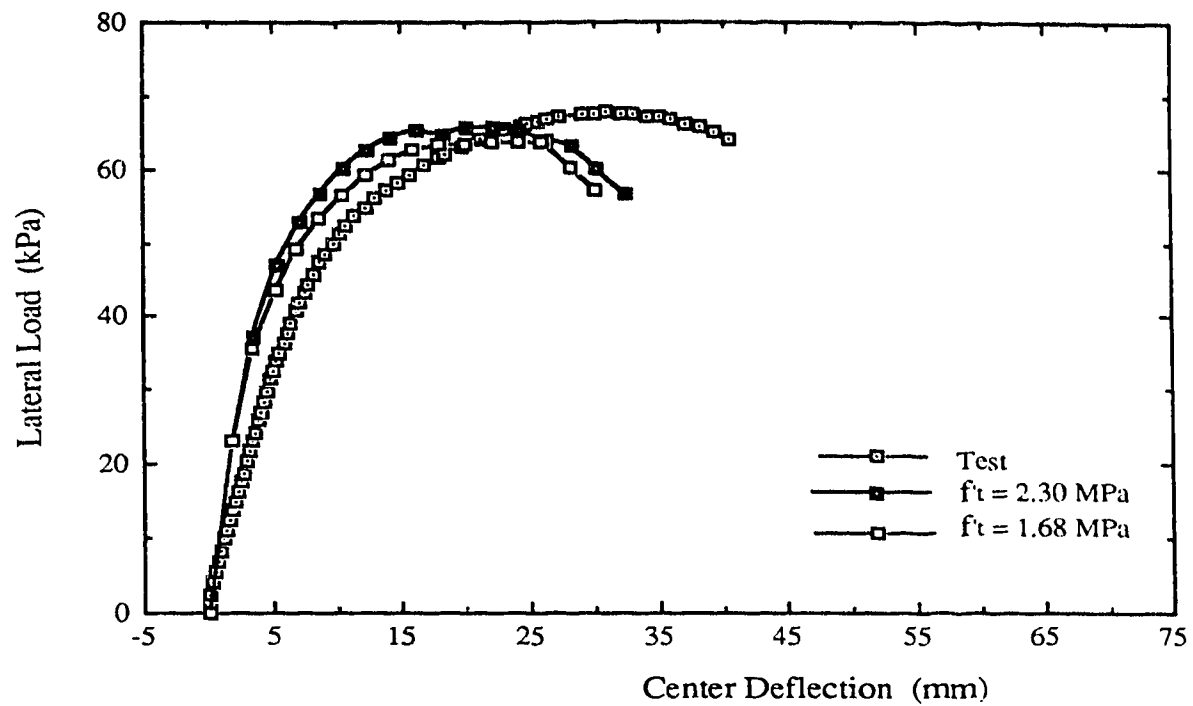


Figure 6.11 Specimen C5 - Effect of the Tensile Strength of Concrete

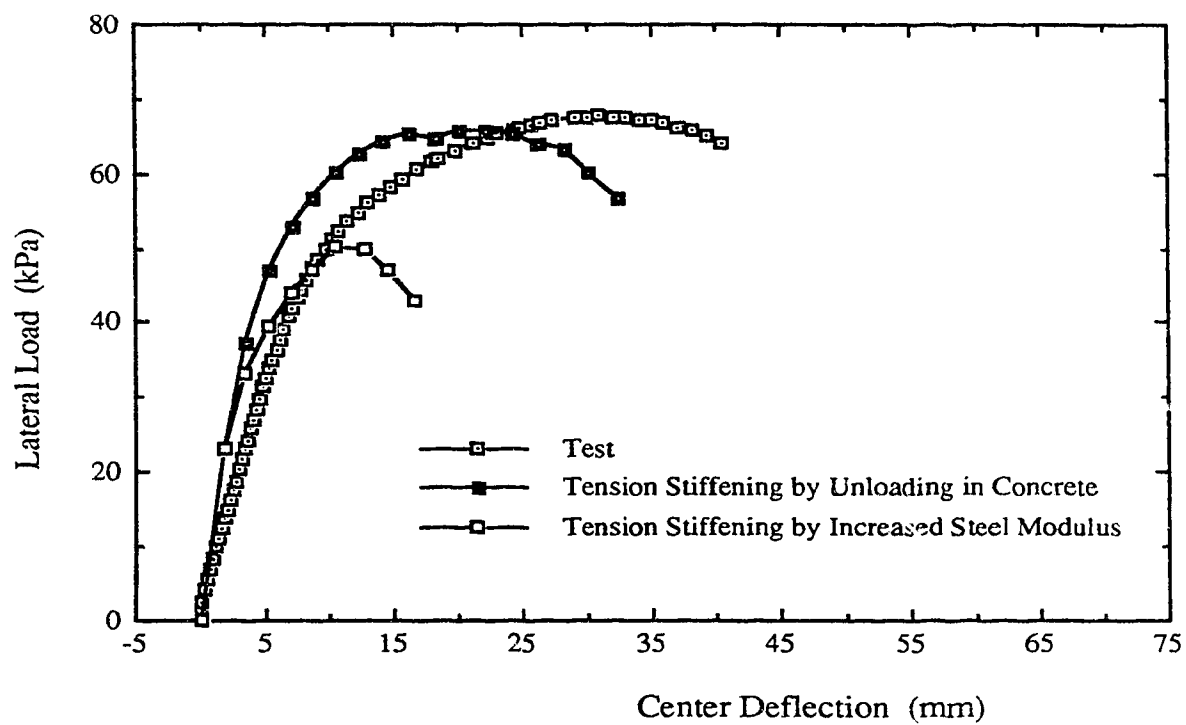


Figure 6.12 Specimen C5 - Comparison Between Tension Stiffening Models

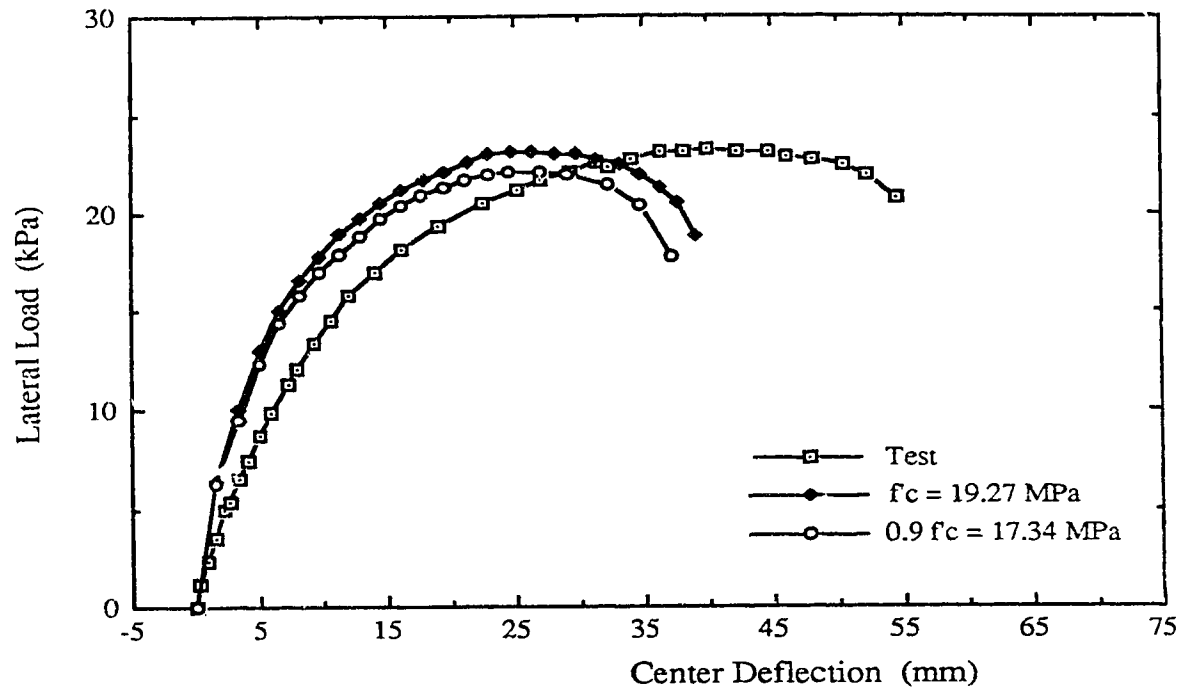


Figure 6.13 Specimen B2 - Effect of the Compressive Strength of Concrete

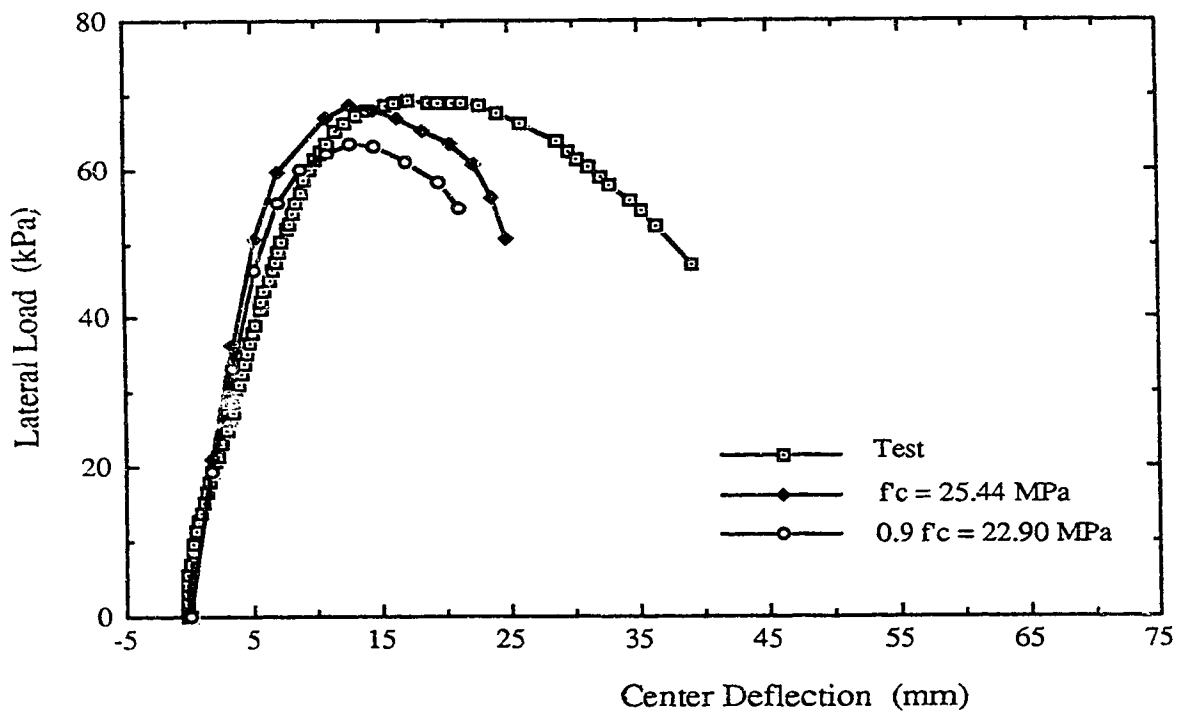


Figure 6.14 Specimen C6 - Effect of the Compressive Strength of Concrete

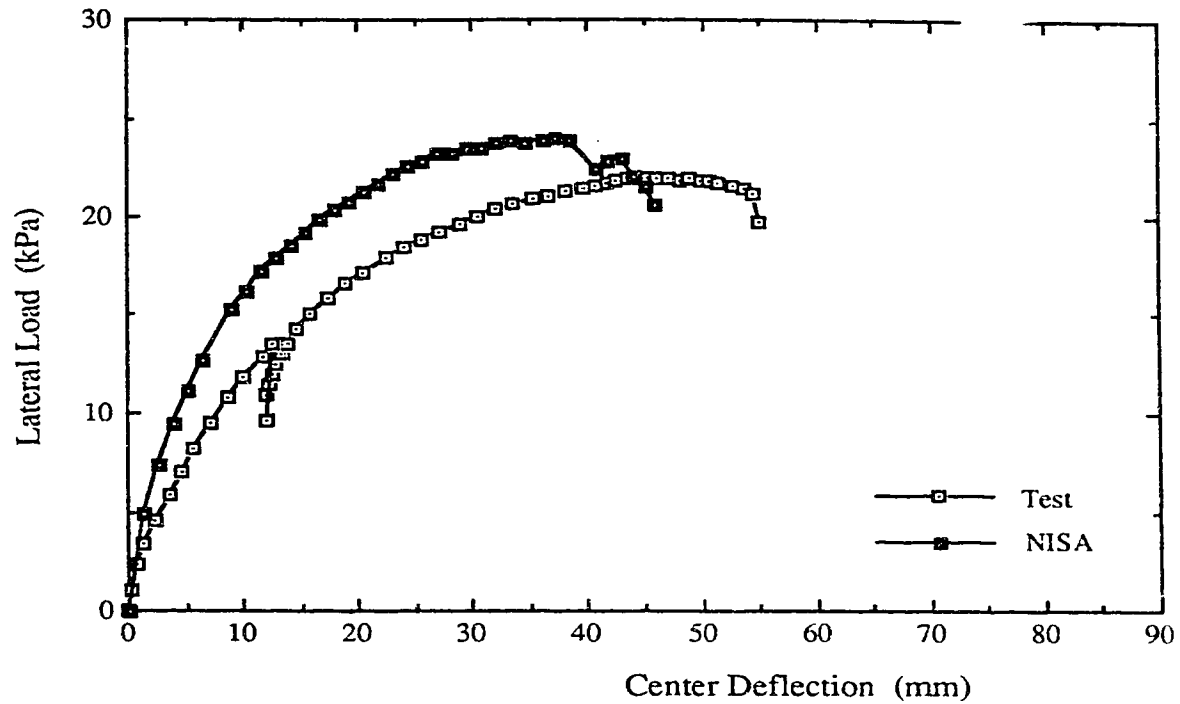


Figure 6.15 Experimental and Analytical Lateral Load versus Central Deflection Curves for Specimen A2

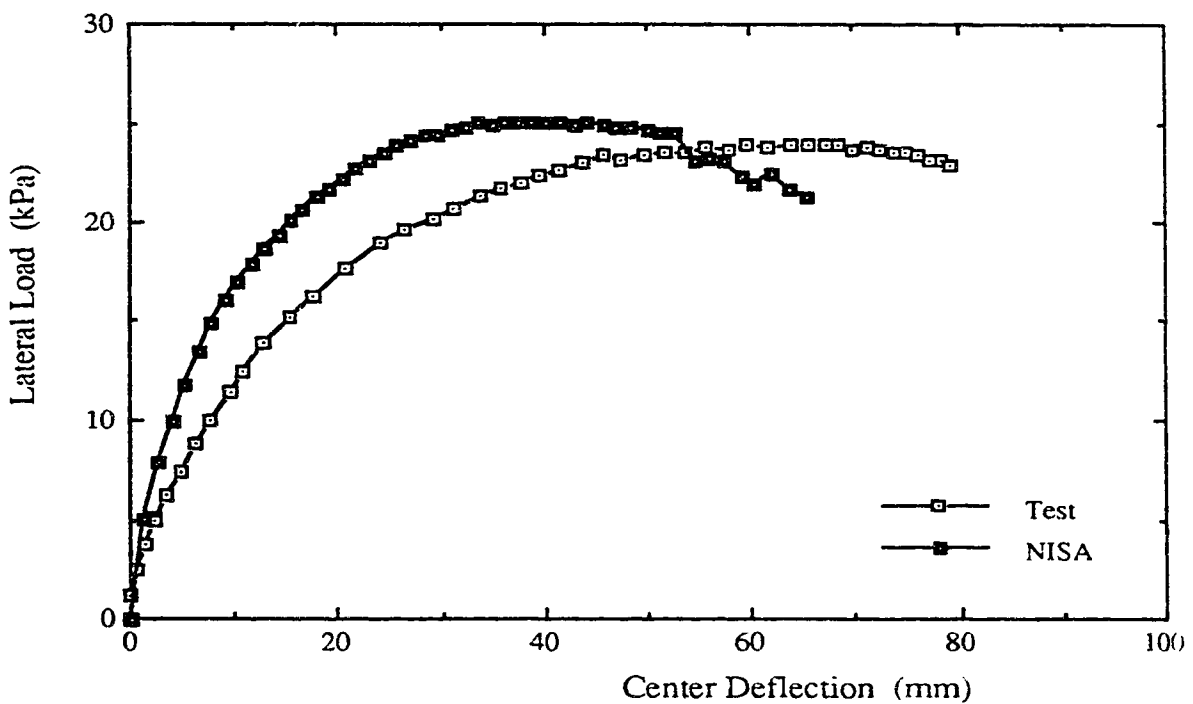


Figure 6.16 Experimental and Analytical Lateral Load versus Central Deflection Curves for Specimen A3

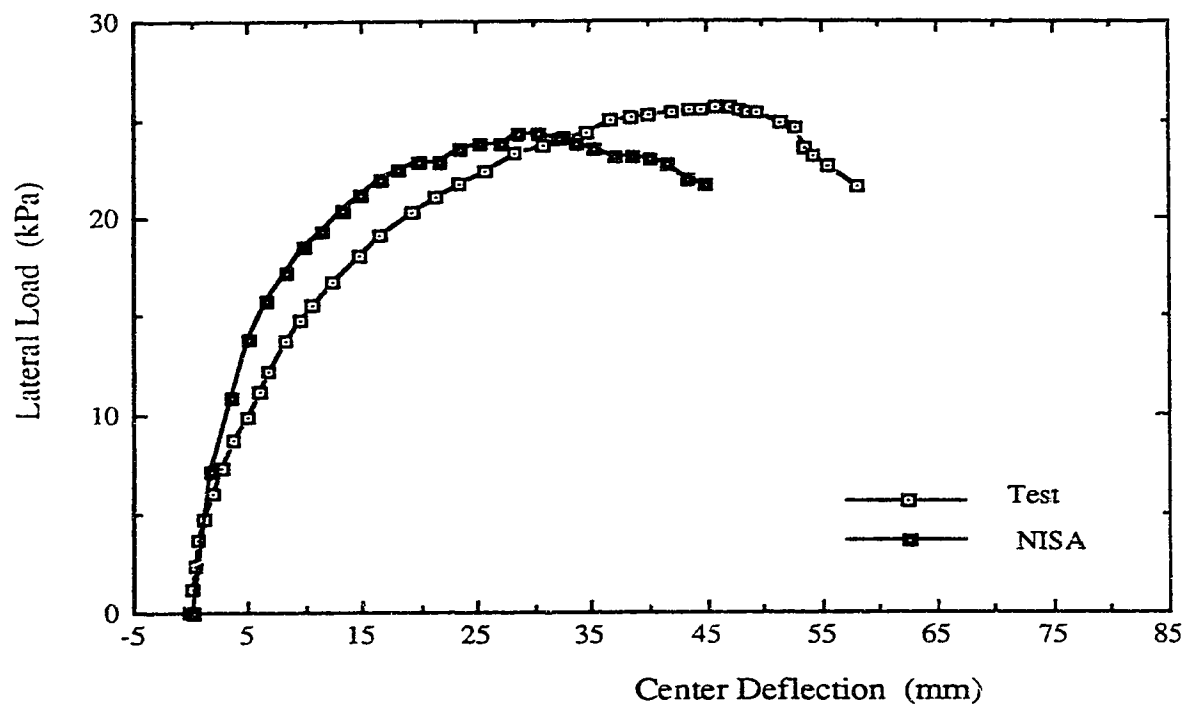


Figure 6.17 Experimental and Analytical Lateral Load versus Central Deflection Curves for Specimen B3

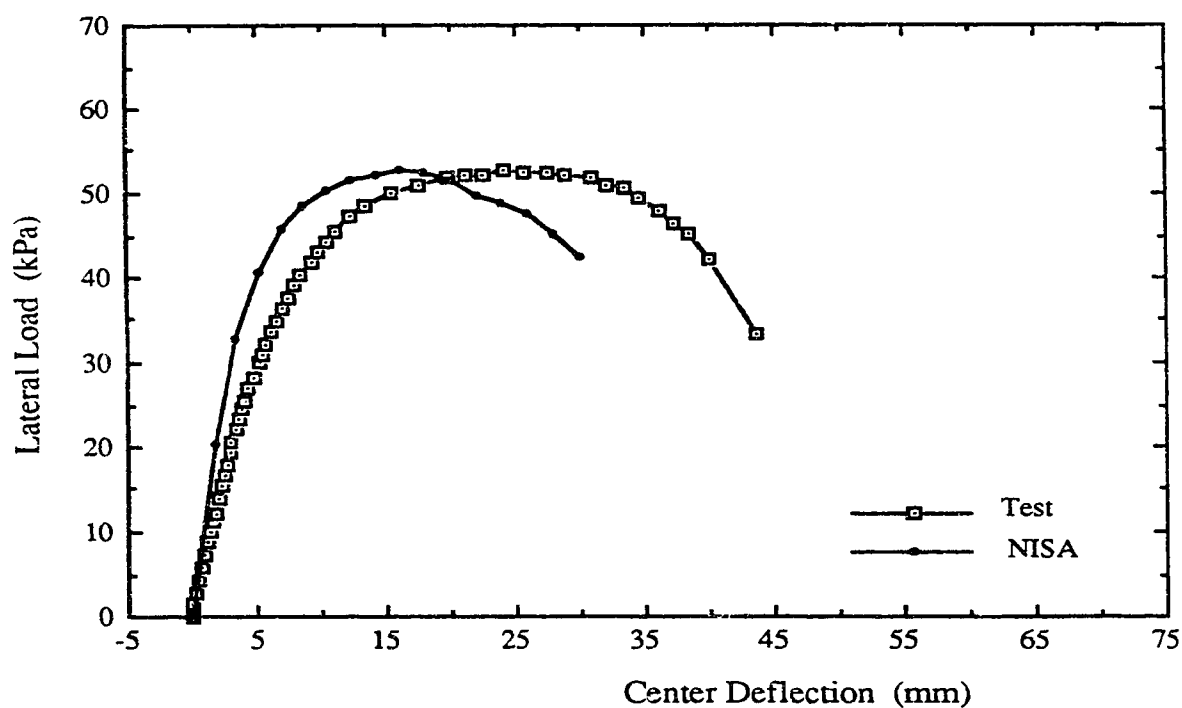


Figure 6.18 Experimental and Analytical Lateral Load versus Central Deflection Curves for Specimen C2

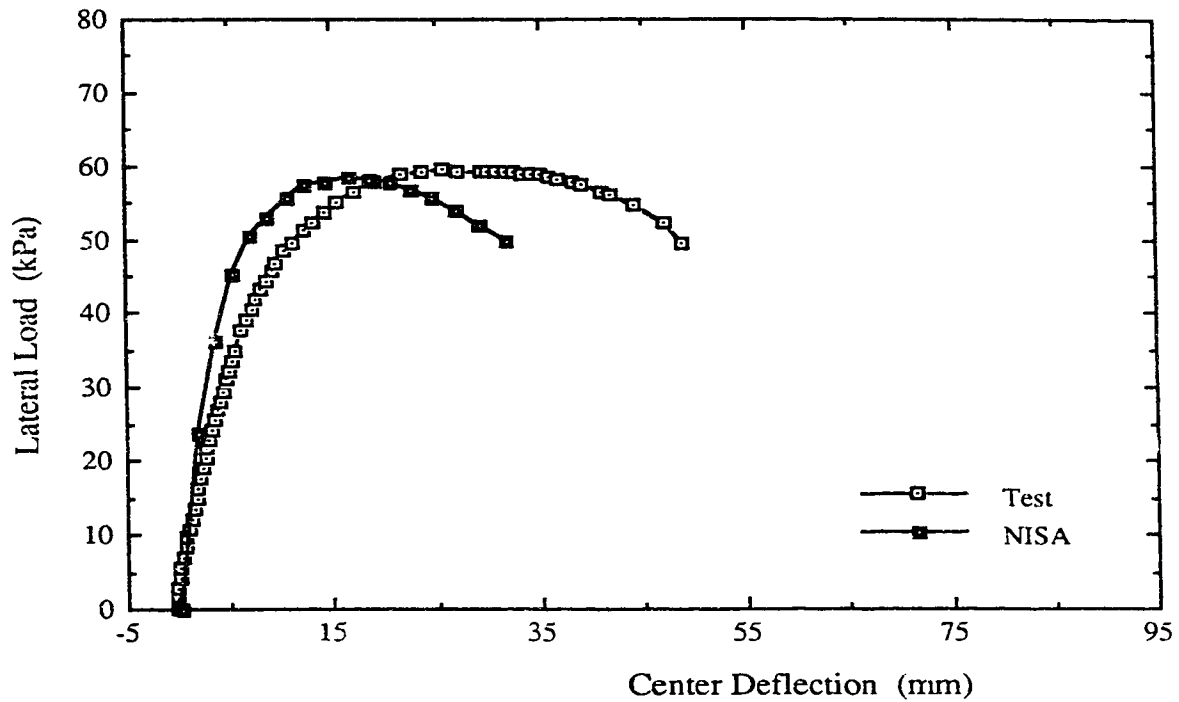


Figure 6.19 Experimental and Analytical Load versus Central Deflection Curves for Specimen C4

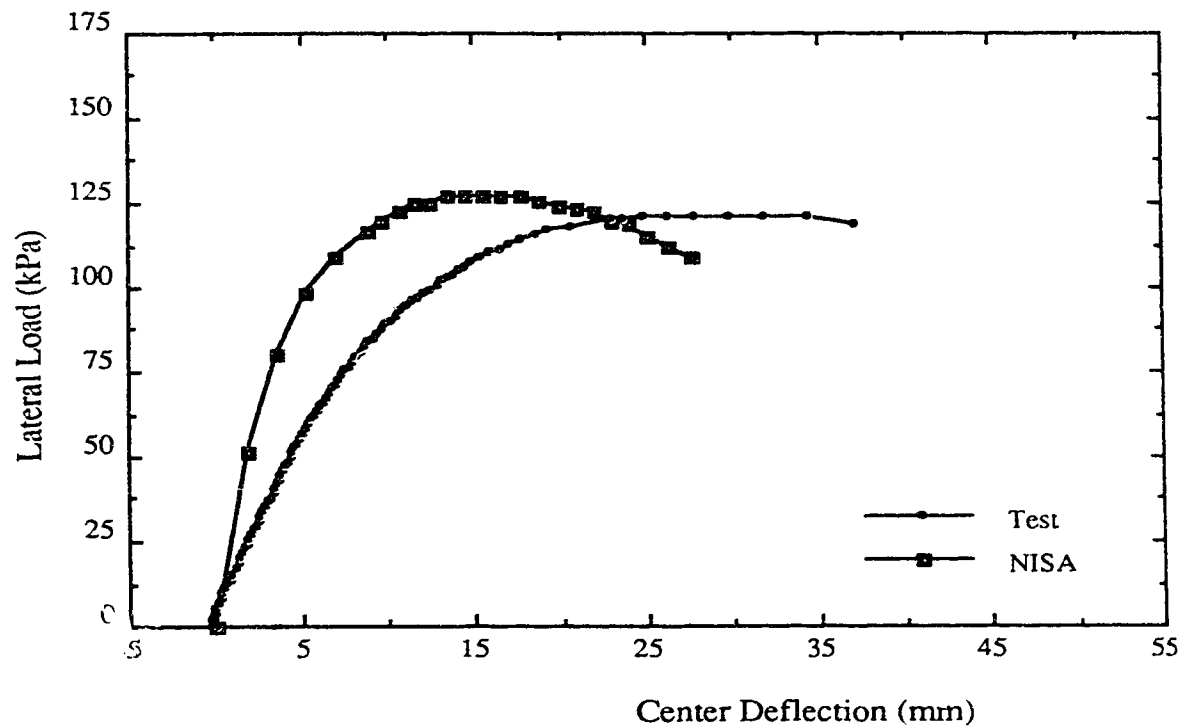


Figure 6.20 Experimental and Analytical Load versus Central Deflection Curves for Specimen D2

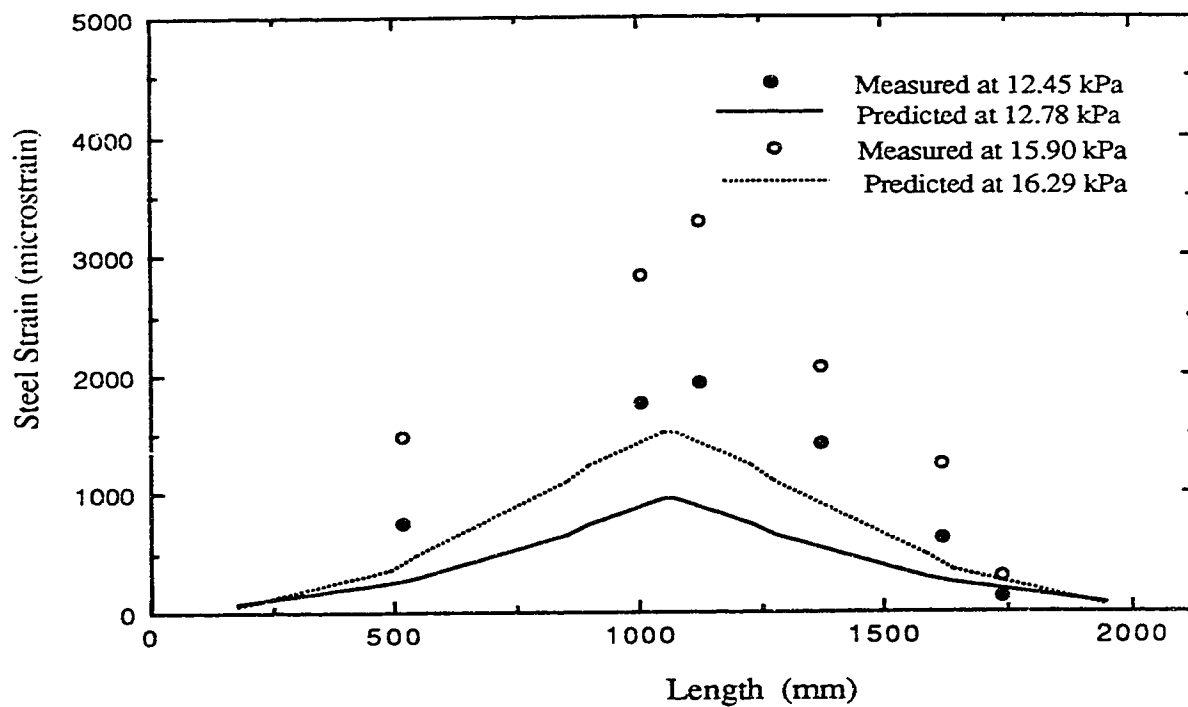


Figure 6.21 Predicted and Measured Strains in Bottom Reinforcement for Specimen A2

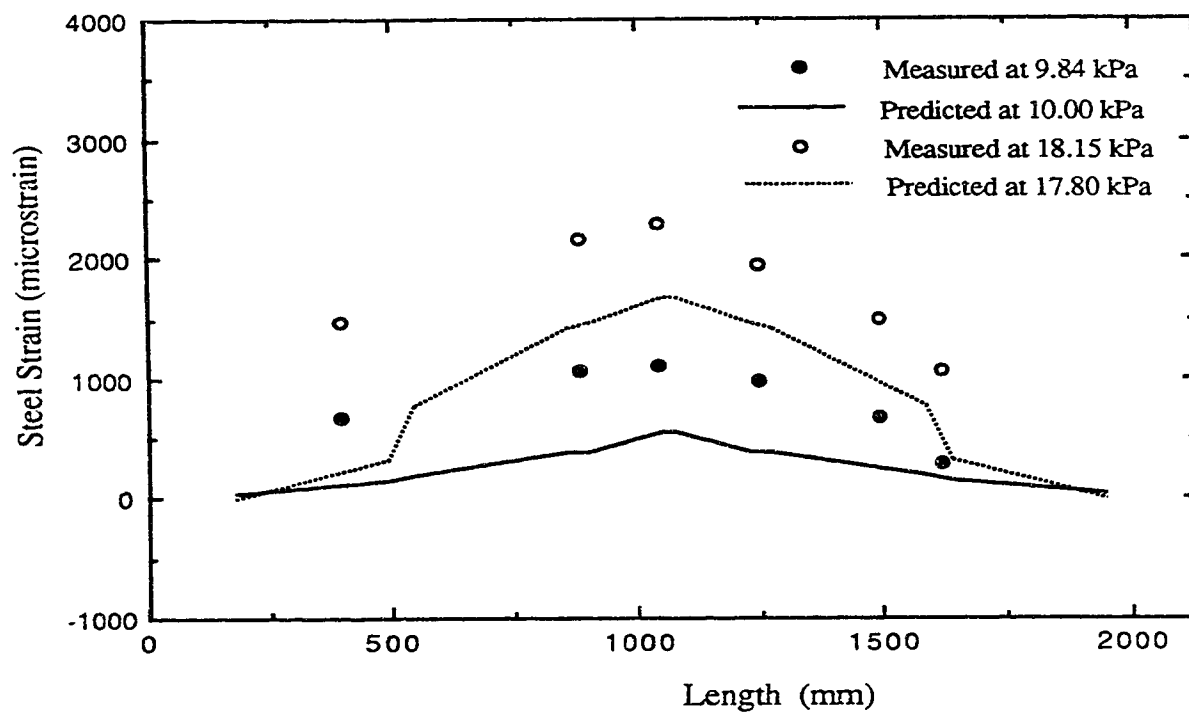


Figure 6.22 Predicted and Measured Strains in Bottom Reinforcement for Specimen B2

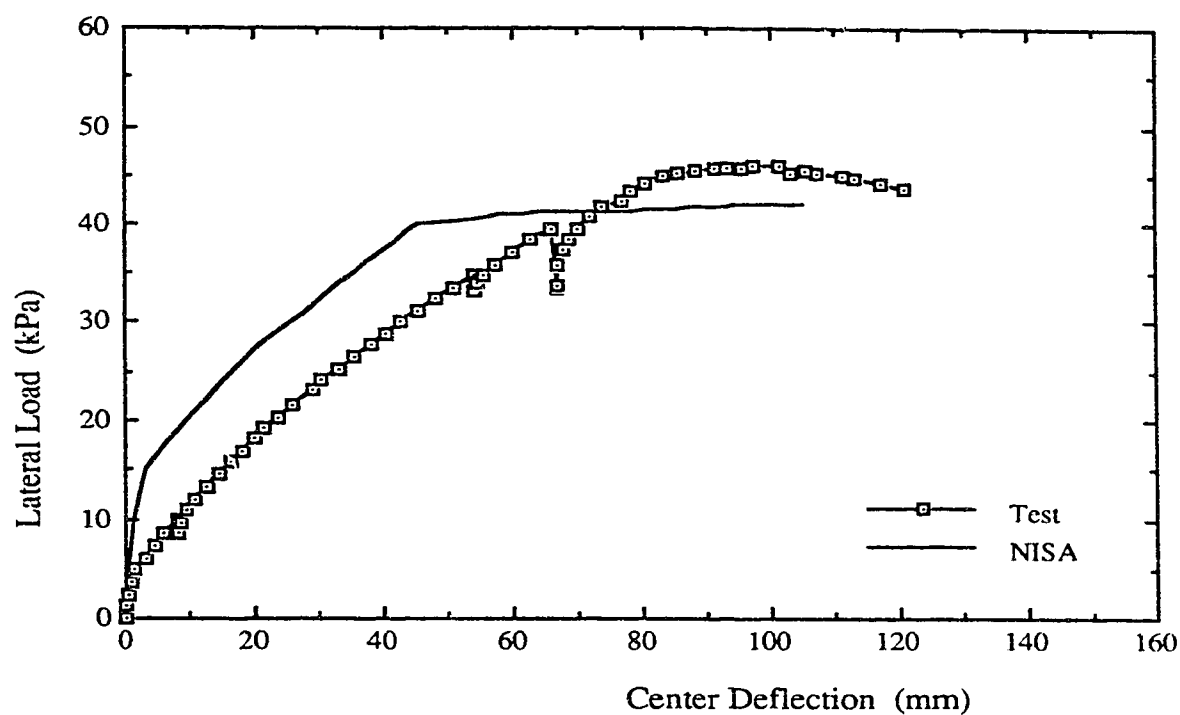


Figure 6.23 Experimental and Analytical Lateral Load versus Central Deflection Curves for Specimen B1

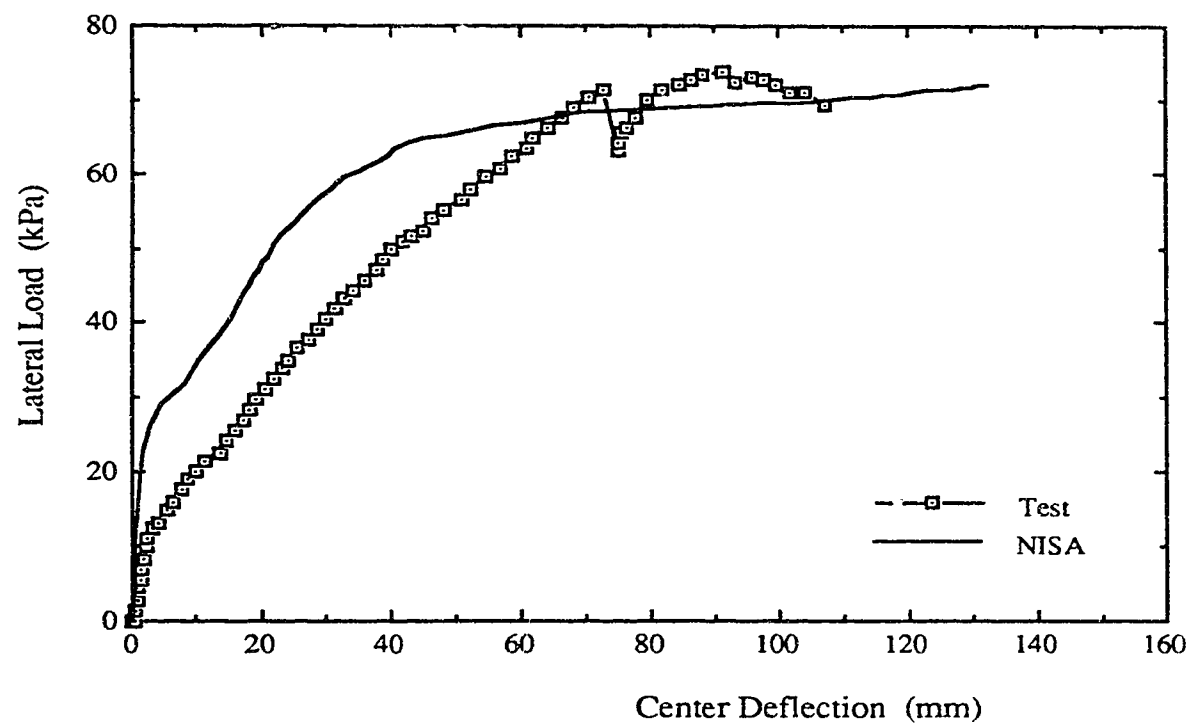


Figure 6.24 Experimental and Analytical Lateral Load versus Central Deflection Curves for Specimen C1

7. Summary, Conclusions and Recommendations

7.1 Summary

The behaviour of reinforced concrete plates simply supported on the four edges and subjected to combined inplane compressive and lateral loads was investigated.

The experimental phase of the study consisted of testing 19 specimens to failure to evaluate the effects of loading type, slenderness, inplane load level, aspect ratio, reinforcement content in the two orthogonal directions and loading sequence on the different aspects of the behaviour. A test frame was constructed to conduct such tests. It was similar to the one used by Aghayere and MacGregor (1988) with new added features to minimize uncertainties in the support boundary conditions and in the method of applying the inplane load. The test specimens were divided into four series, each of which had a specimen which was tested under lateral load only for comparison with those tested under combined loads within the same series.

The analytical phase of the study included the development of a simple model for predicting the lateral load capacity of plates subjected to predefined inplane load. Experimental observations indicated that the model can also be used in cases where the inplane and lateral loads are applied simultaneously in a proportional manner.

The prediction of the response of plates under combined loads using nonlinear finite element analysis was also investigated. The NISA code was used as the analytical tool for the analysis where geometrical nonlinearity was included using Updated Lagrangian formulation and material nonlinearity was included using an incremental hypoelastic plane stress material model for reinforced concrete implemented in a 3D degenerated plate-shell element.

7.2 Conclusions

Based on the experimental observations, the following conclusions are drawn:

1. Specimens tested under lateral loads only carried loads much higher than those predicted by the yield-line analysis. This is partly attributed to the strain hardening of steel and also to the tensile membrane action which developed at large deflections.
2. Specimens tested under combined uniaxial inplane and lateral loads behaved highly anisotropically, since the presence of the inplane compressive load delayed the cracking normal to the inplane load direction.
3. The failure of plates tested under combined loads was either caused by compressive crushing of concrete, before or after yielding of the tension steel, because of the limited deformability of concrete

in compression, or by the instability of the plate where due to the increase in deflection, the external moments increased more rapidly than the internal resisting moments.

4. The effect of the inplane load on the lateral load capacity of reinforced concrete plates depends mainly on the slenderness of the plate. For stocky square plates, the presence of the inplane load increased the lateral load capacity as the geometrical nonlinearity effect of the inplane load consumed only a part of the enhanced moment capacity of the plate cross section in the direction of the inplane load. On the other hand, the presence of the inplane load resulted in serious reduction in their lateral load capacity since the second-order effect of the inplane load dominated the behaviour.

5. For plates tested under combined uniaxial inplane and lateral loads, an increase in the lateral load capacity was achieved more efficiently by increasing the reinforcement ratio in the direction perpendicular to the inplane load than it was by increasing the reinforcement parallel to the inplane load. This was particularly noticeable for rectangular specimens loaded along the short sides.

6. Although the lateral load capacity of the rectangular specimen which had inplane loads applied along the long sides was less than that of an identical one that was uniaxially loaded along the short sides, the reduction in strength was much less than one would expect

for metal plates. This is attributed to the fact that the increased flexural capacity of the plate section in the short direction compensated for part of the reduction of the plate action.

7. For moderate values of inplane load levels, increasing the inplane load level may result in an increase or a decrease of the lateral load capacity of plates carrying combined loads. This depends on several factors such as the aspect ratio of the plate, its slenderness, and whether the inplane load is applied uniaxially or biaxially.

8. The loading sequence is a significant factor in determining the ultimate strength of plates subjected to combined loads. In the cases tested, proportional loading or prior application of the inplane load resulted essentially in the same lateral load-deflection response and the same ultimate strength. On the other hand, the effect of a prior application of the lateral load depended on the state of the cracking and the out-of-plane deflection of the plate when the inplane load was applied.

The analytical model developed gave good predictions of the measured maximum lateral loads. The approximate approach of treating the pronounced anisotropic properties of reinforced concrete plates under combined loads proved to be adequate for practical purposes.

The nonlinear finite element analysis of the test specimens highlighted the effect of the assumptions which influence the load carried by concrete in tension on the prediction of the response of plates subjected to combined inplane and lateral loads. The results contradicted the normally held opinion that the tension stiffening could change the shape of the load deflection response but not the ultimate strength. Although the predicted ultimate strengths were in good agreement with the test results, the predicted load-deflection responses were in general too stiff compared to the measured ones especially in specimens which were tested under lateral loads only. This could be in part attributed to the use of the same tension stiffening model for all concrete layers in tension. Also, the used stress-strain curve of plain concrete in tension that assumed an initial modulus of elasticity equal to that obtained from the compression tests seems to contribute to the apparent stiff predicted response.

7.3 Recommendations for Future Study

Experimental and analytical studies are needed to study the behaviour of plates with boundary conditions other than simply supported under combined loads.

Since most of the floating concrete structures and those used in offshore structures are made of prestressed, post-tensioned concrete, tests and analytical studies on prestressed concrete plates under combined inplane and lateral loads would be of great interest. The

simultaneous effect of positive factors (the increase in the stiffness of the plate, the delay of crack initiation and limitation of their width) and the negative factors (increase in stress level in compressed concrete) may affect the carrying capacity favorably or unfavorably.

In future improvements of the constitutive models for reinforced concrete, attention must be devoted to the need of a tension stiffening model that allow concrete layers in the tension zone to follow different stress-strain curves. The widely used assumption that the initial modulus of elasticity of concrete in tension can be taken as the one in compression seems to be unrealistic even if one is studying short term behaviours. Very little information is available concerning this important property. Additional information on this subject can be a significant improvement. Also, analytical modelling of decay in concrete compressive strength and stiffness due to increasing lateral tensile strains should be investigated. Additional experimental data in this area are needed.

References

Aas-Jakobsen, K., 1983, "Buckling of Walls," Comite Euro-International du Beton, Bulletin D'Information No. 155, pp. 223-250.

Abbasi, A. F. and Siess, C. P., 1969, "Effect of Stress-Strain Characteristics of High-Strength Reinforcement on the Behaviour of Reinforced Concrete Beam-Columns," Civil Engineering Studies, Structural Research Series No. 354, University of Illinois, Urbana, September.

ACI Committee 318-89, 1989, "Building Code Requirements for Reinforced Concrete," American Concrete Institute, Detroit, Michigan.

ACI Committee 357, 1988, "Barge-Like Concrete Structures," ACI Structural Journal, Vol. 85, No.1, January-February, pp. 102-105.

ACI Committee 209, 1982, "Prediction of Creep, Shrinkage, and Temperature Effects in Concrete Structures, in Designing for the Effects of Creep, Shrinkage, and Temperature in Concrete Structures," SP 76, ACI, Detroit, Michigan, pp. 193-300.

Aghayere, A. O. and MacGregor, J. G., 1988, "Stability of Concrete Plates," Structural Engineering Report No. 157, Department of Civil Engineering, University of Alberta, Edmonton, Alberta, 178 p.

Bathe, K.-J., 1982, "Finite Element Procedures in Engineering Analysis," Prentice-Hall, 735 p.

Bazant, Z. P. and Oh, B. H., 1984, "Deformation of Progressively Cracked Reinforced Concrete Beams," ACI Journal, Proceedings Vol. 81, No. 3, May-June, pp. 268-278.

Bazant, Z. P., Cedolin, L. and Tabbara M. R., 1991, "New Method of Analysis for Slender Columns," ACI Structural Journal, Vol. 88, No. 4, pp. 391-401.

Bazant, Z. P. and Cedolin, L., 1991, "Stability of Structures," Oxford University Press, New York, 984 p.

Bell, J. C. and Elms, D. G., 1971, "A Finite element Approach to Post-Elastic Slab Behaviour. Cracking, Deflection, and Ultimate Load of Concrete Slab Systems," SP 30, ACI, Detroit, Michigan, pp. 325-344.

Breen, J. E. and Ferguson, P. M., 1964, "The Restrained Long Concrete Column as a Part of a Rectangular Frame," ACI Journal, Proceedings Vol. 61, No. 5, May, pp. 563-585.

Broms, B. and Viest, I. M., 1961, "Long Reinforced Concrete Columns," A Symposium, Transactions, ASCE , Vol. 126, p. 308, (21D,23).

Canadian Standards Association (CSA), 1990, "Methods of Tests for Concrete," National Standards of Canada, CAN3-A23.2-M90, Canadian Standards Association, Rexdale, Ontario.

Carreira, Domingo J. and Chu, Kuang-Han, 1986, "The Moment-Curvature Relationship of Reinforced Concrete Members," ACI Journal, Vol. 83, No. 2, Mar.-Apr., pp. 191-198.

CEB/FIP, 1978, "Model Code for Concrete Structures," Comite Euro-International du Beton, Bulletin D'Information No. 124/125-E, 348 p.

CEB/FIP, 1985, "Cracking and Deformations," Comite Euro-International du Beton, Bulletin D'Information No. 158, Paris.

CEB/FIP, 1990, "Model Code for Concrete Structures," Comite Euro-International du Beton, First Draft, Bulletin D'Information No. 195, Paris.

Clark, L. A., 1972, "Tests on Slab Elements and Skew Slab Bridges Designed in Accordance with the Factored Elastic Moment Field," Cement and Concrete Association, Technical Report 42.474, September, London, 47 p.

Clark, L. A. and Speirs, D. M., 1978, "Tension Stiffening in Reinforced Concrete Beams and Slabs under Short-Term Load," Cement and Concrete Association, Technical Report 42.521, July, London, 19 p.

Clark, L. A. and White, I. G., 1978, "Tests to Determine the Torsional Stiffness of Flexurally Cracked Slab Elements," Cement and Concrete Association, Technical Report 42.517, January, London, 22 p.

Collins, M. P. and Mitchell, D., 1987, "Prestressed Concrete Basics," Canadian Prestressed Concrete Institute, Ottawa, 614 p.

Ernst, G. C., 1952, "Stability of Thin-Shelled Structures," ACI Journal, Vol. 49, No. 24, December, pp. 277-292.

Favre, R., Charif, H. and Jaccoud, J., 1990, "Improved Serviceability of Reinforced Concrete Slabs with the Use of High Strength Concrete," SP 121, ACI, Detroit, Michigan, pp. 89-108.

Ferry-Borges, J. and Arantes Olivira, E. R., 1963, "Nonlinear Analysis of Reinforced Concrete Structures," Publication, International Association for Bridge and Structural Engineering, Vol. 23, pp. 51-70.

Gilbert, R. I. and Warner, R. F., 1978, "Tension Stiffening in Reinforced Concrete Slabs," Journal of the Structural Division, ASCE, Vol. 104, No. ST12, December, pp. 1885-1900.

Girolami, A. G., Sozen, M. A. and Gamble, W. L., 1970, "Flexural Strength of Reinforced Concrete Slabs with Externally Applied Inplane Forces," and Gamble, W. L., Flug, H. and Sozen, M. A., "Strength of Slabs Subjected to Multiaxial Bending and Compression,"

Civil Engineering Studies, Structural Research Series No. 369, Department of Civil Engineering, University of Illinois, Urbana, Ill.

Ghali, A. and Favre, R., 1986, "Concrete Structures: Stresses and Deformations," Chapman & Hall, New York, 352 p.

Ghosh, S. K. and Cohn, M. Z., 1972, "Ductility of Reinforced Concrete Sections in Combined Bending and Axial Load," SM Study 8, University of Waterloo Press, pp. 147-180.

Hannant, D. J., 1972, "Tensile Strength of Concrete: a Review Paper," Structural Engineering, July, Vol. 50, pp. 253-258.

Hognestad, E., 1952, "Fundamental Concepts in Ultimate Design of Reinforced Concrete Members," ACI Journal, Vol. 48, pp. 809-828.

Hughes, O., 1983, "Ship Structural Design: A Rationally-Based Computer-Aided Optimization Approach," John Wiley & Sons, New York, 566 p.

Jofriet, J. C. and McNeice, G. M., 1971, "Finite Element Analysis of Reinforced Concrete Slabs," Journal of the Structural Division, ASCE, Vol. 97, No. ST3, pp. 785-806.

Kordina, K. and Storkebaum, K. H., 1973, "Untersuchungen uber die Traglasten Ausmitting Beanspruchter Stahlbetonwande," Institute fur Baustoffkunde und Stahlbetonbau, Technischen, Universitat Braunschweig, 87 p.

Kordina, K. and Timm, R., 1979, "Experimentelle Untersuchungen zum Stabilitatsverhalten vpn Bewhrten und Unbeehrten Betonwanden," Institute fur Baustoffkunde und Stahlbetonbau, Technischen, Universitat Braunschweig, 115 p.

Kordina, K. and Kiel, M., 1982, "Stabilität Mehseitig Gelagertes Betonwände, 2. Stufe," Institute für Baustoffkunde und Stahlbetonbau, Technischen, Universität Braunschweig 116 p.

Kotsovos, M. D., 1983, "Effect of Testing Techniques on the Post-Ultimate Behaviour of Concrete in Compression," *Materials and Structures (Materiaux et Constructios)*, Vol. 16, No. 91, pp. 3-12.

Kupfer, H. and Gerstle, K. H., 1973, "Behaviour of Concrete under Biaxial Stresses," *Journal of the Engineering Mechanics Division, ASCE*, Vol. 99, No. EM4, pp. 853-866.

Kupfer, H., Hilsdorf, H. K. and Rüschi, H., 1969, "Behaviour of Concrete under Biaxial Stresses," *ACI Journal*, Vol. 66, No. 8, pp. 656-666.

Lenschow, R. J. and Sozen, M. A., 1966, "A Yield Criterion for Reinforced Concrete under Biaxial Moments and Forces," *Civil Engineering Studies, Structural Research Series No. 311*, University of Illinois, Urbana, July.

Liu, T. C. Y., Nilson, A. H. and Slate, F. O., 1972, "Stress-Strain Response and Fracture of Concrete in Uniaxial and Biaxial Compression," *ACI Journal*, Vol. 69, No. 5, May, pp. 291-295.

MacGregor, J. G., 1988, "Reinforced Concrete: Mechanics and Design," Prentice Hall, Englewood Cliffs, New Jersey, 799 P.

Massicotte, B., Elwi, A. E. and MacGregor, J. G., 1988, "Analysis of Reinforced Concrete Panels Loaded Axially and Transversally," *Structural Engineering Report No. 161*, Department of Civil Engineering, University of Alberta, Edmonton, 254 p.

Massicotte, B., Elwi, A. E. and MacGregor, J. G., 1990, "Tension-Stiffening Model for Planar Reinforced Concrete Members," *Journal of Structural Division, ASCE*, 116(11), pp. 3039-3058.

Oberlander, G. D. and Everard, N. J., 1977, "Investigation of Reinforced Concrete Walls," ACI Journal, June, pp. 256-263.

Park, R. and Gamble, W. L., 1980, "Reinforced Concrete Slabs," John Wiley & Sons, New York, 769 p.

Park, R., 1964, "Ultimate Strength of Rectangular Concrete Slabs under Short-Term Uniform Loading with Edges Restrained against Lateral Movement," Proc. Inst. Civ. Eng., Vol. 28, June, pp. 125-150.

Pfrang, E. O., Siess, C. P. and Sozen, M. A., 1964, "Load-Moment-Curvature Characteristics of Reinforced Concrete Cross Sections," ACI Journal, Vol. 61, No. 7, July, pp. 763-778.

Prakhya, G. K. V. and Morley, C. T., 1990, "Tension Stiffening and Moment-Curvature Relations of Reinforced Concrete Elements," ACI Structural Journal, Vol. 87, No. 5, September-October, pp. 597-605.

Ramm, E., 1976, "Geometrisch Nichtlineare Elastostatik und Finite Elemente," Bericht No. 76-2, Institute Für Baustatik, Universität Stuttgart, Stuttgart, Germany.

Ramm, E., 1977, "A Plate/Shell Element for Large Deflections and Rotations," in: Bathe, K.-J., Oden, J. T., and Wunderlich, W., Eds., "Formulation and Computational Algorithms," U.S.-Germany Symposium, M.I.T., pp. 264-293.

Ramm, E., 1980, "Strategies for Tracing the Nonlinear Response Near Limit Points," in Wunderlich, W., Stein, E., and Bathe, K.-J., Eds., "Nonlinear Finite Element Analysis in Structural Mechanics," Proceedings of the Europe-U.S. Workshop, Ruhr Universität, Bochum, Germany, pp. 63-89.

Rüsch, H., 1960, "Researches Toward a General Flexural Theory for Structural Concrete," ACI Journal, Proceedings Vol. 57, July, pp. 1-28.

Saenz, L. P., 1964, "Discussion of Equation for the Stress-Strain Curve of Concrete by Desayi and Krishnan," ACI Journal, Vol. 61, No. 9, pp. 1229-1235.

Saheb, M. and Desayi, P., 1989, "Ultimate Strength of R. C. Wall Panels in One-Way Inplane Action," Journal of Structural Division, ASCE, 115(10), pp. 2617-2630.

Saheb, M. and Desayi, P., 1990, "Ultimate Strength of R. C. Wall Panels in Two-Way Inplane Action," Journal of Structural Division, ASCE, 116(5), pp. 1384-1402.

Stegmüller, H., 1984, "NISA- Input Description," Institute Für Baustatik, Universität Stuttgart, Stuttgart, Germany.

Stegmüller, H., Häfner, L., Ramm, E. and Sattelle, J. M., 1983, "Theoretische Grundlagen zum FE-Programm System NISA 80,".

Swartz, S. E., Rosebraugh, V. H. and Berman, M. V., 1974, "Buckling Tests on Rectangular Concrete Panels," ACI Journal, Vol. 71, No. 1, January, pp. 33-39.

Sziliard, R., 1974, "Theory and Analysis of Plates," Prentice-Hall, New York, 724 p.

Taylor, R., Maher, D. R. H. and Hayes, B., 1966, "Effect of Arrangement of Reinforcement on the Behaviour of Reinforced Concrete Slabs," Magazine of concrete research, Vol. 18, No. 55, June, pp. 85-94.

Timoshenko, S. P. and Woinowsky-Krieger, S., 1959, "Theory of Plates and Shells," Second edition, McGraw-Hill, 580 p.

Todeschini, C. E., Bianchini, A. C. and Kesler, C. E., 1964, "Behaviour of Columns Reinforced with High Strength Steels," ACI Journal. Vol. 61, pp. 701-715.

Toma, S. and Chen, W. F., 1983, "Post-Buckling Behaviour of Tubular Beam-Columns," Journal of Structural Division, ASCE, Vol. 109, No. 8, August, pp. 1918-1932.

Van Greunen, J., 1979, "Nonlinear Geometric, Material and Time Dependent Analysis of Reinforced Concrete and Prestressed Concrete Slabs and Panels," Ph.D. Dissertation, Department of Civil Engineering, University of California, Berkeley, Report No. 79-3.

Vebo, A. and Ghali, A., 1977, "Moment-Curvature Relation of Reinforced Concrete Slabs," Journal of Structural Division, ASCE, Vol.103, pp. 515-531.

Vecchio, F. J. and Collins, M. P., 1982, "The Response of Reinforced Concrete to Inplane Shear and Normal Stresses," University of Toronto, Department of Civil Engineering Publication No. 82-03, March, 332 p.

Williams, B. A., 1986, "Tests on Large Reinforced Concrete Elements Subjected to Direct Tension," Cement and Concrete Association, Technical Report 562, London, 56 p.

Appendix A

Ancillary Tests Results

The concrete used for all specimens except two was ordered from a ready mix supplier. Concrete placing was done in four phases and the same concrete mix was ordered for each. The concrete used for casting specimens C5 and C9 was produced in the laboratory. Concrete cylinders and modulus of rupture beams were cast at the same time as the specimens. Compressive and tensile strength tests were conducted to determine the parameters necessary to define concrete behaviour as a function of time.

Cylinders were nominally 150 mm in diameter and 300 mm long. Beams were 152x152x914 mm. Five concrete cylinders and two beams were tested the same day as each plate test. Of the five cylinders, three were tested in compression to determine the compressive strength and the static modulus of elasticity of concrete in compression in accordance with CSA A23.2-9C (CSA,1990). The remaining two cylinders were used for a split cylinder tensile test in accordance with CSA A23.2-13C (CSA, 1990). The modulus of rupture beams were tested in accordance with CSA A23.2-8C (CSA, 1990). The results of the ancillary tests are given in detail in Tables A.1 through A.5.

The data from the control tests for each of the main four castings were fitted with regression lines of the form $F(t) = a + bt$ by

the method of least squares, where t is the age of the concrete. Table 2.4 gives the age at which the specimen was tested together with the concrete properties determined for each specimen from the regression equations. As mentioned earlier, specimens C5 and C9 were cast at different times using concrete produced in the laboratory and hence their concrete properties did not follow the regression equations. Their strengths were taken from the tests made at the time these specimens were tested.

Table A-1 Ancillary Tests Results for Series A

Time from Casting, Days	Compression Test		Splitting Test	Rupture Test
	f'_c (MPa)	E_c (MPa)	f_{sp} (MPa)	f_r (MPa)
52	22.92	20740		
	22.03	20825	1.68	3.13
	21.83	21390	1.84	3.57
	$\mu = 22.26$	$\mu = 20985$	$\mu = 1.76$	$\mu = 3.35$
70	24.47	21130		
	20.78	21740	2.36	3.40
	21.06	21405	2.88	3.76
	$\mu = 22.10$	$\mu = 21425$	$\mu = 2.62$	$\mu = 3.58$
80	22.87	21365		
	21.77	21140	2.18	3.43
	22.71	21380	2.32	3.65
	$\mu = 22.45$	$\mu = 21295$	$\mu = 2.25$	$\mu = 3.54$
86	22.96	21415		
	24.11	21005	2.16	3.51
	23.90	21210	2.26	3.79
	$\mu = 23.65$	$\mu = 21210$	$\mu = 2.21$	$\mu = 3.65$

Table A-2 Ancillary Tests Results for Series B

Time from Casting, Days	Compression Test		Splitting Test	Rupture Test
	f_c (MPa)	E_c (MPa)	f_{sp} (MPa)	f_r (MPa)
32	18.31	20115		
	17.83	20440	1.49	2.51
	18.00	20300	1.60	2.85
	$\mu = 18.05$	$\mu = 20285$	$\mu = 1.55$	$\mu = 2.68$
65	19.53	21120		
	20.68	20755	1.57	2.63
	20.10	20930	1.63	2.95
	$\mu = 20.11$	$\mu = 20935$	$\mu = 1.60$	$\mu = 2.79$
80	18.08	21670		
	20.66	20835	2.10	2.87
	20.18	21230	1.74	3.25
	$\mu = 19.64$	$\mu = 21245$	$\mu = 1.92$	$\mu = 3.06$
154	19.16	21465		
	20.91	20915	1.81	3.11
	21.58	21265	2.15	3.67
	$\mu = 20.55$	$\mu = 21215$	$\mu = 1.98$	$\mu = 3.39$

Table A-3 Ancillary Tests Results for Series C

Time from Casting, Days	Compression Test		Splitting Test	Rupture Test
	f'_c (MPa)	E_c (MPa)	f_{sp} (MPa)	f_r (MPa)
29	25.93	21510		
	24.08	21145	1.72	3.20
	24.94	20990	2.38	3.74
	$\mu = 24.98$	$\mu = 21215$	$\mu = 2.10$	$\mu = 3.47$
34	25.68	21515		
	25.14	21645	2.40	3.36
	24.52	21260	2.66	3.88
	$\mu = 25.11$	$\mu = 21475$	$\mu = 2.53$	$\mu = 3.52$
37	25.57	21360		
	27.36	21520	2.38	3.21
	25.52	21750	2.52	3.65
	$\mu = 26.15$	$\mu = 21545$	$\mu = 2.45$	$\mu = 3.43$
42	24.52	21585		
	26.54	21210	2.18	3.19
	25.35	21335	2.44	4.17
	$\mu = 25.47$	$\mu = 21375$	$\mu = 2.31$	$\mu = 3.68$
50	23.55	22090		
	24.96	21815	2.21	3.51
	26.53	22270	2.27	4.05
	$\mu = 25.01$	$\mu = 22060$	$\mu = 2.24$	$\mu = 3.78$
61	24.18	21435		
	26.21	21915	2.27	3.62
	24.97	21560	2.49	4.14
	$\mu = 25.12$	$\mu = 21650$	$\mu = 2.38$	$\mu = 3.88$

Table A-3 Ancillary Tests Results for Series C (continued)

Time from Casting, Days	Compression Test		Splitting Test	Rupture Test
	f_c (MPa)	E_c (MPa)	f_{sp} (MPa)	f_r (MPa)
83	26.02	22340		
	26.88	22440	2.41	3.76
	25.34	22575	—	4.40
	$\mu = 26.08$	$\mu = 22450$	$\mu = 2.41$	$\mu = 4.08$
24 (C5 [*])	25.76	21560		
	26.34	21940	2.67	3.21
	25.33	21900	2.43	3.88
	$\mu = 25.81$	$\mu = 21800$	$\mu = 2.55$	$\mu = 2.70$
39 (C9 [*])	25.02	19430		
	24.12	19040	2.87	3.09
	25.68	19130	2.35	2.61
	$\mu = 26.15$	$\mu = 19200$	$\mu = 2.61$	$\mu = 2.85$

* Concrete for these specimens was produced in the laboratory.

Table A.4 Ancillary Tests Results for Series D

Time from Casting, Days	Compression Test		Splitting Test	Rupture Test
	f'_c (MPa)	E_c (MPa)	f_{sp} (MPa)	f_r (MPa)
32	26.42	21200		
	25.76	20850	2.82	3.39
	25.75	21100	2.57	3.04
	$\mu = 25.98$	$\mu = 21050$	$\mu = 2.70$	$\mu = 3.22$
36	26.49	20550		
	25.71	21350	2.57	3.17
	26.16	20500	2.72	3.34
	$\mu = 26.12$	$\mu = 20800$	$\mu = 2.65$	$\mu = 3.26$

Appendix B

Calculation of Shrinkage Induced Stresses

For a member having equal amount of top and bottom reinforcement, it can be shown (Ghali and Favre, 1986) that uniform shrinkage induces uniform concrete tensile stresses which can be predicted using the formula:

$$\sigma_{sh} = \epsilon_{sh} E_c \left(1 - \frac{A_c}{A'_c}\right) \quad (B.1)$$

where,

ϵ_{sh} = shrinkage strain occurring at time t = age of the specimen at testing.

$E'_c = E_c(t_0)/(1 + \chi\phi(t, t_0))$ = age-adjusted elasticity modulus of concrete.

$\chi(t, t_0)$ = Aging coefficient of concrete.

$\phi(t, t_0)$ = Creep coefficient of concrete

A_c = Cross-section area.

A'_c = Area of the age-adjusted transformed section

$$= A_c + (E_s/E'_c - 1) A_s$$

As recommended by MacGregor (1988), the CEB method (1978) was used for computing shrinkage strains but the ultimate shrinkage strains were taken from the ACI recommendations (1982).

The axial shrinkage strains occurring between times t_0 and t can be predicted using the formula

$$\epsilon_{sh}(t, t_0) = \epsilon_{shu} \alpha_{ss} \alpha_{RH} \alpha_{sL} \beta_s(t - t_0) \quad (B.2)$$

Where,

ϵ_{shu} = basic shrinkage strain at time = ∞ for a member with an effective thickness of 152 mm, in the absence of test data it may be taken as 0.00080.

α_{ss} = factor to account for the size effect on shrinkage.

α_{RH} = factor to account for the relative humidity.

α_{sL} = factor to account for the slump and cement content; can be taken equal to 1.0.

β_s = factor to account for the rate at which shrinkage develops.

The axial shrinkage strains for all specimens, as calculated using Eqn. B.2, are given in Table B.1 together with the values of the parameters used in this equation.

The parameters used in Eqn. B.1 to calculate the tensile stresses due to shrinkage are given in Table B.2 for all of the specimens, and the tensile stresses due to shrinkage are given in Table 5.1.

Table B.1 Calculation of Shrinkage Strains

Specimen Designation	Age (Days)	h (mm)	α_{ss}	β_s	$\epsilon_{sh} \times 10^{-6}$
A1	52	67.3	1.15	0.62	570.0
A2	70	64.7	1.15	0.66	607.0
A3	80	65.3	1.15	0.68	625.0
A4	86	65.3	1.15	0.69	635.0
B1	32	68.2	1.15	0.50	460.0
B2	65	66.8	1.15	0.65	598.0
B3	80	66.7	1.15	0.68	625.0
B4	154	65.3	1.15	0.77	708.0
C1	29	67.8	1.15	0.50	460.0
C2	34	67.6	1.15	0.53	487.0
C3	37	68.5	1.15	0.53	487.0
C4	42	70.0	1.15	0.56	515.0
C5	24	70.1	1.15	0.45	414.0
C6	50	67.4	1.15	0.62	570.0
C7	61	66.5	1.15	0.64	589.0
C8	83	67.8	1.15	0.68	625.0
C9	39	66.9	1.15	0.53	487.0
D1	32	92.8	1.05	0.44	369.0
D2	36	92.7	1.05	0.44	378.0

Table B.2 Parameters Used to Calculate the Tensile Stresses Due to Shrinkage

Specimen Designation	Age (Days)	χ	ϕ	E'_c (MPa)	A'_{cx} (mm ²)	A'_{cy} (mm ²)
A1	52	0.760	1.80	8900.0	77385.0	77385.0
A2	70	0.740	2.10	8305.0	75550.0	75550.0
A3	80	0.740	2.15	8215.0	76270.0	87240.0
A4	86	0.740	2.20	8115.0	87505.0	76405.0
B1	32	0.740	1.50	50.0	77350.0	77350.0
B2	65	0.760	2.00	8255.0	77715.0	77715.0
B3	80	0.740	2.10	8185.0	77710.0	77710.0
B4	154	0.740	2.70	7135.0	78010.0	78010.0
C1	29	0.765	1.46	10060.0	76660.0	76660.0
C2	34	0.760	1.53	9895.0	76620.0	76620.0
C3	37	0.760	1.58	9750.0	77660.0	77660.0
C4	42	0.745	1.68	9575.0	79335.0	88675.0
C5	24	0.840	1.00	11850.0	84990.0	77545.0
C6	50	0.740	1.80	9315.0	77010.0	77010.0
C7	61	0.740	1.95	8980.0	76490.0	76490.0
C8	83	0.680	2.15	9090.0	77660.0	77660.0
C9	39	0.760	1.58	8725.0	77200.0	77200.0
D1	30	0.780	1.45	9785.0	105575.0	105575.0
D2	36	0.760	1.58	9475.0	105920.0	105920.0

Appendix C

Experimental Lateral Load versus Center Deflection Curves

In this appendix, the lateral load versus center deflection plots for all the specimens are given. The lateral load is given as pressure in kPa computed as the sum of the jack loads divided by the area of the plate within the center-lines of the supports. The reference values for the deflection measurements of the specimens were taken at the start of the loading tests.

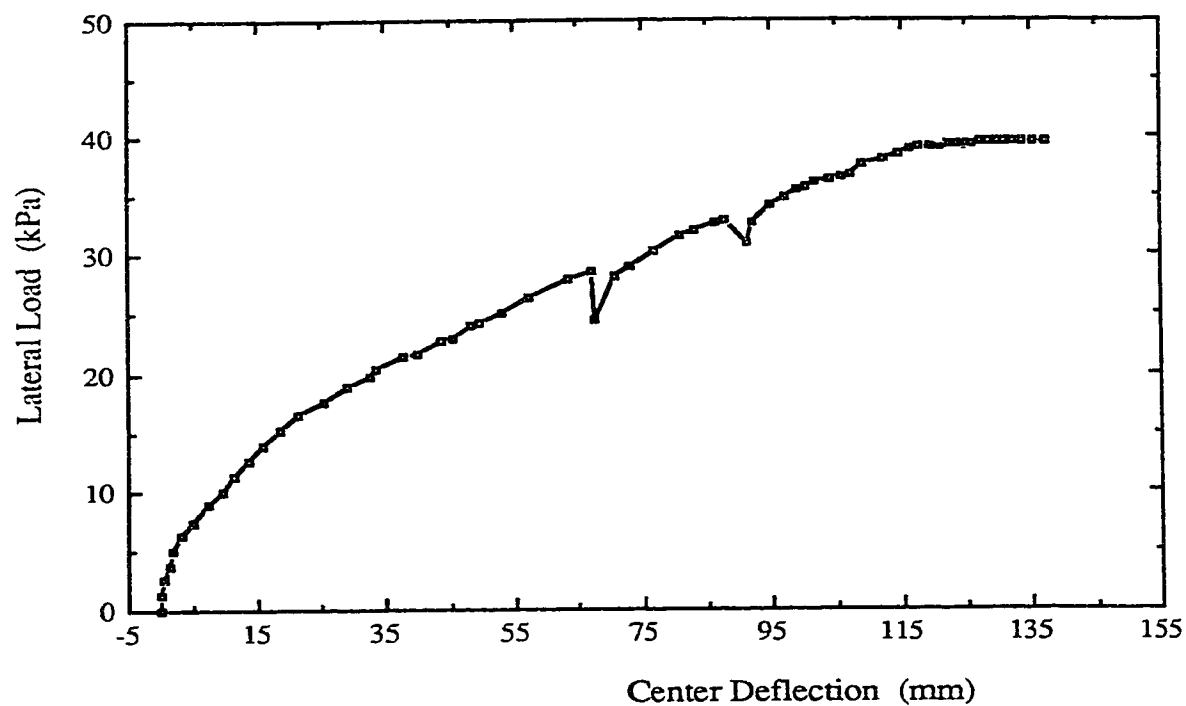


Figure C.1 Lateral Load versus Center Deflection Curve for Specimen A1

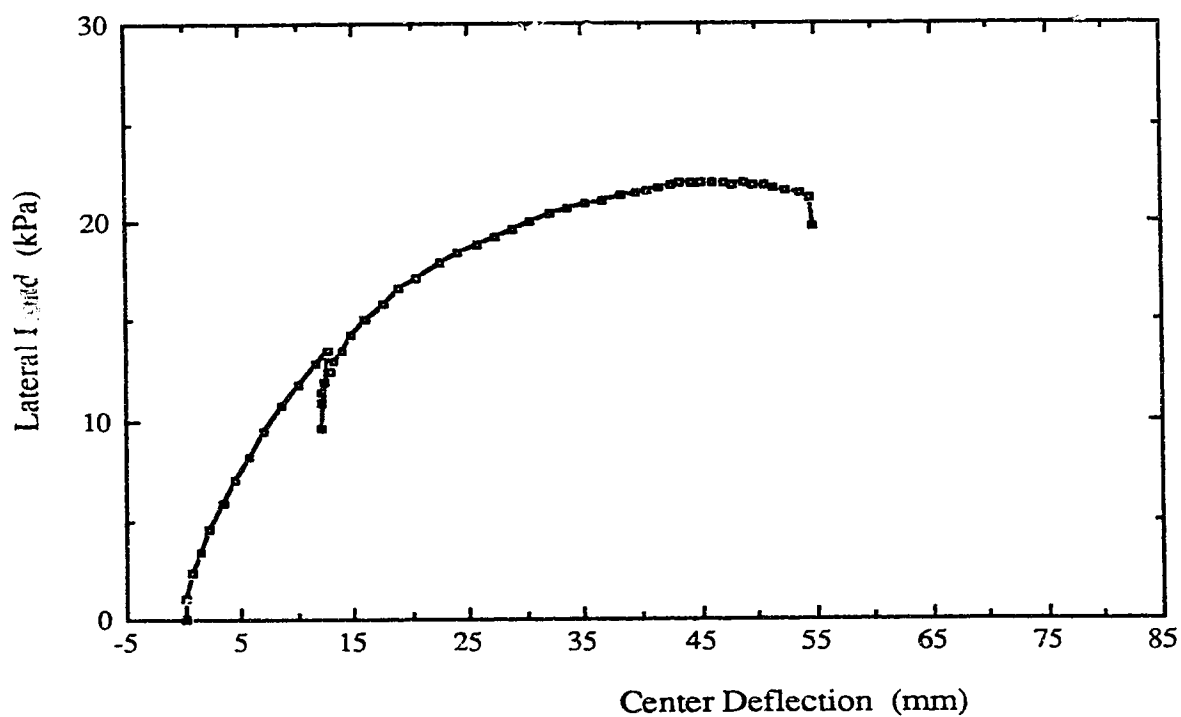


Figure C.2 Lateral Load versus Center Deflection Curve for Specimen A2

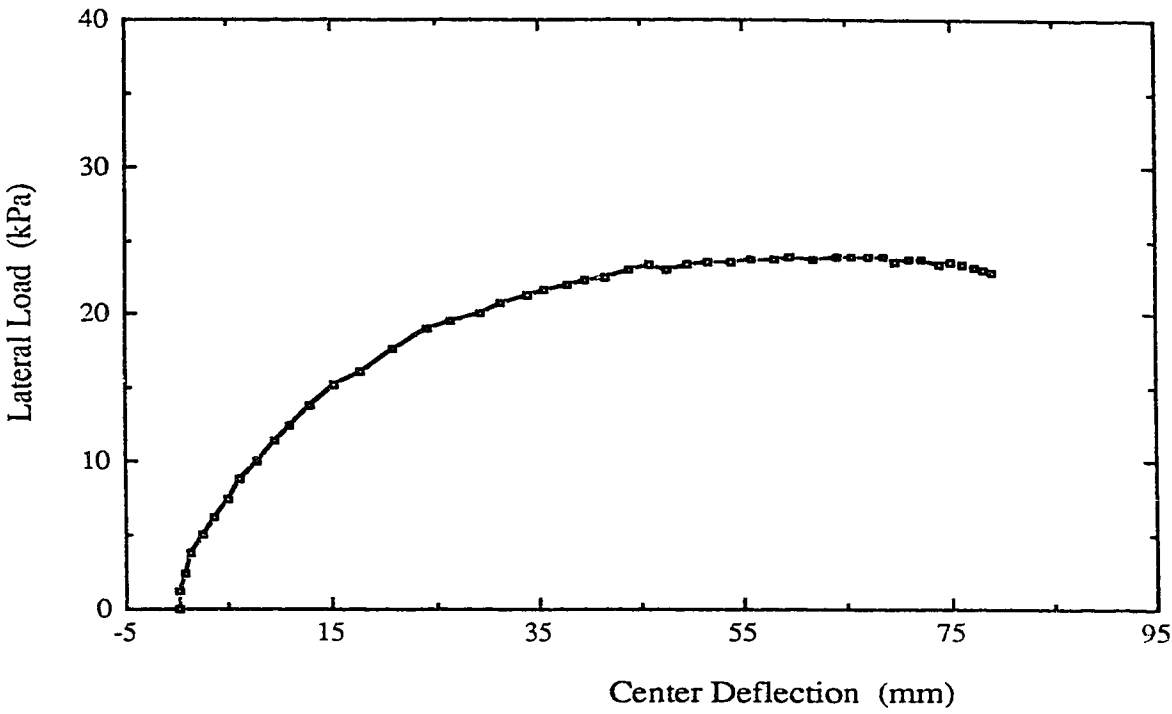


Figure C.3 Lateral Load versus Center Deflection Curve for Specimen A3

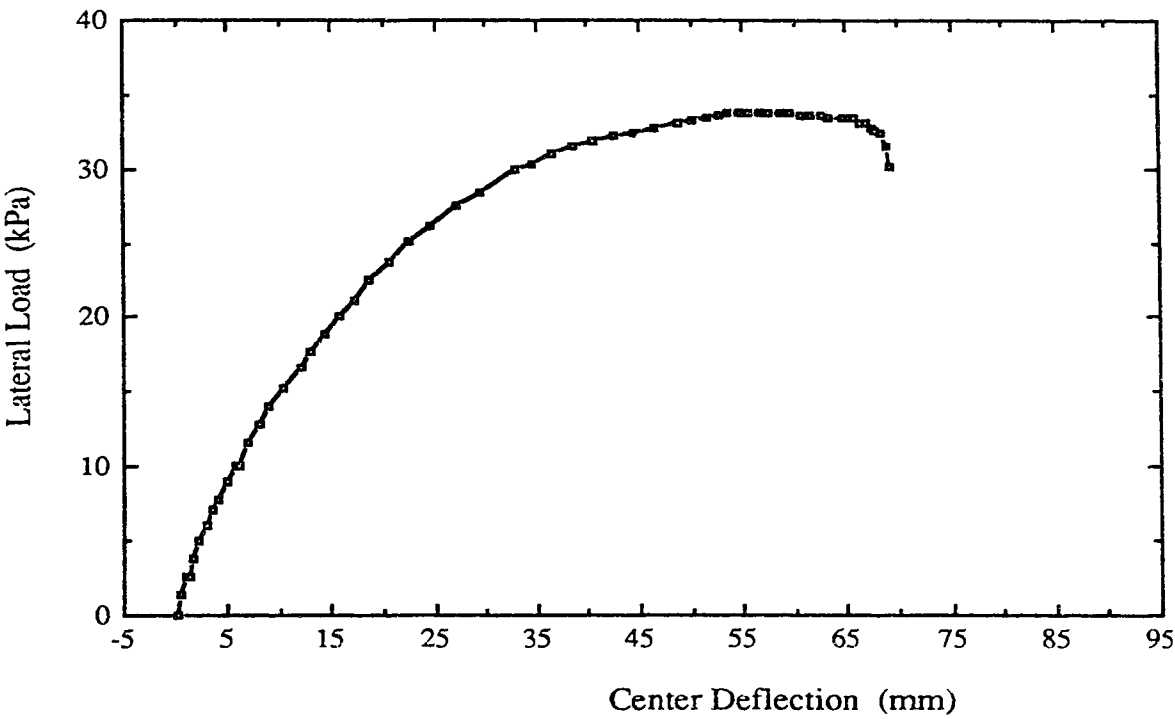


Figure C.4 Lateral Load versus Center Deflection Curve for Specimen A4

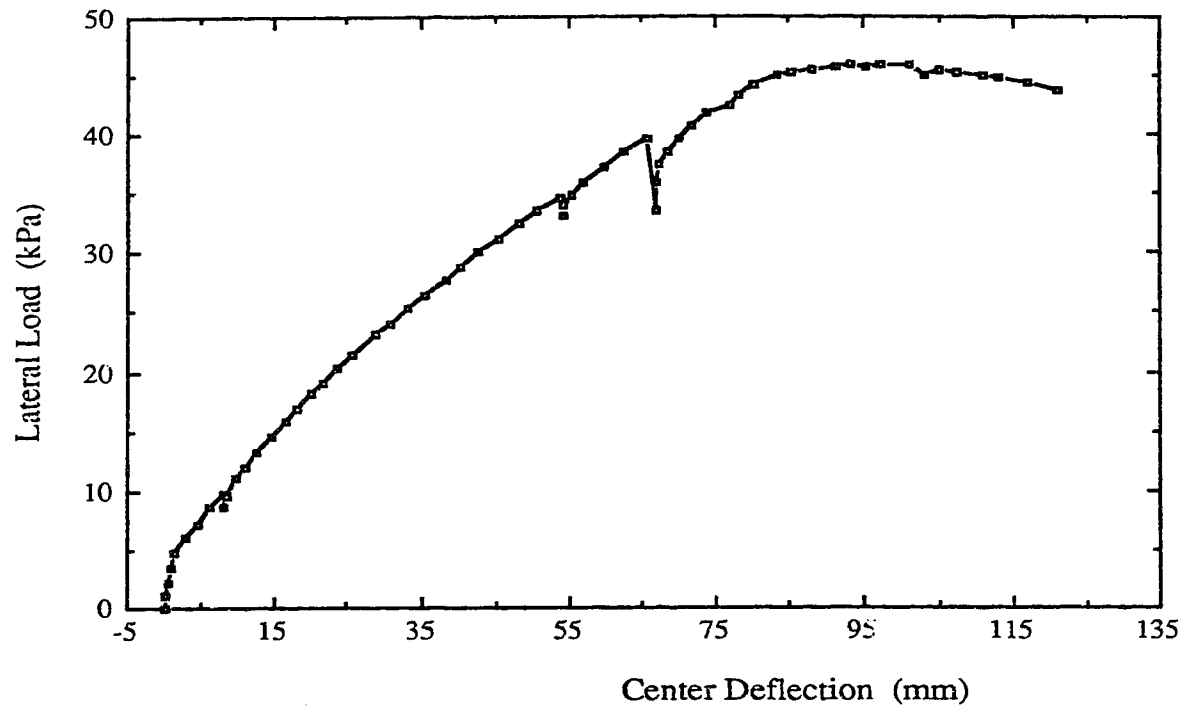


Figure C.5 Lateral Load versus Center Deflection Curve for Specimen B1

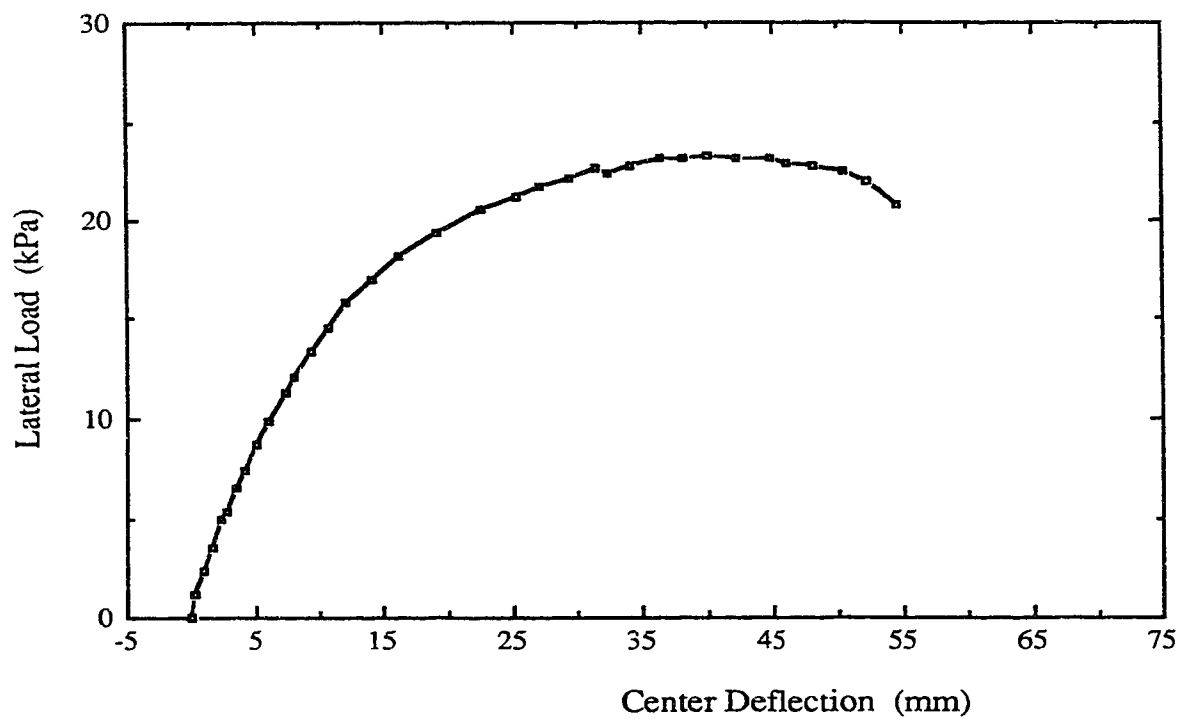


Figure C.6 Lateral Load versus Center Deflection Curve for Specimen B2

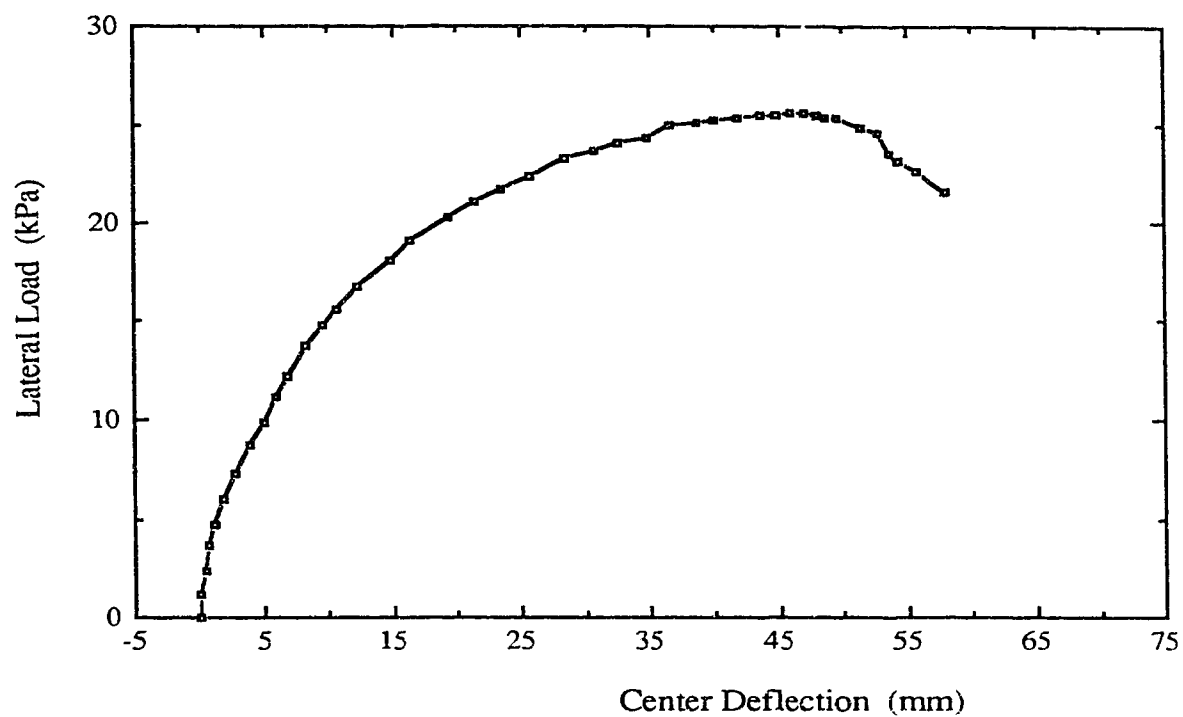


Figure C.7 Lateral Load versus Center Deflection Curve for Specimen B3

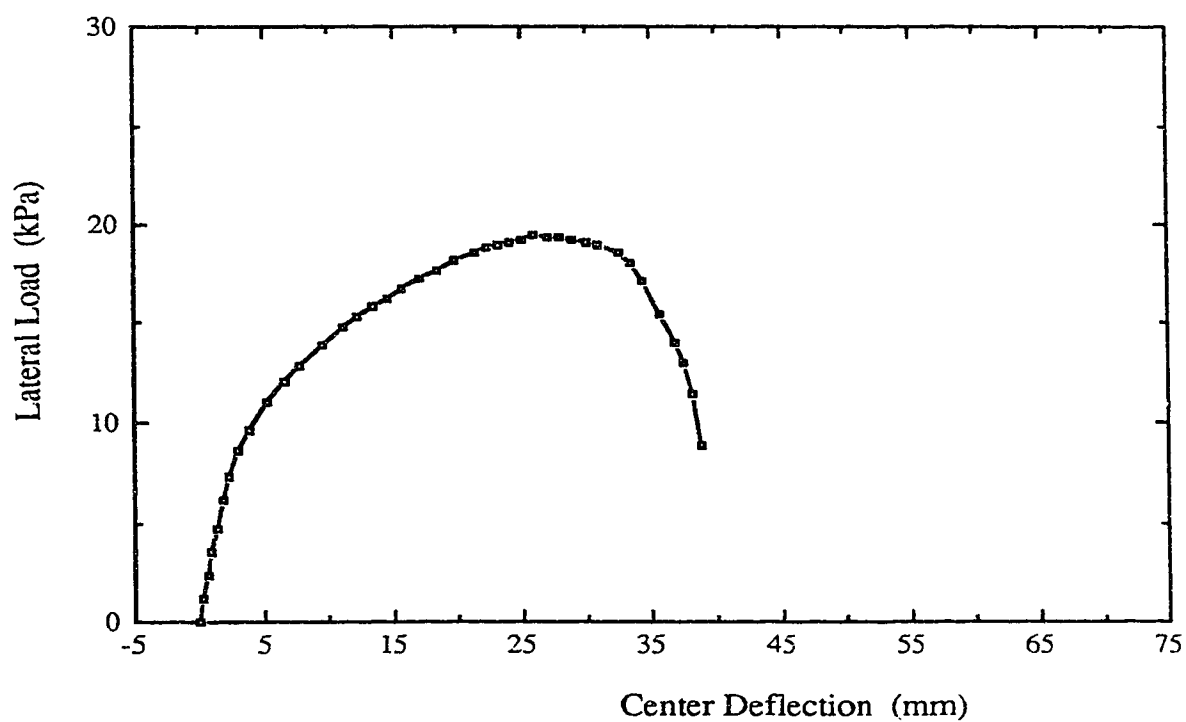


Figure C.8 Lateral Load versus Center Deflection Curve for Specimen B4

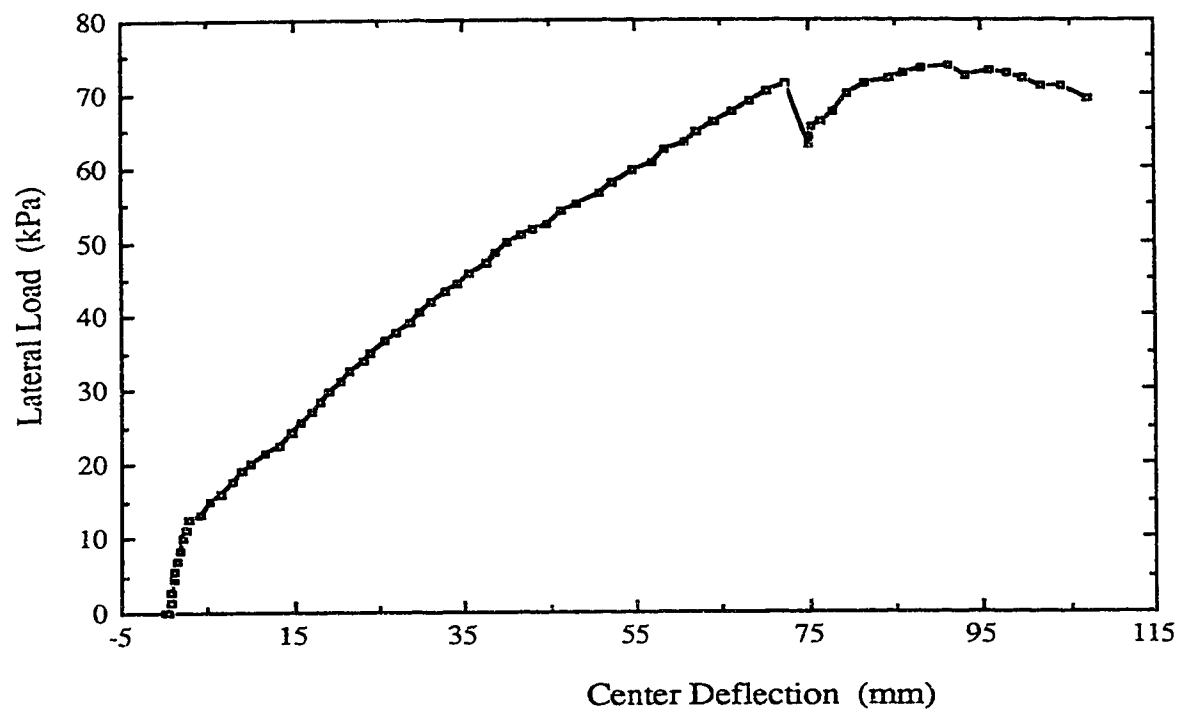


Figure C.9 Lateral Load versus Center Deflection Curve for Specimen C1

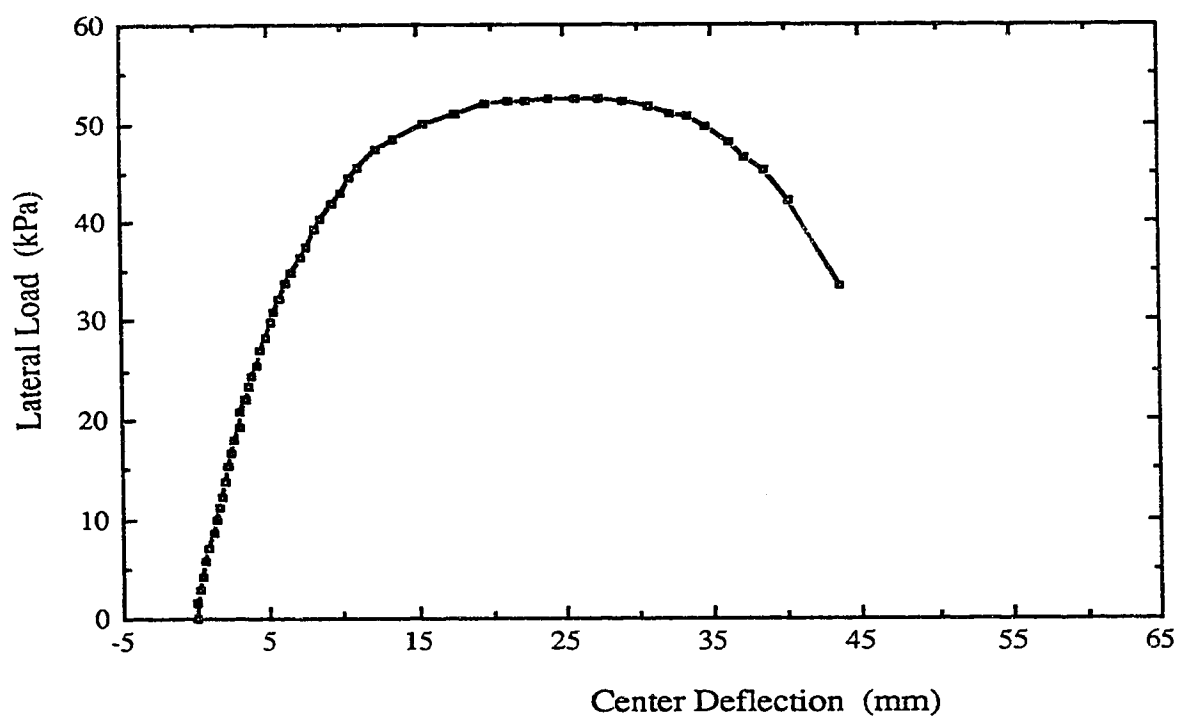


Figure C.10 Lateral Load versus Center Deflection Curve for Specimen C2

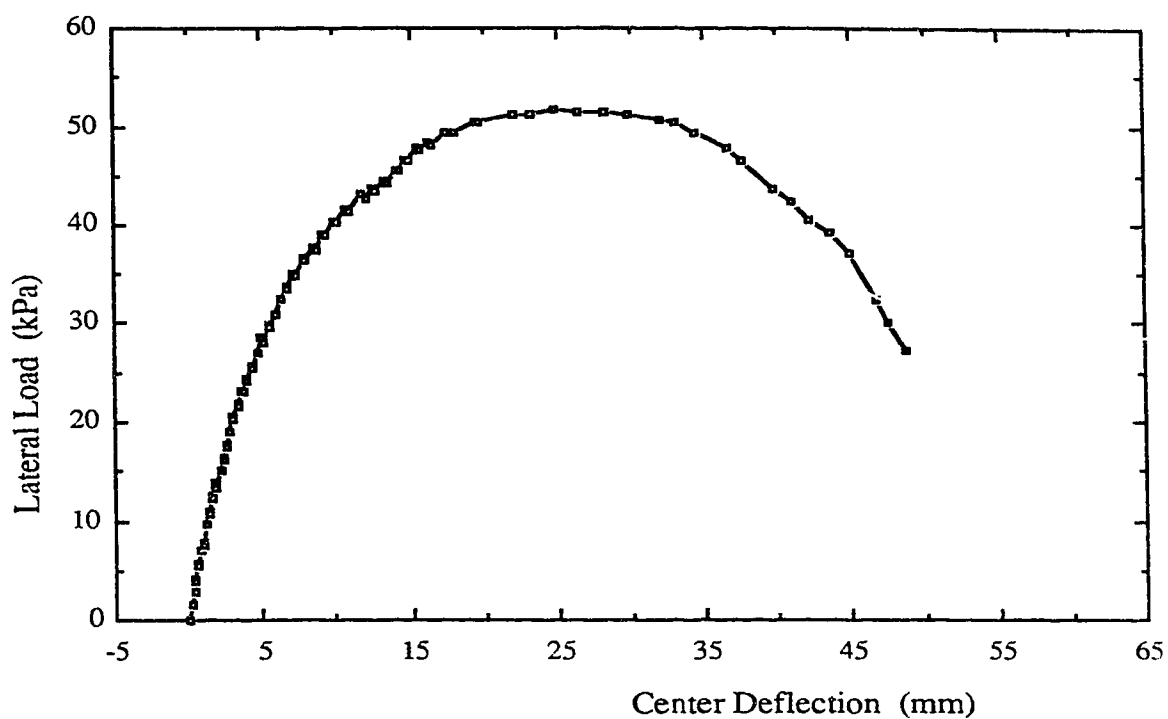


Figure C.11 Lateral Load versus Center Deflection Curve for Specimen C3

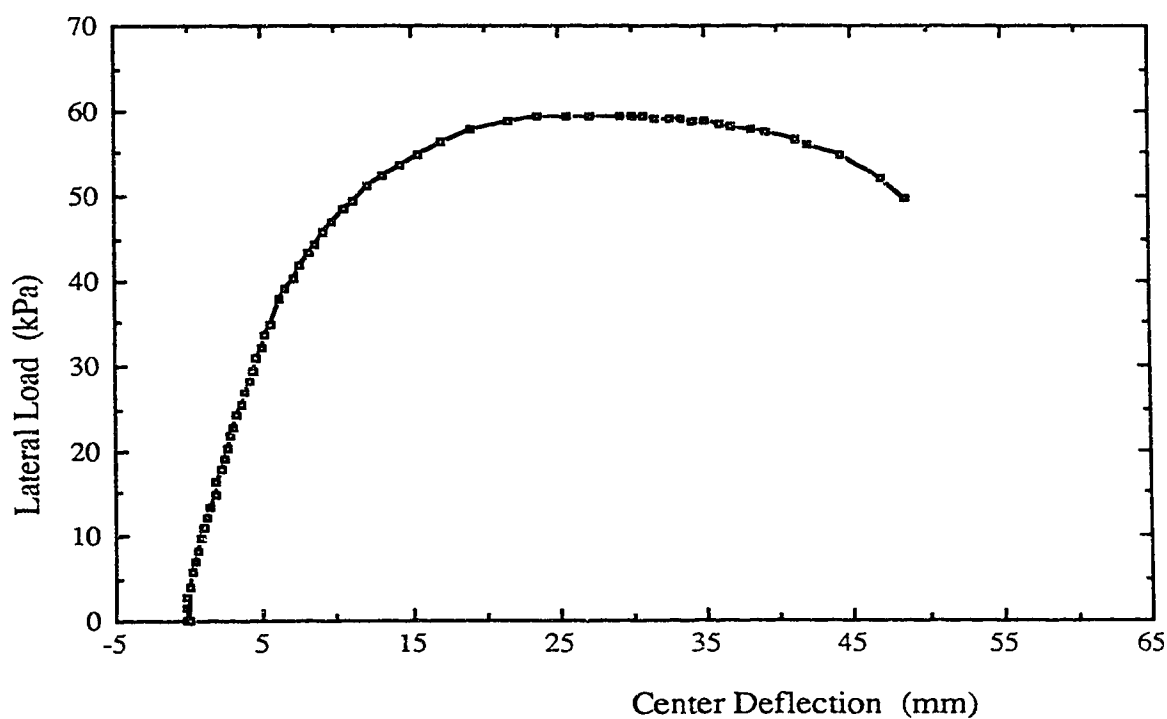


Figure C.12 Lateral Load versus Center Deflection Curve for Specimen C4

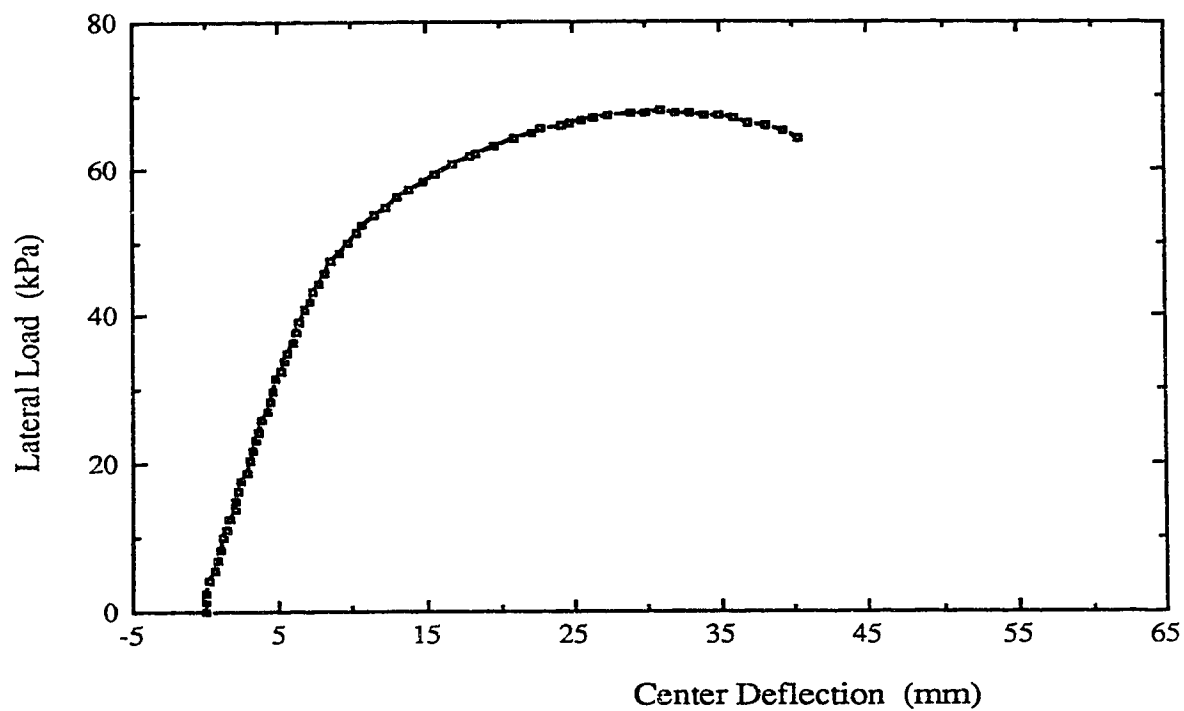


Figure C.13 Lateral Load versus Center Deflection Curve for Specimen C5

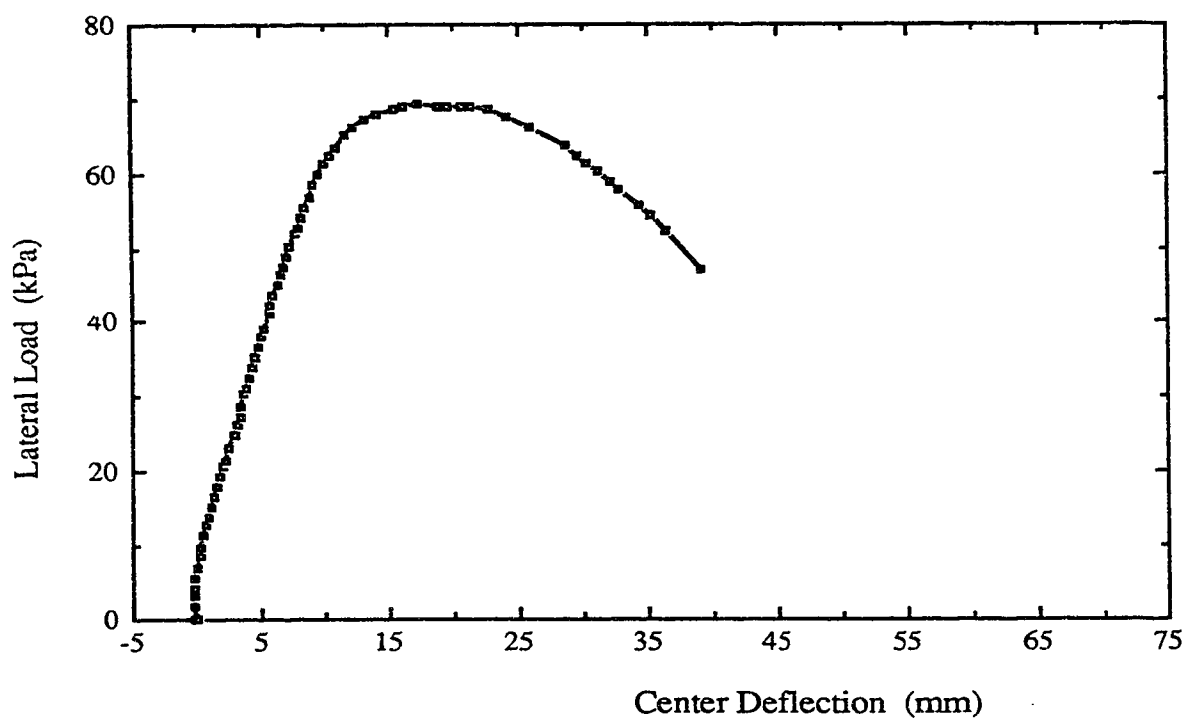


Figure C.14 Lateral Load versus Center Deflection Curve for Specimen C6

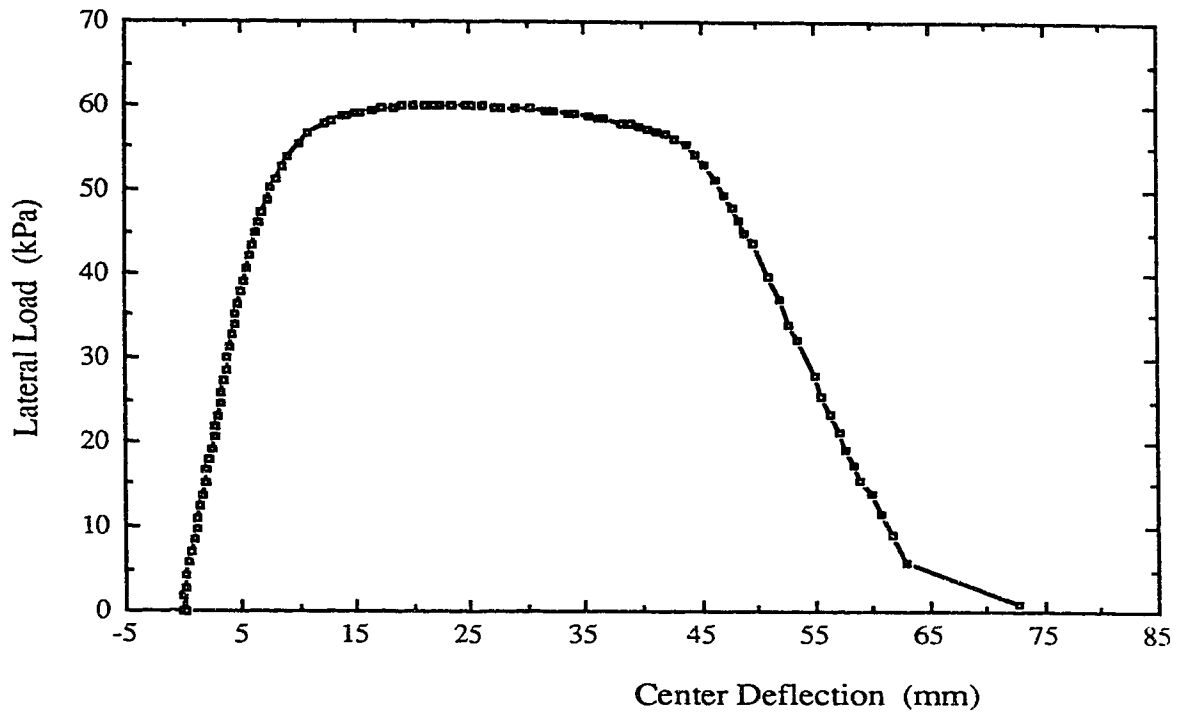


Figure C.15 Lateral Load versus Center Deflection Curve for Specimen C7

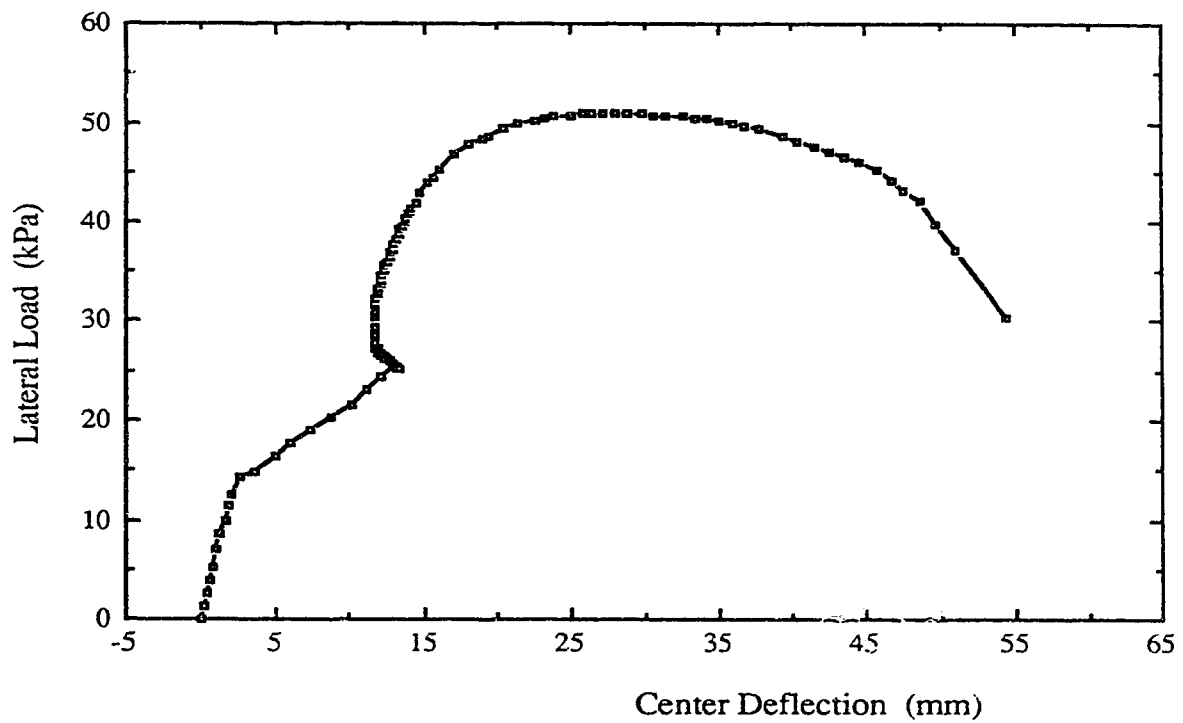


Figure C.16 Lateral Load versus Center Deflection Curve for Specimen C8

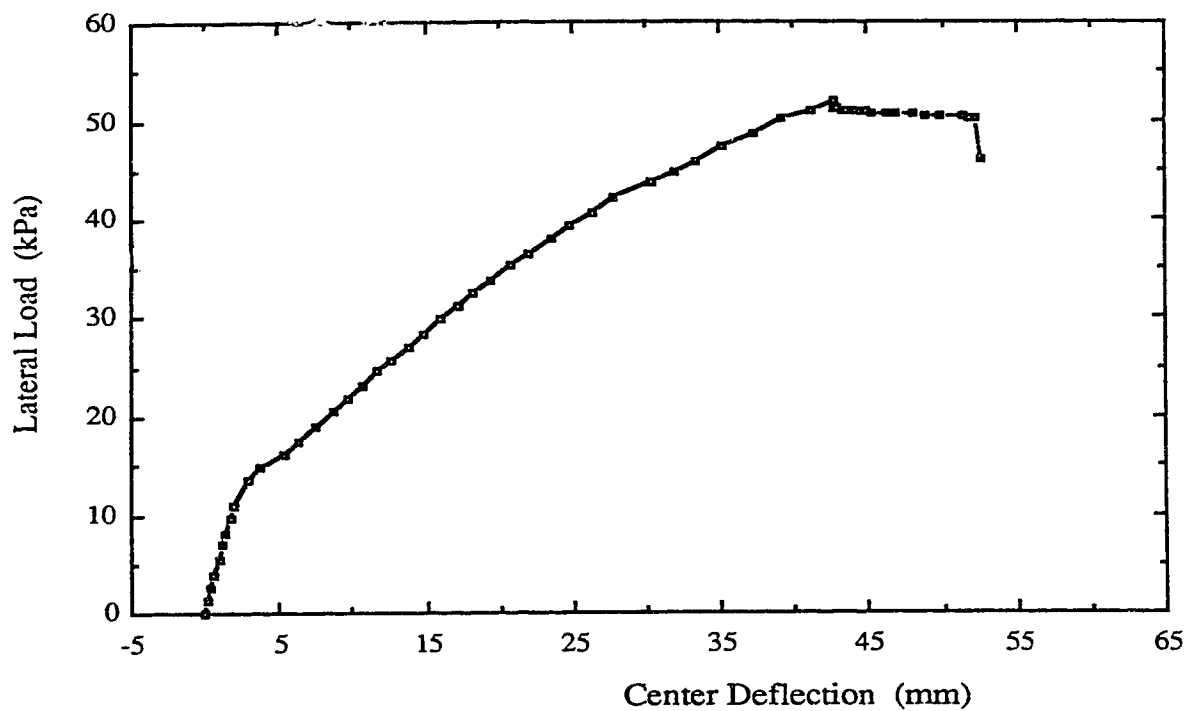


Figure C.17 Lateral Load versus Center Deflection Curve for Specimen C9

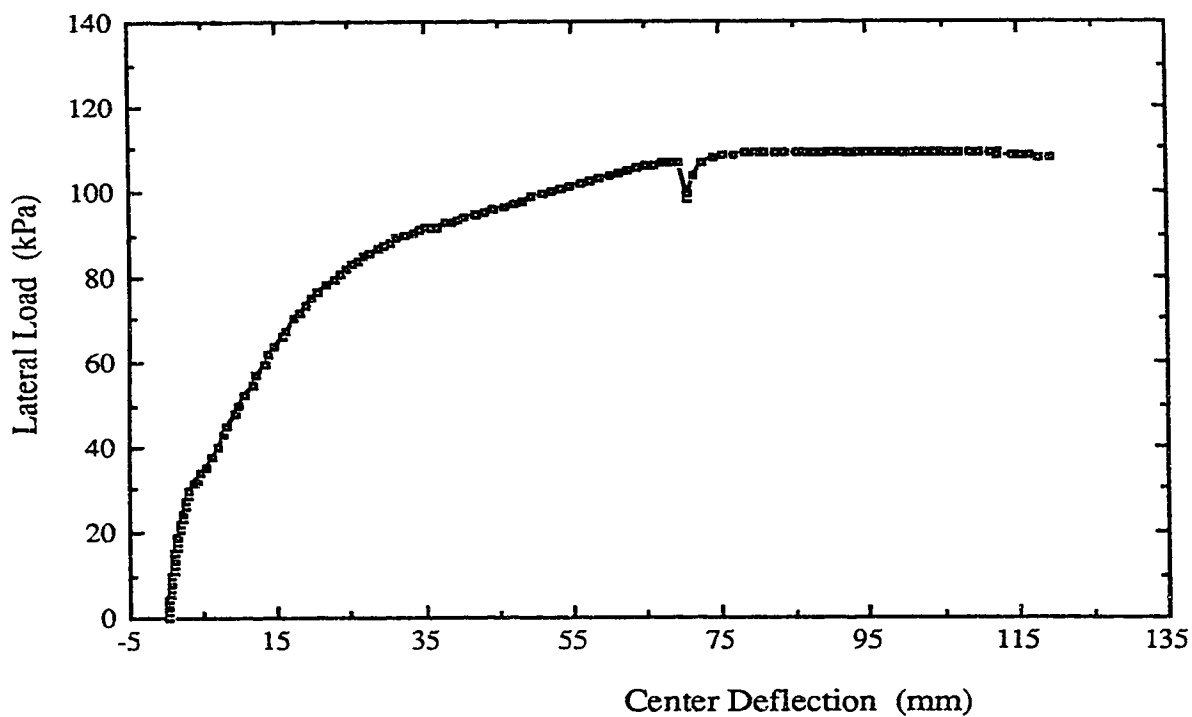


Figure C.18 Lateral Load versus Center Deflection Curve for Specimen D1

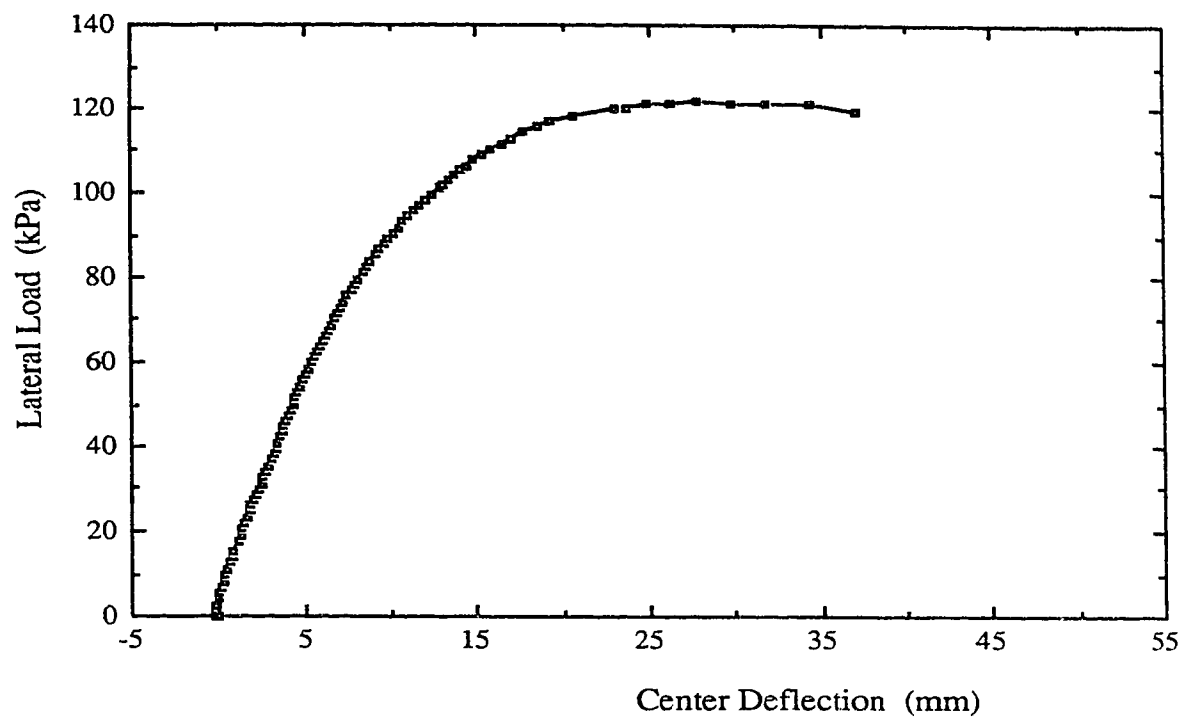


Figure C.19 Lateral Load versus Center Deflection Curve for Specimen D2